

Bose–Einstein Condensation and Applications

Dissertation
zur Erlangung des akademischen Grades

“Doktor der Naturwissenschaften”

an der

Naturwissenschaftlichen Fakultät
der
Leopold-Franzens-Universität Innsbruck

eingereicht von

Mag. rer. nat. Dieter Jaksch

Innsbruck, im Oktober 1999

Contents

I	Cold Bose-gases	7
1	Bose-Einstein Condensation (BEC)	9
1.1	Introduction	9
1.2	BEC of an ideal Bose-gas in a trap	11
1.2.1	Ideal Bose gas at zero temperature	11
1.2.2	What is a Bose-Einstein condensate?	12
1.2.3	Thermodynamic properties	13
1.3	BEC of the weakly interacting Bose-gas	15
1.3.1	Two-particle interaction	16
1.3.2	The Gross-Pitaevskii equation (GPE)	17
1.3.3	The time dependent GPE	18
1.3.4	The quasiparticle spectrum	18
1.3.5	Linear response at $T = 0$	19
1.3.6	Mean field theory at finite temperature	19
1.4	Experimental techniques	20
1.4.1	Trapping neutral atoms	20
1.4.2	Cooling in magnetic traps	21
1.4.3	Probing a BEC	21
II	Quantum kinetic theory (QKT)	27
2	Basics of QKT	29
2.1	Introduction	29
2.2	Applications of QKT	31
2.2.1	Growth of the condensate	31
2.2.2	Properties of the condensate in the stationary state	32
3	PUBLICATION: Quantum kinetic theory IV	35
3.1	Introduction	37
3.2	Main results	38
3.2.1	Fluctuation analysis	38

3.3	Model	41
3.3.1	Description of the system	42
3.3.2	Master equation	45
3.4	Solutions of the master equation	46
3.4.1	Stationary solution	47
3.4.2	Nonstationary solutions	49
3.4.3	Correlation functions	50
3.5	Conclusions	56
3.A	Stationary solution for a canonical bath of particles	56
3.A.1	Excited modes	57
3.A.2	Weakly interacting Bose gas in the canonical ensemble	57
3.A.3	Particle number distribution of the condensate	58
3.B	Calculation of $R_{00}(N)$	62
3.B.1	Simplifying the integral	62
3.B.2	Calculating the function $G(\mathbf{Q})$ for the harmonic oscillator	63
3.B.3	Integration over \mathbf{Q}	64
III	Realization of the Bose Hubbard model	68
4	Introduction	70
5	PUBLICATION	73
5.1	Cold bosonic atoms in optical lattices	73
6	The Bose–Hubbard Model	82
6.1	Hamiltonian	82
6.2	Approximate ground state	82
6.2.1	Gutzwiller ansatz	84
6.3	Phase diagram of the Bose–Hubbard model	84
7	Optical lattices	86
7.1	Optical potentials	86
7.1.1	Influence of spontaneous emission	87
7.1.2	Neglecting spontaneous emission	89
7.2	Bloch bands and Wannier functions	89
7.2.1	Wannier functions	90
7.2.2	Connection between J and the bandstructure	91
7.3	Realizing the Bose–Hubbard Hamiltonian	92
7.3.1	One– two– and three dimensional Bose–Hubbard model	94
7.4	Light–induced inelastic collisions	94

IV Entanglement and quantum computing using neutral atoms	97
8 Introduction	99
8.1 Quantum computing in optical lattices	99
8.2 Electromagnetic microtraps	100
8.2.1 State selective potentials	102
9 PUBLICATION	105
9.1 Entanglement of atoms via cold controlled collisions	105
10 PUBLICATION: Quantum gates with neutral atoms	115
10.1 Introduction	116
10.2 Model	117
10.2.1 Hamiltonian	118
10.2.2 Phase shift due to interaction	119
10.3 Gate operation	121
10.3.1 Switching potential	121
10.3.2 Particles in the same internal state	122
10.3.3 Particles in different internal states	124
10.3.4 Particles at finite temperature	125
10.4 A physical implementation	126
10.4.1 Microscopic electromagnetic trapping potential	126
10.4.2 Results	128
10.5 Conclusions	132
10.A Time evolution	133
10.A.1 Analytical calculation	133
10.A.2 Numerical calculation	134
10.B Interaction phase shift	135
11 PUBLICATION: Quantum computing with neutral atoms	138
11.1 Introduction	139
11.2 Entanglement of atoms via cold controlled collisions	140
11.2.1 Hamiltonian	140
11.2.2 Moving potentials	142
11.2.3 Switching potentials	144
11.3 Physical realizations	149
11.3.1 Two-qubit gates in optical lattices	149
11.3.2 Two-qubit gates in magnetic microtraps	153
11.4 Parallel quantum computing	157
11.4.1 Multi-particle entanglement operations	158
11.4.2 Quantum error correction	161

11.4.3	Fault-tolerant computing	166
11.4.4	Selectivity and “sweep operations”	168
11.5	Final remarks	170
11.A	One particle in a moving harmonic potential	171
11.A.1	Hamiltonian	171
11.A.2	Exact solution	172
11.A.3	Corrections to the adiabatic approximation	172
11.B	Quantum error correction and the implementation of Shor’s code	173
12	Moving optical lattices	184
12.1	State selective optical potentials	184
12.1.1	Optical potential for a three level atom	184
12.1.2	State selective optical potential	185
12.1.3	Laser configuration	186
12.1.4	Resulting optical potential	187
12.2	Evolution of atoms in moving lattices	188
12.2.1	One particle in a moving optical lattice	188
12.2.2	Interaction between two particles	190
12.2.3	Numerical calculations	191
12.3	Fidelity of a gate operation	192
12.3.1	Initial motional state	192
12.3.2	Calculating the fidelity	193
12.4	Ramsey experiment	194
12.4.1	Occupation numbers	195
12.4.2	Special cases	196

Preface

This thesis covers most of my work in the field of Bose–Einstein condensation. It contains several different topics: quantum kinetic theory for describing Bose–gases at finite temperatures, the Bose–Hubbard model and its realization with neutral atoms in an optical lattice, and different ways for implementing quantum computations with neutral atoms in optical lattices and magnetic microtraps. I did all of those works in collaboration with Prof. Peter Zoller, Prof. Crispin Gardiner, and Prof. Ignacio Cirac. I did most of the work at the University of Innsbruck, during a research visit at the Victoria University of Wellington in New Zealand in the beginning of 1998, and while I was staying at the Institute for Theoretical Physics (ITP) in Santa Barbara in the summer of 1998. During my stay in New Zealand I completed the work on quantum kinetic theory. In Santa Barbara I mainly worked on the Bose–Hubbard model.

The thesis is divided into four parts. The first part contains a general brief introduction to the field of Bose–Einstein condensation in dilute gases. I also give a list of references which contain all the details. In the second part I first present the basics of quantum kinetic theory, then a publication mostly dealing with the fluctuations of a condensate in its stationary state is reprinted. In the third part, after a short introduction, I present a publication on the Bose–Hubbard model and its realization using neutral atoms in optical lattices. Some details on the Bose–Hubbard model and on optical lattices that were left out in this publication complete the third part of my thesis. In the fourth part, again after an introduction, three publications are presented. The first shows how neutral atoms in optical lattices may be used to perform quantum computations. The second publication demonstrates how to implement two–qubit gates with magnetic microtraps and in the third publication the ideas of the other two publications are extended. It also shows how parallel quantum computing, error correction schemes and fault–tolerant computing can be implemented. However, some of the contents of the third publication is also contained in one of the preceding two publications. Some details left out in the publications complete the fourth part of my thesis. Each chapter of this thesis has its own bibliography. The abbreviation BEC is used for Bose–Einstein condensate as well as for Bose–Einstein condensation.

Part I

Cold Bose–gases

Chapter 1

Bose–Einstein Condensation (BEC)

1.1 Introduction

Bose–Einstein condensation (BEC) predicted by Einstein [1] and Bose [2] in 1924 was first observed in alkali atomic vapors in 1995. In contrast to much older experiments with Helium where strong interactions between the particles wash out the effects expected due to BEC the relatively weak two–particle interaction in dilute alkali gases allows the study of properties of BEC experimentally. Those experiments and the possibility of a theoretical description of weakly interacting bosonic systems starting from fundamental quantum mechanics has stimulated a lot of experimental and theoretical effort towards a deep understanding of BEC.

Experimental efforts to create BEC in dilute gases started over 15 years ago [3]. The first experiments concentrated on using atomic hydrogen H to obtain BEC. However, mainly the large rates for inelastic collisions in H [3] prevented these experiments from succeeding for a long time. It took until 1998 before BEC was reported in H by T.J. Greytak’s and D. Kleppner’s group [4]. Three years earlier the first successful experiments on BEC were performed by C.E. Wieman’s and E.A. Cornell’s group with a dilute sample of magnetically trapped ^{87}Rb atoms [5]. Soon afterwards W. Ketterle’s group succeeded in producing a BEC using ^{23}Na atoms [6]. In both experiments the s –wave scattering length was positive, i.e. the particles interacted repulsively with each other. In contrast, also in 1995 R.G. Hulet’s group was able to produce a condensate using ^7Li with attractive interactions [7]. The attractive interaction in ^7Li leads to a collapse of the condensate if the number of condensed particles exceeds a certain critical value [8].

After the first experiments in 1995 had shown clear evidence of BEC the

following ones concentrated on investigating the properties of condensates. BEC has led to a much better understanding of ultracold collisions between neutral atoms. It allows the determination of the s -wave scattering length with a very high accuracy [9] and it was also possible to find Feshbach resonances by applying external magnetic fields [9]. Also BEC allows the study of inelastic two- and three-particle processes [10]. Even interactions between mixtures of Bose-condensates of different species of atoms [11, 12] as well as the coherence properties and relative phases of these binary mixtures [13] have been studied experimentally. Furthermore a lot of effort has been put in measuring collective excitations and phonon modes [14], the sound velocity [15], the structure factor [16], the properties of particles coupled out of a condensate [17], and the initiation of the condensation process [18]. The creation of BEC has become a standard task for experimentalists within the last few years which might allow BEC to become a common tool of experimental atomic and molecular physics.

By using the Gross-Pitaevskii equation (GPE) [19] one can study most of the properties of a weakly interacting condensate theoretically. The GPE describes trapped weakly interacting many particle bosonic systems by means of a macroscopic wavefunction at temperature $T = 0$. The two-particle interaction potential is approximated by a contact potential and characterized by the s -wave scattering length [20]. Depletion of the condensate [21], which becomes important in strongly interacting systems, is neglected. The GPE also does not include thermal fluctuations of the condensate. Although the approximations leading to the GPE seem rather severe many of the macroscopic quantum mechanical effects that become visible in BEC experiments can be described well by using the GPE.

The relative phase of a condensate used to describe interference between BECs has been investigated in [22], theoretical studies on vortices and various other topological effects in a BEC can be found in [23] and BECs with two or more components have been studied in [24]. Furthermore most of the theoretical work done on ultracold collisions [25] is in good agreement with the experiments. Mean field theories that describe BEC at finite temperature have been developed in [26, 27, 28]. However, the most powerful method to describe a BEC at finite temperature is quantum kinetic theory (cf. Sec. (3)). Also the initiation of BEC is well understood by using quantum kinetic theory.

However, besides understanding all properties of BEC, one obvious question, concerning both theorists and experimentalists still has a lot of potential for interesting new physics and ideas: *What are the possible applications of Bose-Einstein condensates?* Up to now this question has only been tackled partly. Condensates can be exploited for building a coherent source of neutral atoms as shown in [17]. Cold neutral atoms can be used to study entanglement and for quantum information processing [29, 30]. One of the open questions is: How can the knowledge about BEC in atomic vapors be applied to other

fields of physics [31]? In our opinion it will be most important within the next few years to find many interesting applications of BEC in order to sustain the experimental and theoretical efforts on this subject in laboratories and offices all around the world. This work is mainly devoted to applications of BEC; we will not go into the details on how to find the properties of Bose–Einstein condensates but will concentrate on finding different possible applications of BEC.

There are also several other open questions that are still being investigated. It would be interesting to find experiments that show a clear breakdown of the GPE since this could stimulate new theoretical efforts in the basic description of weakly interacting many particle systems. Furthermore, still a lot of work is done on investigating properties of condensates of mixtures of different internal atomic states [11, 12] as well as on mixtures of cold bosons and fermions [32] and although there were first successful experiments in demonstrating superfluidity and vortices in condensates [33] many experimentalists are still trying to find topological structures in BECs. One further aim would be to produce molecular Bose–condensates.

In the next sections we will give an overview of the most important properties of BECs. The overview given here is not complete, it is merely a collection of some of the most important results and a list of references. In those references detailed theoretical and experimental results on all the subjects mentioned here can be found.

1.2 BEC of an ideal Bose–gas in a trap

In this section we will briefly present the basic properties of a trapped ideal bosonic gas in thermodynamic equilibrium. First we will investigate a Bose–gas at temperature $T = 0$, then we will define a Bose–condensate. Finally, we will compare the description of a Bose gas in the three different thermodynamic ensembles and discuss the applicability of these three ensembles to current experiments.

1.2.1 Ideal Bose gas at zero temperature

1.2.1.1 Hamiltonian

The second quantized Hamiltonian H_{id} of a trapped non–interacting Bose gas is given by

$$H_{\text{id}} = \int d^3x \Psi^\dagger(\mathbf{x}) \left(\frac{\mathbf{p}^2}{2m} + V_T(\mathbf{x}) \right) \Psi(\mathbf{x}), \quad (1.1)$$

where \mathbf{x} is the coordinate space operator, \mathbf{p} is the momentum operator and m denotes the mass of the particles. $\Psi(\mathbf{x})$ is the bosonic field operator obeying

the usual bosonic commutation relations

$$\left[\Psi(\mathbf{x}), \Psi^\dagger(\mathbf{x}') \right] = \delta(\mathbf{x} - \mathbf{x}'). \quad (1.2)$$

The trapping potential is denoted by $V_T(\mathbf{x})$.

1.2.1.2 Eigenstates

In the non-interacting case it is most convenient to choose the eigenstates of the one particle Hamiltonian

$$H_1 = \frac{\mathbf{p}^2}{2m} + V_T(\mathbf{x}), \quad (1.3)$$

as the set of mode functions for describing the many particle system. The eigenfunctions of H_1 are written as $\phi_i(\mathbf{x})$, and the corresponding eigenvalues are ϵ_i . We will assume $\epsilon_i \leq \epsilon_j$ for $i < j$ and i, j to be positive integers. The eigenstates of the many particle system are written as

$$|\psi\rangle = |n_0, n_1, \dots, n_i, \dots\rangle, \quad (1.4)$$

where the n_i give the number of particles occupying the one particle mode ϕ_i . The state of the system is uniquely defined by $|\psi\rangle$ since the bosonic particles are indistinguishable [34].

1.2.1.3 Ground state

At temperature $T = 0$ the system is in its ground state. Since in the case of bosons quantum statistics does not forbid an arbitrary number of particles to occupy a single one-particle state [34] the ground state is immediately found to be given by

$$|\psi_0\rangle = |N, 0, 0, \dots\rangle, \quad (1.5)$$

where N is the number of particles in the system. All N particles occupy the same one particle state in this case, i.e. a *macroscopic* number of particles show the *same quantum properties*. This can be viewed as a macroscopic manifestation of quantum mechanics.

1.2.2 What is a Bose–Einstein condensate?

A Bose–Einstein condensate is defined to be a macroscopic number of bosons that occupy the same one-particle state [35]. Given the density operator ρ of a bosonic system one can find out whether the Bose–gas is condensed by diagonalizing the one particle density operator ρ_1 which is defined by

$$\rho_1 = \text{tr}_{2, \dots, N} \rho, \quad (1.6)$$

where $\text{tr}_{2,\dots,N}$ denotes the trace over particles 2 to N . If one finds an eigenvalue N_c (belonging to the mode function $\phi_c(\mathbf{x})$) which is of the order of the total number of particles N in the system then N_c particles are said to be condensed in the mode function $\phi_c(\mathbf{x})$. According to this definition N particles of an ideal Bose gas are condensed in the mode function $\phi_0(\mathbf{x})$ at $T = 0$. Note, however, that in the case of an interacting Bose-gas even at $T = 0$ not all the particles are condensed. Then no set of mode functions exists where the ground state of the system can be written as $|\psi_0\rangle = |N, 0, 0, \dots\rangle$ [21].

1.2.3 Thermodynamic properties

Here we will briefly mention the three different thermodynamic ensembles commonly used for describing BEC experiments. A detailed comparison of the three ensembles can be found in [36].

1.2.3.1 Grand canonical ensemble

For simplicity we assume $V_T(\mathbf{x})$ to be harmonic and isotropic, i.e. $V_T(\mathbf{x}) = m\omega\mathbf{x}^2/2$, where ω is the trap frequency. A system in the grand canonical ensemble is assumed to be interacting with a heat bath and allowed to exchange particles with a particle reservoir. The density operator in thermal equilibrium is given by

$$\rho_G = \frac{1}{Z_g} e^{-\beta(H_{\text{id}} - \mu\hat{N})}, \quad (1.7)$$

where $\beta = 1/kT$ is the inverse temperature,

$$\hat{N} = \int d^3x \Psi(\mathbf{x})^\dagger \Psi(\mathbf{x}) \quad (1.8)$$

is the number operator, and μ , the chemical potential, fixes the mean number of particles N in the system. Setting the ground state energy equal to zero we find the grand canonical partition function defined by

$$Z_g = \text{tr} \left\{ e^{-\beta(H_{\text{id}} - \mu\hat{N})} \right\}, \quad (1.9)$$

to be given by

$$Z_g = \prod_{j=0}^{\infty} \left(\frac{1}{1 - Ze^{-\beta\hbar\omega j}} \right)^{\frac{(j+1)(j+2)}{2}}, \quad (1.10)$$

where $Z = \exp(\beta\mu)$ is the fugacity. The mean number of particles in the system is given by

$$N = \sum_j \frac{(j+1)(j+2)}{2} n_j, \quad (1.11)$$

where n_j is the number of particles in a one particle state with energy $\epsilon_j = \hbar\omega j$. given by

$$n_j = \frac{1}{Z^{-1}e^{\beta\hbar\omega j} - 1}. \quad (1.12)$$

Approximating the sum Eq. (1.11) by an integral and treating the ground state separately [34] we find

$$N = n_0 + \frac{g_3(Z)}{(\beta\hbar\omega)^3}, \quad (1.13)$$

where $n_0 = Z/(1 - Z)$ and $g_3(Z)$ is the Bose–function

$$g_3(Z) = \frac{1}{2} \int_0^\infty \frac{x^2}{Z^{-1}e^x - 1}. \quad (1.14)$$

Thus in the thermodynamic limit $N \rightarrow \infty$, $\omega \rightarrow 0$ and $\omega^3 N = \text{const.}$ we find

$$\frac{n_0}{N} = \begin{cases} 1 - \left(\frac{T}{T_c}\right)^3 & \text{for } T < T_c \\ 0 & \text{for } T \geq T_c \end{cases}, \quad (1.15)$$

where the critical temperature T_c is defined by

$$kT_c = \hbar\omega \left(\frac{N}{\zeta(3)} \right)^{1/3}, \quad (1.16)$$

with $\zeta(3) = g_3(1)$ the Riemann–zeta function. We do not want to go into the details on how to find the fluctuations in the grand canonical system since these can be found in [34].

The results obtained in the grand canonical ensemble agree rather well with current experiments as long as no fluctuations are being calculated. Since in experimental setups no particle reservoir is at thermal equilibrium with the Bose–gas the huge particle number fluctuations predicted by the grand canonical ensemble for particles in the ground state do not emerge in the experiment.

1.2.3.2 Canonical ensemble

In the canonical ensemble the system is assumed to interact with a heat bath but not to exchange particles with a particle reservoir. The canonical density operator is given by

$$\rho_c = \frac{1}{Z_c} e^{-\beta H_{\text{id}}}, \quad (1.17)$$

where the canonical partition function is defined as

$$Z_c = \text{tr} \left\{ e^{-\beta H_{\text{id}}} \right\}. \quad (1.18)$$

Investigating the ideal Bose-gas in the canonical ensemble turns out to be more complicated than in the grand canonical ensemble. We will not go into the details here but refer to [37] which gives a detailed analysis of the ideal Bose-gas in the canonical ensemble.

Using the canonical ensemble to describe current experiments seems to be more realistic than using the grand canonical ensemble. However in most of the experiments no heat bath exists which is in thermal equilibrium with the Bose-gas, and evaporative cooling and inelastic collisions lead to a change in the number of particles during the experiments.

1.2.3.3 Micro canonical ensemble

In the micro canonical ensemble the system is assumed to be isolated from any environment. There exists neither a heat bath nor a particle reservoir in thermal equilibrium with the Bose-gas. The micro canonical density operator is given by [34]

$$\rho_M = \frac{1}{\Omega} \int_{E-\Delta}^E d\bar{E} \delta(\bar{E} - H_{\text{id}}), \quad (1.19)$$

where the energy of the system is in the interval $[E - \Delta, E]$ with $\Delta \ll E$. (if $\Delta \ll E$ the thermodynamic properties of the system become independent of Δ). The micro canonical partition function is given by

$$\Omega = \text{tr} \left\{ \int_{E-\Delta}^E d\bar{E} \delta(\bar{E} - H_{\text{id}}) \right\}. \quad (1.20)$$

For details on how to find the properties of a Bose-gas in the micro canonical ensemble we refer to [38].

In principle the micro canonical ensemble is best suited for describing current experiments if it is viewed as a starting point for incorporating particle loss due to inelastic collisions and evaporative cooling. Also, it is possible to include heating of the system due to small interactions of the Bose-gas with the environment starting from a micro canonical description.

1.3 BEC of the weakly interacting Bose-gas

Even in dilute alkali Bose-gases as used in current BEC experiments two particle interactions must not be neglected since they strongly influence the behavior of the Bose-gas. Some of the interesting properties of Bose-Einstein condensates determined by the interaction are

- the formation of a BEC [39],
- the shape of the BEC mode function [19],

- collective excitations of a BEC [40],
- the quasiparticle spectrum [40],
- and the domain structure of two species BECs [24].

Also the evaporative cooling mechanism is based on the elastic thermalizing collisions between two particles [41].

1.3.1 Two-particle interaction

The Hamiltonian of two interacting particles (without external trap potential) is given by

$$H_{\text{int}} = \frac{\mathbf{p}_1^2}{2m} + \frac{\mathbf{p}_2^2}{2m} + V(\mathbf{x}_1 - \mathbf{x}_2). \quad (1.21)$$

where \mathbf{p}_i and \mathbf{x}_i are the momentum and the coordinate space operators of particle $i = 1, 2$, respectively. $V(\mathbf{x}_1 - \mathbf{x}_2)$ is a short range potential with an s -wave scattering length denoted by a_s usually of the order of a few Bohr radii a_0 [9]. BEC experiments are commonly performed in the limit where the thermal wave-length λ_T is much larger than the scattering length a_s . Thus only s -wave scattering with a relative wave vector between the two particles k much larger than the inverse of the scattering length $1/a_s \ll k$ will be important. Outside the range of the interaction potential its effect on s -waves is the same as if the potential were a hard sphere potential with radius a_s [20]. The effect of a hard sphere potential is nothing more than a boundary condition for the relative wave function of the two particles at $r = a_s$ (with $\mathbf{r} = \mathbf{x}_1 - \mathbf{x}_2$). As shown by K. Huang in [20] this boundary condition can be enforced by replacing the interaction potential by a pseudo-potential of the form

$$V(\mathbf{x} - \mathbf{x}') \rightarrow \frac{4\pi a_s \hbar^2}{m} \delta(\mathbf{x} - \mathbf{x}'). \quad (1.22)$$

Note that this replacement yields correct results only for the wave function outside the range of the actual interaction potential and thus the wave function of the relative motion has to extend over a space with volume much larger than a_s^3 . Otherwise measurable quantities will strongly depend on the form of the wave function within the range $r < a_s$ where the pseudo-potential approximation is not valid. In the many body case this condition is only satisfied if the mean distance between the particles is much larger than the range of the interaction potential, i.e.,

$$\eta = n a_s^3 \ll 1, \quad (1.23)$$

where n is the particle density and η is called the gas parameter [42]. In current BEC experiments $\eta \leq 10^{-4}$ and $a_s/\lambda_T \leq 10^{-2}$ and thus the pseudo-potential approximation is valid for describing these experiments.

1.3.2 The Gross-Pitaevskii equation (GPE)

In second quantization the Hamiltonian of the weakly interacting Bose-gas reads

$$H = H_{\text{id}} + \frac{1}{2} \int_{-\infty}^{\infty} d^3x \Psi^\dagger(\mathbf{x}) \Psi^\dagger(\mathbf{x}') V(\mathbf{x} - \mathbf{x}') \Psi(\mathbf{x}') \Psi(\mathbf{x}), \quad (1.24)$$

where according to Sec. 1.3.1 the interaction potential is given by Eq. (1.22). We assume the ground state to be of the form

$$|\Phi\rangle = \frac{(a_0^\dagger)^N}{\sqrt{N!}} |\text{vac}\rangle, \quad (1.25)$$

where $|\text{vac}\rangle$ denotes the vacuum state and the creation operator a_0^\dagger is given by

$$a_0^\dagger = \int_{-\infty}^{\infty} d^3x \varphi_0(\mathbf{x}) \Psi^\dagger(\mathbf{x}). \quad (1.26)$$

We want to find the shape of the mode function $\varphi_0(\mathbf{x})$ by minimizing the expression

$$\langle \Phi | H - \mu \hat{N} | \Phi \rangle \rightarrow \min, \quad (1.27)$$

which after some calculation leads to the Gross-Pitaevskii equation (GPE)

$$\left(-\frac{\hbar^2 \nabla^2}{2m} + V_T(\mathbf{x}) + Ng |\varphi_0(\mathbf{x})|^2 - \mu \right) \varphi_0(\mathbf{x}) = 0, \quad (1.28)$$

where $g = 4\pi a_s \hbar^2/m$. This derivation is one of the most intuitive and simple ways to find the GPE. There are several other methods to obtain the GPE which are presented in [19, 43].

In the non-interacting limit $a_s = 0$ the GPE reduces to an eigenvalue equation with the form of a time independent Schrödinger equation for the trap potential $V_T(\mathbf{x})$. This limit agrees with the ideal gas limit Sec. 1.2, the chemical potential equals the ground state energy ϵ_0 and the mode function $\varphi_0(\mathbf{x})$ is the eigenfunction of the corresponding one particle Hamiltonian. In the opposite limit where the interaction energy dominates the kinetic energy, i.e. $\xi \ll R$ where $\xi = (8\pi a_s N/R^3)^{-1/2}$ is the healing length and R is the size of the condensate cloud, we can neglect the kinetic term [19]. This approximation, called the Thomas-Fermi limit, yields the wave function

$$\varphi_0(\mathbf{x}) = \begin{cases} \sqrt{\frac{1}{Ng} (\mu - V_T(\mathbf{x}))} & \text{for } \mu > V_T(\mathbf{x}) \\ 0 & \text{for } \mu < V_T(\mathbf{x}) \end{cases}. \quad (1.29)$$

1.3.3 The time dependent GPE

Performing the above variational calculation for a time dependent mode function $\varphi_0(\mathbf{x}, t)$ yields the time dependent GPE given by

$$i\hbar \frac{\partial}{\partial t} \varphi_0(\mathbf{x}, t) = \left(-\frac{\hbar^2 \nabla^2}{2m} + V_T(\mathbf{x}) + Ng |\varphi_0(\mathbf{x}, t)|^2 \right) \varphi_0(\mathbf{x}, t). \quad (1.30)$$

The applications of this equation have been studied in [43, 44]. We also want to mention the stability analysis of BEC worked out by S.A. Gardiner et al. in [45] which also makes use of the time dependent GPE.

1.3.4 The quasiparticle spectrum

Now we want to investigate the quasiparticle spectrum along the lines of [40]. By assuming spontaneous symmetry breaking [46] we write the bosonic field operator as the sum $\tilde{\Psi}(\mathbf{x}, t) = \sqrt{N} \varphi_0(\mathbf{x}) + \tilde{\Psi}(\mathbf{x})$, where $\varphi_0(\mathbf{x})$ is the condensate wave function and $\tilde{\Psi}(\mathbf{x})$ is assumed to be a small correction. Inserting this into the grand canonical version of the Hamiltonian $K = H - \mu \hat{N}$ and neglecting all terms in $\tilde{\Psi}(\mathbf{x})$ higher than quadratic yields

$$\begin{aligned} K_B \approx & \zeta + \int d^3x \tilde{\Psi}^\dagger(\mathbf{x}) \mathcal{L} \tilde{\Psi}(\mathbf{x}) + \frac{Ng}{2} \int d^3x \tilde{\Psi}^\dagger(\mathbf{x}) (\varphi_0(\mathbf{x}))^2 \tilde{\Psi}(\mathbf{x}) \\ & + \frac{Ng}{2} \int d^3x \tilde{\Psi}(\mathbf{x}) (\varphi_0^*(\mathbf{x}))^2 \tilde{\Psi}(\mathbf{x}), \end{aligned} \quad (1.31)$$

where ζ is a c-number and

$$\mathcal{L} = \frac{\mathbf{p}^2}{2m} + V_T(\mathbf{x}) - \mu + 2Ng |\varphi_0(\mathbf{x})|^2. \quad (1.32)$$

This Hamiltonian K_B may be diagonalized by using the Bogoliubov ansatz

$$\tilde{\Psi}(\mathbf{x}) = \sum_j \left(u_j(\mathbf{x}) \alpha_j + v_j^*(\mathbf{x}) \alpha_j^\dagger \right), \quad (1.33)$$

where $u_j(\mathbf{x})$ and $v_j(\mathbf{x})$ satisfy the Bogoliubov de–Gennes equations

$$\mathcal{L} u_j(\mathbf{x}) + Ng (\varphi_0(\mathbf{x}))^2 v_j(\mathbf{x}) = E_j u_j(\mathbf{x}), \quad (1.34)$$

and

$$\mathcal{L} v_j(\mathbf{x}) - Ng (\varphi_0^*(\mathbf{x}))^2 u_j(\mathbf{x}) = -E_j v_j(\mathbf{x}). \quad (1.35)$$

Up to a c-number the Hamiltonian then reads

$$K_B = \sum_j E_j \alpha_j^\dagger \alpha_j. \quad (1.36)$$

K_B thus describes a collection of noninteracting quasiparticles for which the condensate is the vacuum.

1.3.5 Linear response at $T = 0$

Applying a weak sinusoidal perturbation to the trap potential will cause the condensate to oscillate and its deformed shape can be detected. At small temperatures $T \ll T_c$ the influence of the thermal component on the condensate can be neglected and the linear response behavior of the condensate is well described by [40]

$$i\hbar \frac{\partial}{\partial t} \varphi(\mathbf{x}, t) = \left(-\frac{\hbar^2 \nabla^2}{2m} + V_T(\mathbf{x}) + Ng |\varphi(\mathbf{x}, t)|^2 + f_+(\mathbf{x})e^{-i\omega_p t} + f_-(\mathbf{x})e^{i\omega_p t} \right) \varphi(\mathbf{x}, t). \quad (1.37)$$

The $f_{\pm}(\mathbf{x})$ are the amplitudes of the sinusoidal perturbation and ω_p is the probe frequency. As shown in [40] the linear response behavior of the condensate is given by

$$\varphi(\mathbf{x}, t) = e^{-i\mu t/\hbar} \left(\sqrt{N_0} \varphi_0(\mathbf{x}) + u_j(\mathbf{x})e^{-iE_j t/\hbar} + v_j^*(\mathbf{x})e^{iE_j t/\hbar} \right), \quad (1.38)$$

where N_0 is the number of condensate particles that are not disturbed by the perturbation and the u_j and v_j are found by solving the Bogoliubov de-Gennes equations with the replacement $N \rightarrow N_0$. Note that linear response theory is only valid for small amplitudes. Non-linear effects will prevent a blow up at resonances $\hbar\omega_p = E_j$. Thus it is possible to probe the quasiparticle spectrum of a BEC by studying its linear response to perturbations in the trap potential.

1.3.6 Mean field theory at finite temperature

While the GPE is very widely accepted as the standard tool to describe a BEC at $T = 0$ there are several different mean field approaches to describe a BEC at finite temperature [26, 27, 28] as well as approaches based on quantum kinetic theory (cf. Sec. 3). We will not explain the differences and problems connected to different mean field theories (can be found in [26]) but will rather present the theory for describing BECs at finite temperature developed by A. Griffin in [26]. By assuming spontaneous symmetry breaking we write the field operator as

$$\Psi(\mathbf{x}, t) = \Phi(\mathbf{x}) + \tilde{\Psi}(\mathbf{x}, t), \quad (1.39)$$

where $\Phi(\mathbf{x}) = \langle \Psi(\mathbf{x}) \rangle$ is the condensate part (corresponding to the condensate wave function $\sqrt{N} \varphi_0(\mathbf{x})$ at zero temperature) obeying the equation of motion [26]

$$\left(\frac{\mathbf{p}^2}{2m} + V_T(\mathbf{x}) - \mu \right) \Phi(\mathbf{x}) + g(|\Phi(\mathbf{x})|^2 + 2\tilde{n}(\mathbf{x}))\Phi(\mathbf{x}) + g\tilde{m}(\mathbf{x})\Phi^*(\mathbf{x}) = 0, \quad (1.40)$$

where $\tilde{n}(\mathbf{x}) = \langle \tilde{\Psi}^\dagger(\mathbf{x})\tilde{\Psi}(\mathbf{x}) \rangle$ and $\tilde{m}(\mathbf{x}) = \langle \tilde{\Psi}(\mathbf{x})\tilde{\Psi}(\mathbf{x}) \rangle$. In Hartree–Fock Bogoliubov approximation the Hamiltonian K reduces up to a c-number to [26]

$$\begin{aligned} K_{\text{HFB}} &\approx \int d^3x \tilde{\Psi}^\dagger(\mathbf{x}) \mathcal{L}_T \tilde{\Psi}(\mathbf{x}) + \frac{g}{2} \int d^3x \tilde{\Psi}^\dagger(\mathbf{x}) m(\mathbf{x}) \tilde{\Psi}^\dagger(\mathbf{x}) \\ &+ \frac{g}{2} \int d^3x \tilde{\Psi}(\mathbf{x}) m^*(\mathbf{x}) \tilde{\Psi}(\mathbf{x}), \end{aligned} \quad (1.41)$$

where $m(\mathbf{x}) = \Phi(\mathbf{x})^2 + \tilde{m}(\mathbf{x})$ and

$$\mathcal{L}_T = \frac{\mathbf{p}^2}{2m} + V_T(\mathbf{x}) - \mu + 2g(|\Phi(\mathbf{x})|^2 + \tilde{n}(\mathbf{x})). \quad (1.42)$$

K_{HFB} can be diagonalized by using the Bogoliubov–ansatz Eq. (1.33) where the mode function $u_j(\mathbf{x})$ and $v_j^*(\mathbf{x})$ now have to satisfy the generalized Bogoliubov equations

$$\mathcal{L}_T u_j(\mathbf{x}) - gm(\mathbf{x})v_j(\mathbf{x}) = E_j u_j(\mathbf{x}), \quad (1.43)$$

$$\mathcal{L}_T v_j(\mathbf{x}) - gm^*(\mathbf{x})u_j(\mathbf{x}) = -E_j v_j(\mathbf{x}). \quad (1.44)$$

The closed set of equations Eqs. (1.40,1.43,1.44) has to be solved numerically with self-consistent values for $\tilde{n}(\mathbf{x})$ and $\tilde{m}(\mathbf{x})$ found from Eq. (1.33) and noting that in thermal equilibrium

$$\langle \alpha_j^\dagger \alpha_j \rangle = \frac{1}{e^{\beta E_j} - 1}, \quad (1.45)$$

to find the quasiparticle excitations as described in [26].

1.4 Experimental techniques

One of the ultimate goals of laser cooling is to achieve BEC in dilute gases. Due to reabsorption of photons, spontaneous emission and various other heating and loss mechanism this goal has still not been achieved by purely optical methods. Several other experimental techniques for trapping cooling and probing neutral atoms had to be developed to achieve BEC. In this section we will briefly describe the most important of those experimental techniques.

1.4.1 Trapping neutral atoms

The first stage of creating a BEC is usually to load bosonic atoms into a Magneto–Optical–Trap (MOT) and to cool the atoms by Doppler cooling. Then *all* the laser beams are turned off and the precooled sample of atoms is loaded into a purely magnetic trap. There are various different ways to trap neutral atoms in those magnetic traps. They all work in the adiabatic

regime where the spin of the atom follows the direction of a (possibly time averaged) magnetic field so that the potential felt by the atoms only depends on the magnitude of the field but not on its direction (cf. Sec. 8.2). One of the difficulties is to avoid Majorana spin flips [47] in positions where the magnetic field is close to zero. The first magnetic trap that allowed trapping of neutral atoms and avoided the spin flips was invented by E.A. Cornell [47]. The zero magnetic field appearing in the center of two anti-Helmholtz coils is moved along a circle by an additional time dependent magnetic field. The time averaged magnetic field felt by the atom is never zero and harmonic around the center. In the first experiments by W. Ketterle and collaborators a blue detuned laser producing a repulsive potential barrier at the center of a magnetic trap was used to prevent the atoms from the region of zero magnetic field [6]. Also several other ways of trapping neutral atoms have been invented like, e.g. the Joffe–Pritchard trap [48]. Later the group by W. Ketterle was even able to load a magnetically trapped BEC into a purely optical trap [11].

1.4.2 Cooling in magnetic traps

The cooling mechanism used to achieve BEC is evaporative cooling [41]. The trapping potential is truncated at a certain energy value E_{cut} such that only particles with an energy less than E_{cut} can be trapped. Elastic collisions between the atoms trying to bring the gas into thermal equilibrium produce highly energetic atoms with an energy larger than E_{cut} . They leave the trap and take away more than the average energy of the trapped particles. The effect is twofold: (i) the temperature of the gas cloud and thus its size shrinks which increases the particle density and (ii) the number of particles and thus the density of the cloud decreases. In order for evaporative cooling to work the effect (ii) has to be smaller than (i) so that the elastic collision rate *increases*. This regime is called runaway evaporation. The conditions necessary to achieve runaway evaporation are described in detail in [41].

We also want to mention that care has to be taken about the so called “bad” collisions. These are the inelastic two and three particle collisions that change the hyperfine levels and lead to additional loss from the trap and heating. In certain species of atoms, e.g. in Cs inelastic collisions have prevented successful BEC experiments up to now [49].

1.4.3 Probing a BEC

The experimental techniques on how to measure the properties of a BEC have also undergone some development during the last few years. In the first experiments the BECs were probed by time of flight measurements [5, 50] where the cloud of atoms is released from the trap and allowed to expand for

a certain time. After letting the cloud expand, its shape represents the initial velocity distribution [51], and thus by imaging the atom cloud, density and velocity profiles of the condensate can be measured. Note that this technique is destructive.

To allow for multiple measurements on a single condensate the MIT group developed the phase contrast imaging method [52]. Phase shifts in a very far detuned laser beam induced by the refractive index of the condensate are transformed into intensity variations of the laser. The condensate is not destroyed by the far detuned laser beam so that it is possible to perform a sequence of measurements on a single condensate. Also it has become possible to do quantitative non-destructive measurements of the surface area of a condensate [53].

References

- [1] A. Einstein, Sitzber. Kgl. Preuss. Akad. Wiss., 261 (1924); A. Einstein, *ibid.* 3 (1925).
- [2] S.N. Bose, Z. Phys. **26**, 178 (1924).
- [3] I.F. Silvera and J.T.M. Walraven, J. Appl. Phys. **52**, 2304 (1981); R. Sprik, J.T.M. Walraven, and I.F. Silvera, Phys. Rev. Lett. **51** 479 (1983); R. Sprik, J.T.M. Walraven, and I.F. Silvera, Phys. Rev. B **32** 5668 (1985).
- [4] D.G. Fried, T.C. Killian, L. Willmann, D. Landhuis, S.C. Moss, D. Kleppner, and T.J. Greytak, Phys. Rev. Lett. **81**, 3811 (1998).
- [5] M. Anderson, J.R. Ensher, M.R. Matthews, C.E. Wieman, and E.A. Cornell, Science **269**, 198 (1995).
- [6] K.B. Davis, M-O. Mewes, M.R. Andrews, N.J. van Druten, D.S. Durfee, D.M. Kurn, and W. Ketterle, Phys. Rev. Lett. **75**, 3969 (1995).
- [7] C.C. Bradley, C.A. Sackett, J.J. Tollet, and R. Hulet, Phys. Rev. Lett. **75**, 1687 (1995).
- [8] C.A. Sackett, H.T.C. Stoof, and R.G. Hulet, Phys. Rev. Lett. **80**, 2031 (1998).
- [9] J.L. Roberts, N.R. Claussen, J.P. Burke, Jr., C.H. Greene, E.A. Cornell, and C.E. Wieman, Phys. Rev. Lett. **81**, 5109 (1998); J. Stenger, S. Inouye, M. R. Andrews, H.-J. Miesner, D. M. Stamper-Kurn, and W. Ketterle, Phys. Rev. Lett. **82**, 2422 (1999).
- [10] E.A. Burt, R.W. Ghrist, C.J. Myatt, M.J. Holland, E.A. Cornell, and C.E. Wieman Phys. Rev. Lett. **79**, 337 (1997).
- [11] D.M. Stamper-Kurn, M.R. Andrews, A.P. Chikkatur, S. Inouye, H.-J. Miesner, J. Stenger, and W. Ketterle, Phys. Rev. Lett. **80**, 2027 (1998).

- [12] D.S. Hall, M.R. Matthews, J.R. Ensher, C.E. Wieman, and E.A. Cornell, Phys. Rev. Lett. **81**, 1539 (1998); D.S. Hall, M.R. Matthews, J.R. Ensher, C.E. Wieman, and E.A. Cornell, Phys. Rev. Lett. **81**, 4531 (1998).
- [13] D.S. Hall, M.R. Matthews, C.E. Wieman, and E.A. Cornell, Phys. Rev. Lett. **81**, 1543 (1998); D.S. Hall, M.R. Matthews, C.E. Wieman, and E.A. Cornell, Phys. Rev. Lett. **81**, 4532 (1998).
- [14] D.S. Jin, J.R. Ensher, M.R. Matthews, C.E. Wieman, and E.A. Cornell, Phys. Rev. Lett. **77**, 420 (1996); M.-O. Mewes, M.R. Andrews, N.J. van Druten, D.M. Kurn, D.S. Durfee, C.G. Townsend, and W. Ketterle, Phys. Rev. Lett. **77**, 988 (1996); D.S. Jin, M.R. Matthews, J.R. Ensher, C.E. Wieman, and E.A. Cornell, Phys. Rev. Lett. **78**, 764 (1997).
- [15] M.R. Andrews, D.M. Kurn, H.-J. Miesner, D.S. Durfee, C.G. Townsend, S. Inouye, and W. Ketterle, Phys. Rev. Lett. **79**, 553 (1997); M.R. Andrews, D.M. Kurn, H.-J. Miesner, D.S. Durfee, C.G. Townsend, S. Inouye, and W. Ketterle, Phys. Rev. Lett. **80**, 2967 (1998).
- [16] J. Stenger, S. Inouye, A.P. Chikkatur, D.M. Stamper-Kurn, D.E. Pritchard, and W. Ketterle, Phys. Rev. Lett. **82**, 4569 (1999).
- [17] M.-O. Mewes, M.R. Andrews, D.M. Kurn, D.S. Durfee, C.G. Townsend, and W. Ketterle, Phys. Rev. Lett. **78**, 582 (1997); I. Bloch, T.W. Hänsch, and T. Esslinger, Phys. Rev. Lett. **82**, 3008 (1999).
- [18] D.M. Stamper-Kurn, H.-J. Miesner, A. P. Chikkatur, S. Inouye, J. Stenger, and W. Ketterle, Phys. Rev. Lett. **81**, 2194 (1998); H.-J. Miesner, D.M. Stamper-Kurn, M.R. Andrews, D.S. Durfee, S. Inouye, and W. Ketterle, Science **279**, 1005 (1998).
- [19] V.L. Ginzburg and L.P. Pitaevskii, JETP **34** (7), 858 (1958); L.P. Pitaevskii, JETP **13**, 451 (1961); G. Baym and C.J. Pethick, Phys. Rev. Lett. **76**, 6 (1996).
- [20] K. Huang, *Statistical mechanics II* (John Wiley & Sons, Inc., New York); K. Huang and C.N. Yang, Phys. Rev. **105**, 767 (1957); K. Huang, C.N. Yang, and J.M. Luttinger, Phys. Rev. **105**, 776 (1957).
- [21] S. Giorgini, L. Pitaevskii, and S. Stringari, Phys. Rev. B **49**, 12938 (1994); F. Dalfovo, S. Giorgini, M. Guilleumas, L. Pitaevskii, and S. Stringari, Phys. Rev. A **56**, 3840 (1997).
- [22] J. Javanainen and S. M. Yoo, Phys. Rev. Lett. **76**, 161 (1997); M. Lewenstein and L. You, *ibid.* **77**, 3489 (1997); A. Imamoglu, M. Lewenstein, and L. You, *ibid.* **78**, 2511 (1997); R. Graham, T. Wong, M. J. Collet, S. M. Tan, and D. F. Walls Phys. Rev. A **57**, 493 (1998); Y. Castin and J. Dalibard, Phys. Rev. A **55**, 4330 (1997); J. Javanainen and M. Wilkens, Phys. Rev. Lett. **78**, 4675 (1997); M. J. Steel and D. F. Walls, Phys.

- Rev. A **56**, 3832 (1997); J. I. Cirac, C. W. Gardiner, M. Naraschewski, and P. Zoller, Phys. Rev. A **54**, R3714 (1996); A. Imamoglu and T.A.B. Kennedy, *ibid.* **55**, R849 (1997); J. Ruostekoski and D.F. Walls, *ibid.* **55**, 3625 (1997); J. Ruostekoski and D.F. Walls, *ibid.* **56**, 2996 (1997).
- [23] B. Jackson, J.F. McCann, and C.S. Adams, cond-mat/9907325; T. Winiecki, J.F. McCann, and C.S. Adams, cond-mat/9907224; M. Linn and A.L. Fetter, cond-mat/9907045; A.A. Svidzinsky and A.L. Fetter, cond-mat/9906182 D.L. Feder, C.W. Clark, and B.I. Schneider, Phys. Rev. Lett. **82**, 4956 (1999); P.O. Fedichev and G.V. Shlyapnikov, Phys. Rev. A **60**, R1779 (1999).
- [24] P. Öhberg and S. Stenholm, Phys. Rev. A **57**, 1272 (1998); P. Ao and S.T. Chui, Phys. Rev. A **58**, 4836 (1998); S.T. Chui and P. Ao Phys. Rev. A **59**, 1473 (1999).
- [25] P.S. Julienne, J. Res. Natl. Inst. Stand. Technol. **101**, 487 (1996).
- [26] A. Griffin, Phys. Rev. B **53**, 9341 (1996); A. Griffin, Wen-Chin Wu, and S. Stringari, Phys. Rev. Lett. **78**, 1838 (1997); D.A.W. Hutchinson, E. Zaremba, and A. Griffin, Phys. Rev. Lett. **78**, 1842 (1997).
- [27] S. Giorgini, Phys. Rev. A **57**, 2949 (1998).
- [28] N. P. Proukakis, K. Burnett, and H.T.C. Stoof, Phys. Rev. A **57**, 1230 (1998); M. Houbiers, H.T.C. Stoof, and E.A. Cornell, Phys. Rev. A **56**, 2041 (1997);
- [29] D. Jaksch, H.-J. Briegel, J.I. Cirac, C.W. Gardiner, and P. Zoller, Phys. Rev. Lett. **82**, 1975 (1999).
- [30] H.-J. Briegel, T. Calarco, D. Jaksch, J.I. Cirac, and P. Zoller, to appear in J. Mod. Opt..
- [31] D.W. Snoke and G. Baym in *Bose-Einstein condensation*, edited by A. Griffin, D.W. Snoke, and S. Stringari, (Cambridge University Press 1995).
- [32] K. Mølmer, Phys. Rev. Lett. **80**, 1804 (1998).
- [33] C. Raman, M. Kohl, R. Onofrio, D.S. Durfee, C.E. Kulewicz, Z. Hadzibabic, and W. Ketterle cond-mat/9909109; M.R. Matthews, B.P. Anderson, P.C. Haljan, D.S. Hall, C.E. Wieman, and E.A. Cornell cond-mat/9908209
- [34] R.K. Pathria, *Statistical Mechanics*, (Hartnolls Ltd., Bodmin, Cornwall 1996).
- [35] P. Nozières in *Bose-Einstein condensation*, edited by A. Griffin, D.W. Snoke, and S. Stringari, (Cambridge University Press 1995).

- [36] H.D. Politzer, Phys. Rev. A **54**, 5048 (1996); C. Herzog and M. Olshanii, Phys. Rev. A **55**, 3254 (1997); N.L. Balazs and T. Bergeman, Phys. Rev. A **58**, 2359 (1998).
- [37] P. Borrmann, J. Harting, O. Mülken, and E.R. Hilf, Phys. Rev. A **60**, 1519 (1999).
- [38] S. Grossmann and M. Holthaus, Phys. Rev. E **54**, 3495 (1996); S. Grossmann and M. Holthaus, Phys. Rev. Lett. **79**, 3557 (1997).
- [39] C.W. Gardiner, M.D. Lee, R.J. Ballagh, M.J. Davis, and P. Zoller, Phys. Rev. Lett. **81** 5266 (1998); H.-J. Miesner, D.M. Stamper-Kurn, M.R. Andrews, D.S. Durfee, S. Inouye, and W. Ketterle, Science **279**, 1005 (1998).
- [40] M. Edwards, P.A. Ruprecht, K. Burnett, R.J. Dodd, and C.W. Clark, Phys. Rev. Lett. **77**, 1671 (1996); P.A. Ruprecht, M. Edwards, K. Burnett, and C.W. Clark, Phys. Rev. A **54**, 4178 (1996).
- [41] O.J. Luiten, M.W. Reynolds, and J.T.M. Walraven, Phys. Rev. A **53**, 381 (1996); W. Ketterle and N.J. van Druten, Adv. At. Mol. Opt. Phys. **37**, 181 (1996).
- [42] Yu. Kagan, G.V. Shlyapnikov, and J.T.M. Walraven, Phys. Rev. Lett. **76**, 2670 (1996).
- [43] C.W. Gardiner, Phys. Rev. A **56**, 1414 (1997); Y. Castin and R. Dum, Phys. Rev. A **57**, 3008 (1998).
- [44] Yu. Kagan, E.L. Surkov, and G.V. Shlyapnikov, Phys. Rev. A **54**, R1753 (1996); Y. Castin and R. Dum, Phys. Rev. Lett. **77**, 5315 (1996).
- [45] S.A. Gardiner *et al.*, preprint.
- [46] A.J. Leggett in *Bose–Einstein condensation*, edited by A. Griffin, D.W. Snoke, and S. Stringari, (Cambridge University Press 1995).
- [47] W. Petrich, M.H. Anderson, J.R. Ensher, and E.A. Cornell, Phys. Rev. Lett. **74**, 3352 (1995).
- [48] W. Ketterle, K.B. Davis, M.A. Joffe, A. Martin, and D.E. Pritchard, Phys. Rev. Lett. **70**, 2253 (1993).
- [49] J. Söding, D. Guéry-Odelin, P. Desbiolles, G. Ferrari, and J. Dalibard, Phys. Rev. Lett. **80**, 1869 (1998).
- [50] D.S. Jin, J.R. Ensher, M.R. Matthews, C.E. Wieman, and E.A. Cornell, Phys. Rev. Lett. **77**, 420 (1996).
- [51] J.R. Ensher, D.S. Jin, M.R. Matthews, C.E. Wieman, and E.A. Cornell, Phys. Rev. Lett. **77**, 4984 (1996).

- [52] M.R. Andrews, D.M. Kurn, H.-J. Miesner, D.S. Durfee, C.G. Townsend, S. Inouye, and W. Ketterle, *Phys. Rev. Lett.* **79**, 553 (1997).
- [53] L.V. Hau, B.D. Busch, C. Liu, Z. Dutton, M.M. Burns, and J.A. Golovchenko, *Phys. Rev. A* **58**, R54 (1998).

Part II

Quantum kinetic theory
(QKT)

Chapter 2

Basics of QKT

2.1 Introduction

The observation of Bose–Einstein condensation in dilute alkali gases in the year 1995 [1] has stimulated a lot of theoretical interest to describe the dynamics of weakly interacting Bose–gases. In the classical limit a realistic description of the kinetics of a weakly interacting gas is provided by the Boltzmann equation (BE) whose usefulness is widely accepted. The quantum Boltzmann equation [2, 3] is an extension of the BE to account for quantum statistical effects, i.e. it contains additional factors in the collision term. However, the quantum Boltzmann equation is still not able to describe the emergence of a Bose–Einstein condensate without putting in some seed condensate [3]. On the other hand methods for describing dilute Bose–gases close to temperature $T = 0$ have been developed. The most successful description uses the Gross–Pitaevskii equation (GPE) [4] for describing the condensate at temperature $T = 0$ and its time dependent version for finding the time evolution of a Bose–Einstein condensate. However the GPE provides only a simplified description of the condensate since it does not contain any effects of quantum fluctuations or thermal irreversible effects.

If one wants to describe an experiment where a Bose–Einstein condensate is created by evaporative cooling it is clearly necessary to use a theory whose validity encompasses both regimes. It should contain the BE to describe the first stages of the experiment where the gas acts as a classical gas as well as the Gross–Pitaevskii limit where most of the particles are condensed and the Bose–Einstein condensate is usually well described by means of the GPE.

Mainly for these reasons C.W. Gardiner and P. Zoller developed a quantum kinetic theory (QKT) in [5, 6] for dilute weakly interacting gases in a trap. QKT contains both limits, i.e., the BE and the GPE are limiting cases of QKT. Furthermore the work on QKT has inspired C.W. Gardiner to develop a new

number conserving kind of Bogoliubov theory [7] which allows for finding the phonon modes of a weakly interacting Bose gas in the case of fixed number of particles in the system while previous versions of the Bogoliubov theory [8] were always using the order parameter of the condensate thus assuming the system to be in a superposition state of states with different numbers of particles. Since one essential quantity of QKT is the number of particles in each mode a description with a well known number of particles in all the modes was clearly called for. We want to mention that also the motivation of giving a very systematic expansion in roots of $1/\sqrt{N_c}$ where N_c is the number of condensed particles independently pursued by Y. Castin and R. Dum leads to a very similar version of the Bogoliubov theory [9] as the one presented in [7].

Since a detailed and complete derivation of QKT is very lengthy and given in the series of papers [5, 6, 7, 10, 11, 12, 13, 14] we will not go through the derivation of QKT here. Instead we want to briefly present the main applications of this theory investigated up to now. The most important application is the description of the formation of the condensate. First we used the quantum Boltzmann master equation (QBME), a stochastic version of the quantum Boltzmann equation, to investigate the first stages of the condensation process [10, 15]. Since the QBME does not take any mean field interaction into account it clearly fails as soon as the fraction of condensed particles becomes significant. The effects of mean field interactions as well as the role of quasi-particles in the growth of the condensate were taken into account in later publications by C.W. Gardiner *et al.* [13, 14]. The second main application of QKT is to find the equilibrium properties of the condensate which we did in our publication presented in chapter 3. There, we investigated the number and phase fluctuations of a condensate due to the interaction of the condensed particles in the lowest lying states with the bath of uncondensed particles.

Finally, we want to mention that there have also been other groups investigating the kinetics of Bose–Einstein condensation in recent years. Analytical calculations on kinetic theory can be found in the contributions by Yu. Kagan *et al.* in [2], by R. Walser *et al.* in [16], and by H.T.C. Stoof *et al.* [17]. Numerical calculations have been presented in papers by D.V. Semikoz *et al.* [3] and by M. Holland *et al.* [18], a detailed description of evaporative cooling is given by O.J. Luiten *et al.* in [19]. Kinetic theory was also used by J. Williams *et al.* to find the conditions for achieving steady-state Bose-Einstein condensation [20].

2.2 Applications of QKT

2.2.1 Growth of the condensate

In [10, 15] we presented our first description of the growth of the condensate based on the QBME. This equation is a stochastic equation for the diagonal matrix elements of the density operator ρ , given by $w_{\mathbf{n}} \equiv \langle \mathbf{n} | \rho | \mathbf{n} \rangle$ and takes the following form:

$$\begin{aligned} \dot{w}_{\mathbf{n}} = & -\frac{\pi}{\hbar} \sum_{1234} \delta(\hbar(\omega_1 + \omega_2 - \omega_3 - \omega_4)) |U_{1234}|^2 \\ & \times \{n_1 n_2 (n_3 + 1) (n_4 + 1) [w_{\mathbf{n}} - w_{\mathbf{n} + \mathbf{e}_{1234}}] \\ & + (n_1 + 1) (n_2 + 1) n_3 n_4 [w_{\mathbf{n}} - w_{\mathbf{n} - \mathbf{e}_{1234}}]\}. \end{aligned} \quad (2.1)$$

Here $|\mathbf{n}\rangle = |n_0, n_1, n_2, \dots\rangle$ is a Fock state of the N -particle system, giving the occupation numbers n_i of the one particle eigenstates $\Psi_i(\mathbf{x})$ of the non-interacting gas and \mathbf{n} denotes the vector consisting of the occupation numbers n_i . The vector \mathbf{e}_{1234} is defined similarly to \mathbf{n} as

$$\mathbf{e}_{1234} = [0, \dots, 0, \overset{1}{1}, 0, \dots, 0, \overset{2}{1}, 0, \dots, 0, \overset{3}{-1}, 0, \dots, 0, \overset{4}{-1}, 0, \dots, 0], \quad (2.2)$$

which describes two particle collisions. The state $|\mathbf{n} - \mathbf{e}_{1234}\rangle$ is reached from $|\mathbf{n}\rangle$ by the collision $1 + 2 \rightarrow 3 + 4$. ω_i is the eigenenergy of the one particle eigenstate $\Psi_i(\mathbf{x})$. The interaction matrix elements U_{1234} are determined by the spatial form of the one particle mode functions and the interaction strength characterized by the s -wave scattering length a_s . They can be found by the equation

$$U_{1,2,3,4} = \frac{4\pi\hbar^2 a_s}{m} \int_{R^3} d^3x \Psi_1^*(\mathbf{x}) \Psi_2^*(\mathbf{x}) \Psi_3(\mathbf{x}) \Psi_4(\mathbf{x}), \quad (2.3)$$

where m is the mass of the particles. The QBME leaves out all the coherences of the density operator and also does not include mean field effects of the condensate. Thus it is only valid as long as the mean field energy is much smaller than the separation of the trap levels (for typical situations this limits the number of particles to few hundred).

The simplest description of the growth of the condensate taking into account the mean field energy of the condensate, but not the mean field interaction of the condensate with the uncondensed particles, obtained from QKT is given by the growth equation first studied in detail in [13]

$$\dot{N}_c = 2W^+(N_c)(N_c + 1) - 2W^-(N_c)N_c, \quad (2.4)$$

where the rates $W^\pm(N_c)$ are defined in Eqs. (3.25, 3.26). $W^+(N_c)$ is the rate at which particles from the thermal cloud are transferred to the condensate by

elastic collisions and $W^-(N_c)$ is the rate at which particles are kicked out of the condensate by elastic collisions with thermal particles. Note the +1 term in Eq. (2.4) which is responsible for the initiation of condensation. Although Eq. (2.4) gives a qualitatively correct result for the growth of the condensate many important features of the growth process are left out. Especially one expects particles in the low lying excited states to have significant influence on the growth of the condensate since

- the energies and the wave functions of the low lying levels are affected by the mean field of the condensate particles, and
- there will be many transitions of atoms to and from these low lying states in the initial stages of the condensation process.

Thus it is not possible to describe the particles in these state as if they were particles in a thermal bath uncorrelated with the condensate during the growth process as done in [13]. Indeed, taking into account the particles in the low lying states explicitly has significant influence on the initial stages of the growth of the condensate as was shown in [14].

2.2.2 Properties of the condensate in the stationary state

The second application we were interested in are the stationary properties of the condensate, i.e., the particle number and phase fluctuations of the condensate coupled to a thermal bath of atoms. In the description presented in chapter 3 we assumed the fluctuations to be only introduced by collisions of condensate particles with thermal particles and by one- two- and three particle losses from the trap. All the fluctuations arising from interactions of the condensate with low lying excitations, i.e. phonons were left out. Another way of viewing this approach is to say that we treated all the particles in the low lying states as being in one mode namely the condensate mode itself and found the fluctuations introduced by interactions with the thermal particles.

Note that the coherence properties of the trapped Bose–Einstein condensate determine the coherence properties of particles eventually coupled out of the condensate. Thus the calculations presented in chapter 3 are important for finding the coherence properties of an atom laser produced by coupling out particles of a condensate in its stationary state. The one particle loss from the condensate introduced in chapter 3 does not necessarily have to originate from collisions of the condensate atoms with background particles but may as well describe the output coupler for the condensed atoms.

References

- [1] M. Anderson, J.R. Ensher, M.R. Matthews, C.E. Wieman, and E.A. Cornell, *Science* **269**, 198 (1995); K.B. Davis, M-O. Mewes, M.R. Andrews, N.J. van Druten, D.S. Durfee, D.M. Kurn, and W. Ketterle, *Phys. Rev. Lett.* **75**, 3969 (1995); C.C. Bradley, C.A. Sackett, J.J. Tollet, and R. Hulet, *Phys. Rev. Lett.* **75**, 1687 (1995).
- [2] Yu. M. Kagan, B.V. Svistunov and G.V. Shlyapnikov, *JETP* **75**, 387 (1992); Yu. Kagan and B.V. Svistunov, *Phys. Rev. Lett.* **79**, 3331 (1997).
- [3] D.V. Semikoz and I.I. Tkachev, *Phys. Rev. Lett.* **74**, 3093 (1995).
- [4] V.L. Ginzburg and L.P. Pitaevskii, *Zh. Eksp. Teor. Fiz.* **34**, 1240 (1958) [*Sov. Phys. JETP* **7**, 858 (1958)]; E.P. Gross, *J. Math. Phys.* **4**, 195 (1963).
- [5] C.W. Gardiner and P. Zoller, *Phys. Rev. A* **55**, 2902 (1997).
- [6] C.W. Gardiner and P. Zoller, *Phys. Rev. A* **58**, 536 (1997).
- [7] C.W. Gardiner, *Phys. Rev. A* **56**, 1414 (1997).
- [8] N.N. Bogoliubov, *J. Phys. (USSR)* **11**, 23 (1947); reprinted in D. Pines, *The Many Body Problem* (Benjamin, New York, 1962).
- [9] Y. Castin and R. Dum, *Phys. Rev. A* **57**, 3008 (1998).
- [10] D. Jaksch, C.W. Gardiner, and P. Zoller, *Phys. Rev. A* **56**, 575 (1997).
- [11] D. Jaksch, C.W. Gardiner, K.M. Gheri, and P. Zoller, *Phys. Rev. A* **58**, 1450 (1998).
- [12] C.W. Gardiner, P. Zoller, cond-mat/9905087.
- [13] C.W. Gardiner, P. Zoller, R.J. Ballagh, and M.J. Davis, *Phys. Rev. Lett.* **79**, 1793 (1997).
- [14] C.W. Gardiner, M.D. Lee, R.J. Ballagh, M.J. Davis, and P. Zoller, *Phys. Rev. Lett.* **81**, 5266 (1998).
- [15] D. Jaksch, diploma thesis, University of Innsbruck (1996).
- [16] R. Walser, J. Williams, J. Cooper, and M. Holland, *Phys. Rev. A* **59**, 3878 (1999).
- [17] H.T.C. Stoof, *Phys. Rev. Lett.* **78**, 768 (1997); C.A. Sackett, H.T.C. Stoof, and R.G. Hulet, *Phys. Rev. Lett.* **80**, 2031 (1998); H.T.C. Stoof, *Phys. Rev. A* **45**, 8398 (1992).
- [18] M. Holland, J. Williams, K. Coakley, and J. Cooper, *Quantum Semiclass. Opt.* **8**, 571 (1996); M. Holland, J. Williams, and J. Cooper, *Phys. Rev. A* **55**, 3670 (1997).
- [19] O.J. Luiten, M.W. Reynolds, and J.T.M. Walraven, *Phys. Rev. A* **53**, 381 (1996).

- [20] J. Williams, R. Walser, C. Wieman, J. Cooper, and M. Holland, Phys. Rev. A **57**, 2030 (1998).

Chapter 3

PUBLICATION

QUANTUM KINETIC THEORY IV: INTENSITY AND AMPLITUDE FLUCTUATIONS OF A BOSE-EINSTEIN CONDENSATE AT FINITE TEMPERATURE INCLUDING TRAP LOSS

D. Jaksch¹, C.W. Gardiner², K.M. Gheri¹, and P. Zoller¹

¹ Institut für Theoretische Physik, Universität Innsbruck, 6020 Innsbruck, Austria

² Physics Department, Victoria University, Wellington, New Zealand

Physical Review A **58**, 1450 (1998)

We use the quantum kinetic theory to calculate the steady state and the fluctuations of a trapped Bose-Einstein condensate at a finite temperature. The system is divided in a condensate and a noncondensate part. A quantum-mechanical description based on the number conserving Bogoliubov method is used for describing the condensate part. The noncondensed particles are treated as a classical gas in thermal equilibrium with temperature T and chemical potential μ . We find a master equation for the reduced density operator of the Bose-Einstein condensate, calculate the steady state of the system, and investigate the effect of one-, two-, and three-particle losses on the condensate. Using linearized Ito equations we find expressions for the intensity fluctuations and the amplitude fluctuations in the condensate. A Lorentzian line shape is found for the intensity correlation function that is characterized by a time constant γ_I^{-1} derived in the paper. For the amplitude correlation function we find ballistic behavior for time differences smaller than γ_I^{-1} , and diffusive

behavior for larger time differences.

PACS: 03.75.Fi, 74.40.+k, 42.50.Lc.

3.1 Introduction

In a series of papers we have developed a quantum kinetic (QK) theory with application to Bose condensation of cold dilute gases. In the first two papers, which we shall refer to as QKI [1] and QKII [2], we considered a spatially homogeneous, weakly condensed system, where the interaction between the atoms was assumed to be sufficiently weak for quasiparticle effects to be negligible. In QKIII [3] the theory was extended to a strongly condensed gas in a trapping potential under the assumption that the noncondensed vapor acts as a heat and particle reservoir for the condensate (see also Ref. [4]), a situation which corresponds closely to present experiments of Bose condensation with alkali-metal vapors [5, 6, 7, 8, 9, 10, 11].

In the present paper (QKIV) we will study the steady state, amplitude, and phase fluctuations of a trapped Bose-Einstein condensate at *finite temperature*, including the effects of one-, two-, and three particle losses on the condensate. Such a study seems particularly timely in view of the present interest in the dynamics and measurement of the phase of the Bose condensate (for a review see Ref. [12]). Until now the discussion in the literature has essentially focused on phase collapse or diffusion, and phase revivals in the zero-temperature limit, analyzing the dependence of collapse and revival times on the trap potential, the dimensionality of the gas, atom number fluctuations, and the coherent dynamics of the condensate [13, 14, 15]. In contrast, in the present work we will study in detail fluctuations as a result of interaction of the condensate with a (reservoir of) uncondensed atoms.

We will almost exclusively consider a grand canonical particle reservoir in this work. This particle reservoir will be assumed to have a constant chemical potential and not to be influenced by the mean field of the condensate. The results will therefore only be valid in the case of small condensate and large thermal particle numbers. In all other cases the simple model used here for the thermal particles will have to be replaced by a more sophisticated one. A more detailed discussion on the expected correction to the results due to particle conservation and mean-field effects is given in Appendix 3.A.

The starting point of the theory is to decompose the field operator describing the N -particle system into condensate and noncondensate parts. The division is based on a splitting into two energy regions where the high energy band is supposed to contain particles in a thermal state corresponding to a given temperature T , and chemical potential μ . The condensate band contains the actual condensate as well as quasi-particle excitations. A quantum-mechanical description based on the number conserving Bogoliubov method is used for describing the condensate part [16]. To facilitate the analysis we drop the quasi-particles and describe the condensate by a single mode with destruction operator B , and the spatial wave function $\xi_N(\mathbf{x})$, corresponding

to the solution of the Gross-Pitaevskii equation for N condensate particles. Elimination of the noncondensate part leaves us with a master equation for the (reduced) condensate density operator. The physics contained in this equation is quite rich. The master equation accounts for loss/gain of particles to/from the thermal band, and phase-destroying but number-conserving collisions between condensate and noncondensate particles as well as linear and nonlinear trap loss.

A diagrammatic illustration of the processes described by the master equation is given in Fig. 3.1. We realize that there are two types of processes. On the one hand, there are those which involve particles from both the condensate and the noncondensed band. They comprise processes which lead to a redistribution of particles between the two bands at rates $W^+(N)$ (condensate gain) and $W^-(N)$ (condensate loss), as well as number conserving scattering events of thermal particles off the condensate. The latter occur with a rate $R_{00}(N)$ and will give rise to fluctuations in the condensate phase. Explicit expressions for W^\pm and R_{00} will be given below. On the other hand there are several loss mechanisms at work which deplete the condensate [17, 18]. There is one-particle loss due to collisions with background gas atoms with associated rate γ_1 . Two particles can be lost with rate $\gamma_2(N)$ from the condensate if two condensed particles collide, and one of them changes its internal state. This particle no longer sees the trap, and escapes. Its partner is imparted with the energy difference set free by the collision, and is also lost from the trap. Finally, three-particle loss can occur with rate $\gamma_3(N)$ if in a three-particle collision a dimer is formed. The binding energy is imparted to the third particle, and all of them escape from the trap. Note that the description of the noncondensate particles in terms of a thermal reservoir results in a finite occupation of the condensate mode even in the presence of loss channels.

3.2 Main results

In this section we will give a short overview of the main results to be derived in detail in the remainder of this paper. As a starting point for our analysis of the particle number and phase fluctuations of a Bose-Einstein condensate at a finite temperature, we adopt the theoretical description developed in the precursor papers QKI-III [1, 2, 3].

3.2.1 Fluctuation analysis

In the limit of large condensate particle numbers, we may approximate the master equation [Eq. (3.17)] by an equation that is of Lindblad type. This has the advantage that standard techniques developed in quantum optics for the description of fluctuation properties become applicable [19]. We have thus

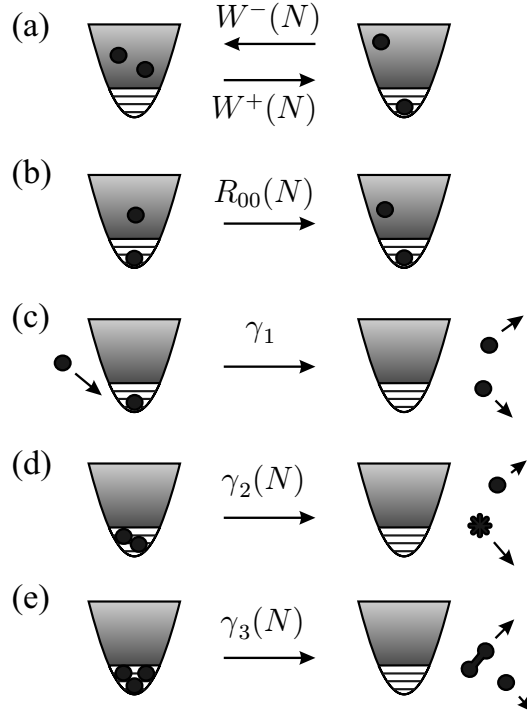


Fig. 3.1: Interpretation of the processes described by the master equation: (a) $W^+(N)$ and $W^-(N)$ are the feeding and depletion rates of the condensate from and to the noncondensed thermal band of particles, respectively. (b) R_{00} is the rate of thermal particles bouncing off the condensate without changing its occupation number. γ_1 (c), $\gamma_2(N)$ (d) and $\gamma_3(N)$ (e) are the rates of one-, two-, and three-particle losses, respectively. We use a star to indicate a change in the internal state of a particle. The barbell represents two atoms having formed a molecule.

derived quantum stochastic differential equations for the condensate particle number $\tilde{N} = B^\dagger B$ and the Glogower-Susskind phase operator $e^{i\phi}$, which is known to characterize phase fluctuations well in the limit of large occupation numbers [20]. Linearization of these equations is permissible in the very same limit of large average occupation $\bar{N} = \langle \tilde{N} \rangle$, and allows us to work out the two-time correlation functions of occupation number and phase. The spectra of condensate occupation number and amplitude fluctuations are then immediately obtainable by Fourier transformation.

3.2.1.1 Condensate particle number fluctuations

For the correlation function of the particle number fluctuations [21] we obtain the following result which holds in the stationary limit, i.e., for times satisfying

$t + s \gg \gamma_I^{-1}$

$$\langle \tilde{N}(t), \tilde{N}(s) \rangle = \frac{\bar{f}_2}{2\gamma_I} e^{-\gamma_I|t-s|} = \sigma^2 e^{-\gamma_I|t-s|}, \quad (3.1)$$

with $\langle a, b \rangle = \langle ab \rangle - \langle a \rangle \langle b \rangle$. In Eq. (3.1)

$$\bar{f}_2/2 = \bar{N}(\bar{W}^+ + \bar{W}^- + \gamma_1) + 4\bar{N}^2\bar{\gamma}_2 + 9\bar{N}^3\bar{\gamma}_3, \quad (3.2)$$

with a bar denoting evaluation at $N = \bar{N}$. Note that σ appearing in Eq. (3.1) is a measure of the width of the particle number distribution. The characteristic time constant γ_I with which the particle number fluctuations regress is given by

$$\gamma_I = 2\bar{N}\partial_{\bar{N}}\bar{W}^- - (\bar{\gamma}_2 + 3\bar{\gamma}_3\bar{N})8\bar{N}/5. \quad (3.3)$$

$\partial_{\bar{N}}$ denotes the derivative with respect to N and evaluation at $N = \bar{N}$. The exact size of this rate depends on the specific experimental setup. A convenient quantity to assess the amount of fluctuations present is the well known Mandel Q parameter defined as

$$Q = \lim_{t \rightarrow \infty} \langle \tilde{N}(t), \tilde{N}(t) \rangle / \langle \tilde{N}(t) \rangle^2 - 1. \quad (3.4)$$

A coherent state would correspond to a value of $Q = 0$, while a number state yields the minimum value $Q = -1$. Assuming two and three particle losses to be insignificant we find for the Mandel Q parameter,

$$Q \approx \frac{5kT}{2\mu_{\bar{N}}} - 1. \quad (3.5)$$

To arrive at this result the approximate expressions of the rates W^+ and W^- as given in Eqs. (3.26,3.25) in terms of the scattering length a , the reservoir temperature T and chemical potential μ have been used.

The results (for details, see Sec. 3.4.3) can now be summarized as follows. The variance of the occupation of the condensate mode is proportional to $kT/\mu_{\bar{N}}$, with $\mu_{\bar{N}}$ the chemical potential for the condensate mode with average occupation \bar{N} . In the Thomas-Fermi approximation μ_N is given by

$$\mu_N = \left(\frac{15N\mu m^{3/2}\omega_x\omega_y\omega_z}{16\sqrt{2}\pi} \right)^{2/5}. \quad (3.6)$$

The constants used in Eq. (3.6) are defined in Sec. 3.3.1. The characteristic rate at which the correlation function drops off is roughly given by $\gamma_I \approx 2\bar{N}\partial_{\bar{N}}\bar{W}^-$, with W^- the loss rate to the noncondensed band.

3.2.1.2 Amplitude and phase fluctuations

In the limit of large and well-defined average occupation number \bar{N} of the condensate mode, the amplitude correlation function $\langle B^\dagger(t)B(s) \rangle$ is well suited to assess phase properties of the condensate mode [21]. In particular, the spectrum of phase fluctuations is identical to the spectrum of amplitude fluctuations. For the amplitude correlation function we obtain for $t > s$

$$\langle B^\dagger(t)B(s) \rangle = \bar{N} e^{(i\frac{\mu\bar{N}}{\hbar} - \frac{16}{25}\bar{R}_{00})(t-s) - \eta(\gamma_I(t-s) + e^{-\gamma_I(t-s)} - 1)}, \quad (3.7)$$

where $\eta = (\sigma\partial_{\bar{N}}\mu_{\bar{N}}/\gamma_I\hbar)^2$. As we will see in Sec. 3.2.1.3 R_{00} is negligible in the above correlation function [Eq. (3.7)] for most of the current experiments. The structure of the correlation function indicates that there are two distinct time regimes:

- For $\gamma_I|t-s| \ll 1$, the term proportional to η in the exponent is proportional to $(t-s)^2$. This is called the ballistic regime.
- For $|t-s|\gamma_I \geq 1$, the phase behaves like that of a system undergoing phase diffusion. A characteristic of such behavior is a linear dependence of the exponent on $|t-s|$. Note that for large time differences we observe the legacy of the ballistic regime in the form of a rescaling of \bar{N} to $\bar{N}_\infty = \bar{N}e^\eta$.

3.2.1.3 Numerical values

Using data from the experiments at JILA [22] and an average occupation number of $\bar{N} = 25000$ Rubidium atoms at a temperature $T = 0.5\mu K$ in a trap with $f_x = f_y = f_z/\sqrt{8} = 47\text{Hz}$ we obtain for the rates $\gamma_I \approx 2\text{Hz}$, $\bar{R}_{00} \approx 4\text{mHz}$, $\bar{W}^\pm \approx 50\text{Hz}$, and $\eta \approx 800$. These values have to be understood as order of magnitude estimates for current experiments. Note that we used a value of $a = 2.6\text{nm}$ for the scattering length of rubidium whereas recent experiments at JILA showed that $a = 5.1\text{nm}$.

3.3 Model

In this section we briefly describe the basic concepts of the quantum kinetic theory developed in Ref. [1, 2, 3, 16, 23]. We do not give a detailed derivation of the master equation used throughout the paper since this can be found in Ref. [3].

3.3.1 Description of the system

The Hamiltonian of a weakly interacting Bose gas confined by a potential $V_T(\mathbf{x})$ in second quantization is written as

$$H = \int d^3\mathbf{x} \psi^\dagger(\mathbf{x}) \left(-\frac{\hbar^2}{2m} \nabla^2 + V_T(\mathbf{x}) \right) \psi(\mathbf{x}) + \frac{1}{2} \int d^3\mathbf{x} \int d^3\mathbf{x}' \psi^\dagger(\mathbf{x}) \psi^\dagger(\mathbf{x}') u(\mathbf{x} - \mathbf{x}') \psi(\mathbf{x}') \psi(\mathbf{x}). \quad (3.8)$$

$\psi(\mathbf{x})$ is the standard bosonic field operator. The two-body interaction potential $u(\mathbf{x} - \mathbf{x}')$ is a short-range potential of the form $u\delta(\mathbf{x} - \mathbf{x}')$ where $u = 4\pi\hbar a/m$ with a the scattering length. We assume the trapping potential to be of the form $V_T(\mathbf{x}) = m(\omega_x^2 x^2 + \omega_y^2 y^2 + \omega_z^2 z^2)/2$.

As was shown in Ref. [3] we can obtain a master equation for the density operator of the condensate mode by dividing the Bose gas into two energy regions called the condensate band R_C and the noncondensate band R_{NC} . The boundary E_R between these two regions is chosen according to Ref. [3] such that R_{NC} is not significantly affected by the mean field of the condensate. The field operator is then written as $\psi(\mathbf{x}) = \psi_{NC}(\mathbf{x}) + \phi(\mathbf{x})$ describing particles in the noncondensate band and in the condensate band, respectively. We will treat the particles in R_{NC} as classical thermalized particles characterized by a temperature T and a chemical potential μ . The particles in R_C are affected by the mean field, and they have to be treated quantum-mechanically. R_C contains all the trap levels that are significantly modified by the mean field of the condensate. As in Ref. [23] we will use the simplest possible description of the condensate band by assuming that only one mode, namely, the condensate mode itself, is important and all the other modes are negligible. The master equation we will use for our calculations is an equation for the reduced density operator ρ_c of the condensate band R_C interacting with the bath of particles in R_{NC} .

3.3.1.1 Condensate band R_C

We use the number-conserving Bogoliubov method derived in Ref. [16] to describe the particles in R_C . In this formulation we can write down the condensate band field operator $\phi(\mathbf{x})$ in the form

$$\phi(\mathbf{x}) = B(N) \left\{ \xi_N(\mathbf{x}) + \sum_m \frac{b_m f_m(\mathbf{x}) + b_m^\dagger g_m(\mathbf{x})}{\sqrt{N}} \right\}. \quad (3.9)$$

The annihilation operator $B(N - 1)$ brings the system R_C from the ground state with N atoms to the ground state with $N - 1$ atoms. The action of the

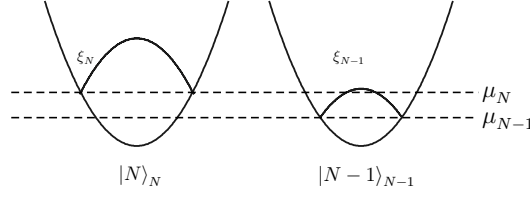


Fig. 3.2: Condensate ground state with N particles $|N\rangle_N$ and with $N-1$ particles $|N-1\rangle_{N-1}$. These two states are connected by the operator B , as described in the text.

operator $B(N-1)$ to the condensate is depicted in Fig. 3.2. $|N\rangle_N$ denotes the ground state with N particles in the condensate. Applying the operator B to this state yields $B|N\rangle_N = \sqrt{N}|N-1\rangle_{N-1}$. Note that the operator B changes the chemical potential of the condensate from μ_N to μ_{N-1} .

As shown in Ref. [16] $\xi_N(\mathbf{x})$ is the condensate wave function, and satisfies the Gross-Pitaevskii equation

$$-\frac{\hbar^2}{2m}\nabla^2\xi_N + V_T\xi_N + Nu|\xi_N|^2\xi_N = \mu_N\xi_N. \quad (3.10)$$

In all our calculations we will use the Thomas-Fermi approximation for the chemical potential [Eq. (3.6)] and for the condensate wave function

$$\xi_N(\mathbf{x}) = \sqrt{\frac{\mu_N - V_T(\mathbf{x})}{Nu}} \quad \text{for } \mu_N > V_T(\mathbf{x}), \quad (3.11)$$

and zero elsewhere. The energy of the condensate is given by

$$E_0 = \frac{5N\mu_N}{7} \quad (3.12)$$

The amplitudes $f_m(\mathbf{x})$ and $g_m(\mathbf{x})$ describe creation and destruction of quasiparticles. They are defined in Ref. [3], but we will not need them in this paper. We will assume there is always a fairly large mean number of particles \bar{N} in the condensate so that we can neglect the influence of the quasiparticles on $\phi(\mathbf{x})$ [24].

3.3.1.2 Noncondensate band R_{NC}

We treat the noncondensate band as a thermal bath of particles in thermal equilibrium. According to Ref. [3] we only need the phase-space density of the noncondensed particles $F(\mathbf{K}, \mathbf{x})$ to calculate all the rates appearing in the master equation for ρ_c [Eq. (3.17)]. In our calculations we will use the classical approximation

$$F(\mathbf{K}, \mathbf{x}) = e^{(\mu - \frac{\hbar^2\mathbf{K}^2}{2m} - V_T(\mathbf{x}))/kT}. \quad (3.13)$$

We expect corrections to the rates W^\pm and R_{00} from using a more detailed description of the noncondensed particles. However, all the calculations presented here will remain valid, since they are mostly independent of the functional form of the rates W^\pm and R_{00} . We only require that it is permissible to linearize the rates $W^\pm(N)$ and $R_{00}(N)$ around the mean number of particles in the condensate \bar{N} . In the present work we will mainly present results obtained by using Eqs. (3.26,3.25) and (3.27,3.28) for the rates $W^\pm(N)$ and $R_{00}(N)$ which were obtained by the assumption of a grand canonical classical bath of particles not influenced by mean-field effects. Corrections to the stationary state due to conservation of the total number of particles as well as mean-field effects and quantum statistics effects are estimated in Appendix 3.A. A further, more detailed, discussion of different models for the uncondensed bath (i.e., the noncondensate band) lies beyond the scope of this paper, and will be presented in other work. However, we want to point out that these models might include canonical baths with a constant particle number [25], evaporatively cooled baths [26] as well as baths that are continuously fed with particles [27].

3.3.1.3 Trap loss

There are several processes leading to losses of condensate particles from the trap. We will consider one-, two-, and three-particle loss with loss rates γ_1 , $\gamma_2(N)$ and $\gamma_3(N)$, respectively. One-particle loss might be caused by background gas particles hitting condensate particles or by coupling condensate particles out of the trap as described in Ref. [21]. Inelastic two-particle collisions changing the internal properties of the particles lead to two particle loss. In most of the current experiments the two particle loss is negligible compared to the three particle loss caused by the inelastic collision of three particles. In the Thomas-Fermi approximation we obtain for the loss rates

$$\gamma_1 = \frac{K_1}{2} \int d^3x |\xi_N(x)|^2 = \frac{K_1}{2}, \quad (3.14)$$

$$\begin{aligned} \gamma_2(N) &= \frac{K_2}{4} \int d^3x |\xi_N(x)|^4 = \frac{K_2 16 \cdot \pi \mu_N^{7/2} \sqrt{2}}{105 m^{3/2} \omega_x \omega_y \omega_z N^2 u^2} \\ &\propto N^{-3/5}, \end{aligned} \quad (3.15)$$

$$\gamma_3(N) = \frac{K_3}{6} \int d^3x |\xi_N(x)|^6 = \frac{4K_3 \mu_N \gamma_2(N)}{9K_2 N u} \propto N^{-6/5}. \quad (3.16)$$

For Rubidium the constants K_i have been measured in [17]. The rates K_i have been calculated analytically in Refs. [28, 29, 30].

3.3.2 Master equation

We simplify Eq. (50) in Ref. [3] for the case that the condensate band consists only of the condensate mode alone. In contrast to Ref. [3] we keep terms including R_{00} , and add the loss terms to the master equation (see Fig. 3.1). We thus obtain the following equation for the reduced density operator of the condensate band ρ_c :

$$\dot{\rho}_c = -\frac{i}{\hbar} [H_0, \rho_c] \quad (3.17)$$

$$+ 2B^\dagger \{W^+(\hat{N})\rho_c\}B - [BB^\dagger, \{W^+(\hat{N})\rho_c\}]_+ \quad (3.18)$$

$$+ 2B \{W^-(\hat{N})\rho_c\}B^\dagger - [B^\dagger B, \{W^-(\hat{N})\rho_c\}]_+ \quad (3.19)$$

$$+ 2BB^\dagger \{R_{00}(\hat{N})\rho_c\}BB^\dagger - [BB^\dagger BB^\dagger, \{R_{00}(\hat{N})\rho_c\}]_+ \quad (3.20)$$

$$+ 2B \{\gamma_1 \rho_c\}B^\dagger - [B^\dagger B, \{\gamma_1 \rho_c\}]_+ \quad (3.21)$$

$$+ 2BB \{\gamma_2(\hat{N})\rho_c\}B^\dagger B^\dagger - [B^\dagger B^\dagger BB, \{\gamma_2(\hat{N})\rho_c\}]_+ \quad (3.22)$$

$$+ 2BBB \{\gamma_3(\hat{N})\rho_c\}B^\dagger B^\dagger B^\dagger - [B^\dagger B^\dagger B^\dagger BBB, \{\gamma_3(\hat{N})\rho_c\}]_+ \quad (3.23)$$

where $\hat{N}\rho_c = [B^\dagger B, \rho_c]_+ / 2$. An intuitive interpretation of the processes described by the master equation [Eqs. (3.17-3.23)] is given in Fig. 3.1. The free evolution of the condensate is described by the Hamiltonian H_0 ,

$$H_0 = E_0(\tilde{N}) \quad \text{where} \quad E_0(N+1) - E_0(N) = \mu_N, \quad (3.24)$$

and μ_N is the chemical potential obtained from the Gross-Pitaevskii equation.

Growth and depletion of the condensate due to interaction with the non-condensed particles is given in Eqs. (3.18,3.19). The growth and the depletion rates $W^\pm(N)$ of the condensate were already calculated in Ref. [3] using the Maxwell-Boltzmann approximation for the phase-space density of the non-condensed particles. They are given by

$$W^+(N) = \frac{4m(akT)^2}{\pi\hbar^3} e^{2\mu/kT} \left\{ \frac{\mu_N}{kT} K_1\left(\frac{\mu_N}{kT}\right) \right\}, \quad (3.25)$$

$$W^-(N) = e^{(\mu_N - \mu)/kT} W^+(N). \quad (3.26)$$

The rate R_{00} defined in Eq. (141) of Ref. [3] can be understood as describing the process of thermal particles bouncing off the condensate. This process does not change the number of particles in the condensate, but does cause phase fluctuations. Using the above expression [Eq. (3.13)] for $F(\mathbf{K}, \mathbf{x})$ and the Thomas-Fermi approximation for the condensate wave function, we find

$$R_{00}(N) = \frac{4kT\mu_N^4}{9\pi^4\hbar^5\omega_x^3\omega_z N^2} e^{\mu/kT} \frac{\text{arsinh}\left(\sqrt{\frac{\omega_z^2 - \omega_x^2}{\omega_x^2}}\right)}{\sqrt{\frac{\omega_z^2 - \omega_x^2}{\omega_x^2}}} \quad (3.27)$$

for $\omega_z > \omega_x = \omega_y$, and

$$R_{00}(N) = \frac{4kT\mu_N^4}{9\pi^4\hbar^5\omega_x^3\omega_zN^2} e^{\mu/kT} \frac{\arcsin\left(\sqrt{\frac{\omega_x^2 - \omega_z^2}{\omega_x^2}}\right)}{\sqrt{\frac{\omega_x^2 - \omega_z^2}{\omega_x^2}}} \quad (3.28)$$

for $\omega_z < \omega_x = \omega_y$. A detailed derivation of R_{00} is given in Appendix 3.B.

Trap loss is accounted for by the last two lines of the master equation Eqs. (3.21,3.22) and (3.23). Note that the only difference between the process including the rate $W^-(N)$ and the one-particle loss rate γ_1 is the dependence of the two rates on the properties μ and T of the noncondensate.

3.4 Solutions of the master equation

In this section we investigate solutions of Eq. (3.17). We find the stationary solution and derive a differential equation for the mean number of particles in the condensate \bar{N} . Using linearized Ito equations, we obtain the correlation functions $\langle N(t), N(s) \rangle$ and $\langle B^\dagger(t)B(s) \rangle$.

We define

$$g_N^\nu := {}_N \langle N - \nu | \rho_c | N \rangle_N. \quad (3.29)$$

From Eq. (3.17), we derive the evolution equation of the matrix elements, expand the terms in this equation for large N in a Kramers-Moyal type expansion to order $1/N$, and obtain

$$\begin{aligned} \dot{g}_N^\nu &= 2\sqrt{(N-\nu)N} \{W^+(N-1)g_{N-1}^\nu - W^-(N)g_N^\nu\} \\ &+ 2\sqrt{(N-\nu+1)(N+1)} \{W^-(N+1)g_{N+1}^\nu - W^+(N)g_N^\nu\} \\ &+ 2\sqrt{(N-\nu+1)(N+1)}\gamma_1 g_{N+1}^\nu - (2N-\nu)\gamma_1 g_N^\nu \\ &+ 2\sqrt{(N-\nu+1)(N-\nu+2)(N+1)(N+2)}\gamma_2(N)g_{N+2}^\nu \\ &- ((N-\nu)(N-\nu-1) + N(N-1))\gamma_2(N)g_N^\nu \\ &+ 2\sqrt{(N-\nu+1)(N-\nu+2)(N-\nu+3)(N+1)(N+2)(N+3)} \\ &\quad \times \gamma_3(N)g_{N+3}^\nu \\ &- ((N-\nu)(N-\nu-1)(N-\nu-2) + N(N-1)(N-2))\gamma_3(N)g_N^\nu \\ &- (1/\tau_N^\nu)g_N^\nu. \end{aligned} \quad (3.30)$$

The time constant

$$\tau_N^\nu = \left\{ \frac{\nu^2}{4N} [W^+(N) + W^-(N)] + \nu^2 R_{00}(N) - \frac{i\nu\mu_N}{\hbar} \right\}^{-1} \quad (3.31)$$

determines the time scale on which the non-diagonal matrix elements decay. We have assumed that $\nu \ll \bar{N}$, and therefore approximated

$$\frac{i}{\hbar} (E_0(N) - E_0(N-\nu)) \approx \frac{i\nu\mu_N}{\hbar}. \quad (3.32)$$

3.4.1 Stationary solution

First we neglect trap loss and solve Eq. (3.30) for the stationary case. All g_N^ν with $\nu \neq 0$ drop off exponentially in time, and we are left with the diagonal terms only. We use the detailed balance condition to calculate the stationary solution \bar{g}_N^0 :

$$\frac{\bar{g}_{N+1}^0}{\bar{g}_N^0} = \frac{W^+(N)}{W^-(N+1)} \approx e^{(\mu - \mu_N)/kT}, \quad (3.33)$$

and therefore

$$\bar{g}_N^0 \propto \prod_{n=0}^N e^{(\mu - \mu_n)/kT}. \quad (3.34)$$

Using the Thomas-Fermi approximation for the chemical potential of the condensate, and replacing the sum occurring in the exponent by an integral, we obtain

$$\bar{g}_N^0 \propto e^{N(\mu - 5\mu_N/7)/kT}. \quad (3.35)$$

This particle distribution has one maximum determined by the condition $\mu_N = \mu$, as expected from thermodynamics. The position of the maximum differs from the mean number of particles in the condensate by an amount of order $1/\bar{N}$.

3.4.1.1 Linearized solution

In the case of $\bar{N} \gg 1$ we may linearize the solution Eq. (3.35) around the mean number of particles in the condensate \bar{N} . We approximate the distribution in Eq. (3.35) by a Gaussian

$$\bar{g}_N^0 \approx \frac{1}{\sqrt{2\pi}\sigma} e^{-\frac{(N - \bar{N})^2}{2\sigma^2}}. \quad (3.36)$$

The width σ of this Gaussian is given by

$$\sigma = \sqrt{\frac{5kT\bar{N}}{2\mu_{\bar{N}}}}. \quad (3.37)$$

In the Thomas-Fermi approximation σ scales with the mean number of condensate particles like $\bar{N}^{3/10}$. The difference between the linearized and nonlinearized solutions can therefore only be seen for very small condensates. Figure 3.3 shows a comparison between the Gaussian approximation and numerical solutions obtained from Eqs. (3.17) and (3.38). As expected both solutions agree very well with each other even for a mean occupation of the condensate of only about $\bar{N} \approx 500$. Note also that the same result for the variance may be obtained from statistical mechanics. Thus the restriction $\mu_{\bar{N}}/kT > 1$ is not necessary for this result to be valid.

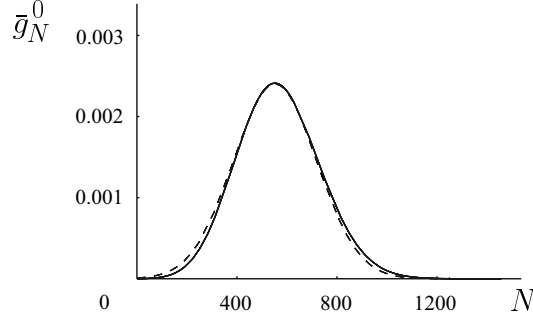


Fig. 3.3: Stationary particle distribution in the condensate. The trap loss is assumed to be zero. $\mu/kT = 0.05$ and $\mu_{N=1}/kT = 0.004$. The solid line represents the numerical stationary solution of the Fokker-Planck equation [Eq. (3.38)] and the detailed balance solution of the master equation [Eq. (3.17)]. The dashed line depicts the Gaussian approximation [Eq. (3.36)]. The trap frequencies are chosen to be $f_x = f_y = f_z/\sqrt{8} = 47\text{Hz}$. The calculation is done for Rubidium.

3.4.1.2 Inclusion of trap loss

In our model the bath of thermal atoms is not depleted by the interaction with the condensate. Experimentally this can be achieved by replenishing the reservoir by some mechanism, or by doing the experiment so quickly that the number of particles lost from the reservoir can be neglected. Furthermore, the calculations presented here for constant T and μ remain valid as long as the heat bath parameters μ and T change slowly compared to the time scale of the condensate dynamics. For the diagonal matrix elements g_N^0 , we therefore obtain a stationary solution different from zero even if we include trap loss. Keeping only the leading order terms in N of Eq. (3.30), we immediately find the Fokker-Planck equation for g_N^0 to be

$$\dot{g}_N^0 = \frac{\partial}{\partial N} \{f_1(N)g_N^0\} + \frac{1}{2} \frac{\partial^2}{\partial N^2} \{f_2(N)g_N^0\} \quad (3.38)$$

where we have defined

$$f_1(N) = -2NW^+(N) + 2N(W^-(N) + \gamma_1) + 4N^2\gamma_2(N) + 6N^3\gamma_3(N), \quad (3.39)$$

and

$$f_2(N) = 2NW^+(N) + 2N(W^-(N) + \gamma_1) + 8N^2\gamma_2(N) + 18N^3\gamma_3(N). \quad (3.40)$$

The Fokker-Planck equation is valid as long as $\bar{N} \gg 1$ and $\sigma \gg 1$.

We approximate the solution of this Fokker-Planck equation by a Gaussian, and obtain the following equation for the mean number of condensate particles \bar{N}_{loss} :

$$\bar{f}_1 = 0. \quad (3.41)$$

The width of the Gaussian σ_{loss} is approximately given by

$$\sigma_{\text{loss}} = \sqrt{\frac{\bar{f}_2}{2\partial_{\bar{N}_{\text{loss}}} \bar{f}_1}}. \quad (3.42)$$

Using the assumption $\mu_{\bar{N}_{\text{loss}}}/kT \ll 1$ Eq. (3.41) can be solved analytically by approximating

$$W^+(N) \approx W_a^+ = \frac{4m(akT)^2}{\pi \hbar^3} e^{2\mu/kT}, \quad (3.43)$$

$$W^-(N) \approx W_a^-(N) = W_a^+ \left(1 + \frac{\mu N}{kT} + \frac{\mu^2 N}{2k^2 T^2}\right) e^{-\mu/kT}. \quad (3.44)$$

For the mean number of particles in the condensate, we obtain

$$\begin{aligned} \bar{N}_{\text{loss}} = & \left(-\frac{\gamma_2(1) + \mu_1 W_a^+ e^{-\mu/kT}/2}{3\gamma_3(1) + \mu_1^2 W_a^+ e^{-\mu/kT}/2} + \right. \\ & \left. \sqrt{\left(\frac{\gamma_2(1) + \mu_1 W_a^+ e^{-\mu/kT}/2}{3\gamma_3(1) + \mu_1^2 W_a^+ e^{-\mu/kT}/2} \right)^2 - \frac{\gamma_1 + W_a^+ (e^{-\mu/kT} - 1)}{3\gamma_3(1) + \mu_1^2 W_a^+ e^{-\mu/kT}/2}} \right)^{5/2}. \end{aligned} \quad (3.45)$$

Here $\mu_1 = \mu_{N=1}/kT$. Trap loss decreases the number of particles in the condensate. Also, the width of the particle distribution is decreased by the nonlinear loss. Both of these effects are well known in nonlinear optics [31]. Figure 3.4 shows the effect of trap loss on the mean number of particles in the condensate for a given T and μ for the parameters measured in Ref. [17]. The dominant contribution to the trap loss comes from three-particle loss, while one,- and two-particle losses are almost negligible. In the following sections we will omit the subscript loss since all the calculations will be done for finite trap loss.

3.4.2 Nonstationary solutions

From Eq. (3.17) we find the evolution equation [32] for the mean number of condensed particles \bar{N} .

$$\begin{aligned} \dot{\bar{N}} = & 2W^+(\bar{N})(\bar{N} + 1) - 2W^-(\bar{N})\bar{N} \\ & - 2\gamma_1 \bar{N} - 4\gamma_2(\bar{N})\bar{N}^2 - 6\gamma_3(\bar{N})\bar{N}^3. \end{aligned} \quad (3.46)$$

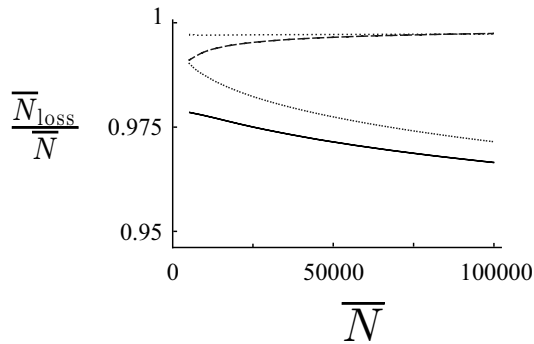


Fig. 3.4: Influence of trap loss on the mean number of particles in the condensate for rubidium. The trap frequencies are $f_x = f_y = f_z/\sqrt{8} = 47\text{Hz}$. The temperature of the thermal cloud is chosen $T = 0.5\mu\text{K}$. One-, two-, and three-particle losses are given by the dotted, dashed, and double dotted lines, respectively. The solid line accounts for all three kinds of loss. We have used $K_1 = 1/70\text{s}^{-1}$, $K_2 = 10^{-22}\text{m}^3/\text{s}$ and $K_3 = 6 \cdot 10^{-42}\text{m}^6/\text{s}$ [17].

By comparing Eq. (3.46) with the results obtained in Ref. [17] we find numerical values for the constants K_i . Equation (3.46) was investigated in Refs. [23, 33] for the case $\gamma_i = 0$. Here we only want to show that trap loss does not change the general behavior of the growth of the condensate. In Fig. 3.5 we show a comparison between the growth curve with and without trap loss. For the parameters chosen the time scale of condensate growth is influenced only slightly by trap loss.

3.4.3 Correlation functions

In this section we calculate the intensity and amplitude correlation functions for a condensate in the stationary state found in Sec. 3.4.1.

3.4.3.1 Ito equation

First we will show that if we restrict ourselves to situations where a large number of particles occupies the condensate and the density operator is almost diagonal in the basis $|N\rangle_N$, we can approximate Eq. (3.17) by a master equation of standard Lindblad form. To do so, we consider terms of the form

$$2C^\dagger\{F(\hat{N})\rho\}C - [CC^\dagger, \{F(\hat{N})\rho\}]_+, \quad (3.47)$$

define the operator $D = \sqrt{F(\tilde{N})}C$, and compare Eq. (3.47) with

$$2D^\dagger\rho D - [DD^\dagger, \rho]_+ \quad (3.48)$$

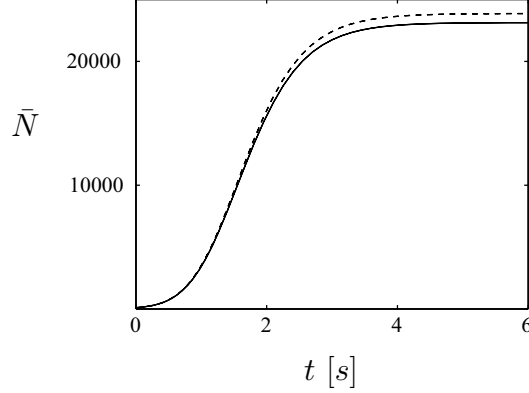


Fig. 3.5: Comparison between the growth of the condensate with trap loss (solid curve) and without trap loss (dashed curve). The parameters are chosen as $K_1 = 1/70\text{s}^{-1}$, $K_2 = 10^{-22}\text{m}^3/\text{s}$, and $K_3 = 6 \cdot 10^{-42}\text{m}^6/\text{s}$ [17]. Parameters for the thermal particles are $T = 0.5\mu\text{K}$ and $\mu = 3 \cdot 10^{-31}\text{J}$. The trap frequencies are chosen to be $f_x = f_y = f_z/\sqrt{8} = 47\text{Hz}$. The calculation is done for rubidium.

for a matrix element g'_N . Since we assume the trap loss to be a small effect compared to the interaction of the condensate with the thermal particles, the terms $C^\dagger C F(\hat{N})$ of the master equation (3.17) are of order $W^+ \bar{N}$. The only exception are the terms involving R_{00} [34]. Therefore, we find for all the terms in our master equation that the difference of Eqs. (3.47) and (3.48) for a matrix element g'_N is of the order of $\bar{N} W^+ (\bar{N}) (\nu/\bar{N})^2$. We will linearize the equations and neglect all terms of order $W^+ (\bar{N})/\bar{N}$. Therefore, we approximate the master equation (3.17) by replacing all the terms of the form Eq. (3.47) by expressions of the form of Eq. (3.48). This enables us to write down the Ito equation straightforwardly for the evolution of the system operators in the Heisenberg picture. Note that the noise terms appearing in the Ito equations do not have a direct physical interpretation. We only need them to have a mathematical equivalence between the solutions of the master equation and the solutions of the Ito equation. The Ito stochastic equation for an operator X in the Heisenberg picture reads

$$\begin{aligned}
dX &= \left\{ \frac{i}{\hbar} [H_0, X] \right. \\
&\quad - [X, \sqrt{W^+} B B^\dagger \sqrt{W^+}]_+ + 2\sqrt{W^+} B X B^\dagger \sqrt{W^+} \\
&\quad - [X, \sqrt{W^- + \gamma_1} B^\dagger B \sqrt{W^- + \gamma_1}]_+ \\
&\quad \quad + 2\sqrt{W^- + \gamma_1} B^\dagger X B \sqrt{W^- + \gamma_1} \\
&\quad - [X, \sqrt{R_{00}} (B B^\dagger)^2 \sqrt{R_{00}}]_+ + 2\sqrt{R_{00}} B B^\dagger X B B^\dagger \sqrt{R_{00}} \\
&\quad \left. - [X, \sqrt{\gamma_2} B^\dagger B^\dagger B B \sqrt{\gamma_2}]_+ + 2\sqrt{\gamma_2} B^\dagger B^\dagger X B B \sqrt{\gamma_2} \right.
\end{aligned}$$

$$\begin{aligned}
& -[X, \sqrt{\gamma_3} B^\dagger B^\dagger B^\dagger BBB \sqrt{\gamma_3}]_+ + 2\sqrt{\gamma_3} B^\dagger B^\dagger B^\dagger X BBB \sqrt{\gamma_3} \} dt \\
& - \left([X, \sqrt{2W^+} B] dC_1 - [X, B^\dagger \sqrt{2W^+}] dC_1^\dagger \right) \\
& - \left([X, \sqrt{2(W^- + \gamma_1)} B^\dagger] dC_2 - [X, B \sqrt{2(W^- + \gamma_1)}] dC_2^\dagger \right) \\
& - \left([X, \sqrt{2R_{00}} BB^\dagger] dC_3 - [X, \sqrt{2R_{00}} BB^\dagger] dC_3^\dagger \right) \\
& - \left([X, \sqrt{2\gamma_2} B^\dagger B^\dagger] dC_4 - [X, BB \sqrt{2\gamma_2}] dC_4^\dagger \right) \\
& - \left([X, \sqrt{2\gamma_3} B^\dagger B^\dagger B^\dagger] dC_5 - [X, BBB \sqrt{2\gamma_3}] dC_5^\dagger \right), \tag{3.49}
\end{aligned}$$

where dC_i are Ito noise increments. The only expectation values that are different from zero are

$$\langle dC_i(t) dC_i^\dagger(t) \rangle = dt. \tag{3.50}$$

Note that all the rates appearing in Eq. (3.49) depend on the number operator \tilde{N} and, that therefore we use relations like [for example, for $W^-(\tilde{N})$]

$$\begin{aligned}
BW^-(\tilde{N}) &= W^-(\tilde{N} + 1)B \approx \left(W^-(\tilde{N}) + \frac{dW^-(\tilde{N})}{d\tilde{N}} \right) B \\
&= (W^- + \partial_{\tilde{N}} W^-) B \tag{3.51}
\end{aligned}$$

to calculate commutators between these rates and B .

3.4.3.2 Intensity fluctuations

We define the operator

$$\delta I_B = \frac{\tilde{N} - \langle \tilde{N} \rangle}{\sqrt{\langle \tilde{N} \rangle}}, \tag{3.52}$$

where we omit the time dependence whenever this can be done without causing confusion. For δI_B we obtain

$$d\delta I_B = -\gamma_I \delta I_B dt + dC_I, \tag{3.53}$$

where

$$\begin{aligned}
dC_I &= \left(\sqrt{2W^+} B dC_1 + B^\dagger \sqrt{2W^+} dC_1^\dagger + \right. \\
& - \sqrt{2(W^- + \gamma_1)} B^\dagger dC_2 - B \sqrt{2(W^- + \gamma_1)} dC_2^\dagger \\
& - 2\sqrt{2\gamma_2} B^\dagger B^\dagger dC_4 - 2BB \sqrt{2\gamma_2} dC_4^\dagger \\
& \left. - 3\sqrt{2\gamma_3} B^\dagger B^\dagger B^\dagger dC_5 - 3BBB \sqrt{2\gamma_3} dC_5^\dagger \right) \frac{1}{\sqrt{N}}. \tag{3.54}
\end{aligned}$$

We expand around \bar{N} and obtain

$$\gamma_I = \partial_{\bar{N}} \bar{f}_1 \approx 2\bar{N} \partial_{\bar{N}} \bar{W}^- + \frac{8}{5} \bar{\gamma}_2 \bar{N} + \frac{24}{5} \bar{\gamma}_3 \bar{N}^2. \quad (3.55)$$

which is now only a function of the expectation value of \tilde{N} . Keeping only these highest-order terms, we can solve Eq. (3.53) and obtain

$$\delta I_B(t) = \delta I_B(0) e^{-\gamma_I t} + \int_0^t e^{-\gamma_I(t-t')} dC_I(t'). \quad (3.56)$$

Using $\langle dC_I(t) dC_I^\dagger(t) \rangle = \bar{f}_2 dt / \bar{N}$ and considering only $t + s \gg \gamma_I^{-1}$ we obtain for the correlation function $\langle \tilde{N}(t), \tilde{N}(s) \rangle$

$$\langle N(t), N(s) \rangle = \frac{\bar{f}_2}{2\gamma_I} e^{-\gamma_I |t-s|} = \sigma^2 e^{-\gamma_I |t-s|}. \quad (3.57)$$

Note that the operator δI_B is of order 1. For $\gamma_2 = \gamma_3 = 0$ we find for the Mandel Q parameter

$$Q \approx \frac{5kT}{2\mu_{\bar{N}}} - 1. \quad (3.58)$$

This means that as long as there is a significant thermal bath, Q will always be larger than 0 since in this case $\mu_{\bar{N}}/kT < 1$ holds. However, since the result for Q also follows from statistical mechanics the restriction $\mu_{\bar{N}}/kT < 1$ is not necessary for this result to be valid, and we obtain sub-Poissonian statistics for $\mu_{\bar{N}}/kT > 5/2$.

3.4.3.3 Amplitude fluctuations

We use the Ito equation introduced above to calculate the phase fluctuations. In particular we calculate the correlation function

$$\langle B^\dagger(t) B(s) \rangle. \quad (3.59)$$

First we simplify Eq. (3.49) for $X = B$ and find

$$dB = -\gamma_B B dt + dC_B, \quad (3.60)$$

where to leading order in \bar{N}

$$\gamma_B = \frac{i\mu_{\bar{N}}}{\hbar} + \frac{16}{25} \bar{R}_{00} + \sqrt{\bar{N}} \delta I_B \left(\frac{i\partial_{\bar{N}} \mu_{\bar{N}}}{\hbar} + \frac{\gamma_I}{2\bar{N}} - \frac{32\bar{R}_{00}}{125\bar{N}} \right). \quad (3.61)$$

The terms of order \bar{W}^\pm/\bar{N} have been neglected. Expressions like Eq. (3.61) appear in optics in connection with the Kerr effect [35]. The noise term reads

$$\begin{aligned}
dC_B = & \left(\sqrt{2W^+} + \frac{\partial_N W^+}{\sqrt{2W^+}} B^\dagger B \right) dC_1^\dagger - \frac{\partial_N W^+}{\sqrt{2W^+}} BB dC_1 \\
& + \left(-\sqrt{2(W^- + \gamma_1)} - \frac{\partial_N W^-}{\sqrt{2(W^- + \gamma_1)}} BB^\dagger \right) dC_2 \\
& + \frac{\partial_N W^-}{\sqrt{2(W^- + \gamma_1)}} BB dC_2^\dagger \\
& + \left(-\frac{\partial_N R_{00}}{\sqrt{2R_{00}}} B^\dagger B - \sqrt{2R_{00}} \right) B (dC_3 - dC_3^\dagger) \\
& + \left(-\frac{\partial_N \gamma_2}{\sqrt{2\gamma_2}} B^\dagger B^\dagger B - 2\sqrt{2\gamma_2} B^\dagger \right) dC_4 + \frac{\partial_N \gamma_2}{\sqrt{2\gamma_2}} BBB dC_4^\dagger \\
& + \left(-\frac{\partial_N \gamma_3}{\sqrt{2\gamma_3}} B^\dagger B^\dagger B^\dagger B - 3\sqrt{2\gamma_3} B^\dagger B^\dagger \right) dC_5 + \frac{\partial_N \gamma_3}{\sqrt{2\gamma_3}} BBBB dC_5^\dagger.
\end{aligned} \tag{3.62}$$

We define the operator $\Phi = \frac{1}{\sqrt{B^\dagger B + 1}} B$ and find the following equation for Φ

$$d\Phi = \left(-\gamma_B dt + dC_\phi - \frac{1}{2\sqrt{N}} d\delta I_B \right) \Phi \tag{3.63}$$

Keeping only the leading terms, we obtain for dC_ϕ

$$dC_\phi = \left(-\frac{\partial_N R_{00}}{\sqrt{2R_{00}}} B^\dagger B - \sqrt{2R_{00}} \right) (dC_3 - dC_3^\dagger) \tag{3.64}$$

and find

$$dC_\phi(t) dC_\phi(t) = 2 \left(-\frac{16}{25} \bar{R}_{00} + \sqrt{\bar{N}} \delta I_B \frac{32\bar{R}_{00}}{125\bar{N}} \right) dt. \tag{3.65}$$

Equation (3.63) can be treated as a c -number equation for Φ , since i times the noise term in this equation has the properties of a classical noise term. We define an operator $\Phi = e^{i\phi}$ and obtain, for its increment,

$$d\phi = \left(-\frac{\mu\bar{N}}{\hbar} - \frac{\partial_{\bar{N}} \mu\bar{N}}{\hbar} \sqrt{\bar{N}} \delta I_B \right) dt - idC_\phi \tag{3.66}$$

In this equation the intensity noise dC_I is independent of the phase noise dC_ϕ , so that the equation for ϕ is very similar to the equations appearing in the phase diffusion model for a laser with colored noise [36]. We may use the same method as used in quantum optics to calculate the correlation function $\langle B^\dagger(t)B(s) \rangle$, and obtain

$$\begin{aligned}
\langle B^\dagger(t)B(s) \rangle = & \bar{N} e^{(i\frac{\mu\bar{N}}{\hbar} - \frac{16}{25}R_{00})(t-s)} \\
& \times e^{\left(-\left(\frac{\sigma_{\bar{N}} \mu\bar{N}}{\gamma_I \hbar} \right)^2 (\gamma_I(t-s) + e^{-\gamma_I(t-s)} - 1) \right)}
\end{aligned} \tag{3.67}$$

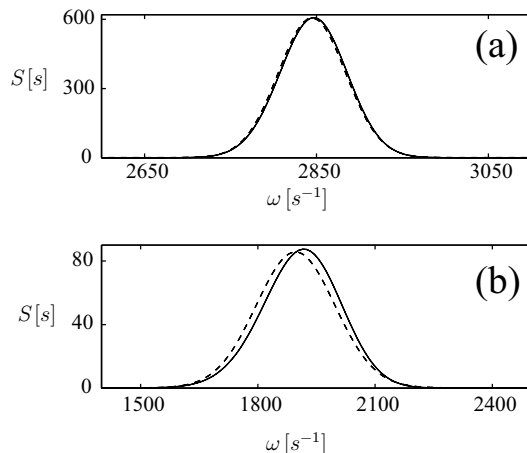


Fig. 3.6: Spectrum of the amplitude fluctuations $S(\omega)$ as defined in Eq. (3.68) against ω for rubidium. The trap frequencies are chosen to be $f_x = f_y = f_z/\sqrt{8} = 47\text{Hz}$. The numerical solutions are given by the solid lines, and the dashed lines represent the analytical results. In (a) the parameters of the thermal cloud are chosen to be $T = 0.25\mu\text{K}$ and $\mu = 3 \cdot 10^{-31}\text{J}$. The mean number of particles therefore is $\bar{N} = 23800$. Plot (b) shows the spectrum for $T = 0.9\mu\text{K}$ and $\mu = 2 \cdot 10^{-31}\text{J}$, and therefore a mean number of condensate particles $\bar{N} = 8640$.

for $t > s$ in the stationary state. In the range of validity of our approximations the result for this correlation function Eq. (3.67) agrees with the result obtained in QKIII [Eq. (184) of Ref. [3]]. If we were to keep the terms of $O(1/\sqrt{\bar{N}})$ in the noise terms the phase noise would no longer be independent of the intensity noise and the solution to Eq. (3.66) would not be so easy to find. The correlation function (3.67) depends only on the time difference $t - s$. The spectrum is found by a Fourier transformation in the time difference $t - s$

$$S(\omega) = \frac{1}{\sqrt{2\pi}} \int_{-\infty}^{\infty} d\Delta t e^{-i\omega\Delta t} \langle B^\dagger(t + \Delta t)B(t) \rangle. \quad (3.68)$$

Fig. 3.6 shows a comparison between the analytic result [Eq. (3.67)] and the direct numerical solution of Eq. (3.17). For a large number of condensate particles \bar{N} , the results agree very well with each other. In case of small particle numbers \bar{N} the linearization used to obtain the analytic result shifts the curve compared to the numerical result. Even so, the shape of the solution is very well approximated by the analytic formula. The spectrum $S(\omega)$ is expected to be of Lorentzian shape around its maximum value. Further away from the center, the shape becomes Gaussian. However, for the parameters chosen in Fig. 3.6 the Gaussian part dominates.

3.5 Conclusions

In this paper we have calculated the correlation functions for amplitude (phase) and intensity fluctuations of a Bose condensate due to interactions with a heat and particle reservoir, representing uncondensed atoms at finite temperature. The present analysis is valid for a strongly condensed system confined in a trapping potential, ignoring contributions from quasiparticle excitations [3]. Finally, we point out that the present theory is readily adapted to a class of highly interesting problems, such as the study of decoherence in Josephson-like situations, where two trapped condensates are brought into contact and the quantum dynamics of the relative phase of the two condensates is observed [12, 37].

Acknowledgments

We like to thank M. Holland, J. Williams, K. Ellinger and H. Ritsch for stimulating discussions. This work was supported by the Marsden Fund under Contract No. PVT-603, and by Österreichische Fonds zur Förderung der wissenschaftlichen Forschung. Part of this work was supported by TMR Network No. ERB 4061 PL 95-0044.

3.A Stationary solution for a canonical bath of particles

We want to investigate the fluctuations in the number of particles of a Bose-Einstein condensate, assuming the system to be in the canonical ensemble. We will include interactions between the Bose particles in our analysis, and investigate their effects on the condensate fluctuations. On first glance one might expect that it would be satisfactory to account for the interaction effects by just including the mean field of the condensate (in the Thomas-Fermi approximation). However, in this approach fluctuations in the size of the condensate lead to an unrealistically large shift of the energy levels, which prevents any condensation [25]. The inclusion of the mean field of the thermal density of particles reduces the shift of the energy levels. As long as fluctuations in the chemical potentials of the thermal cloud μ and the condensate μ_N are small compared to the energy gap between the condensate energy and the first excitation energy, fluctuations will not lead to degeneracy in the thermal cloud. The excitation energies therefore depend mainly on the total number of thermal particles M and the number of particles in the condensate N . We will assume that the eigenenergies of the excited levels depend on M and N but are independent of n_m , i.e., the microstate of the system. As shown in

Ref. [38], the density of particlelike states is much larger than the density of quasiparticles. Thermodynamic quantities of the Bose gas are therefore mainly determined by the particlelike states, which allows us to use the Hartree-Fock approximation for describing the interactions in the thermal cloud.

3.A.1 Excited modes

We denote the energies and the wave functions of the excited states by ϵ_m and $\xi_m(\mathbf{x})$, respectively. The occupation of these levels is n_m . In the Hartree-Fock approximation [39], the effective potential for the thermal particles $V_{\text{eff}}(\mathbf{x})$ is given by

$$V_{\text{eff}}(\mathbf{x}) = V_T(\mathbf{x}) + 2uN |\xi_N(\mathbf{x})|^2 + 2u\tilde{n}(\mathbf{x}), \quad (3.69)$$

with $\tilde{n}(\mathbf{x})$ the density of the noncondensed particles.

3.A.2 Weakly interacting Bose gas in the canonical ensemble

The density operator of a Bose gas in the canonical ensemble is given by

$$\rho_c = \frac{1}{Z_c} e^{-\beta H}, \quad (3.70)$$

where $\beta = 1/kT$, with T the temperature of the system. The partition function Z_c is given by $Z_c = \text{tr} \{e^{-\beta H}\}$. We want to investigate the properties of a Bose condensate in the canonical ensemble. The eigenstates $\{\xi_N(\mathbf{x}), \xi_m(\mathbf{x})\}$ and the corresponding eigenenergies $\{E_0, \epsilon_m\}$ depend on the number of condensate particles N and on the number of particles out of the condensate $M = \sum_m n_m$. The total number of particles N_{tot} is constant,

$$N_{\text{tot}} = N + M = \text{const.} \quad (3.71)$$

The state of the system with N particles in the condensate and n_m particles in the levels ϵ_m is denoted by $|\mathbf{n}\rangle$ where $\mathbf{n} = \{N, n_1, \dots, n_m, \dots\}$. We can therefore write for the matrix elements of the density operator $p(\mathbf{n}) = \langle \mathbf{n} | \rho_c | \mathbf{n} \rangle$

$$p(\mathbf{n}) \propto e^{-\beta E_0(N, M) - \beta \sum_m \epsilon_m(N, M) n_m} \quad (3.72)$$

As can be seen from Eq. (3.72), the condensate energy $E_0(N, M)$ and the excitation energies $\epsilon_m(N, M)$ are functions of the number of condensate particles N and the number of noncondensed particles M . In our calculations we will assume that the influence of the number of noncondensed particles M on the condensate energy is negligible, since the number of noncondensed particles that are inside the condensate region is much smaller than the number of condensed particles. Moreover, the width of the condensate particle distribution is only influenced by the change of the number of noncondensed particles in

the condensate region due to fluctuations in M . The other interaction effects i.e., (i) the influence of the condensate mean field on the excited levels, (ii) the influence of the mean field of the thermal cloud on the excited levels, and (iii) the influence of the condensate mean field on the energy of the condensate, will be included in our calculations.

3.A.3 Particle number distribution of the condensate

Since we are only interested in the probability of finding N particles in the condensate we want to find

$$p(N, M) = \sum_{\{n_m\}} p(N, n_m) \quad (3.73)$$

summed under the constrained $M = \sum_m n_m$. We can do this summation by introducing a contour integral writing

$$p(N, M) \propto e^{-\beta E_0(N, M)} \quad (3.74)$$

$$\times \frac{1}{2\pi i} \int_C \frac{dz}{z} z^{-M} \prod_m \sum_{n_m=0}^{\infty} e^{-\beta \epsilon_m(N, M) n_m} z^{n_m},$$

and integrating using the method of steepest descents to obtain

$$p(N, M) \propto e^{-\beta E_0(N, M) - (M+1) \ln(\bar{z}) - \sum_m \ln(1 - \bar{z} e^{-\beta \epsilon_m(N, M)})}$$

$$\times \left(\frac{M+1}{\bar{z}^2} + \sum_m \frac{e^{-2\beta \epsilon_m(N, M)}}{(1 - \bar{z} e^{-\beta \epsilon_m(N, M)})^2} \right)^{-1/2}. \quad (3.75)$$

\bar{z} depends on M and N , and is given by the solution of

$$M+1 = \sum_m \frac{1}{e^{\beta \epsilon_m(N, M)} \bar{z}^{-1} - 1}. \quad (3.76)$$

By defining

$$F(N, M) = E_0(N, M) + \frac{M}{\beta} \ln(\bar{z})$$

$$+ \frac{1}{\beta} \sum_m \ln(1 - \bar{z} e^{-\beta \epsilon_m(N, M)}), \quad (3.77)$$

$$C(N, M) = \left\{ \ln(\partial_M \ln(\bar{z})) - \ln \left(\bar{z} \sum_m \frac{\beta \partial_M \epsilon_m(N, M)}{e^{\beta \epsilon_m(N, M)} - \bar{z}} \right) \right.$$

$$\left. + \bar{z}^2 \sum_m \frac{\beta \partial_M \epsilon_m(N, M)}{(e^{\beta \epsilon_m(N, M)} - \bar{z})^2} + 1 \right\} \frac{1}{2}, \quad (3.78)$$

and using Eq. (3.76), we may rewrite Eq. (3.75)

$$p(N, M) \propto e^{-\beta F(N, M) + C(N, M)}. \quad (3.79)$$

$C(N, M)$ is a small logarithmic correction to $\beta F(N, M)$ that we neglect in our further calculations. Consistent with the neglect of $C(N, M)$, we approximate $M + 1$ by M in Eq. (3.76) and use the equations

$$M = \sum_m \frac{1}{e^{\beta \epsilon_m(N, M)} \bar{z}^{-1} - 1}, \quad (3.80)$$

and

$$p(N, M) \propto e^{-\beta F(N, M)}. \quad (3.81)$$

$F(N, M)$ is the Helmholtz free energy of the system. The chemical potentials of the condensate and the thermal bath are therefore given by the partial derivatives of $F(N, M)$ with respect to N and M , respectively.

3.A.3.1 Stationary solution

The chemical potential of the condensate in the canonical ensemble $\mu_c(N, M)$ is given by

$$\begin{aligned} \mu_c(N, M) &= \partial_N F(N, M) \\ &= \partial_N E_0(N, M) + \sum_m \frac{\bar{z} \partial_N \epsilon_m(N, M)}{e^{\beta \epsilon_m} - \bar{z}}, \end{aligned} \quad (3.82)$$

and the chemical potential of the noncondensed particles in the canonical ensemble $\mu_v(N, M)$ reads

$$\begin{aligned} \mu_v(N, M) &= \partial_M F(N, M) \\ &= \frac{\ln(\bar{z})}{\beta} + \partial_M E_0(N, M) + \\ &\quad \sum_m \frac{\bar{z} \partial_M \epsilon_m(N, M)}{e^{\beta \epsilon_m} - \bar{z}} \end{aligned} \quad (3.83)$$

If the total number of particles is fixed, the condensate particle distribution will reach its maximum value for $N = \bar{N}$ and $M = \bar{M} = N_{\text{tot}} - \bar{N}$, where \bar{N} can be found by solving

$$\mu_v(\bar{N}, N_{\text{tot}} - \bar{N}) = \mu_c(\bar{N}, N_{\text{tot}} - \bar{N}). \quad (3.84)$$

The width of the stationary canonical distribution σ_{can} is given by

$$\sigma_{\text{can}} = \{\beta \partial_{\bar{N}} (\mu_c(N, N_{\text{tot}} - N) - \mu_v(N, N_{\text{tot}} - N))\}^{-1/2}. \quad (3.85)$$

In the above equations (3.82) and (3.83), the terms including derivatives of $\epsilon_m(N, M)$ are corrections to the chemical potentials due to the shift of the excited energy levels with changing M and N . The term $\partial_M E_0(N, M)$ in Eq. (3.83) is the correction to the chemical potential of the thermal bath due to changes in the condensate energy. By assuming $E_0(N, M) \approx E_0(N)$, we will neglect this term.

3.A.3.2 Method of solving for $p(N, M)$

For simplicity we will assume that the energy and wave function of the condensate are only functions of the number of condensed particles, and use the Thomas-Fermi expressions (3.11) and (3.12), respectively. The influence of the thermal particles on the energy and wave function of the condensate will become important at temperature close to T_c and may therefore only be neglected at very low temperatures [25].

We replace the sum in Eq. (3.80) by an integral

$$\sum_m \rightarrow \int d\epsilon g(\epsilon), \quad (3.86)$$

where $g(\epsilon)$ is the density of states and use the semiclassical expression

$$g(\epsilon) = \frac{1}{(2\pi\hbar)^3} \int d^3x \int d^3p \delta\left(\epsilon - \frac{\mathbf{p}^2}{2m} - V_{\text{eff}}(\mathbf{x})\right), \quad (3.87)$$

to obtain, for a spherically symmetric effective potential and given M and N ,

$$\begin{aligned} M &= 4\pi \int_0^\infty r^2 dr \tilde{n}(r) = \\ &= \left(\frac{mkT}{2\pi\hbar^2}\right)^{3/2} 4\pi \int_0^\infty r^2 dr G_{3/2}\left(\frac{V_{\text{eff}}(\mathbf{x})}{kT} - \ln(\bar{z})\right). \end{aligned} \quad (3.88)$$

Here $G_\sigma(x) = \sum_{n=1}^\infty n^{-\sigma} e^{-nx}$ denotes the Bose functions. By solving this equation numerically we obtain \bar{z} as well as the density of noncondensed particles $\tilde{n}(r)$. Given a fixed total number of particles N_{tot} and a temperature T of the system, we find the particle distribution function $p(N, M)$ from Eq. (3.81) by replacing

$$\begin{aligned} & - \sum_m \ln\left(1 - \bar{z} e^{-\beta\epsilon_m(N, M)}\right) \\ &= \left(\frac{2mkT}{\pi\hbar^2}\right)^{3/2} \frac{\pi}{2} \int_0^\infty r^2 dr G_{5/2}\left(\frac{V_{\text{eff}}(\mathbf{x})}{kT} - \ln(\bar{z})\right). \end{aligned} \quad (3.89)$$

in the expression Eq. (3.77) for $F(N, M)$.

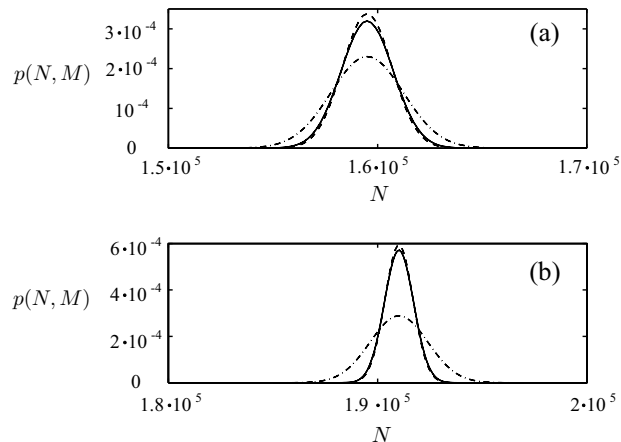


Fig. 3.7: Condensate particle distribution for (a) $T = 0.35\mu K$, $\bar{N} = 1.595 \cdot 10^5$, and $\bar{N}/N_{\text{tot}} \approx 10\%$, and (b) $T = 0.2\mu K$, $\bar{N} = 1.910 \cdot 10^5$, and $\bar{N}/N_{\text{tot}} \approx 33\%$. Both plots are for Rb and a trap frequency of $f_x = f_y = f_z = 66\text{Hz}$. The solid line shows the solution for the canonical ensemble including the mean-field effects, the dashed line is the canonical solution using the mean effective potential $\bar{V}_{\text{eff}}(\mathbf{x})$, and the dash-dotted line is the grand canonical result.

3.A.3.3 Solutions

We want to compare $p(N, M)$ with the solution for a grand canonical bath of thermal particles not influenced by mean-field effects as given in Eq. (3.36). To distinguish between the effect of choosing a different thermodynamic ensemble and the effect of including the change of the mean field due to condensate fluctuations, we will plot a third distribution obtained from the canonical ensemble with a fixed mean effective potential $\bar{V}_{\text{eff}}(\mathbf{x})$ that is given by

$$\bar{V}_{\text{eff}}(\mathbf{x}) = V_T(\mathbf{x}) + 2u\bar{N} |\xi_{\bar{N}}(\mathbf{x})|^2 + 2u\bar{n}(\mathbf{x}), \quad (3.90)$$

where $\bar{n}(\mathbf{x})$ is the thermal density obtained for \bar{N} particles in the condensate, and $N_{\text{tot}} - \bar{N}$ particles in the thermal cloud. In Fig. 3.7, we plot the different particle distributions. For the three curves in each set the number of particles in the condensate \bar{N} is the same. Since the inclusion of the mean-field effects shifts the chemical potential of the noncondensed atoms, the two canonical solutions are not plotted for the same total number of particles. If we were to plot the canonical solutions with and without inclusion of the mean-field effects at the same total number of particles N_{tot} , their maxima would be shifted against each other. As can be seen from Fig. 3.7, the stationary state of a Bose condensate in the canonical ensemble is different from the stationary state of a Bose condensate interacting with a bath of particles in the grand canonical ensemble. When the ratio $\bar{N}/N_{\text{tot}} \approx 10\%$ this difference is

not significant, but for larger condensates, i.e., $\bar{N}/N_{\text{tot}} > 30\%$, the difference might become substantial.

As shown in this appendix, the model used to describe the thermal bath of atoms may have some influence on the particle fluctuations in the condensate. We also expect the intensity relaxation rate γ_I to be influenced by the particular model used for the noncondensed particles. However, a further more detailed analysis of such effects including a treatment of the excitation modes as given in Ref. [40] lies beyond the scope of this paper, and will be presented elsewhere [25, 26].

3.B Calculation of $R_{00}(N)$

We show how the expressions (3.27,3.28) are derived from Eq. (141) in Ref. [3].

3.B.1 Simplifying the integral

R_{00} is defined by

$$\begin{aligned} R_{00}(N) = & \frac{4u^2}{(2\pi)^5 \hbar^2} \int d^3 \mathbf{u} \int d^3 \mathbf{K}_1 \int d^3 \mathbf{K}_2 \int d^3 \mathbf{k} \int d^3 \mathbf{k}' \\ & \times \delta(\mathbf{K}_1 - \mathbf{K}_2 - \mathbf{k} + \mathbf{k}') F(\mathbf{K}_1, \mathbf{u}) (1 + F(\mathbf{K}_2, \mathbf{u})) \\ & \times W_0(\mathbf{u}, \mathbf{k}) W_0(\mathbf{u}, \mathbf{k}') \delta(\Delta\omega_{12}(\mathbf{u})), \end{aligned} \quad (3.91)$$

where

$$W_0(\mathbf{u}, \mathbf{k}) = \frac{1}{(2\pi)^3} \int d^3 \mathbf{v} \xi_N^*(\mathbf{u} + \frac{\mathbf{v}}{2}) \xi_N(\mathbf{u} - \frac{\mathbf{v}}{2}) e^{i\mathbf{k}\cdot\mathbf{v}}, \quad (3.92)$$

and $\Delta\omega_{12}(\mathbf{u})$ accounts for energy conservation. We assume that within the range of the condensate $F(\mathbf{K}, \mathbf{u})$ is constant, and that the factor $1 + F(\mathbf{K}_2, \mathbf{u}) \approx 1$. Integrating over \mathbf{K}_2 and defining $\mathbf{Q} = \mathbf{k} - \mathbf{k}'$ yields

$$\begin{aligned} R_{00}(N) = & \frac{4u^2}{(2\pi)^5 \hbar^2} \frac{2m}{\hbar} \int d^3 \mathbf{K}_1 \int d^3 \mathbf{Q} \delta(\mathbf{Q} \cdot (\mathbf{Q} + 2\mathbf{K}_1)) F(\mathbf{K}_1, 0) \\ & \times \int d^3 \mathbf{k}' \int d^3 \mathbf{u} \frac{1}{(2\pi)^6} \int d^3 \mathbf{v}' \int d^3 \mathbf{v} \xi_N^*(\mathbf{u} + \frac{\mathbf{v}}{2}) \xi_N(\mathbf{u} - \frac{\mathbf{v}}{2}) \\ & \times \xi_N^*(\mathbf{u} + \frac{\mathbf{v}'}{2}) \xi_N(\mathbf{u} - \frac{\mathbf{v}'}{2}) e^{i\mathbf{k}'\cdot(\mathbf{v}+\mathbf{v}') + i\mathbf{Q}\cdot\mathbf{v}}. \end{aligned} \quad (3.93)$$

By integrating over \mathbf{k}' and over \mathbf{v}' and defining

$$\begin{aligned} G^2(\mathbf{Q}) = & \frac{1}{(2\pi)^3} \int d^3 \mathbf{u} \int d^3 \mathbf{v} \left| \xi_N(\mathbf{u} + \frac{\mathbf{v}}{2}) \right|^2 \\ & \left| \xi_N(\mathbf{u} - \frac{\mathbf{v}}{2}) \right|^2 e^{i\mathbf{Q}\cdot\mathbf{v}} \end{aligned} \quad (3.94)$$

we obtain

$$R_{00}(N) = \frac{4u^2}{(2\pi)^5 \hbar^2} \frac{2m}{\hbar} \int d^3 \mathbf{K}_1 \int d^3 \mathbf{Q} \delta(\mathbf{Q} \cdot (\mathbf{Q} + 2\mathbf{K}_1)) F(\mathbf{K}_1, 0) G^2(\mathbf{Q}). \quad (3.95)$$

Now we approximate $\mathbf{Q} + 2\mathbf{K}_1 \approx 2\mathbf{K}_1$, since $G^2(\mathbf{Q})$ is sharply peaked around $\mathbf{Q} = \mathbf{0}$ compared to the width of $F(\mathbf{K}_1, 0)$. Replacing the notation \mathbf{K}_1 by \mathbf{K} , choosing the K_z axis in the direction of \mathbf{Q} , we obtain

$$R_{00}(N) = \frac{4u^2 m}{(2\pi)^5 \hbar^3} \int d^3 \mathbf{Q} \int dK_x \int dK_y \int dK_z \delta(QK_z) e^{(-\frac{\hbar^2(K_x^2 + K_y^2 + K_z^2)}{2m} + \mu)/kT} G^2(\mathbf{Q}). \quad (3.96)$$

Here Q denotes the modulus of \mathbf{Q} . Then we do the integration over \mathbf{K} to obtain

$$R_{00}(N) = \frac{8u^2 \pi m^2 kT}{(2\pi)^5 \hbar^5} e^{\mu/kT} \int d^3 \mathbf{Q} \frac{G^2(\mathbf{Q})}{Q}. \quad (3.97)$$

So far we have not assumed a particular form of the trapping potential or the condensate wave function. These properties are contained in the function $G(\mathbf{Q})$.

3.B.2 Calculating the function $G(\mathbf{Q})$ for the harmonic oscillator

The trapping potential is of the form $V_T(\mathbf{x}) = ax^2 + by^2 + cz^2$ with $a = m\omega_x^2/2$, $b = m\omega_y^2/2$ and $c = m\omega_z^2/2$. We change the variables by defining $\mathbf{x} = \mathbf{u} + \frac{\mathbf{v}}{2}$ and $\mathbf{y} = \mathbf{u} - \frac{\mathbf{v}}{2}$ and get

$$G^2(\mathbf{Q}) = \frac{1}{(2\pi)^3} \int d^3 \mathbf{x} \int d^3 \mathbf{y} |\xi_N(\mathbf{x})|^2 |\xi_N(\mathbf{y})|^2 e^{i\mathbf{Q} \cdot (\mathbf{x} - \mathbf{y})}, \quad (3.98)$$

and therefore

$$G(\mathbf{Q}) = \frac{1}{(2\pi)^{3/2}} \int d^3 \mathbf{x} |\xi_N(\mathbf{x})|^2 e^{i\mathbf{Q} \cdot \mathbf{x}}. \quad (3.99)$$

Using the Thomas-Fermi approximation for the condensate wave function, defining $Q'_x = Q_x/\sqrt{a}$, $Q'_y = Q_y/\sqrt{b}$ and $Q'_z = Q_z/\sqrt{c}$, and changing the variables $x' = x\sqrt{a}$, $y' = y\sqrt{b}$ and $z' = z\sqrt{c}$, simplifies the integral to

$$G(\mathbf{Q}) = \frac{1}{(2\pi)^{3/2} \sqrt{abc} N u} \int_{\mathbf{x}'^2 < \mu_N} d^3 \mathbf{x}' (\mu_N - \mathbf{x}'^2) e^{i\mathbf{Q}' \cdot \mathbf{x}'}. \quad (3.100)$$

Integrating in spherical coordinates we obtain

$$\begin{aligned} G(\mathbf{Q}) &= \frac{2}{\sqrt{2\pi abcNuQ'}} \int_0^{\sqrt{\mu_N}} dr (r\mu_N - r^3) \sin(Q'r) \\ &= \frac{4}{\sqrt{abcNuQ'^5}} [(3 - \mu_N Q'^2) \sin(Q'\sqrt{\mu_N}) - \\ &\quad 3\sqrt{\mu_N} Q' \cos(Q'\sqrt{\mu_N})], \end{aligned} \quad (3.101)$$

where $Q' = \sqrt{Q_x'^2 + Q_y'^2 + Q_z'^2}$.

3.B.3 Integration over \mathbf{Q}

Last we will now find an expression for the integral

$$\Omega = \int d^3\mathbf{Q} \frac{G^2(\mathbf{Q})}{Q}. \quad (3.102)$$

We make use of the fact that $G(\mathbf{Q})$ only depends on Q' by replacing $d^3\mathbf{Q} = \sqrt{abc} d^3\mathbf{Q}'$ using spherical coordinates, and change the variable

$$Q' \rightarrow \sqrt{\mu_N} Q' = T. \quad (3.103)$$

The modulus Q can be expressed in terms of \mathbf{Q}' as

$$Q = Q' \sqrt{a \sin^2 \theta \cos^2 \phi + b \sin^2 \theta \sin^2 \phi + c \cos^2 \theta}. \quad (3.104)$$

We obtain

$$\begin{aligned} \Omega &= \frac{8\mu_N^4}{\pi \sqrt{abcN^2u^2}} \int_0^{2\pi} d\phi \int_0^\pi d\theta \frac{\sin(\theta)}{\sqrt{a \sin^2 \theta \cos^2 \phi + b \sin^2 \theta \sin^2 \phi + c \cos^2 \theta}} \\ &\quad \times \int_0^\infty dT \frac{1}{T^9} [(3 - T^2) \sin(T) - 3T \cos(T)]^2. \end{aligned} \quad (3.105)$$

Next we integrate over T , define $x = \cos \theta$, $\alpha^2 = c - a \cos^2 \phi - b \sin^2 \phi$, and $\beta^2 = (a \cos^2 \phi + b \sin^2 \phi)/\alpha^2$, and write

$$\begin{aligned} \Omega &= \frac{\mu_N^4}{9\pi \sqrt{abcN^2u^2}} \int_0^{2\pi} d\phi \frac{1}{\alpha} \int_{-1}^1 \frac{dx}{\sqrt{x^2 + \beta^2}} \\ &= \frac{2\mu_N^4}{9\pi \sqrt{abcN^2u^2}} \int_0^{2\pi} d\phi \frac{\operatorname{arcsinh}(\beta^{-1})}{\alpha}. \end{aligned} \quad (3.106)$$

In the case $\alpha^2 < 0$ we take the modulus of α^2 and replace $\operatorname{arcsinh} \rightarrow \operatorname{arcsin}$. To further evaluate this integral we now assume that $a = b$. Then $\alpha^2 = c - a$ and $\beta^2 = a/(c - a)$. The integration over ϕ then yields a factor of 2π , and we obtain the expressions given in Eqs. (3.27) and (3.28). $R_{00}(N)$ therefore depends on the number of particles in the condensate as $N^{-2/5}$.

References

- [1] C. W. Gardiner and P. Zoller, Phys. Rev. A **55**, 2902 (1997).
- [2] D. Jaksch, C. W. Gardiner, and P. Zoller, Phys. Rev. A **56**, 575 (1997).
- [3] C. W. Gardiner and P. Zoller, cond-mat/9712002.
- [4] J. Anglin, Phys. Rev. Lett. **79**, 6 (1997).
- [5] M. Anderson, J. R. Ensher, M. R. Matthews, C. E. Wieman, and E. A. Cornell, Science **269**, 198 (1995).
- [6] K. B. Davis, M-O. Mewes, M. R. Andrews, N. J. van Druten, D. S. Durfee, D. M. Kurn, and W. Ketterle, Phys. Rev. Lett. **75**, 3969 (1995).
- [7] C. C. Bradley, C. A. Sackett, J. J. Tollet, and R. Hulet, Phys. Rev. Lett. **75**, 1687 (1995).
- [8] D. J. Heinzen, see <http://storm.ph.utexas.edu/dept/research/heinzen/bose.html>
- [9] L. Hau, see <http://amo.phy.gasou.edu/bec.html/>
- [10] B. Anderson and M. Kasevich, see <http://amo.phy.gasou.edu/bec.html/>
- [11] G. Rempe, see <http://amo.phy.gasou.edu/bec.html/>
- [12] P. Villain, M. Lewenstein, R. Dum, Y. Castin, L. You, A. Imamoglu, and T. B. A. Kennedy, J. Mod. Optics, **44**, 1775 (1997).
- [13] J. Javanainen and S. M. Yoo, Phys. Rev. Lett. **76**, 161 (1997). M. Lewenstein and L. You, *ibid.* **77**, 3489 (1997); A. Imamoglu, M. Lewenstein, and L. You, *ibid.* **78**, 2511 (1997); R. Graham, T. Wong, M. J. Collet, S. M. Tan, and D. F. Walls Phys. Rev. A **57**, 493 (1998).
- [14] Y. Castin and J. Dalibard, Phys. Rev. A **55**, 4330 (1997); J. Javanainen and M. Wilkens, Phys. Rev. Lett. **78**, 4675 (1997); M. J. Steel and D. F. Walls, Phys. Rev. A **56**, 3832 (1997).
- [15] For a discussion of measurement of the phase of the bose condensate see: J. I. Cirac, C. W. Gardiner, M. Naraschewski, and P. Zoller, Phys. Rev. A **54**, R3714 (1996); A. Imamoglu and T.A.B. Kennedy, *ibid.* **55**, R849 (1997); J. Ruostekoski and D.F. Walls, *ibid.* **55**, 3625 (1997). J. Ruostekoski and D.F. Walls, *ibid.* **56**, 2996 (1997).
- [16] C.W. Gardiner, Phys.Rev. A **56**, 1414 (1997).
- [17] E.A. Burt, R.W. Ghrist, C.J. Myatt, M.J. Holland, E.A. Cornell, and C.E. Wieman Phys. Rev. Lett. **79**, 337 (1997).
- [18] W. Ketterle and N. J. van Druten, Adv. At. Mol. Opt. Phys. **37**, 181 (1996).

- [19] C. W. Gardiner, *Quantum Noise* (Springer Berlin 1991).
- [20] K. M. Gheri, D. F. Walls, and M. A. Marte Phys. Rev. A **46**, 6002 (1992).
- [21] The correlation functions [Eqs. (3.1) and (3.7)] refer to fluctuation properties inside the trap. This must be related to the correlation functions describing the response of the atom counter by a proper theory of an output coupler. In this context, see H. Steck, M. Naraschewski, and H. Wallis, LANL preprint quant-ph/9708014; E. V. Goldstein and P. Meystre, LANL preprint physics/9710043. R. J. Ballagh, K. Burnett, and T. F. Scott, Phys. Rev. Lett. **78**, 1607 (1997). M.-O. Mewes, M. R. Andrews, D. M. Kurn, D. S. Durfee, C. G. Townsend, and W. Ketterle, Phys. Rev. Lett. **78**, 582 (1997).
- [22] C. J. Myatt, E. A. Burt, R. W. Ghrist, E. A. Cornell, and C. E. Wieman Phys. Rev. Lett. **78**, 586 (1997).
- [23] C. W. Gardiner, P. Zoller, R. J. Ballagh, and M. J. Davis, Phys. Rev. Lett. **79**, 1793 (1997).
- [24] This implies that fluctuations of particles from the condensate mode to quasiparticle modes as well as to very low-lying one-particle excitations are not included in this approach. Calculations on fluctuations between the condensate mode and low lying excited modes can be found in S. Giorgini, L. P. Pitaevskii and S. Stringari, LANL preprint, cond-mat/9711065.
- [25] C. W. Gardiner and P. Zoller (unpublished).
- [26] M. J. Davis, R. J. Ballagh, C. W. Gardiner and P. Zoller (unpublished).
- [27] M. Holland, K. Burnett, C. Gardiner, J. I. Cirac, and P. Zoller, Phys. Rev. A **54**, R1757 (1996).
- [28] P. Fedichev, M. Reynolds, and G. V. Shlyapnikov, Phys. Rev. Lett. **77**, 2921 (1996).
- [29] B. D. Esry, C. H. Greene, Y. Zhou, and C. D. Lin, J. Phys. B **29**, L51 (1996).
- [30] H. M. J. M. Boesten, A. J. Moerdijk, and B. J. Verhaar, Phys. Rev. A **54**, R29 (1996).
- [31] H. Ritsch, Quantum Opt. **2**, 189 (1990).
- [32] This equation is found by neglecting all fluctuations. Inclusion of fluctuations into this equation has not yet been done, and is clearly desirable. However, in current experiments fluctuations in the initial conditions due to technical uncertainties between two experimental runs are much larger than any fluctuations one could expect from a fundamental point of view.

See H.-J. Miesner, D. M. Stamper-Kurn, M. R. Andrews, D. S. Durfee, S. Inouye, and W. Ketterle, *Science* **279**, 1005 (1998).

- [33] C. W. Gardiner, M. D. Lee, R. J. Ballagh, M. J. Davis, and P. Zoller, LANL preprint, cond-mat/9801027.
- [34] The use of this approximation for the terms involving R_{00} leads to the decay rate of $16/25\bar{R}_{00}$ instead of \bar{R}_{00} , as expected from the expression for $\tau_{\bar{N}}$. However, for parameters chosen according to current experimental setups, the exact value of the rate \bar{R}_{00} has only a minor influence on the correlation function $\langle B^\dagger(t)B(s) \rangle$.
- [35] D. F. Walls and G. J. Milburn *Quantum Optics*, Springer (1994).
- [36] H. Ritsch and P. Zoller, *Phys. Rev. A* **38**, 4657 (1988).
- [37] F. Sols and R. A. Hegstrom, *Fundamental Problems in Quantum Physics*, (Kluwer Dodrecht, 1995), p. 299.
- [38] F. Dalfovo, S. Giorgini, M. Guilleumas, L. Pitaevskii, and S. Stringari, *Phys. Rev. A* **56**, 3840 (1997).
- [39] A. Griffin, *Phys. Rev. B* **53**, 9341 (1996).
- [40] D. A. W. Hutchinson, E. Zaremba, and A. Griffin, *Phys. Rev. Lett.* **78**, 1842 (1997).

Part III

Realization of the Bose Hubbard model

Chapter 4

Introduction

Quantum phase transitions in strongly correlated bosonic systems have attracted a lot of interest in recent years. The simplest system where one can investigate the Mott insulator phase transition occurring in these systems at zero temperature are repulsively interacting bosons with spin zero in a lattice described by the Bose–Hubbard Hamiltonian. This Hamiltonian contains the main physics of strongly interacting bosonic systems which is the competition between kinetic- and interaction energy. There are several ways to study the Mott insulator phase transition. The model may be investigated analytically by mean field theory [1], renormalization group techniques [1, 2], projection methods [3] or by strong coupling expansions [4]. Numerically most of the studies on the Bose–Hubbard model use quantum Monte Carlo methods [5].

Physical realizations of the Bose–Hubbard model include short correlation length superconductors, granular superconductors, Josephson arrays, the dynamics of flux lattices in type II superconductors, and critical behavior of ^4He in porous media. In these realizations the bosonic systems are either tightly bound composites of fermions that act like effective bosonic particles, or correspond to bosonic excitations. The aim of the following publication is to show that also cold neutral bosonic atoms trapped in an optical lattice realize the Bose–Hubbard model. Compared to other physical realizations this system has the big advantage of being highly controllable. By adjusting the intensity of the laser beams producing the lattice one is able to change the interaction matrix element U and the tunneling matrix element J (kinetic energy gained by hopping from one lattice site to the next) which are the only two parameters of the Bose–Hubbard Hamiltonian. Moreover it is possible to realize one– two– and three dimensional systems by turning off the tunneling along several directions independently. Also, while in most of the other realizations impurities are always present and spoil the validity of the simple Bose–Hubbard Hamiltonian this is almost not the case in optical lattices which provide a very regular and well known periodic structure allowing detailed analytical calculation of

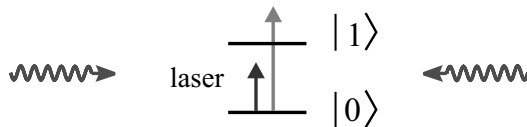


Fig. 4.1: Schematic setup of an optical lattice configuration. A two level atom with internal states $|0\rangle$ and $|1\rangle$ interact with two counterpropagating laser beams which produce a standing wave.

all the relevant parameters. Thus this system is very well suited to study the properties of the Bose–Hubbard model experimentally. Moreover as shown in our publication the possibility to add additional slowly varying potentials to the optical lattice potential adds a new feature to the Bose–Hubbard model. It would also be possible to add random potentials and thus to simulate disordered systems as investigated in [4]. Thus the Bose glass phase could be studied experimentally with bosonic atoms in optical lattices.

Also optical lattices have received much attention in atomic physics because there neutral atom cooled to the microkelvin range interacting with an optical standing wave (schematic setup see Fig. 4.1) are bound in the antinodes of this optical standing wave, thus forming regular microscopic lattices [6, 7]. One of the ultimate goals of working with optical lattices is to achieve atomic densities where the number of atoms trapped in the optical lattice exceeds the number of lattice sites. Several difficulties have to be overcome to achieve such high densities: (i) one has to have a source of neutral atoms that provides densities large enough to fill each of the lattice sites and (ii) it is also necessary to have an optical lattice in which fluorescence effects are strongly suppressed such that the optical trapping potential is hardly influenced by the large number of particles present in the lattice. If these two problems can be overcome it is possible to study the effects of quantum statistics of the particles trapped in the lattice and to investigate the effects of the interaction between the neutral atoms. As has been shown experimentally [7] the problem (ii) can be overcome by using optical lattices that are far blue detuned with respect to the atomic transition. Very recently an average filling factor of $1/2$ has also been achieved experimentally [8].

One of the goals of chapter 5 is to show that by loading a Bose–Einstein condensate into a far blue detuned optical lattice it is possible to reach densities that exceed one particle per lattice site and thus allow to study the effects of interactions between the atoms and the influence of quantum statistics. In particular we showed that a dense sample of bosonic atoms loaded into an optical lattice realizes a Bose–Hubbard model with the Hamiltonian H_{BH} given in Eq. (6.1).

References

- [1] A.P. Kampf and G.T. Zimanyi, Phys. Rev. B **47**, 279 (1993); M.P.A. Fisher, P.B. Weichman, G. Grinstein, and D.S. Fisher, Phys. Rev. B **40**, 546 (1989); K. Sheshadri, H.R. Krishnamurty, R. Pandit, and T.V. Ramkrishnan, Europhys. Lett. **22**, 257 (1993); L. Amico and V. Penna, Phys. Rev. Lett. **80**, 2189 (1998).
- [2] D.S. Rokhsar and B.G. Kotliar, Phys. Rev. B **44**, 10328 (1991); K.G. Singh and D.S. Rokhsar, Phys. Rev. B **46**, 3002 (1992).
- [3] W. Krauth, M. Caffarel, and J.-P. Bouchard, Phys. Rev. B **45**, 3137 (1992).
- [4] J.K. Freericks and H. Monien, Phys. Rev. B **54**, 16172 (1996).
- [5] R.T. Scalettar, G.G. Batrouni, and G.T. Zimanyi, Phys. Rev. Lett. **66**, 3144 (1991); P. Niyaz, R.T. Scalettar, C.Y. Fong, and G.G. Batrouni, Phys. Rev. B **44**, 7143 (1991); W. Krauth, N. Trivedi, and D. Ceperley, Phys. Rev. Lett. **67**, 2307 (1991); A. van Otterlo and K.-H. Wagenblast, Phys. Rev. Lett. **72**, 3598 (1994); G.G. Batrouni, R.T. Scalettar, G.T. Zimanyi, and A.P. Kampf, Phys. Rev. Lett. **74**, 2527 (1995).
- [6] A. Hemmerich and T. Hänsch, Phys. Rev. Lett. **70**, 410 (1993); A. Hemmerich, C. Zimmermann, and T. Hänsch, Europhys. Lett. **22**, 89 (1993); G. Grynberg, B. Lounis, P. Verkerk, J.-Y. Courtois, and C. Salomon, Phys. Rev. Lett. **70**, 2249 (1993); M.G. Prentiss, Science **260**, 1078 (1993); G.P. Collins Physics Today **46**, 17 (1993).
- [7] A. Hemmerich, M. Weidemüller, T. Esslinger, C. Zimmermann, and T. Hänsch, Phys. Rev. Lett. **75**, 37 (1995).
- [8] M.T. DePue, C. McCormick, S.L. Winoto, S. Oliver, and D.S. Weiss, Phys. Rev. Lett. **82**, 2262 (1999).

Chapter 5

PUBLICATION

COLD BOSONIC ATOMS IN OPTICAL LATTICES

D. Jaksch,^{1,2} C. Bruder,^{1,3} J. I. Cirac,^{1,2} C.W. Gardiner^{1,4} and P. Zoller^{1,2}

¹Institute for Theoretical Physics, University of Santa Barbara, Santa Barbara, CA 93106-4030

²Institut für Theoretische Physik, Universität Innsbruck, A-6020 Innsbruck, Austria

³Institut für Theoretische Festkörperphysik, Universität Karlsruhe, D-76128 Karlsruhe, Germany

⁴School of Chemical and Physical Sciences, Victoria University, Wellington, New Zealand

Physical Review Letters **81**, 3108 (1998)

The dynamics of an ultracold dilute gas of bosonic atoms in an optical lattice can be described by a Bose-Hubbard model where the system parameters are controlled by laser light. We study the continuous (zero temperature) quantum phase transition from the superfluid to the Mott insulator phase induced by varying the depth of the optical potential, where the Mott insulator phase corresponds to a commensurate filling of the lattice (“optical crystal”). Examples for formation of Mott structures in optical lattices with a superimposed harmonic trap, and in optical superlattices are presented.

PACS: 32.80.Pj, 03.75.Fi, 71.35.Lk

Optical lattices—arrays of microscopic potentials induced by the AC Stark effect of interfering laser beams—can be used to confine cold atoms [1, 2, 3, 4, 5, 6, 7]. The quantized motion of such atoms is described by the vibrational motion within an individual well and the tunneling between neighbouring wells, leading to a spectrum describable as a band structure [3]. Near-resonant optical lattices, where dissipation associated with optical pumping produces cooling, have given filling factors of about 1 atom per 10 lattice sites [1, 6]. Higher filling factors will require lower temperatures, and hence will also require minimization of the optical dissipation. This can be achieved in a far-detuned optical lattice (especially with blue detuning), where photon scattering times of many minutes have been demonstrated [2]. Thus the lattice then behaves as a conservative potential, which could be loaded with a Bose condensed atomic vapor [8, 9], for which present densities would correspond to tens of atoms per lattice site.

In this Letter we will study the dynamics of ultracold bosonic atoms loaded in an optical lattice. We will show that the dynamics of the bosonic atoms on the optical lattices realizes a Bose-Hubbard model (BHM) [10, 11, 12, 13, 14, 15, 16], describing the hopping of bosonic atoms between the lowest vibrational states of the optical lattice sites, the unique feature being the full control of the system's parameters by the laser parameters and configurations.

The BHM predicts phase transition from a superfluid (SF) phase to a Mott insulator (MI) at low temperatures and with increasing ratio of the onsite interaction U (due to repulsion of atoms) to the tunneling matrix element J [10]. In the case of optical lattices this ratio can be varied by changing the laser intensity: with increasing depth of the optical potential the atomic wave function becomes more and more localized and the onsite interaction increases, while at the same time the tunneling matrix element is reduced. In the MI phase the density (occupation number per site) is pinned at integer $n = 1, 2, \dots$ corresponding to a commensurate filling of the lattice, and thus represents an *optical crystal* with diagonal long range order with period imposed by the laser light. The nature of the MI phase is reflected in the existence of a finite gap U in the excitation spectrum.

Our starting point is the Hamilton operator for bosonic atoms in an external trapping potential

$$\begin{aligned}
 H = & \int d^3x \psi^\dagger(\mathbf{x}) \left(-\frac{\hbar^2}{2m} \nabla^2 + V_0(\mathbf{x}) + V_T(\mathbf{x}) \right) \psi(\mathbf{x}) + \\
 & \frac{1}{2} \frac{4\pi a_s \hbar^2}{m} \int d^3x \psi^\dagger(\mathbf{x}) \psi^\dagger(\mathbf{x}) \psi(\mathbf{x}) \psi(\mathbf{x})
 \end{aligned} \tag{5.1}$$

with $\psi(\mathbf{x})$ a boson field operator for atoms in a given internal atomic state, $V_0(\mathbf{x})$ is the optical lattice potential and $V_T(\mathbf{x})$ describes an additional (slowly

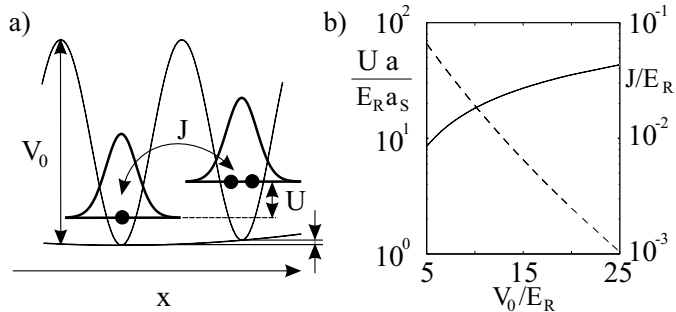


Fig. 5.1: a) Realization of the BHM in an optical lattice (see text). The offset of the bottoms of the wells indicates a trapping potential V_T . b) Plot of scaled onsite interaction U/E_R multiplied by a/a_s ($\gg 1$) (solid line; axis on left-hand side of graph) and J/E_R (dashed line, with axis on right-hand side of graph) as a function of $V_0/E_R \equiv V_{x,y,z0}/E_R$ (3D lattice).

varying) external trapping potential, e.g. a magnetic trap (see Fig. 5.1a). In the simplest case, the optical lattice potential has the form

$$V_0(\mathbf{x}) = \sum_{j=1}^3 V_{j0} \sin^2(kx_j) \quad (5.2)$$

with wavevectors $k = 2\pi/\lambda$ and λ the wavelength of the laser light, corresponding to a lattice period $a = \lambda/2$. V_0 is proportional to the dynamic atomic polarizability times the laser intensity. The interaction potential between the atoms is approximated by a short-range pseudopotential with a_s the s-wave scattering length and m the mass of the atoms. For single atoms the energy eigenstates are Bloch wave functions, and an appropriate superposition of Bloch states yields a set of Wannier functions which are well localized on the individual lattice sites. We assume the energies involved in the system dynamics to be small compared to excitation energies to the second band. Expanding the field operators in the Wannier basis and keeping only the lowest vibrational states, $\psi(\mathbf{x}) = \sum_i b_i w(\mathbf{x} - \mathbf{x}_i)$, Eq. (5.1) reduces to the Bose Hubbard Hamiltonian

$$H = -J \sum_{\langle i,j \rangle} b_i^\dagger b_j + \sum_i \epsilon_i \hat{n}_i + \frac{1}{2} U \sum_i \hat{n}_i (\hat{n}_i - 1) \quad (5.3)$$

where the operators $\hat{n}_i = b_i^\dagger b_i$ count the number of bosonic atoms at lattice site i ; the annihilation and creation operators b_i and b_i^\dagger obey the canonical commutation relations $[b_i, b_j^\dagger] = \delta_{ij}$. The parameters

$$U = \frac{4\pi a_s \hbar^2}{m} \int d^3x |w(\mathbf{x})|^4 \quad (5.4)$$

correspond to the strength of the onsite repulsion of two atoms on the lattice site i ,

$$J = - \int d^3x w(\mathbf{x} - \mathbf{x}_i) \left(-\frac{\hbar^2}{2m} \nabla^2 + V_0(\mathbf{x}) \right) w(\mathbf{x} - \mathbf{x}_j) \quad (5.5)$$

is the hopping matrix element between adjacent sites i, j , and

$$\epsilon_i = \int d^3x V_T(\mathbf{x}) |w(\mathbf{x} - \mathbf{x}_i)|^2 \approx V_T(\mathbf{x}_i) \quad (5.6)$$

describes an energy offset of each lattice site.

For a given optical potential J and U are readily evaluated numerically. For the optical potential given above the Wannier functions can be written as products $w(\mathbf{x}) = w(x)w(y)w(z)$ which can be determined from a one-dimensional bandstructure calculation. Figure 5.1b shows U and J as a function of V_0 in units of the recoil energy $E_R = \hbar^2 k^2 / 2m$. Both the next-nearest neighbor amplitudes and the nearest-neighbor repulsion are typically two orders of magnitude smaller and can thus be neglected. Qualitative insight into the dependence of these parameters is obtained in a harmonic approximation expanding around the minima of the potential wells. The oscillation frequencies in the wells are $\nu_j = \sqrt{4E_R V_{j0}} / \hbar$ which gives the separation to the first excited Bloch band. The oscillator ground state wave function of size $a_{j0} = \sqrt{\hbar / m \nu_j}$ allows us to obtain an estimate for the onsite interaction $U = \hbar \bar{\nu} (a_s / \bar{a}_0) / \sqrt{2\pi}$ with the bar indicating geometric means. Consistency of our model requires $a_s \ll a_{j0} \ll \lambda/2$ and $\Delta E_i = \frac{1}{2} U n_i (n_i - 1) \ll \hbar \nu_j$. The first set of inequalities follows from the pseudopotential approximation, and our requirement of a (large) energy separation from the first excited band. The second inequality expresses the requirement that the onsite interaction associated with the presence of n_i particles at site i , which in our model is calculated in perturbation theory, must be much smaller than the excitation energy to the next band. These inequalities are readily satisfied in practice.

According to mean-field theory (MFT) in the homogeneous case [10, 11] (see also [14]) the critical value of the MI - SF transition for the phase $n = 1$ is at the critical value $U/zJ \approx 5.8$ with $z = 2d$ the number of nearest neighbors. According to Fig. 5.1b this parameter regime is accessible by varying V_0 in the regime of a few tens of recoil energies. As an example, for Sodium [9] we have $E_R = 2\pi \times 8.9$ kHz for a red detuned laser with $\lambda = 985$ nm, and the critical values for the first MI phase in 1D, 2D and 3D are given by $V_{x0} = 10.8$, $V_{x,y0} = 14.4$, and $V_{x,y,z0} = 16.5E_R$, and we assumed in 1D $V_{y,z0} = 25E_R$ for the y and z directions in order to suppress tunneling in these other dimensions, and $V_{z0} = 25E_R$ for 2D. For $V_0 = 15$ we have $U = 0.15$ and $J = 0.07$ in units of E_R . For a blue detuning [9] $\lambda = 514$ nm we find $E_R = 2\pi \times 32$ kHz and the corresponding values are $V_{x0} = 8.4$, $V_{x,y0} = 11.9$ and $V_0 = 14.1$, and $U = 0.2$, $J = 0.02$ for $V_0 = 10$ in units of E_R . For $V_0 \approx 10E_R$ the single particle density

at the center of the optical potential wells will be of order $1/a_0^3 \approx 10^{15} \text{ cm}^{-3}$. Thus we must discuss the role of collisions between ground state atoms (in the presence of a laser field) as a loss and decoherence mechanism [17]. This question is directly related to the problem of collisional loss of Bose-Einstein condensates in optical traps as studied in [9]. We emphasize that in the Mott phase with a single particle per site ($n = 1$) two and more particle loss channels are absent. For a MI phase with $n = 2$ there will be two particle losses: if we take as an order of magnitude the numbers published in Ref. [18] we estimate the corresponding life time to be > 10 s. For $n = 3$ the life time due to three atom losses [18] will be of the order $1/10$ s.

We have performed mean-field calculations for 1D and 2D configurations, as well as an exact diagonalization of the BH Hamiltonian in 1D to illustrate the formation of the Mott insulator phase in optical lattices, in particular for the inhomogeneous case. Our mean field calculations are based on a Gutzwiller ansatz for the ground state wave function $|\Psi_{MF}\rangle = \prod_i |\phi_i\rangle$ with $|\phi_i\rangle = \sum_{n=0}^{\infty} f_n^{(i)} |n\rangle_i$ where $|n\rangle_i$ denotes the Fock state with n atoms at site i [11]. We minimize the expectation value of the Hamiltonian,

$$\langle \Psi_{MF} | H | \Psi_{MF} \rangle - \mu \langle \Psi_{MF} | \sum_i \hat{n}_i | \Psi_{MF} \rangle \rightarrow \min, \quad (5.7)$$

with respect to the coefficients $f_n^{(i)}$. The Lagrange multiplier μ enforces a given mean particle number $N = \sum_i \langle \hat{n}_i \rangle$. This corresponds to a calculation in the grand canonical ensemble with chemical potential μ at temperature $T = 0$. A MI phase is indicated by solutions in the form of single Fock states, $|\phi_i\rangle \rightarrow |n_i\rangle_i$. A signature of a MI phase is integer occupation number (density) $\rho_i = \langle \hat{n}_i \rangle$ and fluctuations, $\sigma_i^2 = (\langle \hat{n}_i^2 \rangle - \langle \hat{n}_i \rangle^2) / \langle \hat{n}_i \rangle \rightarrow 0$. Solutions in the form of superposition of Fock states result in a mean-field $\phi_i = \langle b_i \rangle \neq 0$, indicating the presence of a SF component. The angular brackets indicate an average in the meanfield state. In the homogeneous case ($\epsilon_i = 0$) the phase diagram in the $J - \mu$ plane consists of a series of lobes [10]. Inside the lobes (i.e. for J small in comparison with the onsite repulsion energy U) the system is a Mott phase; outside it is superfluid.

In Fig. 5.2a we plot the density $\rho(x, y)$ and the superfluid component $|\phi(x, y)|^2$ in an optical lattice with a superimposed isotropic harmonic potential at the lattice points $(x/a, y/a) = (i, j)$ ($i, j = 0, \pm 1, \dots$). Fig. 5.2a shows a MI phase with two atoms per site at the center of the trap ($\rho = 2$) surrounded by a Mott phase with a single atom ($\rho = 1$), and superfluid rings between the MI phases. For smaller values of the chemical potential only a single Mott phase would exist at the trap center. Qualitatively, this behavior is readily understood on the basis of the phase diagram in the homogeneous case [10] if we note that the offset $\epsilon_i = V_T(\mathbf{x}_i)$ leads to an effective local chemical potential $\mu - \epsilon_i$.

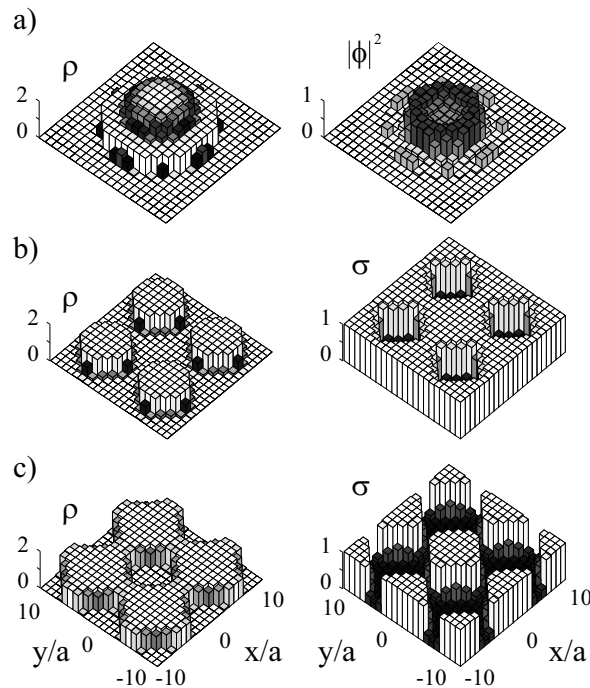


Fig. 5.2: a) MI and SF phases in an optical potential and harmonic trap in 2D. Parameters: $U = 35J$, $V_T(x, y) = J(x^2 + y^2)/a^2$, and $\mu = 50J$. Density $\rho(x, y)$ (left plot), and superfluid density $|\phi(x, y)|^2$ (right plot). b) Superlattice in 2D. Density $\rho(x, y)$ (left plot) and fluctuations $\sigma(x, y)$ (right plot). Parameters: $U = 45J$, $V_T(x, y) = 30J(\sin^2(\pi x/11a) + \sin^2(\pi y/11a))$, and $\mu = 25J$. c) Same as b) with $\mu = 35J$. Four superlattice wells are shown.

By use of interfering laser beams at different angles [4], one can produce a *superlattice*, in which the offset of the optical potential is modulated periodically in space on a scale larger than the lattice period. Fig. 5.2b,5.2c, show the density $\rho(x, y)$ and the scaled density fluctuations $\sigma(x, y)$ of Mott structures formed in a superlattice. With increasing μ we first find a Mott structure at the bottom of the superlattice potential, until the atoms are no longer confined to a particular well of the superlattice but form bridges connecting the superlattice wells.

In general, specific Mott structures can be designed by an appropriate choice of the laser configurations. An experimental signature to detect the Mott state is observation of reduced density-density fluctuations (see $\sigma(x, y)$ in Fig. 5.2). This can be monitored directly in light scattering. Alternatively, the MI phase can be detected spectroscopically by observing the gapped particle-hole excitations.

In 1D and for systems with few atoms per superlattice well we expect fluctuations to be important, and the application of MFT becomes questionable.

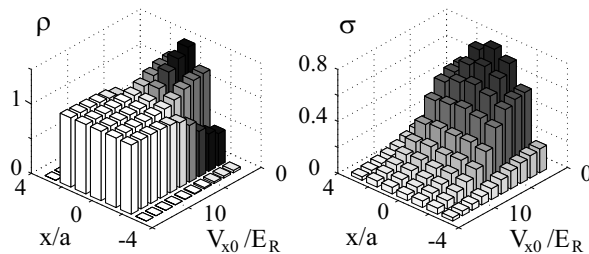


Fig. 5.3: Density ρ and fluctuations σ for the exact ground state in 1D for $N = 5$ atoms in a harmonic well as a function of V_{x0}/E_R for seven lattice cells. The parameters are $a_s/a = 1.1 \cdot 10^{-2}$ (corresponding to Na and $\lambda = 514$ nm, $V_{y0} = V_{z0} = 40E_R$) and $V_T(x) = 0.06 E_R(x/a)^2$.

On the other hand, in this limit it is straightforward to diagonalize the Bose Hubbard Hamiltonian exactly. Fig. 5.3 is a plot of the density and the number fluctuations for the exact ground state for $N = 5$ atoms as a function of V_{x0} . With increasing V_{x0} the density shows a clear transition to the MI phase $\rho = 1$, even for this very small sample. The number fluctuations are suppressed in the MI phase, but remain finite. The phase transition (which according to MFT in the homogeneous limit is expected for $V_0 = 7.4E_R$) is smeared out, and fluctuations are strongly suppressed only for larger values of V_{x0} . Qualitatively, the mean field theory for the inhomogeneous case agrees well with the exact calculations, even for these small systems. Fig. 5.3 can be viewed as an adiabatic transfer into the MI phase as the laser intensity is varied slowly as a function of time.

The atomic level scheme of Fig. 5.1 allows only one adjustable parameter, the depth of the optical potential V_0 . To adjust the tunneling matrix element J independently of the onsite interaction U we can employ atomic configurations with two internal ground state levels $|g_1\rangle$ and $|g_2\rangle$, which are connected by an off-resonant Raman transition (Fig. 5.4a).

We assume that the two internal states move in optical potentials which are shifted relative to each other by $\lambda/4$, as is the case when they have polarizabilities of opposite sign. Expanding the bosonic field operators for the two internal states we obtain a two-species Bose Hubbard Hamiltonian

$$\begin{aligned}
 H = & -(J \sum_{\langle i,j \rangle} a_i^\dagger b_j + h. c.) + \sum_i \epsilon_i a_i^\dagger a_i + \sum_j (\epsilon_j - \delta) b_j^\dagger b_j + \\
 & \frac{U_{aa}}{2} \sum_i a_i^{\dagger 2} a_i^2 + U_{ab} \sum_{\langle i,j \rangle} a_i^\dagger a_i b_j^\dagger b_j + \frac{U_{bb}}{2} \sum_j b_j^{\dagger 2} b_j^2
 \end{aligned} \quad (5.8)$$

with a_i and b_i bosonic destruction operators referring to atoms in the internal states $|g_1\rangle$, and $|g_2\rangle$, respectively. The first term in the Hamiltonian

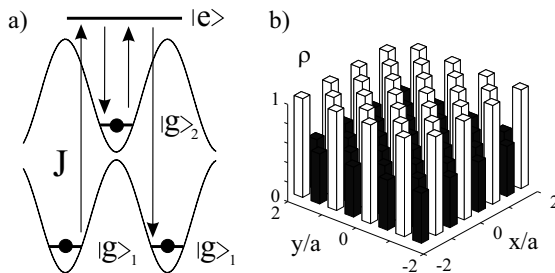


Fig. 5.4: a) Atomic level scheme (see text). b) Checkerboard pattern with a MI phase on one sublattice, and a SF on the other obtained in MFT for the two species BHM, with parameters: $\mu = 25J$, $U_{aa} = U_{bb} = 45J$, $U_{ab} = 0$, $\delta = -25J$, and $\epsilon_i = 0$.

describes the Raman induced hopping between adjacent cells with coupling $J = \frac{1}{2} \int d^3\mathbf{x} w_a(\mathbf{x})^* \Omega_{\text{eff}}(\mathbf{x}) w_b(\mathbf{x} - \lambda/4)$, where Ω_{eff} is the effective two-photon Rabi frequency (including a possible phase). Direct tunneling has been neglected. The second and third term contain offsets due to a trapping potential, and in addition a Raman detuning term $-\delta$ for atoms in state $|g_2\rangle$. The second line contains onsite interactions of atoms a and b described by U_{aa} and U_{bb} , and a nearest-neighbor interaction U_{ab} whose value depends on the overlap of the Wannier functions between a and b . A Raman detuning δ shifts the chemical potential of species b relative to a . We can adjust the value of this detuning to generate checkerboard patterns, e.g. a MI phase of species a and a Mott phase of species b can coexist with different site occupation numbers. As an example, Fig. 5.4b plots the density $\rho(x, y)$ for a specific 2D homogeneous situation where a MI phase $|g_1\rangle$ coexists with a superfluid component in $|g_2\rangle$.

While the present discussion has emphasized periodic (ordered) Bose systems, adding a further optical potential with incommensurate lattice spacing allows the realization of a (pseudo)random potential [5] which leads to the study of disordered Bose systems and appearance of a Bose glass phase [10, 15]. A study of the growth and fluctuations of the MI phase due to coupling to a finite temperature particle reservoir based on a master equation treatment [19] will be presented elsewhere. The ability to manipulate both the lattice and the system parameters in our realization of a Bose-Hubbard model brings a new aspect to condensed matter physics: models and simplifying assumptions may be systematically investigated using the experimental techniques of quantum optics.

The authors thank the members of the BEC98 program at ITP UCSB for discussions. Work supported in part by the NSF, the Austrian Science Foundation, EU TMR networks and the Marsden contract PVT-603.

References

- [1] G. Raithel *et al.*, Phys. Rev. Lett. **78**, 630 (1997); T. Müller-Seydlitz *et al.*, *ibid.* **78**, 1038 (1997); S. E. Hamann *et al.*, *ibid.* **80**, 4149 (1998); and references cited.
- [2] S. Friebel *et al.*, Phys. Rev. A **57**, R20 (1998)
- [3] M. Raizen, C. Salomon, and Q. Niu, Physics Today **50**, 30 (1997).
- [4] L. Guidoni and P. Verkerk, Phys. Rev. A **57**, R1501 (1998) and references cited.
- [5] L. Guidoni *et al.*, Phys. Rev. Lett. **79**, 3363 (1997)
- [6] K. I. Petsas, A. B. Coates, and G. Grynberg, Phys. Rev. A **50**, 5173 (1994)
- [7] I.H. Deutsch and P.S. Jessen, Phys. Rev. A **57**, 1972 (1998).
- [8] M. Anderson *et al.*, Science **269**, 198 (1995); K.B. Davis *et al.*, Phys. Rev. Lett. **75**, 3969 (1995); C.C. Bradley *et al.*, Phys. Rev. Lett. **75**, 1687 (1995); see the BEC homepage <http://amo.phy.gasou.edu/bec.html>
- [9] D.M. Stamper-Kurn *et al.*, Phys. Rev. Lett. **80**, 2027 (1998); S. Inouye *et al.*, Nature **392**, 151 (1998);
- [10] M.P.A. Fisher *et al.*, Phys. Rev. B **40**, 546 (1989).
- [11] W. Krauth, M. Caffarel, and J.-P. Bouchard, Phys. Rev. B **45**, 3137 (1992); K. Sheshadri *et al.*, Europhys. Lett. **22**, 257 (1993).
- [12] A.P. Kampf and G.T. Zimanyi, Phys. Rev. B **47**, 279 (1993).
- [13] C. Bruder, R. Fazio, and G. Schön, Phys. Rev. B **47**, 342 (1993); A. van Otterlo *et al.*, Phys. Rev. B **52**, 16176 (1995).
- [14] J.K. Freericks and H. Monien, Europhys. Lett. **26**, 545 (1994).
- [15] W. Krauth, N. Trivedi, and D. Ceperley, Phys. Rev. Lett. **67**, 2307 (1991); N.V. Prokofev, B.V. Svistunov, and I.S. Tupitsyn, Phys. Lett. A **238**, 253 (1998).
- [16] For other experimental realizations like granular superconductors, Josephson junction arrays, and Helium films, see references cited in [10, 13].
- [17] For a discussion of various aspects of inelastic processes in the presence of light see: P. O. Fedichev *et al.*, Phys. Rev. Lett. **77**, 2913 (1996); K.-A. Suominen *et al.*, Phys. Rev. A **57**, 3724 (1998).
- [18] For decay rates of a Rb condensate in a magnetic trap see: E. A. Burt *et al.*, Phys. Rev. Lett. **79**, 337 (1997).
- [19] C.W. Gardiner, and P. Zoller, Phys. Rev. A **58**, 536 (1998).

Chapter 6

The Bose–Hubbard Model

In this chapter we discuss some of the details needed to obtain the results of the preceding publication (chapter 5).

6.1 Hamiltonian

The Bose–Hubbard model Hamiltonian is given by

$$H_{\text{BH}} = -J \sum_{\langle i,j \rangle} a_i^\dagger a_j + \frac{U}{2} \sum_i a_i^\dagger a_i^\dagger a_i a_i + \sum_i (\epsilon_i - \mu) a_i^\dagger a_i, \quad (6.1)$$

where a_i is the bosonic annihilation operator of a particle in the mode i with a mode function $\psi_i(x)$ centered around the site position x_i . J is the hopping (tunneling) matrix element for a particle to jump from site x_i to one of the nearest neighbors x_j , and $\langle i, j \rangle$ denotes all pairs of nearest neighbors. ϵ_i is the energy offset of the site x_i and μ , the chemical potential, acts as a Lagrangian multiplier to fix the mean number of particles in the grand canonical case. The repulsive interaction between particles in the same site is described by the interaction matrix element $U > 0$.

6.2 Approximate ground state for fixed number of particles

First, we would like to characterize the ground state of H_{BH} for $\epsilon_i = 0$. Solving for the ground state of H_{BH} in mean field theory yields two different regimes. For U/J small (for details see the following Sec. 6.3) the ground state is a superfluid state. The number of particles per site fluctuates and the coherences between particles in different sites are large. The wave function of the ground

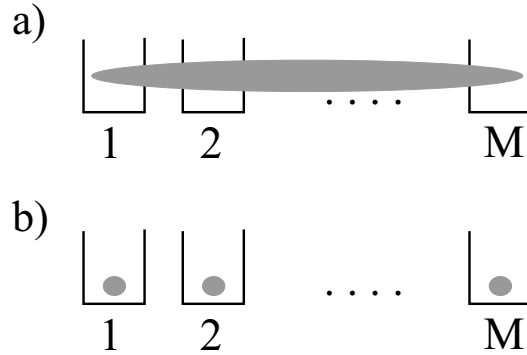


Fig. 6.1: Visualization of a) the superfluid phase and b) the Mott–insulator phase with commensurate filling predicted by the Bose–Hubbard model.

state is then approximately given by

$$|\Psi_{\text{SF}}\rangle \propto \left(\sum_{i=1}^M a_i^\dagger \right)^N |0\rangle, \quad (6.2)$$

where N is the total number of particles and M is the number of lattice sites. $|0\rangle$ denotes the vacuum state. This kind of state is visualized in Fig. 6.1a.

By increasing the repulsive interaction U compared to J a quantum phase transition (at temperature $T = 0$) from the superfluid to a Mott–insulator phase takes place. It becomes less favorable for the particles to jump from one site to the next, since the interaction between two particles in one site increases the energy. For commensurate filling of the sites the ground state thus turns into a state where the number of particles per site is integer and the particle number fluctuations in the sites tend to zero. The ground state is then approximately given by

$$|\Psi_{\text{MIC}}\rangle \propto \prod_{i=1}^M \left(a_i^\dagger \right)^{N/M} |0\rangle. \quad (6.3)$$

A ground state of this form can be viewed as shown in Fig. 6.1b. Commensurate filling means that N/M is an integer. If the filling is not commensurate each site will host $[N/M]$ particles (where $[x]$ denotes the largest integer contained in x). The remaining particles will act as a superfluid above the Mott–insulator core. The ground state is then approximately given by

$$|\Psi_{\text{MINC}}\rangle \propto \left(\sum_{i=1}^M a_i^\dagger \right)^{N-[N/M]M} \prod_{i=1}^M \left(a_i^\dagger \right)^{[N/M]} |0\rangle, \quad (6.4)$$

6.2.1 Gutzwiller ansatz

In our numerical calculations in chapter 5 we used the Gutzwiller ansatz [1] for the wave function

$$|\Psi_{\text{MF}}\rangle = \prod_{i=1}^M |\Phi_i\rangle, \quad (6.5)$$

where

$$|\Phi_i\rangle = \sum_{n=0}^{\infty} f_n^{(i)} |n\rangle_i, \quad (6.6)$$

with $|n\rangle_i$ being the Fock state with n particles in mode i . The $f_n^{(i)}$ are constants. The Gutzwiller ansatz contains the superfluid wave function $|\Psi_{\text{SF}}\rangle$ as well as the Mott–insulator wave function $|\Psi_{\text{MINC}}\rangle$ and is thus well suited for describing the quantum phase transition from the superfluid to the Mott–insulator phase. We determined the $f_n^{(i)}$ by minimizing the energy

$$\langle \Psi_{\text{MF}} | H_{\text{BH}} | \Psi_{\text{MF}} \rangle \rightarrow \min \quad (6.7)$$

as a function of $f_n^{(i)}$.

6.3 Phase diagram of the Bose–Hubbard model

To give a more quantitative picture of the phase transition described above we will show some results obtained by a Pade analysis by N. Elstner and H. Monien [2] for $\epsilon_i = 0$. The calculations there are carried out for a given chemical potential μ and thus for a fixed mean number of particles corresponding to a grand canonical calculation. In this case the superfluid phase is characterized by a finite order parameter $\langle a_i \rangle \neq 0$ while in the Mott–insulator phase the order parameter $\langle a_i \rangle = 0$ (For a fixed number of particles the order parameter is always zero). Figure 6.2 shows the phase diagram obtained in [2] for the square lattice in two dimensions. The phase diagram shows the boundary between the Mott–insulator phase and the superfluid phase as a function of J/U and μ/U . The two lobes represent Mott–insulator phases with one and two particles per lattice site, respectively. If the chemical potential is increased further lobes with larger number of particles per lattice site can be found. In [2] the boundary between the superfluid and the Mott–insulator phase is found by calculating the energy difference of particle and hole excitations from a Mott–insulator state $|\Psi_{\text{MIC}}\rangle$. The values of μ/U and J/U where this energy difference vanishes defines the boundary between the two phases (for details see [2, 3]). Using mean field calculations [1] one finds the condition

$$U_c = (3 + 2\sqrt{2})JZ \quad (6.8)$$

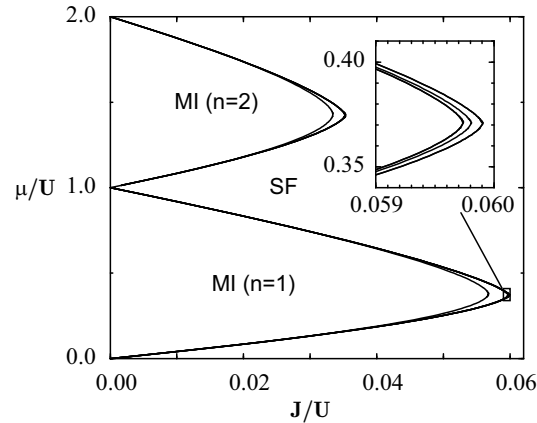


Fig. 6.2: Phase diagram obtained in [2]. The different curves represent different degrees of approximation but are all very close to each other. The calculation was performed for a two dimensional square lattice with $Z = 4$ nearest neighbors. This figure is published with the kind permission of N. Elstner.

for the onset of the Mott-insulator phase with one particle per site, where Z is the number of nearest neighbors of one cell. This estimate agrees well with more rigorous calculations like [2].

References

- [1] A.P. Kampf and G.T. Zimanyi, Phys. Rev. B **47**, 279 (1993); M.P.A. Fisher, P.B. Weichman, G. Grinstein, and D.S. Fisher, Phys. Rev. B **40**, 546 (1989); K. Sheshadri, H.R. Krishnamurty, R. Pandit, and T.V. Ramkrishnan, Europhys. Lett. **22**, 257 (1993); L. Amico and V. Penna, Phys. Rev. Lett. **80**, 2189 (1998).
- [2] N. Elstner and H. Monien, cond-mat/9807033; N. Elstner and H. Monien, cond-mat/9905367.
- [3] J.K. Freericks and H. Monien, Phys. Rev. B **54**, 16172 (1996).

Chapter 7

Optical lattices

7.1 Optical potentials

We consider first a two-level atom with the internal ground state $|0\rangle$ and the excited state $|1\rangle$ in one dimension coupled to a monochromatic classical laser field with frequency ω as schematically shown in Fig. 4.1. The spontaneous emission rate of the excited state is given by γ . In the rotating frame the stochastic Schrödinger equation (with $\hbar = 1$) for the atom is given by [1]

$$d|\Psi(t)\rangle = \left\{ -iH_{\text{eff}}dt + \int_{-k}^k du \sqrt{\gamma N(u)} e^{-iux} dB_u(t)^\dagger |0\rangle \langle 1| \right\} |\Psi(t)\rangle, \quad (7.1)$$

where $|\Psi(t)\rangle = |\Psi_1(t)\rangle \otimes |1\rangle + |\Psi_0(t)\rangle \otimes |0\rangle$ and H_{eff} is the effective Hamiltonian given by

$$H_{\text{eff}} = \frac{p^2}{2m} + \left(\delta - i\frac{\gamma}{2} \right) |1\rangle \langle 1| - \frac{\Omega(x)}{2} (|1\rangle \langle 0| + |0\rangle \langle 1|). \quad (7.2)$$

x and p are the coordinate and momentum operators, respectively. The mass of the atom is m and the detuning δ between the atomic transition frequency ω_{10} and the laser field is given by $\delta = \omega_{10} - \omega$. We denote the Rabi frequency which is proportional to the electric field strength and the dynamic polarizability of the atom by Ω . $dB_u(t)$ is an Ito noise increment, $N(u)$ is normalized and determined by the spatial distribution of the spontaneously emitted photons [1]. k is the wave number of the classical light field. The equations of motion for the wave functions $|\Psi_1(t)\rangle$ and $|\Psi_0(t)\rangle$ are given by

$$\frac{d|\Psi_1(t)\rangle}{dt} = -i \left\{ \delta - i\frac{\gamma}{2} + \frac{p^2}{2m} \right\} |\Psi_1(t)\rangle + i\frac{\Omega(x)}{2} |\Psi_0(t)\rangle, \quad (7.3)$$

and

$$d|\Psi_0(t)\rangle = -i \left(\frac{p^2}{2m} \right) dt |\Psi_0(t)\rangle$$

$$+ \left\{ i \frac{\Omega(x)}{2} dt + \int_{-k}^k du \sqrt{\gamma N(u)} e^{-iux} dB_u(t)^\dagger \right\} |\Psi_1(t)\rangle. \quad (7.4)$$

We want to consider the case of a far detuned optical lattice, i.e. the case where the detuning is much larger than the Rabi frequency $|\delta| \gg |\Omega|$. Furthermore we will assume the spontaneous emission rate to be much smaller than the detuning, i.e. $\gamma \ll |\delta|$. Also we will assume the kinetic energy of an excited atom (and thus also the recoil energy $E_R = k^2/2m$) to be much smaller than the detuning $E_R \ll |\delta|$. In this case it is permissible to adiabatically eliminate the excited internal state of the atom $|1\rangle$. We do this by setting the left hand side of Eq. (7.3) equal to zero and by neglecting the kinetic energy term which yields

$$|\Psi_1(t)\rangle = \frac{\Omega(x)}{2\delta - i\gamma} |\Psi_0(t)\rangle. \quad (7.5)$$

Combining Eqs. (7.4, 7.5) and defining the operator

$$c = \frac{\sqrt{\gamma}\Omega(x)}{2\delta - i\gamma}, \quad (7.6)$$

We find

$$d|\Psi_0(t)\rangle = \left\{ -i \left(\frac{p^2}{2m} - \frac{\Omega(x)^2\delta}{4\delta^2 + \gamma^2} - \frac{i}{2} c^\dagger c \right) dt + \int_{-k}^k du \sqrt{N(u)} e^{-iux} dB_u(t)^\dagger c \right\} |\Psi_0(t)\rangle. \quad (7.7)$$

We define the optical potential as

$$V_\gamma(x) = -\frac{\Omega(x)^2|\delta|}{4\delta^2 + \gamma^2}. \quad (7.8)$$

Furthermore we will always assume the atom to be interacting with a standing light wave. The spatial dependence of the Rabi frequency is then given by

$$\Omega(x) = \Omega_0 \sin(kx). \quad (7.9)$$

7.1.1 Influence of spontaneous emission

Next we want to investigate the effect of spontaneous emission, i.e. to estimate the mean time until a spontaneous emission occurs if an atom is interacting with a standing light wave and trapped in the vibrational ground state of one of the potential minima of the optical potential Eq. (7.8).

7.1.1.1 Ground state wave function

We assume the size of the ground state wave function a_0 in the optical potential to be much smaller than the periodicity of $V_\gamma(x)$ given by $a = \pi/k$, i.e.

$$\pi \sqrt[4]{\frac{|\delta|}{\frac{k^2}{2m}} \frac{\Omega_0^2}{4\delta^2 + \gamma^2}} \gg 1, \quad (7.10)$$

which can be fulfilled without violating the previous assumptions $|\delta| \gg |\Omega_0|$, $|\delta| \gg \gamma$ and $|\delta| \gg p^2/2m$. For finding the ground state wave function we expand the optical potential around its minimum to second order

$$V_\gamma(x) \approx \mathcal{C} + \frac{m\omega_T^2 x^2}{2}, \quad (7.11)$$

with the trapping frequency

$$\omega_T^2 = \frac{2\Omega_0^2 |\delta| k^2}{(4\delta^2 + \gamma^2)m}, \quad (7.12)$$

and a constant \mathcal{C} that is proportional to the light intensity in the center of the harmonic trap. The ground state of one of the potential minima of the optical potential is then approximately given by the ground state of the approximating harmonic oscillator

$$\bar{\Psi}_0(x) = \sqrt[4]{\frac{1}{\pi a_0^2}} e^{-\frac{x^2}{2a_0^2}}, \quad (7.13)$$

where $a_0 = \sqrt{1/m\omega_T}$. If condition Eq. (7.10) is not fulfilled but the particle may still be trapped in the optical lattice anharmonicity effects will change the shape of the ground state wave function but the following estimates will still be valid qualitatively.

7.1.1.2 Blue detuned optical lattice

In the case of a blue detuned optical lattice (dark optical lattice) $\delta < 0$ the potential minima coincide with the points of no light intensity and thus $\mathcal{C} = 0$. The time between two spontaneously emitted photons is determined by the rate

$$\gamma_{\text{eff}} = \langle \bar{\Psi}_0 | c^\dagger c | \bar{\Psi}_0 \rangle \approx -\frac{\gamma}{4\delta} \omega_T \ll \omega_T. \quad (7.14)$$

As was shown recently in an experiment by Friebel et al. [2] the spontaneous emission rate in far blue detuned optical lattices can be of the order of several minutes.

7.1.1.3 Red detuned optical lattice

In a red detuned optical lattice (bright optical lattice) $\delta > 0$ the potential minima coincide with the points of maximum light intensity and thus

$$C = -\frac{\Omega_0^2 \delta}{4\delta^2 + \gamma^2}. \quad (7.15)$$

In this case the time between two spontaneously emitted photons is determined by the rate

$$\gamma_{\text{eff}} = \langle \bar{\Psi}_0 | c^\dagger c | \bar{\Psi}_0 \rangle \approx \frac{\gamma}{4\delta} \left(\frac{4\Omega_0^2 \delta}{4\delta^2 + \gamma^2} - \omega_T \right). \quad (7.16)$$

Since $\Omega_0^2/\delta \gg \omega_T$ due to assumption Eq. (7.10) the spontaneous emission in a red detuned optical lattice will always be more significant than in a blue detuned optical lattice.

7.1.2 Neglecting spontaneous emission

Spontaneous emission may be neglected as long as we assume the experiment to be performed within a time much smaller than $1/\gamma_{\text{eff}}$. Then the equation for the wave function becomes

$$\frac{d|\Psi_0(t)\rangle}{dt} = -iH|\Psi_0(t)\rangle, \quad (7.17)$$

with the Hamiltonian

$$H = \frac{p^2}{2m} + V_0(x), \quad (7.18)$$

where the optical potential $V_0(x)$ is given by

$$V_0(x) = -\frac{\Omega(x)^2}{4\delta}. \quad (7.19)$$

The Hamiltonian H is the starting point of the calculations in the preceding publication.

7.2 Bloch bands and Wannier functions

The optical potential $V_0(x) = (\Omega_0^2/4\delta) \sin^2(kx) \equiv V_0 \sin^2(kx)$ is periodic in space and it is thus useful to work out the Bloch eigenstates

$$\phi_q^{(n)}(x) = e^{iqx} u_q^{(n)}(x), \quad (7.20)$$

where q is the Bloch wave number and $u_q^{(n)}(x)$ are eigenstates of the Hamiltonian

$$H_q = \frac{(p+q)^2}{2m} + V_0(x), \quad (7.21)$$

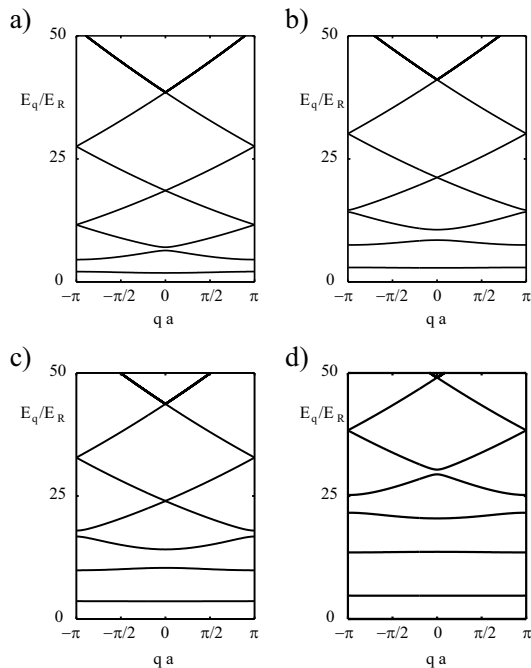


Fig. 7.1: Band structure of an optical lattice with the optical potential $V_0(x) = V_0 \sin^2(kx)$ for different depths of the potential. a) $V_0 = 5E_R$, b) $V_0 = 10E_R$, c) $V_0 = 15E_R$, and d) $V_0 = 25E_R$.

with energy $E_q^{(n)}$ and periodicity a of the optical potential $V_0(x)$, i.e.

$$H_q u_q^{(n)}(x) = E_q^{(n)} u_q^{(n)}(x). \quad (7.22)$$

In Figure 7.1 the bandstructure (eigenenergies $E_q^{(n)}$ as a function of q) is shown for different depths of the optical potential V_0 . For the lowest lying bands the separation of the different bands n is approximately given by the frequency ω_T while particles in higher bands with energies larger than V_0 behave as free particles. All the calculations in the preceding publication assume the particles to be in the lowest band which implies cooling to temperatures T much lower than the trapping frequency ω_T .

7.2.1 Wannier functions

A set of orthogonal normalized wave functions that fully describe particles in band n of the optical potential and that are localized at the sites (regions around the potential minima) of the optical lattice is given by the Wannier

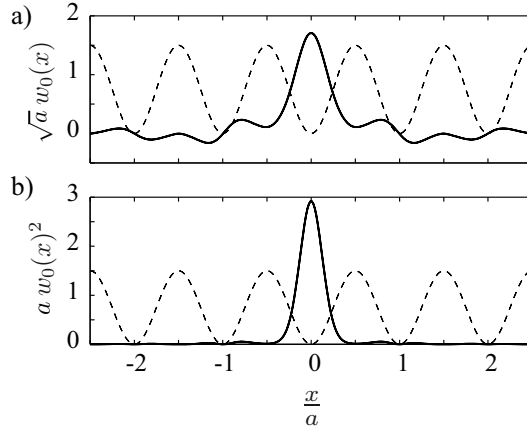


Fig. 7.2: Wannier function for an optical lattice with $V_0 = 10E_R$. Plot a) shows the mode function $w_0(x)$ (solid curve) and plot b) the probability distribution $w_0(x)^2$ (solid curve) as a function of position x . The dashed curves indicate the shape of the optical potential $V_0(x) = V_0 \sin^2(kx)$.

functions [3]

$$w_n(x - x_i) = \mathcal{N}^{-1/2} \sum_q e^{-iqx_i} \phi_q^{(n)}(x), \quad (7.23)$$

where x_i is the position of the lattice site and \mathcal{N} is a normalization constant. Figure 7.2 shows an example of a Wannier function with $n = 0$. These Wannier functions $w_0(x - x_i)$ tend towards the ground state wave functions Eq. (7.13) of one of the lattice sites when $V_0 \rightarrow \infty$ at constant k since we may then neglect all the terms involving the Bloch wave number q and it is valid to approximate the optical potential by a harmonic potential. The advantages of using Wannier functions $w_0(x - x_i)$ to describe particles in the lowest band are that

- a mean position x_i may be attributed to the particle if it is found to be in the mode corresponding to the Wannier function $w_0(x - x_i)$ (cf. Fig. 7.2) and
- local interactions between particles can be described easily since the dominant contribution comes from particles located at the same position x_i .

7.2.2 Connection between J and the bandstructure

In the case where $U = 0$ the Hamiltonian H_{BH} Eq. (6.1) reduces to a tight binding model Hamiltonian. We assume periodic boundary conditions and

that the one particle eigenstates of H_{BH} are of the form

$$|\Psi\rangle = \sum_n e^{i\alpha n} a_n^\dagger |0\rangle, \quad (7.24)$$

with the constant α obeying the equation $\alpha l = 2\pi M$ where l is an integer. The eigenvalue equation for $|\Psi\rangle$ reads

$$H_{BH} |\Psi\rangle = E_\alpha |\Psi\rangle, \quad (7.25)$$

from which we find

$$-2J \cos(\alpha) = E_\alpha. \quad (7.26)$$

From Eq. (7.26) it is clear that the hopping matrix element is given by

$$J = \frac{\max(E_q^{(0)}) - \min(E_q^{(0)})}{4} \quad (7.27)$$

7.3 Realizing the Bose–Hubbard Hamiltonian

We will now show how to reduce the Hamiltonian H_{full} of many interacting particles in an optical lattice to the Bose–Hubbard Hamiltonian Eq. (6.1).

$$\begin{aligned} H_{\text{full}} &= \int dx \psi^\dagger(\mathbf{x}) \left(\frac{\mathbf{p}^2}{2m} + V_0(\mathbf{x}) + V_T(\mathbf{x}) \right) \psi(\mathbf{x}) \\ &\quad + \frac{g}{2} \int dx \psi^\dagger(\mathbf{x}) \psi^\dagger(\mathbf{x}) \psi(\mathbf{x}) \psi(\mathbf{x}) \end{aligned} \quad (7.28)$$

with $\psi(\mathbf{x})$ the bosonic field operator for atoms in the given internal atomic state $|0\rangle$, $V_T(\mathbf{x})$ describes a (slowly varying compared to $V_0(\mathbf{x})$) external trapping potential, e.g. a magnetic trap. g is the interaction strength between the particles. We assume all the particles to be in the lowest band of the optical lattice and expand the field operator in terms of the Wannier functions $\psi(\mathbf{x}) = \sum_i a_i w^{(0)}(\mathbf{x} - \mathbf{x}_i)$, where a_i is the destruction operator for a particle in site \mathbf{x}_i . $w^{(0)}(\mathbf{x} - \mathbf{x}_i)$ is the three dimensional version of the Wannier functions discussed in Sec. 7.2.1. We find

$$H_{\text{full}} = - \sum_{i,j} J_{ij} a_i^\dagger a_j + \frac{1}{2} \sum_{i,j,k,l} U_{ijkl} a_i^\dagger a_j^\dagger a_k a_l, \quad (7.29)$$

where

$$J_{ij} = - \int dx w_0(\mathbf{x} - \mathbf{x}_i) \left(\frac{p^2}{2m} + V_0(\mathbf{x}) + V_T(\mathbf{x}) \right) w_0(\mathbf{x} - \mathbf{x}_j) \quad (7.30)$$

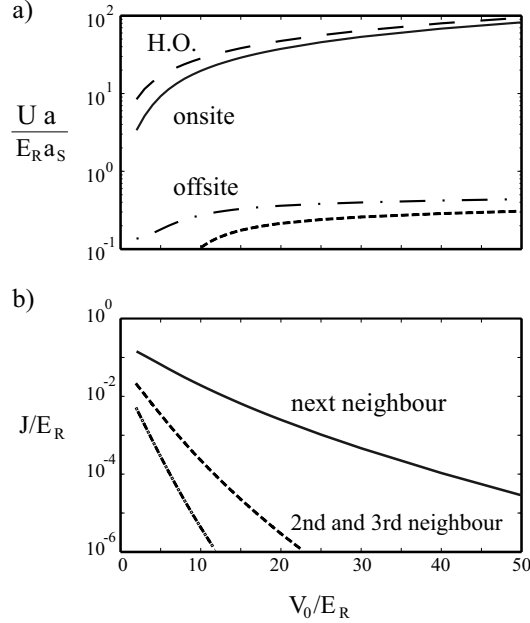


Fig. 7.3: a) Comparison of on site U_{0000} (solid curve) to off site interactions U_{0101} (dash dotted curve) and U_{0001} (dashed curve). The dashed curve labeled HO is the interaction matrix element U_{0000} if the Wannier functions are approximated by the ground state wave function of a harmonic oscillator approximating the optical potential around its minimum. b) Comparison of nearest neighbor hopping J_{01} (solid curve) and hopping to the 2nd J_{02} (dashed curve) and 3rd J_{03} (dash dotted curve) neighbors. All calculations presented in this figure are for a three dimensional optical lattice with equal lattice properties in each direction x, y and z .

and

$$U_{ijkl} = g \int dx w_0(\mathbf{x} - \mathbf{x}_i) w_0(\mathbf{x} - \mathbf{x}_j) w_0(\mathbf{x} - \mathbf{x}_k) w_0(\mathbf{x} - \mathbf{x}_l). \quad (7.31)$$

We first compare the interaction matrix element for particles in the same site U_{0000} with the interaction matrix elements for particles in two adjacent sites U_{0101} and the interaction matrix element U_{0001} as shown in Fig. 7.3a. We find the offsite interaction matrix elements U_{0101} and U_{0001} to be more than one order of magnitude smaller than the onsite interaction matrix element U_{0000} which allows us to neglect offsite interactions. Due to the orthogonality of the Wannier functions hopping is only possible along the x, y and z directions. In Fig. 7.3b the hopping matrix elements between nearest neighbors J_{01} and between 2nd J_{02} and 3rd J_{03} nearest neighbors (along one of the axes) are compared with each other. For $V_0 > 5E_R$ the latter are at least one order

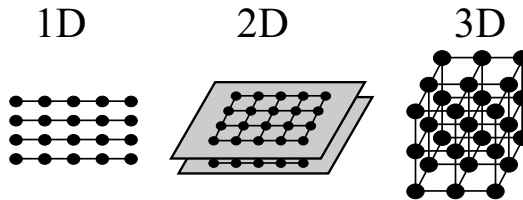


Fig. 7.4: One– two– and three dimensional Bose–Hubbard model. Hopping is only possible along sites connected by lines. In the other directions hopping is turned off by choosing a large laser intensity and thus producing high optical barrier.

of magnitude smaller than the the hopping matrix elements between nearest neighbors and may thus be neglected.

Therefore we arrive at the standard Bose–Hubbard Hamiltonian

$$H_{\text{BH}} = -J \sum_{\langle i,j \rangle} a_i^\dagger a_j + \frac{U}{2} \sum_i a_i^\dagger a_i^\dagger a_i a_i + \sum_i \epsilon_i a_i^\dagger a_i, \quad (7.32)$$

where $J \equiv J_{01}$ and $U \equiv U_{0000}$. The terms ϵ_i arise from the additional (in comparison to the localization of the Wannier functions slowly varying) trapping potential, and are given by

$$\epsilon_i = V_T(x_i). \quad (7.33)$$

7.3.1 One– two– and three dimensional Bose–Hubbard model

The intensities of the laser beams producing the optical potentials in x, y and z direction can be adjusted independently. Also the frequencies have to be adjusted such that the potentials add and do not interfere. Choosing the laser intensity large enough tunneling along different directions can selectively be turned off since the tunneling matrix element decreases rapidly for large V_0 (cf. Fig. 7.3b). By choosing the laser intensity large along one direction a two dimensional Bose–Hubbard model can be realized whereas by choosing a large laser intensity along two dimensions a one dimensional Bose–Hubbard model is created. The different situations are shown in Fig. 7.4.

7.4 Light–induced inelastic collisions

When two particles get close to each other the interaction changes the energy between different internal states [4]. An example is shown in Fig. 7.5 where the potential curves for two atoms with relative distance r are given schematically for the different internal states ($S + S$) and ($P + S$). As a consequence the detuning δ of the laser field changes as the particles come close to each other

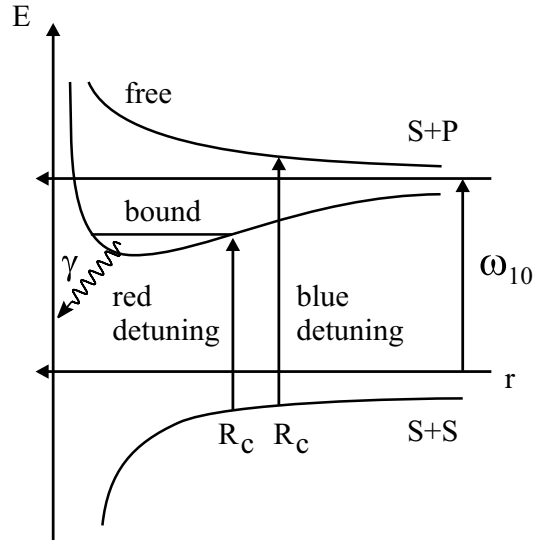


Fig. 7.5: Schematic interaction potential curves for two atoms at distance r .

and becomes $\delta = 0$ at the Condon point R_C . The probability for the two particles to be excited to the states $P + S$ increases around the Condon point. The particles can either form a quasistable molecule (red detuning) which decays by emitting spontaneously a photon γ or they can be promoted to an unbound $S + P$ state with a large kinetic energy equal to the detuning of the laser at $r = \infty$. Both of these effects should be kept as small as possible to minimize loss from the optical lattice. There are several ways to do so:

- Avoid a Condon point by detuning far to the red. However, this will lead to a large spontaneous emission rate compared to the case of a blue detuned optical lattice (cf. Sec. 7.1.1).
- Avoid a red detuning that puts the Condon point close to a quasibound state (shown in Fig. 7.5).
- Choose the detuning such that the two potential curves have an angle close to 90° to each other at the Condon point which makes the probability of finding the two particles in the region where $\delta \approx 0$ small.

References

- [1] P. Zoller and C.W. Gardiner, quant-ph/9702030. C.W. Gardiner and P. Zoller, *Quantum noise II*, to be published.

- [2] S. Friebel, C. D'Andrea, J. Walz, M. Weitz, and T.W. Hänsch, *Phys. Rev. A* **57**, R20 (1998)
- [3] C. Kittel, *Quantum Theory of Solids*, John Wiley & Sons, (New York 1963).
- [4] P.S. Julienne, *J. Res. Natl. Inst. Stand. Technol.* **101**, 487 (1996).

Part IV

Entanglement and quantum computing using neutral atoms

Chapter 8

Introduction

8.1 Quantum computing in optical lattices

In the publication discussed in the previous part III we were mainly interested in how to obtain regular fillings of an optical lattice. We will now concentrate on possible new experiments and applications which might emerge from making use of very well controlled neutral atoms in an optical lattice. We will show how it is possible to move an optical lattice state selectively and thus to be able to control the interaction between atoms. These “handmade” collisions of neutral atoms in moving optical lattices are the basis of many of the experiments discussed in the following publications (chapters 9 and 11). In particular the suggested experiments should allow one to create EPR-pairs and GHZ-states of neutral atoms in optical lattices, it should be possible to measure the s -wave scattering length a_s of the atoms and eventually also to discover some effects of the trapping on the interaction between neutral atoms, since the ground state size in the optical lattices can be made comparable to the scattering length a_s . Using the techniques described below it should also be possible to discriminate Mott-insulator states from superfluid states of the atoms in the lattice (cf. chapter 5).

Another very prominent example of possible applications of neutral atoms in moving optical lattices is the implementation of two-qubit quantum gates and performing quantum computations in parallel as described in detail in chapter 11. There the qubit is represented by two internal states of the trapped atoms. One qubit rotations are easily performed by applying laser pulses to the atoms. Two qubit gates are implemented by selectively letting particles in specific internal states interact with each other as described in chapter 9. Another way to build two-qubit quantum gates is suggested in [1]. There dipole-dipole interactions between neutral atoms trapped in an optical lattice are used in order to build two-qubit quantum gates.

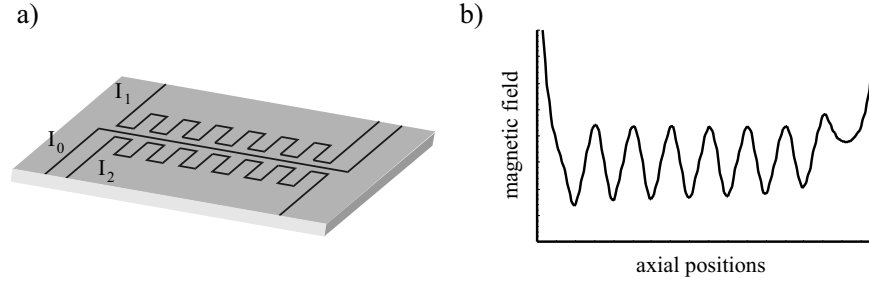


Fig. 8.1: a) Magnetic motor for neutral atoms as introduced in [10]. b) Potential created by the configuration shown in a).

8.2 Electromagnetic microtraps

While we have discussed optical lattices as a possible way to trap and manipulate neutral atoms for purposes of quantum computing and entanglement operations there is a second possibility which we want to consider now. As is standard in Bose–Einstein condensation experiments neutral atoms can be trapped by magnetic fields [2, 3, 4]. While in these magnetic traps the number of trapped atoms is usually on the order of 10^5 several groups including J. Schmiedmayer [5], T. Hänsch [6], K.G. Libbrecht [7], and E. Hinds [8] are experimentally working on guiding and trapping neutral atoms in magnetic micro-traps which allow for storage of single atoms. New advances in nanofabrication techniques [9] promise unique trap designs on a nano-scale and control over the trapped atoms on the quantum level. The major advantages of magnetic micro-traps compared to optical lattices are

- that the static magnetic fields are much more stable and less distorted by the presence of atoms than the laser beams of an optical lattice,
- the geometry of the trap can be designed much more easily than in an optical lattice,
- there is no spontaneous emission in magnetic traps,
- and – in principle – the magnetic traps can be highly integrated and might thus turn out to be more useful for commercial use than optical setups.

However, there are also several disadvantages of magnetic traps compared to optical lattices, e.g.,

- it is easier to load a cold bosonic sample of atoms into an optical lattice [11] which has been achieved experimentally than into an array of mag-

netic microtraps (which has not been done up to now to the best of my knowledge),

- manipulating the atoms usually requires extra laser beams (one qubit gates, preparation of the initial internal states, readout of the information) which is much harder in magnetic micro-traps since there the atoms are always close to a surface.
- The distance between the different trapping potential is determined by the laser wavelength in the case of an optical lattice which can easily be on the order of a few hundreds of nanometers, while it is much more difficult to obtain arrays of magnetic trap potentials with centers less than $1\mu\text{m}$ away from each other.

In order to do entanglement operations in electromagnetic microtraps it is necessary to control the trapping potential in a state selective way. This can be achieved by combining electric and magnetic static fields as we show in Sec. 8.2.1. In chapter 10 these static selective potentials are the starting point for showing how to implement a two-qubit quantum gate. The scheme presented there allows for a quantum gate between two atoms in neighboring potential wells (cf. Fig. 8.2). One way to perform gate operations between an arbitrary pair of atoms would be to move *one* column of atoms along the y -axis (in the scheme presented in Fig. 8.2) while leaving the neighboring atoms in their places. Although it might not be easy to do this experimentally first experiments towards this direction have been presented recently by the group of T. Hänsch [10]. The basic principle is shown in Fig. 8.1, where in Fig. 8.1a we show the experimental setup while in Fig. 8.1b the potential generated by this setup is shown. By changing the currents I_0 , I_1 and I_2 with time the wells of the potential move along the axial position.

We also want to mention that in the publication presented in chapter 10 D. Jaksch was mainly responsible for the theoretical part and for how to solve numerically for the state vectors which works in a similar way as described in detail for the optical lattice in Sec. 12.2.3. T. Calarco was mainly involved into finding the physical implementations of the theoretical schemes described in the paper and running simulations for experimentally feasible situations given to us by the experimental authors of the paper. In the publication presented in chapter 11 it was the main responsibility of H. Briegel to do the theoretical part on quantum computation while D. Jaksch was mainly responsible for how the physical requirements on the system used for doing the computations could be satisfied.

8.2.1 State selective potentials

In the electromagnetic microtraps we consider in chapters 10 and 11 neutral atoms are trapped by static inhomogeneous electric and magnetic fields. We assume that the magnetic field changes slowly enough so that the magnetic moment of the trapped atom can follow the direction of the field adiabatically. In this adiabatic regime the potential energy of the atom depends on the magnitude $|\mathbf{B}|$ of the magnetic field but not on its direction and is given by

$$E_{\text{magn}} = g_F \mu_B m_F |\mathbf{B}|, \quad (8.1)$$

where g_F is the gyromagnetic factor of the atom. μ_B denotes the Bohr magneton and m_F is the z -component of the total spin of the atom's hyperfine level, i.e., the interaction energy of the atom with the magnetic field depends on the internal hyperfine state of the atom. The potential energy of an atom interacting with a static electric field is given by

$$E_{\text{el}} = \frac{\alpha_{\text{el}}}{2} |\mathbf{E}|^2, \quad (8.2)$$

where α_{el} is the static polarizability of the internal state. This polarizability depends on the form of the spatial wave function and is thus independent of the atom's hyperfine level. $|\mathbf{E}|$ is the magnitude of the electric field applied.

Combining electric and magnetic fields and being able to change them independently allows for switching the potential state dependently as described in Sec. 10. One of the situations we were considering is depicted in Fig. 8.2. There we assumed a magnetized magnetic mirror [12] lying in the x, y -plane with the surface magnetization

$$M(x) = \sum_{n=1}^2 \frac{2B_n}{\mu_0 (1 - e^{-k_n b})} \cos(k_n x + \delta_n) \quad (8.3)$$

changing only along the x -direction. $\mu_0 = 4\pi 10^{-7} \text{Vs/Am}$, B_n, k_n and δ_n are constants that can be chosen within limits determined by the properties of the magnetic mirror. In addition a static magnetic field of the form

$$\mathbf{B} = \{B_0 \cos \Theta, B_y, B_0 \sin \Theta\} \quad (8.4)$$

is applied, where B_0, B_y and Θ are constants. For appropriate parameters this setup produces the potential shown in Fig. 8.2a with paired wells assumed to trap the atoms. A charged dot is put below the two paired wells (depicted in Fig. 8.2b) and by changing the charge of this dot it is possible to state selectively remove the barrier between the two potential wells.

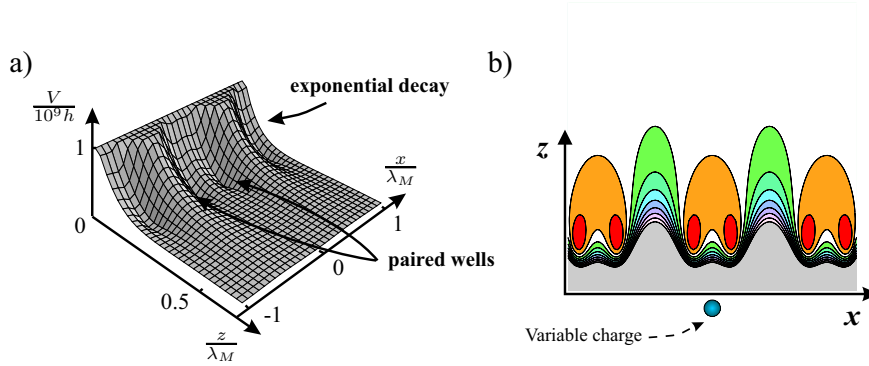


Fig. 8.2: Magnetic potential considered to build a two-qubit quantum gate. a) Three dimensional plot of the magnetic potential V along the x and z axes. b) Contour plot of the magnetic potential shown in a). The parameters are chosen as $B_1 = 37.5\text{mT}$, $B_2 = 120\text{mT}$, $\delta_1 = 0$, $\delta_2 = \pi$, $B_0 = 12\text{mT}$, $B_y = 1\text{mT}$, $\Theta = 0$, $k_1 = 2\pi/\lambda_M$, $k_2 = 4\pi/\lambda_M$, $b = \lambda_M$, and $\lambda_M = 2\mu\text{m}$.

References

- [1] G.K. Brennen, C.M. Caves, P.S. Jessen, and I.H. Deutsch, *Phys. Rev. Lett.* **82**, 1060 (1999).
- [2] M.H. Anderson, J.R. Ensher, M.R. Matthews, C.E. Wieman and E.A. Cornell, *Science*, **269**, 198 (1995).
- [3] K.B. Davis, M-O. Mewes, M.R. Andrews, N.J. van Druten, D.S. Durfee, D.M. Kurn, and W. Ketterle, *Phys. Rev. Lett.*, **75**, 3969 (1995).
- [4] C.C. Bradley, C.A. Sackett, J.J. Tollet, and R. Hulet, *Phys. Rev. Lett.*, **75**, 1687 (1995).
- [5] J. Denschlag, D. Cassettari, and J. Schmiedmayer, *Phys. Rev. Lett.* **82**, 2014 (1999); J. Denschlag, G. Umshaus, and J. Schmiedmayer, *Phys. Rev. Lett.* **81**, 737 (1998);
- [6] V. Vuletic, T. Fischer, M. Praeger, T.W. Hänsch, and C. Zimmermann, *Phys. Rev. Lett.*, **80**, 1634 (1998).
- [7] J.D. Weinstein and K.G. Libbrecht, *Phys. Rev. A*, **52**, 4004 (1995).
- [8] E.A. Hinds, M.G. Boshier, and I.G. Hughes, *Phys. Rev. Lett.* **80**, 645 (1998).
- [9] J. Schmiedmayer, private communication.
- [10] J. Reichel, W. Hänsel, and T.W. Hänsch, unpublished.
- [11] B.P. Anderson and M.A. Kasevich, *Science* **282**, 1686 (1998).

- [12] I.G. Hughes, P.A. Barton, T.M. Roach, M.G. Boshier, and E.A. Hinds, *At. Mol. Opt. Phys.* **30**, 647 (1997); I.G. Hughes, P.A. Barton, T.M. Roach, and E.A. Hinds, *At. Mol. Opt. Phys.* **30**, 2119 (1997).

Chapter 9

PUBLICATION

ENTANGLEMENT OF ATOMS VIA COLD CONTROLLED COLLISIONS

D. Jaksch,¹ H.-J. Briegel,¹ J.I. Cirac,¹ C. W. Gardiner,² and P. Zoller¹

¹Institut für Theoretische Physik, Universität Innsbruck, A-6020 Innsbruck, Austria.

²School of Chemical and Physical Sciences, Victoria University, Wellington, New Zealand.

Physical Review Letters **82**, 1975 (1999)

We show that by using *cold controlled collisions* between two atoms one can achieve conditional dynamics in moving trap potentials. We discuss implementing two qubit quantum-gates and efficient creation of highly entangled states of many atoms in optical lattices.

PACS: 03.67.-a, 32.80.Pj, 03.67.Lx, 34.90.+q.

The controlled manipulation of entangled states of N -particle systems is fundamental to the study of basic aspects of quantum theory [1, 2], and provides the basis of applications such as quantum computing and quantum communications [3, 4]. Engineering entanglement in real physical systems requires precise control of the Hamiltonian operations and a high degree of coherence. Achieving these conditions is extremely demanding, and only a few systems, including trapped ions, cavity QED and NMR, have been identified as possible candidates to implement quantum logic in the laboratory [3]. On the other hand, in atomic physics with *neutral atoms* recent advances in cooling and trapping have led to an exciting new generation of experiments with Bose condensates [5], experiments with optical lattices [6], and atom optics and interferometry. The question therefore arises, to what extent these new experimental possibilities and the underlying physics can be adapted to provide a new perspective in the field of experimental quantum computing.

In this Letter we propose coherent cold collisions as the basic mechanism to entangle neutral atoms. The picture of *atomic collisions* as *coherent interactions* has emerged during the last few years in the studies of Bose Einstein condensation (BEC) of ultracold gases. In a field theoretic language these interactions correspond to Hamiltonians which are quartic in the atomic field operators, analogous to Kerr nonlinearities between photons in quantum optics. By storing ultracold atoms in arrays of microscopic potentials provided, for example, by optical lattices these collisional interactions can be controlled via laser parameters. Furthermore, these nonlinear atom-atom interactions can be large [7], even for interactions between individual pairs of atoms, thus providing the necessary ingredients to implement quantum logic.

Let us consider a situation where two atoms 1 and 2 in internal states $|a\rangle_1$ and $|b\rangle_2$ (labelled a and b) are trapped in the ground states $\psi_0^{a,b}$ of two potential wells $V^{a,b}$. Initially, at time $t = -\tau$, these wells are centered at positions \bar{x}^a and \bar{x}^b , sufficiently far apart (distance $d = \bar{x}^b - \bar{x}^a$) so that the particles do not interact. The positions of the potentials are moved along trajectories $\bar{x}^a(t)$ and $\bar{x}^b(t)$ so that the wavepackets of the atoms overlap for certain time, until finally they are restored to the initial position at the final time $t = \tau$. This situation is described by the Hamiltonian

$$H = \sum_{\beta=a,b} \left[\frac{(p^\beta)^2}{2m} + V^\beta \left(x^\beta - \bar{x}^\beta(t) \right) \right] + u^{ab}(x^a - x^b). \quad (9.1)$$

Here, $x^{a,b}$ and $p^{a,b}$ are position and momentum operators,

$$V^{a,b} \left(x^{a,b} - \bar{x}^{a,b}(t) \right) \quad (9.2)$$

describe the displaced trap potentials and u^{ab} is the atom-atom interaction term.

Ideally, we would like to implement the transformation from $t = -\tau$ to $t = \tau$

$$\psi_0^a(x^a - \bar{x}^a)\psi_0^b(x^b - \bar{x}^b) \rightarrow e^{-i\phi}\psi_0^a(x^a - \bar{x}^a)\psi_0^b(x^b - \bar{x}^b), \quad (9.3)$$

where each atom remains in the ground state of its trapping potential and preserves its internal state. The phase ϕ will contain a contribution from the interaction (collision). Transformation (9.3) can be realized in the *adiabatic limit*, [8] whereby we move the potentials so that the atoms remain in the ground state. In the absence of interactions ($u^{\text{ab}} = 0$) adiabaticity requires $|\dot{\bar{x}}^{a,b}(t)| \ll v_{\text{osc}} \quad \forall t$, where $v_{\text{osc}} \approx a_0\omega$ is the rms velocity of the atoms in the vibrational ground state, a_0 is the size of the ground state of the trap potential, and ω is the excitation frequency. The phase ϕ can be easily calculated in the limit $|\ddot{\bar{x}}^{a,b}(t)| \ll v_{\text{osc}}/\tau$. In this case, $\phi = \phi^a + \phi^b$ where

$$\phi^{a,b} = \frac{m}{2\hbar} \int_{-\tau}^{\tau} dt \dot{\bar{x}}^{a,b}(t)^2, \quad (9.4)$$

are the *kinetic phases*. In the presence of interactions ($u^{\text{ab}} \neq 0$), we define the time-dependent energy shift due to the interaction as

$$\Delta E(t) = \frac{4\pi a_s \hbar^2}{m} \int dx \prod_{\beta=a,b} |\psi_0^\beta(x - \bar{x}^\beta(t))|^2, \quad (9.5)$$

where a_s is the s -wave scattering length. We assume that: (i) $|\Delta E(t)| \ll \hbar\omega$ so that no sloshing motion is excited; (ii) $|\dot{\bar{x}}^{a,b}(t)| \ll v_{\text{osc}}$ (adiabatic condition); (iii) v_{osc} is sufficiently small for the zero energy s -wave scattering approximation to be valid [9]. In that case, (9.3) still holds with $\phi = \phi^a + \phi^b + \phi^{\text{ab}}$ with the *collisional phase*

$$\phi^{\text{ab}} = \frac{1}{\hbar} \int_{-\tau}^{\tau} dt \Delta E(t). \quad (9.6)$$

In the case of quasi-harmonic potentials (as is realized with optical potentials, see below) (9.3) still holds, even in the non-adiabatic regime, i.e. at higher velocities. For harmonic traps one can solve exactly the evolution for $u^{\text{ab}} = 0$, and identify the condition for adiabaticity:

$$\left| \int_{-\tau}^t \dot{\bar{x}}^{a,b}(t') e^{i\omega t'} dt' \right| \ll a_0, \quad \forall -\tau \geq t \geq \tau. \quad (9.7)$$

This is consistent with condition (ii). Actually, for (9.3) to hold the inequality (9.7) only has to be fulfilled for $t = \tau$ (and not for all times). This means that the particle need not be in the ground state of the moving potential at all times, but only at the final time. The phase $\phi = \phi^a + \phi^b$, as well as the wave functions $\psi^{a,b}(x^{a,b}, t)$, can be calculated exactly [8]. For $u^{\text{ab}} \neq 0$ if conditions (i) and (iii)

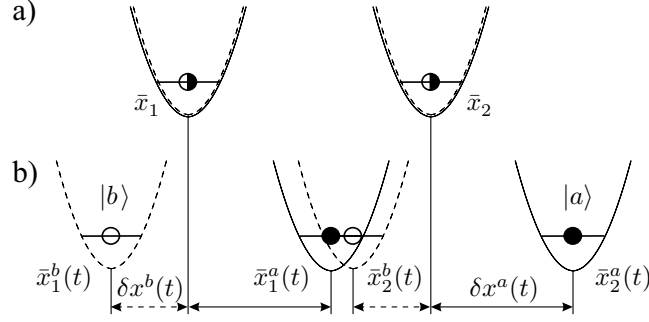


Fig. 9.1: Configurations at times $\pm\tau$ (a) and at t (b). The solid (dashed) curves show the potentials for particles in the internal state $|a\rangle$ ($|b\rangle$), respectively. Center positions $\bar{x}_j^\beta(t)$ and displacements $\delta x^\beta(t)$ as defined in the text.

are satisfied, then (9.3) is still valid. There is an additional phaseshift (with respect to $u^{ab} = 0$) ϕ^{ab} which is given by Eqs. (9.5,9.6) with the replacement $\psi_0^{a,b}(x^{a,b} - \bar{x}^{a,b}(t)) \rightarrow \psi^{a,b}(x^{a,b}, t)$. It is also straightforward to generalize these results to the case in which the trap frequency changes with time [10].

So far, we have shown that one can use cold collisions as a coherent mechanism to induce phase shifts in two-atom interactions in a controlled way. Our goal is now to use these interactions to implement conditional dynamics. We consider two atoms 1 and 2, each of them with two internal levels $|a\rangle_{1,2}$ and $|b\rangle_{1,2}$. We will use the superscripts $\beta = a, b$ and the subscripts $j = 1, 2$ to label the internal levels and atoms, respectively. Atoms in the internal state $|\beta\rangle_j$ experience a potential V_j^β which is initially ($t = -\tau$) centered at position \bar{x}_j . We assume that we can move the centers of the potentials as follows (Fig. 9.1): $\bar{x}_j^\beta(t) = \bar{x}_j + \delta x^\beta(t)$. The trajectories $\delta x^\beta(t)$ are chosen in such a way that $\delta x^\beta(-\tau) = \delta x^\beta(\tau) = 0$ and the first atom collides with the second one only if they are in states $|a\rangle$ and $|b\rangle$, respectively ($|\bar{x}_1^b(t) - \bar{x}_2^a(t)| \gg a_0 \forall t$). This choice is motivated by the physical implementation considered below. The fact that \bar{x}_j does not depend on the internal atomic state allows one to easily change this internal state at times $t = \pm\tau$ by applying laser pulses. If the conditions stated above are fulfilled, depending on the initial internal atomic states we have:

$$\begin{aligned}
 |a\rangle_1|a\rangle_2 &\rightarrow e^{-i2\phi^a}|a\rangle_1|a\rangle_2, \\
 |a\rangle_1|b\rangle_2 &\rightarrow e^{-i(\phi^a+\phi^b+\phi^{ab})}|a\rangle_1|b\rangle_2, \\
 |b\rangle_1|a\rangle_2 &\rightarrow e^{-i(\phi^a+\phi^b)}|b\rangle_1|a\rangle_2, \\
 |b\rangle_1|b\rangle_2 &\rightarrow e^{-i2\phi^b}|b\rangle_1|b\rangle_2,
 \end{aligned} \tag{9.8}$$

where the motional states remain unchanged. The kinetic phases ϕ^β and the

collisional phase ϕ^{ab} can be calculated as stated above. We emphasize that the ϕ^{β} are (trivial) one particle phases that, if known, can always be incorporated in the definition of the states $|a\rangle$ and $|b\rangle$.

In the language of Quantum Information, transformation (9.8) corresponds to a fundamental two-qubit gate [4]. In order to illustrate to what extent the mechanism presented above is able to perform this ideal gate, we have carried out a numerical study in 3 dimensions. We have integrated the time-dependent Schrödinger equation with the Hamiltonian (9.1). We have taken harmonic potentials with various time dependent displacements $\delta x^{\beta}(t)$ and frequencies. Their form as well as the parameter range are motivated by the specific implementations outlined below. The figure of merit that we have used is the minimum fidelity [11], which is defined as $F = \min_{|\psi\rangle} \langle \tilde{\psi} | \text{tr}_{\text{ext}} (\mathcal{U} |\psi\rangle \langle \psi| \otimes \rho_{\text{ext}} \mathcal{U}^{\dagger}) | \tilde{\psi} \rangle$. Here $|\psi\rangle$ is an arbitrary internal state of both atoms, $|\tilde{\psi}\rangle$ is the state resulting from $|\psi\rangle$ using the mapping (9.8). The trace is taken over motional states, \mathcal{U} is the evolution operator for the internal states coupled to the external motion (including the collision), and ρ_{ext} the density operator corresponding to both atoms in the motional ground state at $t = -\tau$. In the ideal case the fidelity will be one. We have taken the potential u^{ab} as proportional to a delta function and used a truncated moving harmonic oscillator basis (10 states for each degree of freedom). The first illustration corresponds to a fixed trap frequency $\omega^a = \omega^b$ and displacements $\delta x^b(t) = 0$ and $\delta x^a(t)$ as specified in Fig. 9.2a. In Fig. 9.2b we present a contour plot of F as a function of the parameters characterizing the displacement $\delta x^a(t)$. The fidelity is very close to one for a surprisingly wide range of parameters, even well into the non-adiabatic regime. We have also studied numerically the effect of time-varying trap frequencies (see Fig. 9.3a) and finite temperatures, so that ρ_{ext} describes a thermal distribution of temperature T . For temperatures $kT \leq 0.2\hbar\omega$ (where ω is the initial trap frequency) the fidelity remains very close to one (of the order of 0.997), and this result is still robust with respect to changes in the parameters. We have also included loss due to collisions by adding an imaginary part to the scattering length. In that case, the fidelity is reduced (see Fig. 9.3b).

So far we have assumed that there is one atom per potential well. In practice, the particle number might not be controlled. Nevertheless, one can easily generalize the above results to this case by using a second quantized picture. For example, in the adiabatic regime we denote by a_i and b_i the annihilation operators for a particle in the ground state of the potential centered at the position i , and corresponding to the internal levels $|a\rangle$ and $|b\rangle$, respectively. The effective Hamiltonian in this regime is

$$H = \sum_i \left[\omega^a(t) a_i^{\dagger} a_i + \omega^b(t) b_i^{\dagger} b_i + u^{\text{aa}}(t) a_i^{\dagger} a_i^{\dagger} a_i a_i + \right.$$

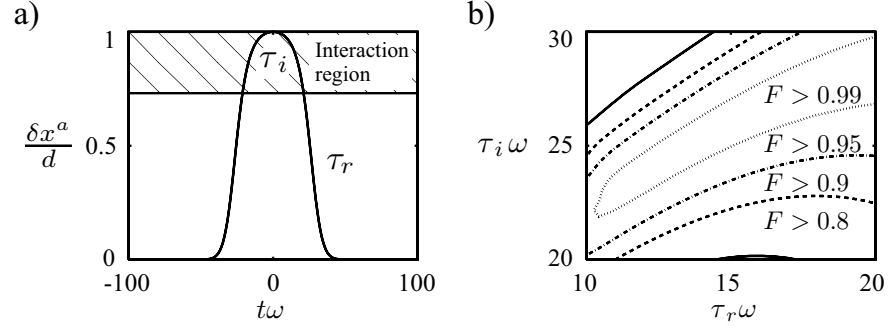


Fig. 9.2: a) Displacement as a function of time ωt , $\delta x^a(t)/d = (1 + \exp(-(\tau_i/\tau_r)^2)) / (1 + \exp((t^2 - \tau_i^2)/\tau_r^2))$ and $\delta x^b(t) = 0$ (see text), with $\tau_r = 30/\omega$ and $\tau_i = 20/\omega$. The shaded region indicates where the particles interact. b) Fidelity F against rise time τ_r and interaction time τ_i for ^{87}Rb with $a_s = 5.1\text{nm}$, $\omega = 2\pi \times 100\text{kHz}$ and $d = 10 a_0$.

$$u^{bb}(t)b_i^\dagger b_i^\dagger b_i b_i] + \sum_{i,j} u_{ij}^{ab}(t)a_i^\dagger a_i b_j^\dagger b_j, \quad (9.9)$$

where the ω 's and u 's depend on the specific way the potentials are moved. This Hamiltonian corresponds to a Quantum–Non–Demolition situation [12], whereby the particle number can be measured non–destructively.

A physical implementation of this scenario requires an interaction which produces internal state dependent conservative trap potentials and the possibility of moving these potentials independently. Furthermore, the choice of the internal atomic states $|a\rangle$ and $|b\rangle$ has to be such that they are collisionally stable (i.e. the internal states do not change after the collision). These requirements can be satisfied in an optical lattice. We consider a specific but relevant example of alkali atoms with a nuclear spin equal to $3/2$ (^{87}Rb , ^{23}Na) trapped by standing waves in 3 dimensions. The internal states of interest are hyperfine levels corresponding to the ground state $S_{1/2}$. Along the z axis, the standing waves are in the lin \angle lin configuration (two linearly polarized counter-propagating traveling waves with the electric fields forming an angle 2θ [13]). The electric field is a superposition of right and left circular polarized standing waves (σ^\pm) which can be shifted with respect to each other by changing θ ,

$$\vec{E}^+(z, t) = E_0 e^{-i\omega t} [\vec{e}_+ \sin(kz + \theta) + \vec{e}_- \sin(kz - \theta)], \quad (9.10)$$

where \vec{e}_\pm denote unit right and left circular polarization vectors, $k = \nu/c$ is the laser wavevector and E_0 the amplitude. The lasers are tuned between the $P_{1/2}$ and $P_{3/2}$ levels so that the dynamical polarizabilities of the two fine structure $S_{1/2}$ states corresponding to $m_s = \pm 1/2$ due to the laser polarization σ^\mp vanish, whereas the ones due to σ^\pm are identical ($\equiv \alpha$). The optical potentials

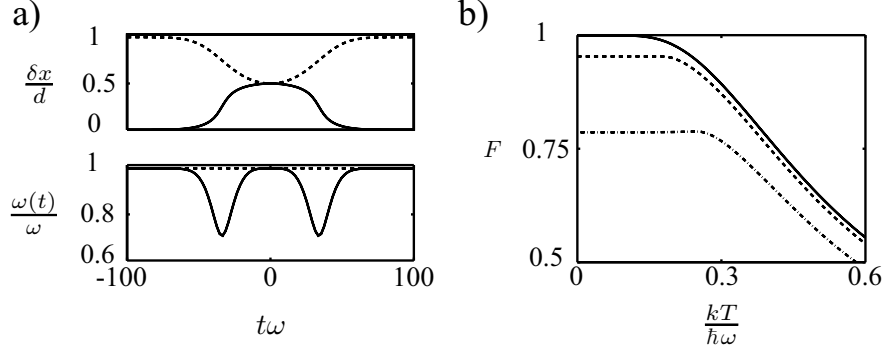


Fig. 9.3: a) Upper plot: Displacements $\delta x^a(t)/d$ (solid line) and $1 + \delta x^b(t)/d$ (dashed line). Lower plot: Trap frequencies $\omega^a(t)/\omega$ (solid line) and $\omega^b(t)/\omega$ (dashed line). b) Fidelity F against temperature $kT/\hbar\omega$ for ^{87}Rb with $a_s = 5.1\text{nm}$ (solid line), $a_s = (1 - 0.01i) \times 5.1\text{nm}$ (dashed line) and $a_s = (1 - 0.05i) \times 5.1\text{nm}$ (dash-dotted line). Here $\omega = 2\pi \times 100\text{kHz}$ and $d = 390\text{nm}$.

for these two states are $V_{m_s=\pm 1/2}(z, \theta) = \alpha|E_0|^2 \sin^2(kz \pm \theta)$. We choose for the states $|a\rangle$ and $|b\rangle$ the hyperfine structure states $|a\rangle \equiv |F = 1, m_f = 1\rangle$ and $|b\rangle \equiv |F = 2, m_f = 2\rangle$. Due to angular momentum conservation, these states are stable under collisions (for the dominant central electronic interaction [14]). The potentials “seen” by the atoms in these internal states are

$$V^a(z, \theta) = [V_{m_s=1/2}(z, \theta) + 3V_{m_s=-1/2}(z, \theta)] / 4 \quad (9.11)$$

$$V^b(z, \theta) = V_{m_s=1/2}(z, \theta). \quad (9.12)$$

If one stores atoms in these potentials and they are deep enough, there is no tunneling to neighboring wells and we can approximate them by harmonic potentials. By varying the angle θ from $\pi/2$ to 0, the potentials V^b and V^a move in opposite directions until they completely overlap. Then, going back to $\theta = \pi/2$ the potentials return to their original positions. The shape of the potential V^a changes as it moves. By choosing

$$\theta(t) = \pi \left(1 - \frac{1 + \exp(-(\tau_i/\tau_r)^2)}{1 + \exp((t^2 - \tau_i^2)/\tau_r^2)} \right) / 2 \quad (9.13)$$

with $\tau_r = 30/\omega$ and $\tau_i = 20/\omega$, the frequencies and displacements of the harmonic potentials approximating (9) are exactly those plotted in Fig. 9.3a. Therefore, that figure shows that under this realistic situation one can obtain very high fidelities.

The scheme presented here can be used in several interesting experiments: (a) One can use this method to measure the phase shift ϕ^{ab} and therefore determine the scattering length corresponding to a - b collisions. For that, one can use ideas borrowed from Ramsey spectroscopy, namely: (i) prepare

all atoms in the superposition $(|a\rangle + |b\rangle)/\sqrt{2}$ by applying a $\pi/2$ laser pulse; (ii) shift their potentials as described above; (iii) apply another $\pi/2$ laser pulse; (iv) detect the population of the internal states by fluorescence. It can easily be shown that such populations depend in a simple way on the phase shift ϕ^{ab} . One can even determine the sign of the scattering length by applying laser pulses with pulse area different from $\pi/2$ [15]. (b) In a similar way, one can also measure the spatial correlation function by applying the second laser pulse (iii) and population detection (iv) without moving the potential back to the origin. This would be a way of discriminating between Mott and superfluid phases for particles in an optical lattice [7]. (c) Apart from that, if one is able to address individual wells with a laser, one can also perform certain experiments which are interesting both from the quantum information and fundamental point of view. For example, one could create an entangled EPR pair of two particles $(|a\rangle_1|b\rangle_2 - |b\rangle_1|a\rangle_2)/\sqrt{2}$ [1]. This could be done by having two atoms in neighboring wells and: (i) prepare each of them in the superposition $(|a\rangle + |b\rangle)/\sqrt{2}$; (ii) shift their potentials back and forth so that the phase shift $\phi^{ab} = \pi$; (iii) apply a $\pi/2$ laser pulse to the second atom. In this case one could test Bell inequalities and perform other fundamental experiments. (d) With more than two particles one could create higher entangled states with simple lattice operations. For example, if one has N particles in N potential wells, one could create GHZ states of the form $(|a\rangle_1|a\rangle_2 \dots |a\rangle_N - |b\rangle_1|b\rangle_2 \dots |b\rangle_N)/\sqrt{2}$ [2]. This could be easily done, for example, if one could use a different internal state $|c\rangle_1$ in the first atom instead of $|b\rangle_1$ [16]. The procedure would be as follows: (i) prepare the first atom in the state $(|a\rangle_1 + |c\rangle_1)/\sqrt{2}$, and the others in the state $(|a\rangle + |b\rangle)/\sqrt{2}$; (ii) Move the potential corresponding to the internal level $|c\rangle$ back and forth so that if the first atom is in that state it interacts with all the other atoms for a time such that in each “collision” the phase shift difference between the collision $a-c$ and $b-c$ is π ; (iii) apply a $\pi/2$ pulse (in transition $a-b$) to all the atoms except the first one, which is transferred from $|c\rangle$ to $|b\rangle$. We emphasize that the optical lattice configuration allows the preparation of these states in a *single sweep* of the lattice. (e) Finally, it is clear that one could use optical lattices in the context of quantum information since the above procedure provides a fundamental two bit gate (9.8) which, combined with single particle rotations allows to perform any quantum computation between an arbitrary number of two-level systems. In particular, the optical lattice setup would be very well suited to implement fault tolerant quantum computations due to the possibility of doing gate operations [4] in parallel [15].

So far we have neglected some processes that may lead to decoherence, and therefore limit the performance of our scheme. This includes spontaneous emission of atoms in the off-resonant optical lattice potentials, and inelastic collisions to wrong final atomic states. The spontaneous emission lifetime of

a single atom in the lattice is from seconds to many minutes, depending on the laser detuning [6]. The problem of collisional loss is closely related to the loss mechanism in Bose condensates in magnetic and optical traps, a problem studied extensively in recent experiments. By choosing proper internal hyperfine states one can maximize the lifetime due to inelastic collisions to be of the order of at least several seconds [17].

Finally, by filling the lattice from a Bose condensate, and using the ideas related to Mott transitions in optical lattices [7] it is possible to achieve uniform lattice occupation (“optical crystals”) or even specific atomic patterns, as well as the low temperatures necessary for performing the experiments proposed in this letter.

This research was supported by the Austrian Science Foundation, by the TMR network ERB-FMRX-CT96-0087, by the NSF under Grant No. PHY94-07194, and by the Marsden fund, contract PVT-603.

Note added: After this work was completed we became aware of [18] where dipole–dipole interactions controlled by optical lattices are proposed as a mechanism to implement a two bit quantum gate.

References

- [1] J. S. Bell, *Physics* **1**, 195 (1964).
- [2] D. M. Greenberger *et al.*, *Am J. Phys.* **58**, 1131 (1990).
- [3] C. P. Williams and S.H. Clearwater, *Explorations in Quantum Computing* (Springer Verlag, New York 1997).
- [4] D. P. DiVincenzo, *Phys. Rev. A* **51**, 1015 (1995); C. H. Bennett, *Phys. Today* **48**, 24 (1995); A. Barenco *et al.*, *Phys. Rev. A* **52**, 3457 (1995).
- [5] F. Dalfovo *et al.*, cond-mat/9806038.
- [6] S. Friebel *et al.*, *Phys. Rev. A* **57**, R20 (1998);
S. E. Hamann *et al.* *Phys. Rev. Lett.* **80**, 4149 (1998), and references cited.
- [7] D. Jaksch *et al.*, *Phys. Rev. Lett.* **81**, 3108 (1998).
- [8] see, e.g., A. Galindo, P. Pascual, *Quantum Mechanics II* (Springer Berlin 1991).
- [9] The justification parallels the arguments presented in the context of the pseudo–potential approximation in BEC see, e.g., H. T. C. Stoof, M. Bijlsma, and M. Houbiers, *J. Res. Natl. Inst. Stand. Technol.* **101**, 443 (1996).
- [10] Yu. Kagan *et al.*, *Phys. Rev. A* **54**, R1753, (1996).

- [11] B. Schumacher, Phys. Rev. A **54**, 2614 (1996).
- [12] V. B. Braginsky, Y. I. Vorontsov, and F. Y. Khalili, Sov. Phys. JETP **46**, 705 (1977).
- [13] V. Finkelstein, P. R. Berman, and J. Guo, Phys. Rev. A, **45**, 1829 (1992).
- [14] J. Weiner et al., Rev. Mod. Phys. in press; E. Tiesinga, B. J. Verhaar, and H. T. C. Stoof, Phys. Rev. A, **47**, 4114 (1993).
- [15] for details see: H. Briegel and D. Jaksch, unpublished.
- [16] In ^{87}Rb and ^{23}Na one could use $|a\rangle \equiv |F = 1, m_F = -1\rangle$, $|b\rangle \equiv |F = 2, m_F = 2\rangle$ and $|c\rangle \equiv |F = 1, m_F = 1\rangle$ (see [15]).
- [17] D. M. Stamper-Kurn *et al.*, Phys. Rev. Lett. **80**, 2027 (1998).
- [18] G. K. Brennen *et al.*, Phys. Rev. Lett., in print.

Chapter 10

PUBLICATION

QUANTUM GATES WITH NEUTRAL ATOMS: CONTROLLING COLLISIONAL INTERACTIONS IN TIME DEPENDENT TRAPS

T. Calarco^{1,2}, E. A. Hinds³, D. Jaksch¹, J. Schmiedmayer⁴, J.I. Cirac¹, and
P. Zoller¹

¹Institut für Theoretische Physik, Universität Innsbruck, A-6020 Innsbruck, Austria

²ECT*, European Centre for Theoretical Studies in Nuclear Physics and Related Areas

Villa Tambosi, Strada delle Tabarelle 286, I-38050 Villazzano (Trento), Italy

³ Sussex Centre for Optical and Atomic Physics, University of Sussex, Brighton, BN1 9QH, United Kingdom

⁴ Institut für Experimentalphysik, Universität Innsbruck, A-6020 Innsbruck, Austria

to appear in Phys. Rev. A

We theoretically study specific schemes for performing a fundamental two-qubit quantum gate via controlled atomic collisions by switching microscopic potentials. In particular we calculate the fidelity of a gate operation for a configuration where a potential barrier between two atoms is instantaneously removed and restored after a certain time. Possible implementations could be based on microtraps created by magnetic and electric fields, or potentials induced by laser light.

10.1 Introduction

The creation and manipulation of many-particle entangled states offers new perspectives for the investigation of fundamental questions of quantum mechanics, and is the basis of applications such as quantum information processing. Several proposals to implement quantum logic [1] have been made including ion-traps [2], cavity QED and photons [3], and molecules in the context of NMR [4]. Very recently, we have identified a new way of entangling neutral atoms by using *cold controlled collisions* [5] (see also [6]). Neutral atoms are good candidates for quantum information processing, since they suffer a comparatively weak dissipative coupling to the environment. Techniques to cool and trap atoms by means of magnetic and optical potentials have been developed in the context of laser cooling and trapping, and Bose-Einstein condensation (BEC) [7]. In particular the ongoing development of magnetic microtraps [8] offers an interesting new perspective for storing and manipulating arrays of atoms [9, 10] and possible applications in quantum information [11].

Motivated by these new experimental possibilities we will study in this paper specific configurations of atoms stored in time dependent microtraps. We will assume that two internal states of the atoms $|a\rangle$ and $|b\rangle$ represent the logical states $|0\rangle$ and $|1\rangle$ of a qubit, respectively. The aim is to implement a fundamental two-qubit quantum gate between two atoms with the truth table

$$\begin{aligned}
 |0\rangle|0\rangle &\rightarrow |0\rangle|0\rangle, \\
 |0\rangle|1\rangle &\rightarrow |0\rangle|1\rangle, \\
 |1\rangle|0\rangle &\rightarrow |1\rangle|0\rangle, \\
 |1\rangle|1\rangle &\rightarrow -|1\rangle|1\rangle,
 \end{aligned} \tag{10.1}$$

by switching the trapping parameters. Eq. (10.1) represents a so called phase gate. To realize this transformation we will consider state selective switching of the trapping potential such that the atoms pick up a phase due to collisional interaction [12] only if they are in state $|b\rangle$. This can be achieved by raising and lowering a potential barrier between the two atoms as shown in Fig. 10.1. According to Fig. 10.1a the potential is initially composed of two separated wells. Ideally the atoms have been cooled to the vibrational ground states of the two wells. At time $t = 0$ the shape of the trapping potential is changed for particles in state $|b\rangle$ (dashed line in Fig. 10.1b) while the potentials for the atoms in the state $|a\rangle$ remains unchanged (solid line in Fig. 10.1b). By removing the barrier the particles in state $|b\rangle$ start to oscillate and will collide. The “cold” collision represents a coherent interaction described by a pseudo-potential with a strength proportional to the s -wave scattering length [5]. This results in a phase shift of the wave function for both atoms in the internal state

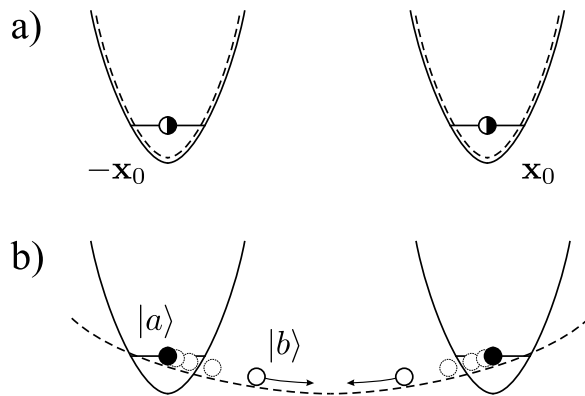


Fig. 10.1: Configuration at times $t < 0$, $t > \tau$ (a) and during the gate operation (b). The solid (dashed) curves show the potentials for particles in the internal state $|a\rangle$ ($|b\rangle$).

$|b\rangle$. The size of the phase shift can be controlled by the number of oscillations and the effective collisional interaction strength (see Sec. 10.2.1). As a last step the atoms have to be restored to the motional ground state of the trapping potential of Fig. 10.1a. This whole process of switching the potentials can be performed either as (i) switching the shape of the potential *instantaneously* at times $t = 0$ and $t = \tau$ where τ is a multiple of the oscillation period in the well of Fig. 10.1b (dashed line), or, (ii) deforming the shape of the potential between Fig. 10.1a and b *adiabatically*. The aim of the present paper is to investigate the gate dynamics for the scenario (i), when the switching is instantaneous: In particular we are interested in the required physical parameters and the corresponding fidelities characterising the quality of the phase gate. We will also study the dependence of the fidelity on the temperature of the atoms. The paper is organized as follows. Section 10.2 describes the model and derives an expression for the collisional phase shift. In Sec. 10.3 we study the gate dynamics for the case of instantaneous switching while in Sec. 10.4 we present numerical results for the fidelity.

10.2 Model

In the present section we will write down the Hamiltonian for two interacting particles trapped in conservative time dependent potentials and derive an expression for the collisional phase shift.

10.2.1 Hamiltonian

The dynamics of atoms in a time-varying, state-dependent trapping potential $V_\alpha(\mathbf{x}, t)$ (where t is time and $\mathbf{x} \equiv (x, y, z)$ is the three-dimensional coordinate) can be described by the Hamiltonian operator

$$\begin{aligned}
 H = & \sum_{\alpha \in \{a, b\}} \int d^3x \hat{\Psi}_\alpha^\dagger(\mathbf{x}) \left[-\frac{\hbar^2}{2m} \nabla^2 + V_\alpha(\mathbf{x}, t) \right] \hat{\Psi}_\alpha(\mathbf{x}) \\
 & + \sum_{\alpha, \beta \in \{a, b\}} \frac{1}{2} \int d^3x d^3x' \hat{\Psi}_\alpha^\dagger(\mathbf{x}) \hat{\Psi}_\beta^\dagger(\mathbf{x}') \\
 & \quad \times U_{\alpha\beta}(\mathbf{x}, \mathbf{x}') \hat{\Psi}_\beta(\mathbf{x}') \hat{\Psi}_\alpha(\mathbf{x}), \tag{10.2}
 \end{aligned}$$

where m is the mass of the atoms, $\hat{\Psi}_\alpha(\mathbf{x})$ is a field operator for atoms in internal state $|\alpha\rangle$, and $U_{\alpha\beta}(\mathbf{x}, \mathbf{x}')$ is the potential for the interaction between two atoms in states $|\alpha\rangle$ and $|\beta\rangle$, where $\alpha, \beta \in \{a, b\}$. We take a trapping potential of the form

$$V_\alpha(\mathbf{x}, t) = v_\alpha(x, t) + v_\perp(y) + v_\perp(z), \tag{10.3}$$

i.e. we assume the same shape along y and z , which is independent of time and of the internal state.

For cold atoms the dominant collisional interaction is the s -wave scattering term described by a contact potential of the form

$$U_{\alpha\beta}(\mathbf{x}, \mathbf{x}') = \frac{4\pi a_s^{\alpha\beta} \hbar^2}{m} \delta^3(\mathbf{x} - \mathbf{x}'), \tag{10.4}$$

where $a_s^{\alpha\beta}$ is the s -wave scattering length for the corresponding internal states. Note that for identical atoms in the same internal state s -wave scattering is only possible for bosonic atoms (cf. the b - b collision in Fig. 10.1b). We therefore require, in the following, the field operators $\hat{\Psi}_\alpha(\mathbf{x})$ to describe bosonic atoms and to obey the usual bosonic commutation relations.

Furthermore, we assume much stronger confinement along the y and z directions than in x , so that the probability of transverse excitations can be neglected. If each atom is initially in the ground state $|\psi_\perp\rangle$ of the transverse potentials, it will then remain in that state to a good approximation and the corresponding degrees of freedom can be integrated out. In this case the dynamics becomes effectively one-dimensional and is described by the Hamiltonian operator

$$H_x = \sum_{\alpha \in \{a, b\}} \int dx \hat{\psi}_\alpha^\dagger(x) \left[-\frac{\hbar^2}{2m} \frac{d^2}{dx^2} + v_\alpha(x, t) \right] \hat{\psi}_\alpha(x)$$

$$\begin{aligned}
& + \sum_{\alpha, \beta \in \{a, b\}} \frac{1}{2} \int dx dx' \hat{\psi}_\alpha^\dagger(x) \hat{\psi}_\beta^\dagger(x') \\
& \quad \times u_{\alpha\beta}(x - x') \hat{\psi}_\beta(x') \hat{\psi}_\alpha(x). \tag{10.5}
\end{aligned}$$

Here $\hat{\psi}_\alpha(x)$ is the one-dimensional analogue of $\hat{\Psi}_\alpha(\mathbf{x})$, and

$$\begin{aligned}
u_{\alpha\beta}(x - x') &= \int dy dy' dz dz' U_{\alpha\beta}(\mathbf{x}, \mathbf{x}') \\
& \quad \times |\psi_\perp(y) \psi_\perp(y') \psi_\perp(z) \psi_\perp(z')|^2 \\
&= \frac{4\pi a_s \hbar^2}{m} \delta(x - x') \left[\int dy |\psi_\perp(y)|^4 \right]^2, \tag{10.6}
\end{aligned}$$

is an effective interaction potential taking into account the transverse confinement of the atoms. The ψ_\perp are the ground-state wavefunctions in the transverse directions (having energy $\hbar\omega_\perp/2$ each). Their time evolution will just contribute an overall phase factor (with a phase proportional to ω_\perp), irrelevant for the quantities we are going to compute. We see that the effective interaction strength can be adjusted by changing the trapping parameters.

Eq. (10.5) holds for an arbitrary number of atoms. We now consider the case of two bosonic atoms 1 and 2, with internal states $|a\rangle_{1,2}$ and $|b\rangle_{1,2}$. Their evolution is governed by the first-quantized Hamiltonian

$$\mathcal{H} = \sum_{\alpha, \beta \in \{a, b\}} \mathcal{H}_{\alpha\beta} \otimes |\alpha\rangle_1 \langle \alpha| \otimes |\beta\rangle_2 \langle \beta|, \tag{10.7}$$

where

$$\mathcal{H}_{\alpha\beta} \equiv \mathcal{H}_{\alpha\beta}^0 + u_{\alpha\beta}, \tag{10.8}$$

$$\mathcal{H}_{\alpha\beta}^0 = \mathcal{H}_\alpha(p_1, x_1, t) + \mathcal{H}_\beta(p_2, x_2, t), \tag{10.9}$$

$$\mathcal{H}_\alpha(p_i, x_i, t) = \frac{p_i^2}{2m} + v_\alpha(x_i, t). \tag{10.10}$$

Here x_i and p_i are the position and momentum operator for particle $i = 1, 2$ respectively.

10.2.2 Phase shift due to interaction

We call $|\psi_{\alpha\beta}^{(0)}(t)\rangle$ and $|\psi_{\alpha\beta}(t)\rangle$ the two-particle states at time t evolved from the same initial state $|\psi_{\alpha\beta}(0)\rangle$ in the absence and in the presence of interaction, respectively:

$$i\hbar\partial_t|\psi_{\alpha\beta}^{(0)}(t)\rangle = \mathcal{H}_{\alpha\beta}^0|\psi_{\alpha\beta}^{(0)}(t)\rangle, \quad (10.11)$$

$$i\hbar\partial_t|\psi_{\alpha\beta}(t)\rangle = \mathcal{H}_{\alpha\beta}|\psi_{\alpha\beta}(t)\rangle. \quad (10.12)$$

We also define the overlaps

$$O_0(\psi_{\alpha\beta}, t) \equiv \langle\psi_{\alpha\beta}(t)|\psi_{\alpha\beta}^{(0)}(t)\rangle; \quad (10.13)$$

$$O(\psi_{\alpha\beta}, t) \equiv \langle\psi_{\alpha\beta}(t)|\psi_{\alpha\beta}(0)\rangle. \quad (10.14)$$

The condition that both atoms end up at time $t = \tau$ with the same spatial distribution they had at the beginning will not be exactly fulfilled in realistic situations. However, in order for our scheme to work it is required that this is true at least approximately:

$$|O(\psi_{\alpha\beta}, \tau)| \approx 1 \quad \forall \alpha, \beta, \quad (10.15)$$

i.e. the two-atom final state should differ from the initial one just by a phase factor $\Phi_{\alpha\beta}(\tau) \equiv \arg[O(\psi_{\alpha\beta}, \tau)]$:

$$|\psi_{\alpha\beta}(\tau)\rangle \approx e^{-i\Phi_{\alpha\beta}(\tau)}|\psi_{\alpha\beta}(0)\rangle. \quad (10.16)$$

We also assume that the interaction between atoms does not induce any significant alteration in the shape of the wave functions, *i.e.*

$$|O_0(\psi_{\alpha\beta}, t)| \approx 1 \quad \forall \alpha, \beta, t. \quad (10.17)$$

Hence

$$|\psi_{\alpha\beta}(t)\rangle \approx e^{-i\phi_{\alpha\beta}(t)}|\psi_{\alpha\beta}^{(0)}(t)\rangle, \quad (10.18)$$

having defined the *collisional phase*

$$\phi_{\alpha\beta}(t) \equiv \arg[O_0(\psi_{\alpha\beta}, t)], \quad (10.19)$$

accounting for the contribution of the interaction to the total phase $\Phi_{\alpha\beta}(\tau)$. The rest of the phase comes from the motion of the particles in the time-dependent trapping potential. From Eqs. (10.15) and (10.17) it follows that

$$|O(\psi_{\alpha\beta}^{(0)}, \tau)| \approx 1 \quad \forall \alpha, \beta, \quad (10.20)$$

which implies, by analogy with Eq. (10.16),

$$|\psi_{\alpha\beta}^{(0)}(\tau)\rangle \approx e^{-i[\phi_{\alpha}(\tau)+\phi_{\beta}(\tau)]}|\psi_{\alpha\beta}(0)\rangle. \quad (10.21)$$

Here the *kinematic phase* $\phi_\alpha(\tau)$ [$\phi_\beta(\tau)$] is defined as the phase that one atom would acquire after evolving for a time τ in the potential v_α [v_β] in the absence of the other particle. By substituting Eq. (10.21) into Eq. (10.18) evaluated at $t = \tau$, and comparing it with Eq. (10.16), the collisional phase can be reexpressed as

$$\phi_{\alpha\beta}(\tau) \approx \Phi_{\alpha\beta}(\tau) - [\phi_\alpha(\tau) + \phi_\beta(\tau)]. \quad (10.22)$$

By combining Eqs. (10.2.2), (10.17) and (10.18), we find

$$\hbar\partial_t\phi_{\alpha\beta}(t) \approx \langle\psi_{\alpha\beta}^{(0)}(t)|u_{\alpha\beta}|\psi_{\alpha\beta}^{(0)}(t)\rangle \equiv \Delta E_{\alpha\beta}(t), \quad (10.23)$$

which is precisely the result one would expect from perturbation theory. In order for Eq. (10.17) to hold, the time-dependent energy shift defined in Eq. (10.23) has to satisfy the condition $\Delta E_{\alpha\beta}(t) \ll \hbar\omega$, with $\hbar\omega$ the first excitation energy of the system. Integration of Eq. (10.23) gives a perturbative expression for the collisional phase:

$$\phi_{\alpha\beta}(t) \approx \frac{1}{\hbar} \int_0^t dt' \Delta E_{\alpha\beta}(t'). \quad (10.24)$$

10.3 Gate operation

To proceed further, we have to specify the functional form of the potential $v_\alpha(x, t)$ in Eq. (10.3). The two atoms are initially trapped along x in two separate harmonic wells of frequency ω_0 , centered at $\pm x_0$. In order to simplify the analytic calculations, the confinement in the transverse directions is also assumed to be harmonic. At $t = 0$ the barrier between the wells is suddenly removed in a selective way for atoms in internal state $|b\rangle$: an atom in state $|a\rangle$ feels no change, whereas one in state $|b\rangle$ finds itself in a new harmonic potential, centered on $x = 0$ with frequency $\omega < \omega_0$. The atoms are allowed to oscillate for some time, and then at $t = \tau$ the barrier is suddenly raised again to trap them at the original positions. During this process the atoms acquire a kinematic phase due to their oscillations within the wells, and also – if they collide – an interaction phase due to the collision. Here we calculate these phases and consider the appropriate switching time τ for a quantum gate. In Sect. 10.4 we make a quantitative estimate of the gate fidelity.

10.3.1 Switching potential

We take the potential in Eq. (10.3) to be explicitly

$$v_a(x, t) = \frac{m\omega_0^2}{2} [\theta(x)(x - x_0)^2 + \theta(-x)(x + x_0)^2]; \quad (10.25)$$

$$v_b(x, t) = \begin{cases} v_a(x, t) & t < 0, t > \tau; \\ \frac{m\omega^2}{2}x^2 & 0 \leq t \leq \tau; \end{cases} \quad (10.26)$$

$$v_{\perp}(y) = \frac{m\omega_{\perp}^2}{2}y^2, \quad (10.27)$$

as shown in Fig. 10.1.

As long as the single-well ground-state width $a_0 = \sqrt{\hbar/m\omega_0}$ satisfies $a_0^2 \ll x_0^2$ and there are no significant excitations to higher levels of $v_a(x, t)$, the actual behavior of that potential around the origin does not really matter and we can use Eq. (10.25) regardless of the experimental shape of the barrier around $x = 0$. The ground state wavefunctions $\psi_{\pm}(x)$ of the right and left well of the potential $v_a(x, t)$ are given by

$$\psi_{\pm}(x) = \left(\frac{m\omega_0}{2\pi\hbar}\right)^{\frac{1}{4}} e^{-\frac{m\omega_0}{2\hbar}(x_0 \mp x)^2}, \quad (10.28)$$

while the ground state wavefunction in the transverse directions is given by

$$\psi_{\perp}(y) = \left(\frac{m\omega_{\perp}}{2\pi\hbar}\right)^{\frac{1}{4}} e^{-\frac{m\omega_{\perp}}{2\hbar}y^2}. \quad (10.29)$$

By assumption the overlap between the two wavefunctions $\psi_{+}(x)$ and $\psi_{-}(x)$ is negligible since the two particles are kept separated from each other in the potential $v_a(x, t)$. At $t = 0$, the central barrier between the two wells is selectively switched off for state $|b\rangle$. A particle in this state will start moving towards the other atom along x and an interaction will take place. We shall separately study the evolution of the system at $t \geq 0$ for each combination of internal states (α, β) . For operation of the quantum gate analyzed here, it is important that $v_b(x, t)$ be accurately harmonic while $0 \leq t \leq \tau$.

10.3.2 Particles in the same internal state

10.3.2.1 Initial state

If both particles are in the same internal state $|\alpha\rangle$, this factorizes from the motional degrees of freedom and the initial state is

$$|\psi_{\alpha\alpha}(0)\rangle = \frac{|\psi_{-}\rangle|\psi_{+}\rangle + |\psi_{+}\rangle|\psi_{-}\rangle}{\sqrt{2}} \otimes |\alpha\rangle|\alpha\rangle. \quad (10.30)$$

The calculation can be simplified by introducing the center of mass (CM) and relative coordinates for the x -motion, thus rewriting

$$\begin{aligned} \psi_{\alpha\alpha}(x_1, x_2, 0) &\equiv \frac{1}{\sqrt{2}} [\psi_{-}(x_1)\psi_{+}(x_2) + \psi_{+}(x_1)\psi_{-}(x_2)] \\ &= \psi_{\text{CM}}(R, 0)\psi_{\text{rel}}(r, 0), \end{aligned} \quad (10.31)$$

where

$$\psi_{\text{CM}}(R, 0) = \left(\frac{M\omega_0}{\pi\hbar} \right)^{\frac{1}{4}} e^{-\frac{M\omega_0}{2\hbar} R^2}, \quad (10.32)$$

$$\psi_{\text{rel}}(r, 0) = \left(\frac{\mu\omega_0}{4\pi\hbar} \right)^{\frac{1}{4}} \sum_{\varsigma=-1,+1} e^{-\frac{\mu\omega_0}{2\hbar} (2x_0+\varsigma r)^2}, \quad (10.33)$$

with $M = 2m$, $\mu = m/2$, $R = (x_1 + x_2)/2$, $r = x_2 - x_1$.

10.3.2.2 Time evolution

For $t \leq 0$, the particles are stored in the displaced wells and no interaction takes place. If both particles are in state $|a\rangle$, the potential remains unchanged also for $t \geq 0$; there is no collision and thus the collisional phase $\phi_{aa} = 0$. The state simply picks up the phase due to the free evolution:

$$|\psi_{\alpha\alpha}(t)\rangle = e^{-i\omega_0 t} |\psi_{\alpha\alpha}(0)\rangle. \quad (10.34)$$

We shall now consider the situation in which both particles are in state $|b\rangle$. In this case, after the barrier is switched off, the particles start oscillating in the harmonic trapping potential. In the absence of interaction they would come back to the initial state after an oscillation period $T_{\text{osc}} = 2\pi/\omega$, having acquired a phase $4\pi\omega_{\perp}/\omega$ because of the transverse confining potential. The interaction causes an additional phase to be accumulated by the wavefunction as the number of oscillations increases, and a slight decrease in the oscillation frequency, because the atoms acquire a small delay in their motion inside the trap as they come out from a collision. If the latter feature is not too strong, by choosing a switching time $\tau \approx 2N\pi/\omega$ it should be possible to get back the original state plus an interaction phase, that is adjusted to $\pm\pi$ by a proper choice of the trap parameters and of the number of collisions occurring during the actual gate operation, *i.e.* for $0 < t < \tau$. We shall therefore focus on the dynamics in this time interval.

In the center of mass–relative coordinate system we get

$$\mathcal{H}_{bb} = \frac{P^2}{2M} + \frac{M\omega^2}{2} R^2 + \frac{p^2}{2\mu} + \frac{\mu\omega^2}{2} r^2 + u_{bb}(r), \quad (10.35)$$

where $P = p_1 + p_2$, $p = (p_1 - p_2)/2$. If the interaction is neglected we can solve the two–particle Schrödinger equation for Hamiltonian Eq. (10.35) analytically as shown in Appendix 10.A.1. It can be seen from Eqs. (10.55–10.61) that the unperturbed two-atom motion has a period of $T_{\text{osc}}/2$ instead of T_{osc} . This happens because the initial state, symmetric with respect to the origin, has

nonzero projection only on the even eigenstates, having energies $(2n + 1/2)\hbar\omega$: therefore, after a time π/ω , each component of the wavefunction gets the same constant phase $\exp[i(2n + 1/2)\pi] = \exp(i\pi/2)$. This has a simple physical interpretation: if the atoms do not interact, after half an oscillation period each particle is at its turning point, coinciding with the other atom's starting location; so at that time the two atoms have interchanged their positions, but since they are indistinguishable this has to be regarded as exactly the same motional state they had at the beginning (apart from a phase factor).

When we take into account the interaction between particles, the center of mass motion is unaffected but the relative motion can no longer be treated analytically. The numerical method we use to carry out this calculation is outlined in Appendix 10.A.2.1. It is, however, possible to take the interaction into account perturbatively as shown in the following section.

10.3.2.3 Perturbative calculation of the phase shift

Eqs. (10.6) and (10.29) combine to yield

$$u_{\alpha\beta}(x_1 - x_2) = 2a_s^{\alpha\beta}\hbar\omega_{\perp}\delta(x_1 - x_2). \quad (10.36)$$

When both particles are in state $|b\rangle$, the time-dependent energy shift defined in Eq. (10.23) can be calculated analytically:

$$\begin{aligned} \Delta E_{bb}(t) &= \int dRdr |\psi_{CM}(R, t)\psi_{\text{rel}}^{(0)}(r, t)|^2 u_{bb}(r) \\ &= a_s^{bb}\hbar\omega_{\perp} \sqrt{\frac{8m\Omega(t)}{\pi\hbar}} e^{-\frac{2m\omega_0}{\hbar}x_0^2} \left[1 - \sin^2(\omega t) \frac{\omega_0\Omega(t)}{\omega^2}\right], \end{aligned} \quad (10.37)$$

where $\Omega(t)$ is defined in Eq. (10.56). The corresponding interaction-induced phase shift accumulated after an oscillation period is

$$\phi_{bb}(T_{\text{osc}}) \approx \frac{4a_s^{bb}\omega_{\perp}}{\sqrt{x_0^2\omega^2 - a_0^2\omega_0^2/4}}, \quad (10.38)$$

which has been evaluated by means of the well-known saddle-point approximation.

10.3.3 Particles in different internal states

10.3.3.1 Initial state

When the internal states of the atoms are different, they no longer factorize as in Eq. (10.30) and the initial state is given by

$$|\psi_{ab}(0)\rangle = \frac{1}{\sqrt{2}} [|\psi_{-}\rangle_1 |\psi_{+}\rangle_2 \otimes |a\rangle_1 |b\rangle_2 + (1 \leftrightarrow 2)], \quad (10.39)$$

where without loss of generality we assumed that the particle in the left (right) well is in internal state $|a\rangle$ ($|b\rangle$).

10.3.3.2 Time evolution

The relevant quantities can again be expressed in terms of the projection of the evolved state on the initial one. By virtue of symmetry under particle interchange, this turns out to be

$$O(\psi_{ab}, t) = \langle \psi_- | \langle \psi_+ | e^{-\frac{i}{\hbar} \mathcal{H}_{ab} t} | \psi_- \rangle | \psi_+ \rangle. \quad (10.40)$$

Therefore we can restrict our analysis, as in the previous case, to the one-dimensional motion, starting from the non-symmetrized wavefunction

$$\psi_-(x_1) \psi_+(x_2). \quad (10.41)$$

The Hamiltonian for $0 < t < \tau$ reads

$$\begin{aligned} \mathcal{H}_{ab} &= \frac{p_1^2}{2m} + \frac{p_2^2}{2m} + \frac{m\omega_0^2}{2} (x_1 + x_0)^2 + \frac{m\omega^2}{2} x_2^2 \\ &\quad + u_{ab}(x_1 - x_2) \\ &= \frac{P^2}{2M} + \frac{p^2}{2\mu} + \frac{m}{2} (\omega^2 - \omega_0^2) Rr + \frac{m}{2} \omega_0^2 x_0^2 \left(1 - \frac{\omega_0^2}{\tilde{\omega}^2} \right) \\ &\quad + \frac{M}{2} \tilde{\omega}^2 \left(R + \frac{\omega_0^2}{2\tilde{\omega}^2} x_0 \right)^2 + \frac{\mu}{2} \tilde{\omega}^2 \left(r - \frac{\omega_0^2}{\tilde{\omega}^2} x_0 \right)^2 \\ &\quad + u_{ab}(r) \end{aligned} \quad (10.42)$$

where $\tilde{\omega} \equiv \sqrt{(\omega^2 + \omega_0^2)}/2$. Only the left well of $v_a(x_1, t)$ has been considered since the wavefunction remains negligible in the region $x_1 > 0$ for $t > 0$, as it is at $t = 0$. It can be seen from Eq. (10.42) that the center of mass no longer decouples from the relative motion, unlike in the previous symmetrical case. A numerical calculation is needed to evaluate the phase shift ϕ_{ab} . This is done in Appendix 10.A.2.2.

10.3.4 Particles at finite temperature

Up to now we have assumed the particles to be in a well known motional state. In realistic experimental situations this may not be the case. The temperature T of the particles in the trap will be different from 0 and thus the initial state of the system with particles in internal states α, β is given by the density operator

$$\rho_{\alpha\beta}(T, t = 0^-) \propto e^{-\mathcal{H}_{\alpha\beta}(0^-)/k_B T}. \quad (10.43)$$

This takes the average over different initial excited states, with a thermal probability distribution corresponding to T . As shown in Appendix 10.B the collisional phase accumulated is independent of the shape of the wave function if the particles move at a constant velocity with respect to each other and the shape of the one particle wavefunction does not change during the interaction. This is a good approximation for the interaction between particles in the same internal state $|b\rangle$. The particles interact in the vicinity of the center of the well where their velocity $v \approx x_0\omega$ is almost constant and the shape of the one particle wavefunction does not change substantially as long as the conditions

$$a_x \ll x_0, \quad \text{and} \quad a \ll x_0 \quad (10.44)$$

hold, where a is the width of the one particle wavefunction when the particles cross the center of the trap and $a_x = \sqrt{\hbar/m\omega}$. Therefore the collisional phase $\phi_{bb}(T_{\text{osc}})$ is almost independent of the temperature T as long as mainly excitations fulfilling conditions Eq. (10.44) are populated. Note that we are neglecting transverse excitations. If all three motional degrees of freedom are characterized by the same temperature T , this is realistic as long as the condition $k_B T \ll \hbar\omega_{\perp}$ is satisfied. However, in principle it is also possible to cool the transverse motion separately, allowing a higher temperature along x . Of course this would require that the rethermalization time is much larger than the experimental time scale. This lack of sensitivity to temperature applies quite generally, for example to atoms interacting in an optical lattice as discussed in [5], provided that the velocity at which the atoms are made to interact (in that case the velocity of lattice movements) is kept constant during the interaction.

10.4 A physical implementation

We now consider the implementation of a switching potential by means of static electric and magnetic trapping forces. We first discuss the possibility of obtaining the desired state dependence by means of devices which are experimentally available [9, 11], when the present magnetic devices can be combined with nanofabricated electrodes. Then we compute the performance of a quantum gate for realistic trapping parameters.

10.4.1 Microscopic electromagnetic trapping potential

The interaction between the magnetic dipole moment of an atom in some hyperfine state $|F, m_F\rangle$ and an external static magnetic field \mathbf{B} entails an energy $U_{\text{magn}} \approx g_F \mu_B m_F |\mathbf{B}|$ depending on the atomic internal state via the quantum number m_F (here μ_B is the Bohr magneton and g_F is the Landé

factor). The Stark shift induced on an atom by an electric field \mathbf{E} gives an energy (independent on the hyperfine sublevel) $U_{\text{el}} \approx \frac{1}{2}\alpha_{\text{el}}|\mathbf{E}|^2$, where α_{el} is the atomic polarizability. The interplay between these two effects can be exploited in order to obtain a trapping potential whose shape depends on the internal state of the atoms. As an example, we consider an atomic mirror like the one recently realized [9] from a conventional video tape with sinusoidal magnetization $\mathbf{M} = (M_0 \cos[k_M x], 0, 0)$ along the x -axis. The period of the pattern, $2\pi/k_M$, can be as small as $1\mu\text{m}$ with the system studied in [9], or even close to 100 nm using existing magnetic storage technologies. In order to get a microscopic trapping potential [11], it is necessary to apply an external bias field $\mathbf{B}^{\text{ext}} \equiv (0, B_y^{\text{ext}}, B_z^{\text{ext}})$, oriented mainly along the z axis, normal to the mirror's surface, and with a small component along y in order to prevent trap losses due to spin flips occurring at magnetic field zeros. In this case the magnetic trapping potential is

$$V_{m_F}(\mathbf{x}) = g_F \mu_B m_F \left\{ B_0^2 e^{-2k_M z} \cos^2(k_M x) + (B_y^{\text{ext}})^2 + \left[B_0 e^{-k_M z} \sin(k_M x) + B_z^{\text{ext}} \right]^2 \right\}^{\frac{1}{2}}, \quad (10.45)$$

where $B_0 = \mu_0 M_0 (1 - e^{-k_M \delta})/2$ and δ is the tape thickness. The minima of V_{m_F} form a periodic pattern above the tape surface, at a height $z_0 = \ln(\mu_0 M_0/B_0)/k_M$ typically of the order of some fractions of μm . The spacing between two nearest minima along x is just the period of the magnetization, $2\pi/k_M$. With present-day technology, trapping frequencies can range from a few tens of kHz up to some MHz. Microscopic electrodes can be nanofabricated on the mirror's surface [10], thus allowing for the design of a potential with the characteristics described in Sect. 10.3.

For the states $|a\rangle$ and $|b\rangle$ we choose the hyperfine structure states $|a\rangle \equiv |F = 1, m_F = -1\rangle$ and $|b\rangle \equiv |F = 2, m_F = 2\rangle$ of the $5S_{1/2}$ level of ^{87}Rb , having scattering lengths $a_s^{bb} \approx a_s^{ab} \approx 5.1$ nm. Several schemes of loading atoms into the trap have been envisaged (see for example [9, 11]). Most of them rely on an intermediate step, where atoms can be trapped and cooled without coming in contact with the magnetic mirror. This pre-loading stage can be either a magnetic trap initially displaced from the surface, or a different kind of trap (for instance an evanescent wave mirror, where different internal states can be trapped by gravity close to the surface [13] before the atoms are put in the correct states for magnetic trapping), to be replaced by the electromagnetic microtrap with a gradual switch-on of the electric and bias magnetic fields in the final stage of loading [10]. This could also allow for implementing a controlled filling of the trap sites by adiabatically turning on the periodic potential, in a similar way to that discussed in [14].

10.4.2 Results

10.4.2.1 Time evolution during gate operation

If both particles are in state $|a\rangle$, there is no interaction-induced phase shift, as expressed in Eq. (10.34). The results for both particles in state $|b\rangle$ are shown in Fig. 10.2a, while those for differing internal states appear in Fig. 10.2b. The harmonic potential ensures that the system comes periodically back to its initial state. In the absence of interaction, the frequency of recurrences is twice as high for $|\psi_{bb}(t)\rangle$ as it is for $|\psi_{ab}(t)\rangle$, as already discussed at the end of Sect. 10.3.2.2. The interaction also makes the two cases substantially different from each other. Its effect on the atomic motion is not dramatic if both particles are in state $|b\rangle$: actually, the oscillation period in the presence of interaction is increased by only $\delta t \approx 1.4 \times 10^{-3} T_{\text{osc}}$ with the parameters used here. The collisional phase ϕ_{bb} increases in steps at the times $t_k \equiv (2k + 1)T_{\text{osc}}/4$, when the atoms meet at the center of the well, and remains constant at intermediate times while they are apart. Note that since the particles are indistinguishable the amplitude for the particles to bounce back during the collision does not harm the performance of our scheme. The contributions of the reflected and the non-reflected part to the wavefunction are indistinguishable. What matters is whether or not the two-particle spatial distribution approaches the initial one, and this is satisfied to a high accuracy in our case.

The behavior is quite different if the atoms are in different internal states. The phase shift increases in larger steps since the collision is close to the turning point of the particle in state $|b\rangle$, near $x = x_0$. Here the velocity of the particle is much smaller than at the center of the trap and thus the interaction time is longer, allowing a larger phase to accumulate. The collision also excites vibrations of the particle in state $|a\rangle$. The resulting loss of energy from the particle in state $|b\rangle$ leads to a decreasing oscillation amplitude of that particle, and the initial state is no longer recovered. This problem can be avoided if the potential minimum for state $|a\rangle$ is displaced along the transverse direction from the one for state $|b\rangle$ by means of an additional electrostatic field [11], so that the atoms interact if and only if they are both in state $|b\rangle$.

10.4.2.2 Gate fidelity at $T = 0$

Ideally, the scheme described above should realize the mapping

$$\begin{aligned}
 |a\rangle|a\rangle &\rightarrow e^{-i2\phi_a}|a\rangle|a\rangle, \\
 |a\rangle|b\rangle &\rightarrow e^{-i(\phi_a+\phi_b+\phi_{ab})}|a\rangle|b\rangle, \\
 |b\rangle|a\rangle &\rightarrow e^{-i(\phi_b+\phi_a+\phi_{ab})}|b\rangle|a\rangle, \\
 |b\rangle|b\rangle &\rightarrow e^{-i(\phi_{bb}+2\phi_b)}|b\rangle|b\rangle,
 \end{aligned} \tag{10.46}$$

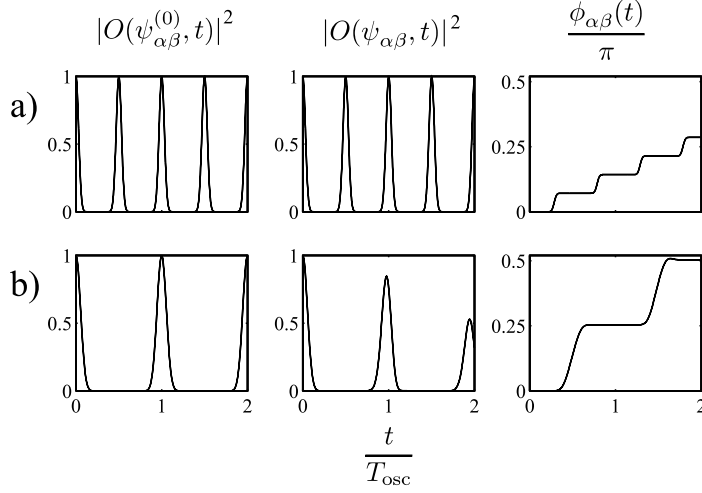


Fig. 10.2: Dynamics during gate operation: projection of the initial state on the state evolved without (left) and with interaction (center); interaction-induced phase shift (right). Results are shown for different combinations of internal states: a) $\alpha = \beta = b$; b) $\alpha \neq \beta$. We choose $\omega = 2\pi 17.23$ kHz and $\omega_{\perp} = 2\pi 150$ kHz, corresponding to ground-state widths $a_x \approx 82$ nm, $a_{\perp} \approx 28$ nm, with the initial wells having frequency $\omega_0 = 2\omega$ and displaced by $x_0 = 5a_x$. Time is in units of the oscillation period T_{osc} .

where ϕ_a and ϕ_b are the phases due to the time evolution without taking into account the interaction. We assume, as above, that the trapping potential is designed to prevent the atoms interacting if they are in different internal states. Therefore we set $\phi_{ab} = 0$ in Eq. (10.46) and consider only ϕ_{bb} in the following. We use the minimum fidelity F [15] to characterize the quality of the gate. F is defined as

$$F = \min_{|\tilde{\chi}\rangle} \left(\text{tr}_{\text{ext}} \left\{ \langle \tilde{\chi} | \mathcal{U} S [|\chi\rangle \langle \chi| \otimes \rho_0] S^{\dagger} \mathcal{U}^{\dagger} | \tilde{\chi}\rangle \right\} \right), \quad (10.47)$$

where $|\chi\rangle$ is an arbitrary internal state of both atoms, and $|\tilde{\chi}\rangle$ is the state resulting from $|\chi\rangle$ using the mapping (10.46). The trace is taken over properly symmetrized motional states, \mathcal{U} is the evolution operator for the internal states coupled to the external motion (including the collision), S represents symmetrization under particle interchange and ρ_0 is the density operator for the initial two-particle motional ground state. A straightforward calculation gives

$$F = \frac{1}{2} \frac{1 - A^2 - B^2 [(1 + A^2)B^2 - 4ABC + 2C^2] \cos^2(\phi_{bb})}{(1 + A) \{ 2 + B[(1 - A)B + 2C] \cos(\phi_{bb}) \} - B^2 (B - C)^2 \cos^2(\phi_{bb})} \quad (10.48)$$

where $A = |O(\psi_{bb}^{(0)}, \tau)|^{\frac{1}{2}}$, $B = |O(\psi_{bb}, \tau)|^{\frac{1}{2}}$, $C = |O_0(\psi_{bb}, \tau)|^{\frac{1}{2}}$. With the parameters quoted above, we obtain $F \approx 0.99$ either by choosing a gate operating time $\tau = 7(T_{\text{osc}} + \delta t)$, maximizing B , or $\tau = 7T_{\text{osc}}$, maximizing instead

A. We prefer this latter choice since, after a time $\tau = NT_{\text{osc}} = 2N\pi/\omega$, the j^{th} component of the x -wavefunction of an atom in state $|b\rangle$ in the basis of eigenstates of $v_b(0 \leq t \leq \tau)$ gets a phase $2N(j + 1/2)\pi$ (here $N = 7$). This brings some simplifications: e.g., the kinematic phases can be written as

$$\phi_a = N\pi \frac{\omega_0 + 2\omega_{\perp}}{\omega}, \quad \phi_b = N\pi \frac{\omega + 2\omega_{\perp}}{\omega}. \quad (10.49)$$

The general form of ϕ_b is much more complicated. Fig. 10.3a shows that after 7 complete oscillations Eq. (10.19) yields a phase shift $\phi_{bb}(7T_{\text{osc}}) \approx \pi$ due to the interaction, whereas the perturbative formula Eq. (10.38) gives $7\phi_{bb}(T_{\text{osc}}) \approx 0.97\pi$. The figure also shows that the overlap $|O_0(\psi_{bb}, t)|$ remains close to 1, satisfying Eq. (10.17). The curve has local minima at the times t_k defined in Sect. 10.4.2.1, signalling that a collision is taking place, and shows a global decrease due to the accumulating delay of the interacting motion with respect to the noninteracting one. The fidelity turns out to be

$$F = \frac{1}{2} \{1 - |O_0(\psi_{bb}, \tau)| \cos[\phi_{bb}(\tau)]\}. \quad (10.50)$$

10.4.2.3 Gate fidelity at $T \neq 0$

In order to compute the temperature dependence $F(T)$ of the fidelity, the density matrix for the motional degrees of freedom in Eq. (10.47) has to be replaced by

$$\rho_{\text{ext}}(T) = \sum_{l,n} P_{ln}(T) |l\rangle_R \langle l| \otimes |n\rangle_r \langle n|, \quad (10.51)$$

which coincides with ρ_0 at $T = 0$. Here we have introduced the eigenstates $|l\rangle_R$ for the center of mass and $|n\rangle_r$ for the relative motion. The probabilities $P_{ln}(T)$ for occupation of the CM and relative motion excited states are calculated assuming for each atom a thermal distribution corresponding to temperature T , as expressed by Eq. (10.43). We obtain

$$F(T) = \frac{1}{2} \left\{ 1 - \sum_{l,n} P_{ln}(T) |O_0(\psi_{(n)}, \tau)| \cos[\phi_{(n)}(\tau)] \right\}, \quad (10.52)$$

where

$$\begin{aligned} \psi_{(n)}(r) &= \left(\frac{m\omega_0}{2\pi\hbar} \right)^{\frac{1}{4}} \sum_{\varsigma=-1,+1} \frac{e^{-\frac{m\omega_0}{4\hbar}(2x_0+\varsigma r)^2}}{\sqrt{n!2^{n+1}}} \\ &\quad \times H_n \left[\sqrt{\frac{m\omega_0}{2\hbar}}(2x_0 + \varsigma r) \right]. \end{aligned} \quad (10.53)$$

In particular, $\psi_{(0)} \equiv \psi_{bb}$ and $\phi_{(0)} \equiv \phi_{bb}$. The corresponding interaction-induced phase shifts $\phi_{(n)}(t)$ are shown in Fig. 10.3b,c. The discrepancy be-

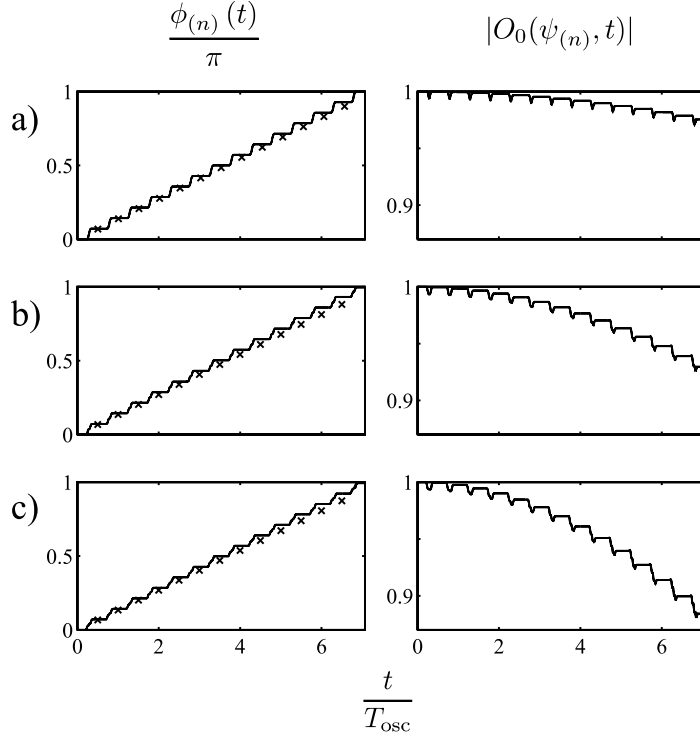


Fig. 10.3: Dynamics for both atoms in state $|b\rangle$, with relative-motion excitations: a) $n = 0$; b) $n = 1$; c) $n = 2$. On the left: interaction-induced phase shift; the crosses refer to the perturbative result from Eq. (10.24), explicitly given by Eq. (10.38) for $n = 0$, and evaluated numerically for $n > 0$. On the right: projection of the evolved state on the corresponding state evolved without interaction. Trap parameters have the same values as in Fig. 10.2 and satisfy Eq. (10.74) since $a_0\omega_0/(4x_0\omega) = 0.07$ in this case.

tween the interacting and the noninteracting motion increases with n , but nevertheless the phase shift $\phi_{(n)}$ remains still close to π (Fig. 10.3b and c), as already discussed in Sect. 10.3.2.3. Consequently the fidelity is not rapidly suppressed with temperature.

For example, one might well be interested in the values of $F(T)$ for temperatures up to $k_B T \approx \hbar\omega_0$. Let us therefore define $\gamma \equiv \exp(-\hbar\omega_0/k_B T)$ and neglect terms of $\mathcal{O}(\gamma^7)$ in the evaluation of Eq. (10.52) to obtain

$$\begin{aligned}
 F(T) \approx F(0) - \frac{1}{2} \sum_{n=1}^6 \gamma^n \left\{ |O_0(\psi_{(n)}, \tau)| \cos[\phi_{(n)}(\tau)] \right. \\
 \left. - |O_0(\psi_{(n-1)}, \tau)| \cos[\phi_{(n-1)}(\tau)] \right\}. \quad (10.54)
 \end{aligned}$$

This still gives a high fidelity $F(T) \approx 0.96$ even at $k_B T = 2\hbar\omega_0$, for which

$\gamma^7 \approx 0.03$. We note that, in order to reach such a high fidelity, the timing has to be quite precise, with a resolution better than $10^{-3}T_{\text{osc}}$ corresponding to tens of ns in this case.

10.5 Conclusions

We have shown that entanglement among ultracold neutral atoms can be controlled by means of microscopic switching potentials. The fidelity for a fundamental two-qubit quantum gate turns out to be quite robust with respect to temperature: in fact, with the parameters quoted below Fig. 10.2, we find $F(T) \approx 0.96$ for $T \approx 3\mu\text{K}$ in the x -motion, while assuming ground-state cooling in the transverse directions. We find a gate operation time of $\tau \approx 0.4\text{ms}$, over which coherence can probably be preserved with presently available experimental systems. Static microtraps based on available atomic mirrors [9, 11] provide a good opportunity for a first implementation of our scheme. Here nanofabrication technologies allow steep potentials to be achieved with small charges and/or currents. Trapping fields can be controlled electronically in a fast and accurate way [10].

Some problems remain to be addressed. To perform even a single gate operation, the trap should be loaded with exactly one atom per well. Read-out should be done possibly without removing atoms from the trap. In order to build up more complex operations, gates should be arranged in a periodic structure where coherent atom transport may take place between different locations. This would permit gate operations either on one pair of atoms at a time, or on several pairs in parallel, a fact which could be exploited for efficient implementation of quantum error correcting schemes and fault-tolerant quantum computing [16]. This will be the subject of future work.

Acknowledgments

We thank S. A. Gardiner for many useful discussions. One of us (T. C.) thanks M. Traini and S. Stringari for the kind hospitality at the Physics Department of Trento University, and the ECT* for partial support during the completion of this work. This work was supported in part by the Österreichischer Fonds zur Förderung der wissenschaftlichen Forschung, the European Community under the TMR networks ERB-FMRX-CT96-0087 and Nanofab, the UK Engineering and Physical Sciences Research Council, and the Institute for Quantum Information GmbH.

10.A Time evolution

10.A.1 Analytical calculation

If both particles are in state $|b\rangle$ we start from the Hamiltonian Eq. (10.35), neglect the interaction term, and solve the Schrödinger equation. We find (omitting the internal state indices bb)

$$\psi_{\text{CM}}(R, t) = \left[\frac{M\Omega(t)}{\pi\hbar} \right]^{\frac{1}{4}} e^{i\phi_{\text{CM}}(R, t) - \frac{M\Omega(t)}{2\hbar} R^2}, \quad (10.55)$$

where

$$\Omega(t) = \frac{\omega^2 \omega_0}{[\omega^2 \cos^2(\omega t) + \omega_0^2 \sin^2(\omega t)]}, \quad (10.56)$$

$$\begin{aligned} \phi_{\text{CM}}(R, t) &= \frac{M\Omega(t)}{2\hbar} \frac{\omega_0^2 - \omega^2}{\omega_0 \omega} R^2 \cos(\omega t) \sin(\omega t) - \frac{\omega t}{2} \\ &\quad - \frac{1}{2} \arctan \left[\frac{(\omega_0 - \omega) \cos(\omega t) \sin(\omega t)}{\omega \cos^2(\omega t) + \omega_0 \sin^2(\omega t)} \right]. \end{aligned} \quad (10.57)$$

From Eqs. (10.32) and (10.55) it follows

$$|O(\psi_{\text{CM}}, t)|^2 = \left[1 + \frac{(\omega_0^2 - \omega^2)^2}{4\omega_0^2 \omega^2} \sin^2(\omega t) \right]^{-\frac{1}{2}}. \quad (10.58)$$

If the particles did not interact, the relative motion would be

$$\begin{aligned} \psi_{\text{rel}}^{(0)}(r, t) &= \sqrt{\frac{\mu\Omega(t)}{4\pi\hbar}} \left(e^{i\phi_{\text{rel}}(-r, t) - \frac{\mu\Omega(t)}{2\hbar} [r+2x_0 \cos(\omega t)]^2} \right. \\ &\quad \left. + e^{i\phi_{\text{rel}}(r, t) - \frac{\mu\Omega(t)}{2\hbar} [r-2x_0 \cos(\omega t)]^2} \right), \end{aligned} \quad (10.59)$$

where

$$\begin{aligned} \phi_{\text{rel}}(r, t) &= -\frac{\omega t}{2} - \frac{1}{2} \arctan \left[\frac{(\omega_0 - \omega) \cos(\omega t) \sin(\omega t)}{\omega \cos^2(\omega t) + \omega_0 \sin^2(\omega t)} \right] \\ &\quad + \frac{2\mu\Omega(t)}{\hbar\omega\omega_0} \sin(\omega t) \left[\left(\frac{\omega_0^2 - \omega^2}{4} r^2 + \omega_0^2 x_0^2 \right) \cos(\omega t) + \omega_0^2 x_0 r \right]. \end{aligned} \quad (10.60)$$

The overlap between the states Eqs. (10.33) and (10.59) is

$$\begin{aligned} |O(\psi_{\text{rel}}^{(0)}, t)|^2 &= \left(e^{-\frac{8m\omega_0\omega^2 x_0^2 \cos^2(\omega t)}{\hbar\omega_+^2(t)}} + e^{-\frac{8m\omega_0\omega^2 x_0^2 \sin^2(\omega t)}{\hbar\omega_-^2(t)}} \right. \\ &\quad \left. + \frac{2 \cos \left[\frac{4m\omega}{\hbar} \frac{\omega_0^2(\omega_0^2 + \omega^2)}{\omega_+^2(t)\omega_-^2(t)} x_0^2 \right]}{e^{\frac{4m\omega_0}{\hbar} \left[\frac{\cos^2(\omega t)}{\omega_+^2(t)} + \frac{\sin^2(\omega t)}{\omega_-^2(t)} \right] \omega^2 x_0^2}} \right) \\ &\quad \times \left[1 + \frac{(\omega_0^2 - \omega^2)^2}{4\omega_0^2 \omega^2} \sin^2(\omega t) \right]^{-\frac{1}{2}} \end{aligned} \quad (10.61)$$

with $\omega_{\pm}(t) = \sqrt{\omega^2 + \omega_0^2 \pm (\omega^2 - \omega_0^2) \cos(\omega t)}$.

This result for the relative motion should be compared to the actual evolution in the presence of interaction, which cannot be computed analytically. If the particles are in different internal states we also have to resort to numerical methods.

10.A.2 Numerical calculation

10.A.2.1 Particles in the same internal state

We write the state vector as a sum over the eigenstates $|n\rangle$ of a harmonic oscillator of mass μ and frequency ω ,

$$|\psi_{\text{rel}}(t)\rangle = \sum_n e^{-i(n+1/2)\omega t} c_n(t) |n\rangle \quad (10.62)$$

and approximate the potential by a truncated sum

$$\begin{aligned} \delta(r) &\approx \sum_{k,l}^{N_{\text{max}}} |k\rangle \langle k| \delta(r) |l\rangle \langle l| \\ &= \sum_{k,l}^{N_{\text{max}}} \psi_k^*(0) \psi_l(0) |k\rangle \langle l|, \end{aligned} \quad (10.63)$$

where $\psi_n(x) = \langle x|n\rangle$. We have checked that the final result is independent of N_{max} , with N_{max} of the order of some tens. The Schrödinger equation for $|\psi_{\text{rel}}(t)\rangle$ gives

$$\dot{c}_n(t) = -i2a_s^{bb} \omega_{\perp} \psi_n^*(0) \sum_{l=0}^{N_{\text{max}}} \psi_l(0) e^{i(n-l)\omega t} c_l(t), \quad (10.64)$$

which we solve numerically for $c_n(t)$ with $0 \leq n \leq N_{\text{max}}$. The initial conditions, from Eq. (10.33), read

$$\begin{aligned} c_n(0) &= \frac{e^{-\frac{m\omega_0\omega}{\hbar(\omega_0+\omega)}x_0^2}}{\sqrt{n!2^n}} \frac{(\omega_0\omega)^{\frac{1}{4}}}{\sqrt{\omega_0+\omega}} \left(\frac{\omega_0-\omega}{\omega_0+\omega}\right)^{\frac{n}{2}} \\ &\times \left[H_n\left(\sqrt{\frac{2m\omega\omega_0^2x_0^2}{\hbar(\omega_0^2-\omega^2)}}\right) + H_n\left(\sqrt{\frac{2m\omega\omega_0^2x_0^2}{\hbar(\omega^2-\omega_0^2)}}\right) \right]. \end{aligned} \quad (10.65)$$

10.A.2.2 Particles in different internal states

In order to solve the Schrödinger equation for the Hamiltonian Eq. (10.42) we decompose the state vector

$$|\psi_{ab}(t)\rangle = \sum_{j,k} e^{-i(j+k+1)\tilde{\omega}t} c_{jk}(t) |\tilde{j}\rangle_R |\tilde{k}\rangle_r, \quad (10.66)$$

(where now $\tilde{\psi}_j(x) = \langle x | \tilde{j} \rangle$ are the eigenfunctions of a harmonic oscillator with frequency $\tilde{\omega}$ and mass m) and obtain for the coefficients

$$\begin{aligned}
\dot{c}_{jk}(t) = & i \frac{\tilde{\omega}(\omega_0^2 - \omega^2)}{2(\omega_0^2 + \omega^2)} \left\{ c_{j+1,k+1}(t) e^{-i2\tilde{\omega}t} \sqrt{(j+1)(k+1)} \right. \\
& + c_{j-1,k+1}(t) \sqrt{j(k+1)} + c_{j-1,k-1}(t) e^{i2\tilde{\omega}t} \sqrt{jk} \\
& + c_{j+1,k-1}(t) \sqrt{(j+1)k} + \frac{m\tilde{\omega}}{\hbar} \frac{\omega^2 - \omega_0^2}{\omega_0^2} \xi^2 c_{jk}(t) \\
& + \sqrt{\frac{2m\tilde{\omega}}{\hbar}} \xi \left[e^{i\tilde{\omega}t} (c_{j-1,k}(t) \sqrt{j} - c_{j,k-1}(t) \sqrt{k}) \right. \\
& + e^{-i\tilde{\omega}t} (c_{j+1,k}(t) \sqrt{j+1} - c_{j,k+1}(t) \sqrt{k+1}) \left. \right] \left. \right\} \\
& - i\sqrt{2} a_s^{ab} \omega_{\perp} \tilde{\psi}_k^*(-\xi) \sum_l \tilde{\psi}_l^*(-\xi) e^{i(k-l)\tilde{\omega}t} c_{jl}(t)
\end{aligned} \tag{10.67}$$

where $\xi = x_0 \omega_0^2 / \sqrt{2} \tilde{\omega}^2$.

This can again be solved numerically, starting from the initial conditions, derived from Eqs. (10.32), (10.33),

$$\begin{aligned}
c_{jk}(0) = & \frac{e^{-\frac{m\omega_0\omega(\xi^2 + x_0^2 - \sqrt{2}x_0\xi)}{\hbar(\omega_0 + \omega)}}}{\sqrt{j!k!2^{j+k-2}}} \frac{\sqrt{\omega_0\omega}}{\omega_0 + \omega} \left(\frac{\omega_0 - \omega}{\omega_0 + \omega} \right)^{\frac{j+k}{2}} \\
& \times \left[H_j \left(\sqrt{\frac{m\omega\omega_0^2(\sqrt{2}x_0 - \xi)^2}{\hbar(\omega_0^2 - \omega^2)}} \right) + H_k \left(\sqrt{\frac{m\omega\omega_0^2\xi^2}{\hbar(\omega_0^2 - \omega^2)}} \right) \right].
\end{aligned} \tag{10.68}$$

10.B Interaction phase shift for excited initial states

Let us consider two bosonic atoms in the same internal state $|\alpha\rangle$, but in two different single-particle motional states $|\varphi_{-}\rangle$ and $|\varphi_{+}\rangle$ with vanishing overlap. The initial motional state has the form

$$|\varphi(0)\rangle = \frac{|\varphi_{-}\rangle|\varphi_{+}\rangle + |\varphi_{+}\rangle|\varphi_{-}\rangle}{\sqrt{2}}. \tag{10.69}$$

We assume that: (i) the particles move against each other, come in contact during a certain time interval $[t_i, t_f]$ and then separate again; (ii) the velocity of each particle and the shape of its wavefunction do not vary during the interaction. Thus for $t_i \leq t \leq t_f$ we write:

$$\langle x_1 | \varphi_{-}(t) \rangle = \varphi'(x_1 - vt), \tag{10.70}$$

$$\langle x_2 | \varphi_{+}(t) \rangle = \varphi''(x_2 + vt), \tag{10.71}$$

where v is a positive constant. It follows

$$\begin{aligned}
\phi_{\alpha\alpha}(T_{\text{osc}}) &\approx \frac{1}{\hbar} \int_{t_i}^{t_f} dt \langle \varphi(t) | u_{\alpha\alpha}(x_1, x_2) | \varphi(t) \rangle \\
&= 4a_s^{\alpha\alpha} \omega_{\perp} \int_{t_i}^{t_f} dt \int_{-\infty}^{+\infty} dx_1 \\
&\quad \times |\varphi'(x_1 - vt)|^2 |\varphi''(x_1 + vt)|^2 \\
&\approx \frac{2a_s^{bb} \omega_{\perp}}{v} \int_{-\infty}^{+\infty} dx dy |\varphi'(x)|^2 |\varphi''(y)|^2 \\
&= \frac{2a_s^{bb} \omega_{\perp}}{v}, \tag{10.72}
\end{aligned}$$

where a change of variables $x = x_1 - vt$, $y = x_1 + vt$ has been introduced, and the limits of integration in t have been extended to $\pm\infty$ since the single-particle wavefunctions Eqs. (10.70)-(10.71) overlap just for a finite time. The result turns out to be independent of the initial state. We can compare it to Eq. (10.38), which was obtained in the harmonic potential Eq. (10.26) starting from the single-particle states $|\psi_{\pm}\rangle$ instead of $|\varphi_{\pm}\rangle$. In this case

$$v \equiv \left| \partial_t \langle \psi_{\pm} | e^{\frac{i}{\hbar} \mathcal{H}_b t} x e^{-\frac{i}{\hbar} \mathcal{H}_b t} | \psi_{\pm} \rangle \Big|_{t=t_k} \right| = x_0 \omega, \tag{10.73}$$

and the atoms collide twice during one oscillation period. Therefore the collisional phase Eq. (10.38) should be twice as big as Eq. (10.72). This is true provided that the maximum velocity for the atomic motion in the well $v_b(x, 0 \leq t \leq \tau)$ is large with respect to the analogous quantity for the ground-state motion in the wells $v_a(x, t)$, *i.e.* if

$$x_0 \omega \gg a_0 \omega_0 / 4. \tag{10.74}$$

References

- [1] For a review on quantum computing in general see, for example, A. M. Steane, Rept. Prog. Phys. **61**, 117-173 (1998).
- [2] J. I. Cirac and P. Zoller, Phys. Rev. Lett. **74**, 4091 (1995); Q. A. Turchette, C. S. Wood, B. E. King, C. J. Myatt, D. Leibfried, W. M. Itano, C. Monroe, and D. J. Wineland, *ibid.* **81** 3631 (1998).
- [3] Q. A. Turchette, C. J. Hood, W. Lange, H. Mabuchi, and H. J. Kimble, Phys. Rev. Lett. **75**, 4710 (1995); X. Maître, E. Hagley, G. Nogues, C. Wunderlich, P. Goy, M. Brune, J. M. Raimond, and S. Haroche, *ibid.* **79**, 769 (1997); E. Hagley, X. Maître, G. Nogues, C. Wunderlich, M. Brune, J. M. Raimond, and S. Haroche, *ibid.* **79**, 1 (1997); T. Pellizzari, S. A. Gardiner, J. I. Cirac, and P. Zoller, *ibid.* **75**, 3788 (1995).

- [4] D. G. Cory, A. F. Fahmy, and T. F. Havel, Proc. Natl. Acad. Sci. USA **94**, 1634 (1997); N. A. Gershenfeld, and I. L. Chuang, Science **275**, 350 (1997).
- [5] D. Jaksch, H.-J. Briegel, J. I. Cirac, C. W. Gardiner, and P. Zoller, Phys. Rev. Lett. **82**, 1975 (1999).
- [6] G. K. Brennen, C. M. Caves, P. S. Jessen, and I. H. Deutsch, Phys. Rev. Lett. **82**, 1060 (1999).
- [7] M. H. Anderson, J. R. Ensher, M. R. Matthews, C. E. Wieman, and E. A. Cornell, Science, **269**, 198 (1995). C. C. Bradley, C. A. Sackett, J. J. Tollett, and R. G. Hulet, Phys. Rev. Lett. **75**, 1687 (1995). K. B. Davies, M.-O. Mewes, M. R. Andrews, N. J. van Druten, D. S. Durfee, D. M. Kurn, and W. Ketterle, *ibid.* **75**, 3969 (1995). D. S. Hall, M. R. Matthews, C. E. Wieman, and E. A. Cornell, *ibid.* **81**, 1543 (1998); **81**, 4532 (1998). D. S. Hall, M. R. Matthews, J. R. Ensher, C. E. Wieman, and E. A. Cornell 1998, *ibid.* **81**, 1539 (1998); **81**, 4531 (1998). D. M. Stamper-Kurn, M. R. Andrews, A. P. Chikkatur, S. Inouye, H.-J. Miesner, J. Stenger, and W. Ketterle, *ibid.* **80**, 2027 (1998).
- [8] J. Schmiedmayer in *XVIII International Conference on Quantum Electronics*: Technical Digest, edited by G. Magerl (Technische Universität Wien, Vienna 1992), Series 1992, Vol. 9, p.284 (1992); J. Schmiedmayer, Phys. Rev. A **52**, R13 (1995); J. D. Weinstein, K. Libbrecht, Phys. Rev. A **52**, 4004 (1995). V. Vuletic *et al.*, Phys. Rev. Lett. **80**, 1634 (1998); J. Fortagh *et al.*, Phys. Rev. Lett. **81**, 5310 (1998); J. Denschlag, D. Cassettari, J. Schmiedmayer, Phys. Rev. **82**, 2014 (1998).
- [9] T. M. Roach, H. Abele, M. G. Boshier, H. L. Grossman, K. P. Zetie, and E. A. Hinds, Phys. Rev. Lett. **75**, 629 (1995); E. A. Hinds, M. G. Boshier, and I. G. Hughes. *ibid.* **80**, 645 (1998).
- [10] J. Schmiedmayer, Eur. Phys. J. D **4**, 57 (1998).
- [11] E. A. Hinds, Phil. Trans. Roy. Soc. **357**, 1 (1999)
- [12] This was measured for example in an atom interferometer: J. Schmiedmayer *et al.*, Phys. Rev. Lett. **74**, 1043 (1995).
- [13] Yu. B. Ovchinnikov, I. Manek, and R. Grimm, Phys. Rev. Lett. **79**, 2225 (1997).
- [14] D. Jaksch, C. Bruder, J. I. Cirac, C. W. Gardiner, and P. Zoller, Phys. Rev. Lett. **81**, 3108 (1998).
- [15] B. Schumacher, Phys. Rev. A **54**, 2614 (1996).
- [16] H.-J. Briegel, T. Calarco, D. Jaksch, J. I. Cirac, and P. Zoller (submitted to J. Mod. Opt.).

Chapter 11

PUBLICATION

QUANTUM COMPUTING WITH NEUTRAL ATOMS

H.-J. Briegel,¹ T. Calarco,^{2,3} D. Jaksch,² J.I. Cirac,² and P. Zoller²

¹Sektion Physik, Ludwig-Maximilians-Universität München, D-80333 München, Germany

²Institut für Theoretische Physik, Universität Innsbruck, 6020 Innsbruck, Austria

³ECT*, European Centre for Theoretical Studies in Nuclear Physics and Related Areas
Villa Tambosi, Strada delle Tabarelle 286, Villazzano (Trento), Italy 38050

to appear in J. Mod. Opt.

We develop a method to entangle neutral atoms using cold controlled collisions. We analyze this method in two particular set-ups: optical lattices and magnetic micro-traps. Both offer the possibility of performing certain multi-particle operations in parallel. Using this fact, we show how to implement efficient quantum error correction and schemes for fault-tolerant computing.

11.1 Introduction

Entanglement is one of the most intriguing features of Quantum Mechanics. However, there are very few physical systems in which entanglement can be systematically studied in a controlled way. Those systems include ion-traps [1, 2, 3, 4, 5, 6, 7, 8], cavity QED [9, 10, 11, 12, 13, 14, 15, 16], photons [17, 18, 19, 20, 21, 22, 23, 24, 25], and molecules in the context of NMR [26, 27, 28, 29] (see [30] however). Very recently, we have identified a new way of entangling particles by using *cold controlled collisions* with which one could study experimentally basic issues of quantum information theory [31]. Given the impressive experimental advances made so far in the fields of neutral atom trapping and cooling [32, 33, 34, 35], and in the studies of Bose Einstein condensation (BEC) of ultracold gases [36, 37, 38, 39, 40, 41], that proposal opens a new perspective to several experimental groups who so far have concentrated their efforts in other fields of Atomic Physics.

In the present paper, we build upon the work in [31] and explore the idea of using atomic controlled cold collisions for entangling neutral atoms in optical lattices (see also [42]) and in arrays of magnetic micro-traps. We show how to perform two-qubit gate operations with those systems obtaining very high fidelities. We propose a variety of experiments to entangle particles using state-of-the-art technology. We also concentrate on the unique possibilities that these set-ups offer to perform multi-particle entanglement operations in parallel [43, 44, 45, 46]. Using such parallelism, we show how to implement efficient error correction [47, 48, 49, 50, 51, 52, 53, 54] and fault-tolerant quantum computation schemes [55, 56, 57, 58, 59, 60, 61, 62].

The paper is organized as follows. In Sec. II we discuss the use of ultracold collisions as a mechanism for entangling neutral atoms. Such collisions can be brought about by either moving the potentials in certain spatial directions or by modifying the shape of the trapping potentials. In Sec. III we describe two systems in which such operations can be implemented. These are optical lattices [42, 63, 64, 65, 66] and magnetic microtraps [67, 68, 69, 70, 71] both of which have been studied experimentally in detail in the past. In Sec. IV we describe a class of multi-particle entanglement operations that can be realized in these systems (we concentrate here on optical lattices). The usefulness of such operations for quantum computing depends on certain conditions that need to be satisfied in an experiment. Among these conditions, the filling problem, i.e. how to fill the potentials with regular patterns of atoms, is most outstanding. We discuss these matters and show that even under present-day experimental conditions, very interesting entanglement studies could be performed. Section V summarizes the main results and discusses their relevance for future research.

11.2 Entanglement of atoms via cold controlled collisions

In this Section, we consider two bosonic neutral atoms with two internal states trapped by conservative potentials and cooled to the motional ground states. Initially these two particles are sufficiently far apart so that they do not interact with each other. We then assume the shape of the potentials to be varied in a way that depends on the internal state of the atoms so that the two particles come close to each other if they are in certain internal states. As we will show, this can be done e.g. by moving the center position of the trapping potentials state selectively, or by switching off a potential barrier between the two atoms for one of the two internal states. In both cases the particles will interact via s -wave scattering with each other in a coherent way when they are close to each other. After the interaction has taken place the particles are restored to their initial position. In this way one can implement conditional dynamics and realize a fundamental two-qubit gate.

Note that we are dealing with bosons. Therefore, we have to use symmetrized wave functions for describing the two particles. It will turn out that if the center positions of the trapping potentials are moved state selectively, particles in the same internal state will always be so far apart that their wave functions never overlap. Thus, we will not care about the symmetrization in this case. On the other hand, if the potential barrier is switched off for one internal state, particles in the same internal state will come close to each other and symmetrizing the wave function is essential.

11.2.1 Hamiltonian

Here we deal with the interaction Hamiltonian of two neutral atoms 1 and 2 with internal states $|a\rangle_{1,2}$ and $|b\rangle_{1,2}$ trapped by conservative potentials $V^{\beta_i}(\mathbf{x}_i, t)$ whose functional dependence on the coordinate \mathbf{x}_i , with $i = 1, 2$ the particle index, depends on the internal state of the particle $\beta_{1,2} = a, b$. Initially, the two particles are in the ground state of the trapping potentials and the centers of the two potential wells are sufficiently far apart so that the particles do not interact. Then the form of the potential wells is changed such that there is some overlap of the wave functions of the two atoms, and the particles will interact with each other. This interaction between the atoms in two given internal states β_1 and β_2 can be described by a contact potential

$$u^{\beta_1\beta_2}(\mathbf{x}_1 - \mathbf{x}_2) = \frac{4\pi a_s^{\beta_1\beta_2} \hbar^2}{m} \delta^3(\mathbf{x}_1 - \mathbf{x}_2), \quad (11.1)$$

where $a_s^{\beta_1\beta_2}$ is the s -wave scattering length for the corresponding internal states describing elastic collisions and m is the mass of the particles. This zero energy

s -wave scattering approximation will be valid as long as we assume that v_{osc} , the rms velocity of the atoms in the vibrational ground state, approximately given by $v_{\text{osc}} \approx a_0\omega$, is sufficiently small [72]. Here a_0 is the size of the ground state of the trap potential, and ω is the first excitation frequency. Thus we can describe the evolution of the system by the Hamiltonian

$$H = \sum_{\beta_1, \beta_2} H^{\beta_1 \beta_2} \otimes |\beta_1\rangle_1 \langle \beta_1| \otimes |\beta_2\rangle_2 \langle \beta_2|, \quad (11.2)$$

where

$$H^{\beta_1 \beta_2} = \sum_{i=1,2} \left[\frac{(\mathbf{p}_i)^2}{2m} + V^{\beta_i}(\mathbf{x}_i, t) \right] + u^{\beta_1 \beta_2}(\mathbf{x}_1 - \mathbf{x}_2). \quad (11.3)$$

Here \mathbf{p}_i is the momentum operator.

11.2.1.1 Interaction in perturbation theory

We want to treat the interaction term in the Hamiltonian Eq. (11.3) perturbatively. For particles in two different internal states $\beta_1 \neq \beta_2$ we find the correction to the energy due to the interaction as

$$\Delta E^{\beta_1 \beta_2}(t) = \frac{4\pi a_s^{ab} \hbar^2}{m} \int d\mathbf{x} \prod_i \left| \psi_i^{\beta_i}(\mathbf{x}, t) \right|^2, \quad (11.4)$$

where $\psi_i^{\beta_i}(\mathbf{x}, t)$ is the normalized one-particle wave function of particle i in internal state β_i in the time dependent potential $V^{\beta_i}(\mathbf{x}, t)$. If the particles are in the same internal state $\beta_1 = \beta_2 = \beta$, we have to account for the Bose statistics i.e. use the properly normalized symmetrized two-particle wave function for calculating the energy shift. We therefore find

$$\Delta E^{\beta\beta}(t) = \frac{8\pi a_s^{\beta\beta} \hbar^2}{m(1 + |\alpha|^2)} \int dx \prod_i \left| \psi_i^\beta(\mathbf{x}, t) \right|^2, \quad (11.5)$$

where

$$\alpha = \int dx \left(\psi_1^\beta(\mathbf{x}, t) \right)^* \psi_2^\beta(\mathbf{x}, t). \quad (11.6)$$

For general β_1, β_2 we find the phase accumulated due to the interaction in the time interval $[-\tau, \tau]$ by

$$\phi^{\beta_1 \beta_2} = \frac{1}{\hbar} \int_{-\tau}^{\tau} dt \Delta E^{\beta_1 \beta_2}(t). \quad (11.7)$$

11.2.2 Moving potentials

One way of controlling the interaction between the particles is to move the center position of the potentials $V^{\beta_i}(\mathbf{x}_i, t) = V(\mathbf{x}_i - \bar{\mathbf{x}}_i^{\beta_i}(t))$ towards each other in a state-dependent way while leaving the shape of the potential unchanged. By moving the potential we get two kinds of phase shifts. A kinetic phase which is a single-particle phase due to the kinetic energy of the particles and an interaction phase due to coherent interactions between two atoms. First we will define these two phases for general trapping potentials and afterwards specialize them to moving harmonic potentials. Finally, we will show how conditional dynamics can be realized.

11.2.2.1 Kinetic phase

First we want to consider a single atom in internal state $|\beta\rangle$ trapped in the instantaneous ground state ψ_0 of a moving potential well $V(\mathbf{x} - \bar{\mathbf{x}}^\beta(t))$. The center position of the potential is moved along a trajectory $\bar{\mathbf{x}}^\beta(t)$. Ideally, we want the atom to remain in the ground state of its trapping potential and to preserve its internal state during the motion. This corresponds to the transformation from $t = -\tau$ to $t = \tau$

$$\psi_0[\mathbf{x} - \bar{\mathbf{x}}^\beta(-\tau)] \rightarrow e^{-i\phi^\beta} \psi_0[\mathbf{x} - \bar{\mathbf{x}}^\beta(\tau)], \quad (11.8)$$

where the atom remains in the ground state of the trapping potential and preserves its internal state. Transformation (11.8) can be realized in the *adiabatic limit* [73], where we move the potentials so that the atoms remain in the instantaneous motional ground state. Adiabaticity requires $|\dot{\bar{\mathbf{x}}}^\beta(t)| \ll \hbar\omega/2mv_{\text{osc}}$, for all times t . Here ω is the smallest excitation frequency in the potential and $v_{\text{osc}}^2 = \langle \psi_0(0) | q^2 | \psi_0(0) \rangle / m^2$. q is the momentum operator in the direction the optical lattice is moved. The phase ϕ^β can be easily calculated in the limit $|\ddot{\bar{\mathbf{x}}}^\beta(t)| \ll v_{\text{osc}}/\tau$. We find the *kinetic phase*

$$\phi^\beta = \frac{m}{2\hbar} \int_{-\tau}^{\tau} dt \left(\dot{\bar{\mathbf{x}}}^\beta(t) \right)^2. \quad (11.9)$$

11.2.2.2 Interaction phase

Let us now consider two particles $i = 1, 2$ in different internal states $|\beta_i\rangle_i$ trapped in the ground states of two moving potentials. Initially, at time $t = -\tau$, these wells are centered at positions $\bar{\mathbf{x}}_i$, sufficiently far apart (distance $d = \bar{\mathbf{x}}_1 - \bar{\mathbf{x}}_2$) so that the particles do not interact. The positions of the potentials are moved along trajectories $\bar{\mathbf{x}}_i^{\beta_i}(t)$ so that the wave packets of the atoms overlap for certain time, until finally they are restored to the initial position at the time $t = \tau$. We assume that: (i) $|\dot{\bar{\mathbf{x}}}_i^{\beta_i}(t)| \ll v_{\text{osc}}$ (adiabatic

condition) so that the particles remain in the ground states of the moving trapping potentials; (ii) The interaction can be treated perturbatively, where $|\Delta E^{\beta_1\beta_2}(t)| \ll \hbar\omega$ so that no sloshing motion is excited. In that case, we realize the transformation

$$\begin{aligned} \psi_0(\mathbf{x}_1 - \bar{\mathbf{x}}_1)\psi_0(\mathbf{x}_2 - \bar{\mathbf{x}}_2) \rightarrow \\ e^{-i\phi}\psi_0(\mathbf{x}_1 - \bar{\mathbf{x}}_1)\psi_0(\mathbf{x}_2 - \bar{\mathbf{x}}_2), \end{aligned} \quad (11.10)$$

where $\phi = \phi^{\beta_1} + \phi^{\beta_2} + \phi^{\beta_1\beta_2}$ with the *collisional phase* $\phi^{\beta_1\beta_2}$ defined in Eq. (11.7).

11.2.2.3 Moving harmonic potentials

Here we specialize to harmonic trapping potentials. The wave function $\psi_i^{\beta_i}(\mathbf{x}, t)$ of a particle in a moving harmonic potential can be found analytically. In the Appendix 11.A we show that when we start to move the harmonic potential at time $-\tau$ with the particle in its motional ground state and stop to move the potential at time τ , the condition for the particle to end up in the motional ground state at τ is given by

$$\left| \int_{-\tau}^{\tau} \dot{\bar{\mathbf{x}}}_i^{\beta_i}(t') e^{i\omega t'} dt' \right| \ll a_0. \quad (11.11)$$

This condition is weaker than the condition $|\dot{\bar{\mathbf{x}}}_i^{\beta_i}(t)| \ll v_{\text{osc}}$ for adiabaticity, and means that the particle need not be in the instantaneous ground state of the moving potential at all times, but only at the final time. The kinetic phases can be found exactly (cf. Eq. (11.52)). If $|\Delta E^{\beta_1\beta_2}(t)| \ll \hbar\omega$ is satisfied, the interaction phase can be found by Eq. (11.7) since the $\psi_i^{\beta_i}(\mathbf{x}, t)$ are known. It is also possible to generalize these results to the case in which the trap frequency changes with time [74].

11.2.2.4 Implementation of conditional dynamics

Let us now assume that we can design the potentials such that atoms in the internal state $|\beta_i\rangle_i$ experience a potential $V^{\beta_i}(\mathbf{x}_i, t) = V(\mathbf{x}_i - \bar{\mathbf{x}}_i^{\beta_i}(t))$ which is initially ($t = -\tau$) centered at position $\bar{\mathbf{x}}_i$. We assume that we can move the centers of the potentials as follows: $\bar{\mathbf{x}}_i^{\beta_i}(t) = \bar{\mathbf{x}}_i + \delta\mathbf{x}^{\beta_i}(t)$. As shown in Fig. 11.1 the trajectories $\delta\mathbf{x}^{\beta_i}(t)$ are chosen in such a way that $\delta\mathbf{x}^{\beta_i}(-\tau) = \delta\mathbf{x}^{\beta_i}(\tau) = 0$ and the first atom collides with the second one only if they are in states $|a\rangle$ and $|b\rangle$, respectively ($|\bar{\mathbf{x}}_1^b(t) - \bar{\mathbf{x}}_2^a(t)| \gg a_0 \forall t$). This choice is motivated by the physical implementation considered in Sec. 11.3.1. The fact that $\bar{\mathbf{x}}_i$ does not depend on the internal atomic state and the shape of the two potentials is the same at times $\pm\tau$ allows one to easily change the internal state at times

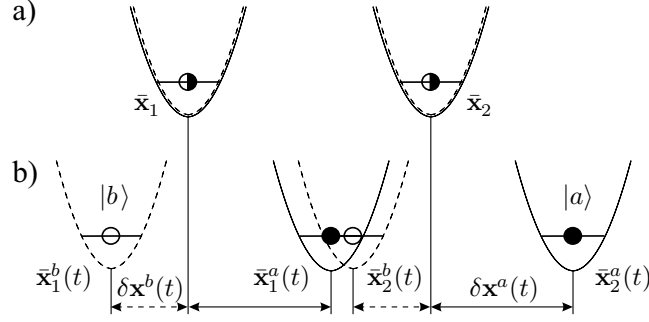


Fig. 11.1: Configurations at times $\pm\tau$ (a) and at t (b). The solid (dashed) curves show the potentials for particles in the internal state $|a\rangle$ ($|b\rangle$). Center positions $\bar{x}_i^{\beta i}(t)$ and displacements $\delta x^{\beta i}(t)$ as defined in the text.

$t = \pm\tau$ by applying laser pulses. If the conditions stated above are fulfilled, depending on the initial internal atomic states we have:

$$\begin{aligned}
 |a\rangle_1 |a\rangle_2 &\rightarrow e^{-i2\phi^a} |a\rangle_1 |a\rangle_2, \\
 |a\rangle_1 |b\rangle_2 &\rightarrow e^{-i(\phi^a + \phi^b + \phi^{ab})} |a\rangle_1 |b\rangle_2, \\
 |b\rangle_1 |a\rangle_2 &\rightarrow e^{-i(\phi^a + \phi^b)} |b\rangle_1 |a\rangle_2, \\
 |b\rangle_1 |b\rangle_2 &\rightarrow e^{-i2\phi^b} |b\rangle_1 |b\rangle_2,
 \end{aligned} \tag{11.12}$$

where the motional states remain unchanged. The kinetic phases ϕ^β and the collisional phase ϕ^{ab} can be calculated as stated above. We emphasize that the ϕ^β are (trivial) one-particle phases that, as long as they are known, can always be incorporated in the definition of the states $|a\rangle$ and $|b\rangle$. This realizes a fundamental two-qubit quantum gate for certain values of ϕ^{ab} , e.g. $\phi^{ab} = \pi$.

11.2.3 Switching potentials

The interaction between the particles can be controlled also in another way, for example by changing with time the shape of the potentials depending on the particles' internal states. Different regimes for the time-dependence of the potential are possible. The two limits of extremely slow (adiabatic) or extremely fast (sudden) potential changes are both interesting and lead to peculiar schemes. Here we will analyze the latter case. We consider two atoms initially trapped in two displaced wells. At a certain time the barrier between the wells is suddenly removed in a selective way for atoms in state $|b\rangle$, whereas it remains unchanged for atoms in state $|a\rangle$. The atoms are allowed to oscillate for some time, and then the barrier is raised again suddenly such as to trap

them back at the original positions. During the process they will acquire both a kinematic phase due to the oscillations within their respective wells, and an interaction phase due to the collision. We will calculate such quantities and look for the optimal switching time required in order to maximize the fidelity for a quantum gate relying on this scheme, which we will estimate quantitatively for the relevant physical example in Sec. 11.3.2.

11.2.3.1 Kinematic phase

Let us first consider the time-independent problem of an atom subject to a three-dimensional potential whose functional form along x depends on the internal atomic state $\beta = a, b$:

$$V^\beta(\mathbf{x}) = v^\beta(x) + v_\perp(y) + v_\perp(z). \quad (11.13)$$

Here the v 's are single-well trapping potentials, and v^a, v^b are centered around $x = x_0, x = 0$, respectively. We assume that the atom is initially prepared in the motional state $|\Psi_+\rangle$, where

$$\langle \mathbf{x} | \Psi_+\rangle \equiv \Psi_+(\mathbf{x}) = \psi_+(x)\psi_\perp(y)\psi_\perp(z) \quad (11.14)$$

and ψ_+, ψ_\perp are the ground-state wave functions of v^a, v_\perp with eigenvalues E^a, E_\perp respectively. Thus $\Psi_+(\mathbf{x})$ is peaked around the position $\mathbf{x}_0 \equiv (x_0, 0, 0)$, coinciding with the center of $V^a(\mathbf{x})$ but displaced from the one of $V^b(\mathbf{x})$. Therefore, if the atom is in internal state $|a\rangle$, its motional state after a time t will be unchanged up to a phase $\phi^a = (E^a + 2E_\perp)t/\hbar$. If it is instead in state $|b\rangle$, it will start oscillating within the well, thus picking up a different phase ϕ^b due to the kinematical evolution, and possibly coming back at the initial position after some time.

11.2.3.2 Interaction phase

We now consider two atoms 1 and 2 initially (at $t = 0$) prepared in the motional states $|\Psi_+\rangle$ and $|\Psi_-\rangle$, the latter being defined as in Eq. (11.14) but with $\psi_-(x) \equiv \psi_+(-x)$ replacing $\psi_+(x)$. We assume that the particles are subject to the potentials $\sum_{\zeta=+,-} \Theta(\zeta x) V^{\beta_i}(\zeta \mathbf{x}_i)$, where Θ denotes the step function. If any one of them is in state $|b\rangle$, for $t > 0$ it will start oscillating within the well, eventually interacting with the other one. If v_\perp is much steeper than v^β , then the probability of transversal excitations can be neglected, *i.e.* each atom remains in the ground state along y and z . By integrating over these variables, the problem is then reduced to a one-dimensional two-particle Schrödinger equation, with

$$\mathcal{H}^{\beta_1\beta_2} = \sum_{i=1}^2 \left[\frac{(p_i)^2}{2m} + w^{\beta_i}(x_i, t) \right] + u_x^{\beta_1\beta_2}(x_1 - x_2) \quad (11.15)$$

replacing the Hamiltonian (11.3) in Eq. (11.2). Here $w^\beta(x, t)$ is a combination of the $v^\beta(x)$ whose form changes with time, and $u_x^{\beta_1\beta_2}$ is an effective interaction potential taking into account the integration over y and z , and therefore depending on the shape of v_\perp . We shall study the dynamics at $t \geq 0$ for different values of (β_1, β_2) separately. If $\beta_1 = \beta_2 \equiv \beta$ the total initial normalized state, symmetric under particle interchange, is

$$|\psi^{\beta\beta}(0)\rangle \approx \frac{|\psi_+\rangle_1|\psi_-\rangle_2 + |\psi_-\rangle_1|\psi_+\rangle_2}{\sqrt{2}} \otimes |\beta\rangle_1 \otimes |\beta\rangle_2, \quad (11.16)$$

where the initial overlap $\langle\psi_-|\psi_+\rangle \ll 1$ has been neglected in computing the normalization. If both particles are in state $|a\rangle$, no interaction takes place and thus the collisional phase $\phi^{aa} = 0$. Therefore, we shall now consider in more detail the situation in which both particles are in state $|b\rangle$ and thus move within the well v^b . In the absence of interaction, after an oscillation period T they would come back exactly to the initial state. Due to the interaction, two effects arise: an additional phase, which is accumulated by the wave function as the number of undergone oscillations increases; and a slight decrease in their frequency, because the atoms acquire a small delay in their motion inside the trap as they come out from a collision. These effects have to be evaluated in detail, since they influence the attainable fidelity for a quantum gate based on this scheme. For symmetry reasons, the relative coordinate motion decouples from the center of mass motion, which is not affected by the interaction and can be solved analytically. For an explicit calculation, it is now needed to specify the form of the potentials in Eq. (11.13).

11.2.3.3 Switching harmonic potentials

In order to perform the calculations analytically, the potentials in Eq. (11.13) are chosen to be harmonic:

$$\begin{aligned} v^a(x) &= \frac{m\omega_0^2}{2}(x - x_0)^2, \\ v^b(x) &= \frac{m\omega^2}{2}x^2, \\ v_\perp(y) &= \frac{m\omega_\perp^2}{2}y^2, \end{aligned} \quad (11.17)$$

where $\omega_\perp \gg \omega_0 > \omega$. Our scheme for gate operation is as follows: initially the two particles are separately stored in two displaced harmonic wells at $\pm x_0$ as described above, *i.e.* with the potential (Fig. 11.2a)

$$w^a(x, t < 0) = \sum_{\varsigma=+,-} \Theta(\varsigma x) v^a(\varsigma x), \quad (11.18)$$

$$w^b(x, t < 0) = w^a(x, t < 0) \quad (11.19)$$

in the one-dimensional Hamiltonian Eq. (11.15). At $t = 0$ the potential undergoes a sudden change, namely the barrier between the two wells is selectively switched off for state $|b\rangle$ only (Fig. 11.2b):

$$w^a(x, 0 < t < \tau) = w^a(x, t < 0); \quad (11.20)$$

$$w^b(x, 0 < t < \tau) = v^b(x). \quad (11.21)$$

Then at $t = \tau$, the potential barrier is suddenly restored: $w^{a,b}(x, t > \tau) = w^{a,b}(x, t < 0)$. The time evolution at $0 < t < \tau$ is characterized by oscillations with periodicity $T \equiv 2\pi/\omega$. The projection of the evolved CM wave function on the initial one

$$\left| \langle \psi_{\text{CM}}^{bb}(t) | \psi_{\text{CM}}^{bb}(0) \rangle \right|^2 = \left[1 + \frac{(\omega_0^2 - \omega^2)^2}{4\omega_0^2\omega^2} \sin^2(\omega t) \right]^{-\frac{1}{2}} \quad (11.22)$$

has instead a period of $T/2$, because of the parity of the spatial wave function. The time-dependent energy shift (11.4) due to the interaction turns out to be

$$\Delta E^{bb}(t) = a_s^{bb} \hbar \omega_{\perp} \sqrt{\frac{8m\Omega(t)}{\pi\hbar}} e^{-\frac{2m\omega_0}{\hbar} x_0^2 \left[1 - \sin^2(\omega t) \frac{\omega_0 \Omega(t)}{\omega^2} \right]}, \quad (11.23)$$

where

$$\Omega(t) = \omega^2 \omega_0 / [\omega^2 \cos^2(\omega t) + \omega_0^2 \sin^2(\omega t)]. \quad (11.24)$$

Hence the interaction-induced phase shift (11.7) accumulated after each oscillation period T is (evaluating the integral in a saddle-point approximation)

$$\begin{aligned} \phi_T^{bb} &= \int_0^T \frac{\Delta E^{bb}(t)}{\hbar} dt \\ &\approx 8a_s^{bb} \sqrt{\frac{m\omega_0}{\hbar} \frac{\omega_y \omega_z}{\omega_0^2 + \omega^2 (4x_0^2 m\omega_0/\hbar - 1)}}. \end{aligned} \quad (11.25)$$

If the particles are in different internal states, the center of mass does not decouple from the relative motion. No analytical solution is found in this case, and one must resort to numerical techniques to evaluate the collisional phase ϕ^{ab} .

11.2.3.4 Implementation of conditional dynamics

If at time τ the atoms have come back to their initial spatial distribution, corresponding to a symmetrized product of the ground states of the two wells, then after the barrier is raised they will remain trapped around the original position. The only change in the overall state will be a phase $\phi_{\tau}^{\beta_1} + \phi_{\tau}^{\beta_2} + \phi_{\tau}^{\beta_1\beta_2}$ as discussed in Sect. 11.2.2.2. Therefore, the gate operation time τ has to be

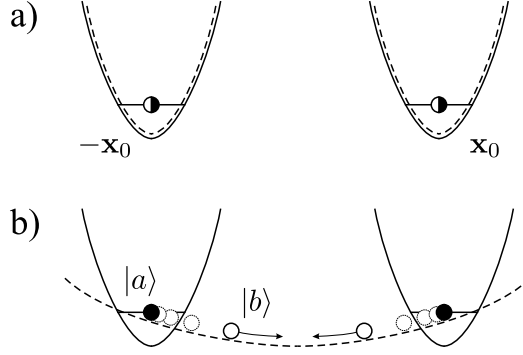


Fig. 11.2: Configuration at times $t < 0$, $t > \tau$ (a) and at $0 \leq t \leq \tau$ (b). The solid (dashed) curves show the potentials for particles in the internal state $|a\rangle$ ($|b\rangle$).

chosen in such a way as to maximize the overlap $|\langle \psi^{\beta_1 \beta_2}(\tau) | \psi^{\beta_1 \beta_2}(0) \rangle|^2$ for all β_1, β_2 . If the modifications in the atomic motion due to interaction are not too strong, this condition will be satisfied to a good approximation after an integer number n of oscillations. Thus, for $\tau \approx nT$, the following mapping is realized:

$$\begin{aligned}
 |a\rangle_1 |a\rangle_2 &\rightarrow e^{-i(2\phi_\tau^a + \phi_\tau^{aa})} |a\rangle_1 |a\rangle_2, \\
 |a\rangle_1 |b\rangle_2 &\rightarrow e^{-i(\phi_\tau^a + \phi_\tau^b + \phi_\tau^{ab})} |a\rangle_1 |b\rangle_2, \\
 |b\rangle_1 |a\rangle_2 &\rightarrow e^{-i(\phi_\tau^b + \phi_\tau^a + \phi_\tau^{ba})} |b\rangle_1 |a\rangle_2, \\
 |b\rangle_1 |b\rangle_2 &\rightarrow e^{-i(2\phi_\tau^b + \phi_\tau^{bb})} |b\rangle_1 |b\rangle_2,
 \end{aligned} \tag{11.26}$$

where $\phi_\tau^{aa} = 0$ as discussed in Sect. 11.2.3.2. If we apply a further single-bit rotation $|0\rangle\langle 0|e^{-i\phi_\tau^a} + |1\rangle\langle 1|e^{-i(\phi_\tau^b + \phi_\tau^{ab})}$ (where the logical states are defined as $|0\rangle \equiv |a\rangle$ and $|1\rangle \equiv |b\rangle$) and take into account that for symmetry reasons $\phi_\tau^{ab} = \phi_\tau^{ba}$, the mapping Eq. (11.26) realizes the fundamental phase gate

$$\begin{aligned}
 |0\rangle|0\rangle &\rightarrow |0\rangle|0\rangle, \\
 |0\rangle|1\rangle &\rightarrow |0\rangle|1\rangle, \\
 |1\rangle|0\rangle &\rightarrow |1\rangle|0\rangle, \\
 |1\rangle|1\rangle &\rightarrow e^{-in(\phi_\tau^{bb} - 2\phi_\tau^{ab})} |1\rangle|1\rangle,
 \end{aligned} \tag{11.27}$$

where the phase difference $\phi_\tau^{bb} - 2\phi_\tau^{ab}$ has to be adjusted to $\pm\pi$ by a proper choice of the trap parameters.

11.3 Physical realizations

A physical implementation of the scenarios described in Sec. 11.2 requires an interaction which produces internal-state-dependent conservative trap potentials and the possibility of manipulating these potentials independently. The choice of the internal atomic states $|a\rangle$ and $|b\rangle$ has to be such that they are elastic (i.e. the internal states do not change after the collision). To achieve entanglement operations with high fidelity, one has to be able to load or cool the atoms to the ground states of the trapping potentials. Finally, for the application of parallel quantum computing one needs periodic structures (e.g. optical lattices), together with the ability to control the positions of the atoms and to fill the lattice sites selectively.

11.3.1 Two-qubit gates in optical lattices

In this Section we want to discuss how a number of difficulties can be overcome that one encounters when trying to use optical lattices for quantum computing. We will first show how one can achieve a filling factor of 1 with particles in the ground states (lowest band) of the lattice. This can be achieved by using an ultracold very dense sample of weakly interacting atoms, namely a Bose-Einstein condensate, and slowly turning on an optical potential. The repulsive interaction between the particles increases as the optical potential is made deeper. At the same time the hopping rate at which particles move from one site to the next decreases. If the optical lattice is turned on on a time scale much slower than the hopping rate and the temperature kT can be kept much smaller than the interaction energy between two particles in one site, one can achieve a filling of the optical lattice with exactly one particle per lattice site. [75] Finally, we note that a filling factor of one out of two lattice sites has been achieved in very recent optical lattice experiments. [65]

We will also discuss how the lattice potentials can be moved in a state-selective way for implementing the two-qubit gate [31]. For alkali atoms with a nuclear spin equal to $3/2$ we show how atoms in different hyperfine levels can be moved into different directions. It is clear that other difficulties like e.g. addressing single qubits exist, but they will not be discussed here since their experimental solution is not specific to the present implementation.

11.3.1.1 Hamiltonian for a Bose-Einstein condensate in an optical lattice

We assume a Bose-Einstein condensate of atoms in internal state $|a\rangle$ to be loaded into an optical lattice potential $V_T(\mathbf{x}) + V_0(\mathbf{x})$, where

$$V_0(\mathbf{x}) = V_{x0} \sin^2(kx) + V_{y0} \sin^2(ky) + V_{z0} \sin^2(kz) \quad (11.28)$$

is a periodic optical lattice potential and $V_T(\mathbf{x})$ is a superlattice potential slowly varying in space compared to $V_0(\mathbf{x})$. k is the wave number of the lasers producing the lattice potential. The Hamiltonian reads [75]

$$H = \int d^3x \psi^\dagger(\mathbf{x}) \left(-\frac{\hbar^2}{2m} \nabla^2 + V_0(\mathbf{x}) + V_T(\mathbf{x}) - \mu \right) \psi(\mathbf{x}) + \frac{1}{2} \frac{4\pi a_s^{\text{aa}} \hbar^2}{m} \int d^3x \psi^\dagger(\mathbf{x}) \psi^\dagger(\mathbf{x}) \psi(\mathbf{x}) \psi(\mathbf{x}), \quad (11.29)$$

where $\psi(\mathbf{x})$ is the bosonic field operator and μ is the chemical potential i.e. a Lagrangian multiplier to fix the number of particles. Expanding the field operators in the Wannier basis while keeping only the dominant terms [75] Eq. (11.29) reduces to the Bose-Hubbard Hamiltonian

$$H = -J \sum_{\langle i,j \rangle} b_i^\dagger b_j + \sum_i (\epsilon_i - \mu) \hat{n}_i + \frac{1}{2} U \sum_i \hat{n}_i (\hat{n}_i - 1), \quad (11.30)$$

where the operators $\hat{n}_i = b_i^\dagger b_i$ count the number of bosonic atoms at lattice site i ; the annihilation and creation operators b_i and b_i^\dagger obey the canonical commutation relations $[b_i, b_j^\dagger] = \delta_{ij}$. J is the tunneling matrix element and U describes the (repulsive) interaction between particles at the same lattice site. $\epsilon_i = V_T(x_i)$ is the value of the slowly varying superlattice potential at site i . The ratio U/J is controlled by the depth of the optical lattice potential V_{j0} . Increasing V_{j0} (via the intensity of the trapping lasers) reduces the tunneling matrix element J and increases the repulsive interaction between the atoms U [75].

11.3.1.2 Loading the lattice

In order to perform gate operations in optical lattices we have to be able to selectively fill the lattice sites with exactly one particle. This can be achieved by making use of the phase transition from a superfluid BEC phase to a Mott insulator (MI) phase at low temperatures, which can be induced by increasing the ratio of the onsite interaction U to the tunneling matrix element J predicted by the Bose-Hubbard model [76, 77]. In the MI phase the density ρ_i (occupation number per site) is pinned at integer $n = 0, 1, 2, \dots$ corresponding to a commensurate filling of the lattice, and thus represents an *optical crystal* with diagonal long range order with period imposed by the laser light. Particle number fluctuations are thereby drastically reduced and thus the number of particles per lattice site is fixed. The number of particles per lattice site depends on the chemical potential μ in the isotropic case $\epsilon_i = 0$ [76]. In the non-isotropic case we may view $\mu - \epsilon_i$ as a local chemical potential. Therefore ρ_i can be controlled by the superlattice potential $V_T(\mathbf{x})$.

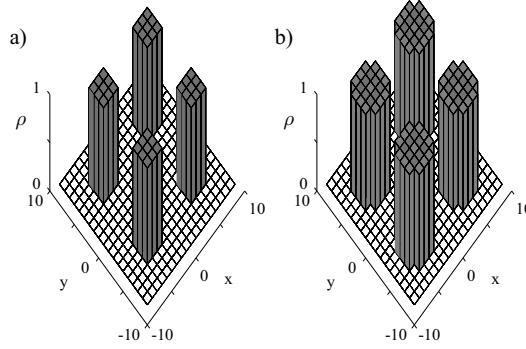
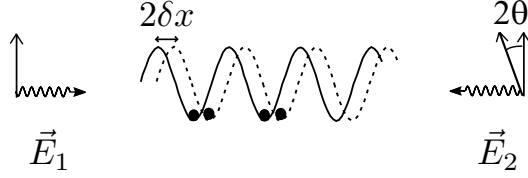
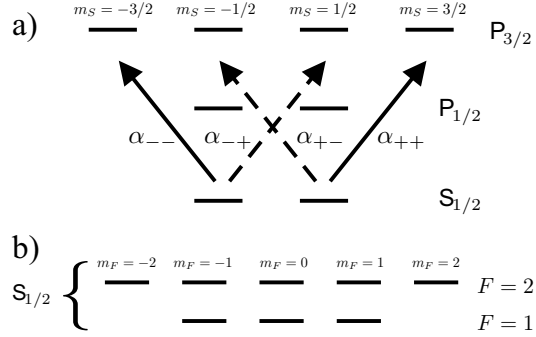


Fig. 11.3: Superlattice potential in 2D with $V_T(x, y) = 40J (\sin^2(\pi x/9a) + \sin^2(\pi y/9a))$ with a the spacing between the lattice sites. The particle density $\rho(x, y)$ for four superlattice wells is shown. Parameters: a) $U = 30J$ and $\mu = 15J$, b) $U = 50J$ and $\mu = 27J$.

Using a Gutzwiller ansatz [75, 78, 79] for the wave function we have performed a mean field calculation to demonstrate how, by a proper choice of the potential $V_T(\mathbf{x})$, one can fill certain blocks of the optical lattice with exactly one particle at temperature $T = 0$. Figure 11.3 shows the result of this mean field calculation, a MI phase where the lattice sites are either filled with 0 or 1 particles. The number fluctuations are almost equal to zero and thus not shown in this plot. To achieve a MI phase at finite temperature $T \neq 0$ one has to fulfill the requirement $kT \ll U$ where the interaction strength U gives the order of magnitude of the first excitation energy in a MI phase. One also has to ensure that particles do not move from a filled site with energy ϵ_i to an adjacent empty site with energy ϵ_j i.e. the temperature has to be much smaller than the energy difference between these two sites $kT \ll \epsilon_j - \epsilon_i$. In Sec. 11.4, we will need periodic fillings of optical lattices as shown in Fig. 11.3 to implement efficient multi-particle entanglement operations and for parallel quantum computing.

11.3.1.3 Moving the lattice potentials state selectively

We consider the example of alkali atoms with a nuclear spin equal to $3/2$ (^{87}Rb , ^{23}Na) trapped by standing waves in three dimensions and thus confined by a potential of the shape as given in Eq. (11.28). The internal states of interest are hyperfine levels corresponding to the ground state $S_{1/2}$ as shown in Fig. 11.5b. Along the z axis, the standing waves are in the lin \angle lin configuration (two linearly polarized counter-propagating traveling waves with the electric fields \vec{E}_1 and \vec{E}_2 forming an angle 2θ [80]) as shown in Fig. 11.4. The total electric field is a superposition of right and left circularly polarized standing waves

Fig. 11.4: Laser configuration along the z -axis.Fig. 11.5: Level scheme of ^{87}Rb and ^{23}Na and laser configuration. (a) Fine structure energy levels and laser configuration. The detuning is chosen such that the polarizabilities α_{+-} and α_{-+} vanish. (b) Hyperfine level structure.

(σ^\pm) which can be shifted with respect to each other by changing θ ,

$$\vec{E}^+(z, t) = E_0 e^{-i\nu t} [\vec{e}_+ \sin(kz + \theta) + \vec{e}_- \sin(kz - \theta)], \quad (11.31)$$

where \vec{e}_\pm denote unit right and left circular polarization vectors, $k = \nu/c$ is the laser wave vector and E_0 the amplitude. The lasers are tuned between the $P_{1/2}$ and $P_{3/2}$ levels so that the dynamical polarizabilities $\alpha_{\pm\mp}$ of the two fine structure $S_{1/2}$ states corresponding to $m_s = \pm 1/2$ due to the laser polarization σ^\mp vanish ($\alpha_{+-} = \alpha_{-+} = 0$), whereas the polarizabilities $\alpha_{\pm\pm}$ due to σ^\pm are identical ($\alpha_{++} = \alpha_{--} \equiv \alpha$). This configuration is shown in Fig. 11.5a and can be achieved by tuning the lasers between the $P_{3/2}$ and $P_{1/2}$ fine state levels so that the ac-Stark shifts of these two levels cancel each other. The optical potentials for these two states are $V_{m_s=\pm 1/2}(z, \theta) = \alpha |E_0|^2 \sin^2(kz \pm \theta)$.

We choose for the states $|a\rangle$ and $|b\rangle$ the hyperfine structure states $|a\rangle \equiv |F = 1, m_f = 1\rangle$ and $|b\rangle \equiv |F = 2, m_f = 2\rangle$. Due to angular momentum conservation, these states are stable under collisions (for the dominant central electronic interaction [81, 82]). The potentials “seen” by the atoms in these internal states are

$$V^a(z, \theta) = [V_{m_s=1/2}(z, \theta) + 3V_{m_s=-1/2}(z, \theta)] / 4$$

$$V^b(z, \theta) = V_{m_s=1/2}(z, \theta). \quad (11.32)$$

If one stores atoms in these potentials and they are deep enough, there is no tunneling to neighboring wells and we can approximate them by harmonic potentials. By varying the angle θ from $\pi/2$ to 0, the potentials V^b and V^a move in opposite directions until they completely overlap. Then, going back to $\theta = \pi/2$ the potentials return to their original positions. The shape of the potential V^a changes as it moves. By choosing

$$\theta(t) = \pi \left(1 - \left(1 + \exp(-(\tau_i/\tau_r)^2) \right) / \left(1 + \exp((t^2 - \tau_i^2)/\tau_r^2) \right) \right) / 2 \quad (11.33)$$

with $\tau_r = 25/\omega$ and $\tau_i = 25/\omega$, the frequencies and displacements of the harmonic potentials approximating (11.32) are exactly those plotted in Fig. 11.6a.

11.3.1.4 Gate fidelity

We use the minimum fidelity F [83] to characterize the quality of the gate. F is defined as

$$F = \min_{\tilde{\varphi}} \langle \tilde{\varphi} | \text{tr}_{\text{ext}} \left(\mathcal{U} |\varphi\rangle\langle\varphi| \otimes \rho_{\text{ext}} \mathcal{U}^\dagger \right) | \tilde{\varphi} \rangle, \quad (11.34)$$

where $|\varphi\rangle$ is an arbitrary internal state of both atoms, $|\tilde{\varphi}\rangle$ is the state resulting from $|\varphi\rangle$ using the mapping (11.12). The trace is taken over motional states, \mathcal{U} is the evolution operator for the internal states coupled to the external motion (including the collision), and ρ_{ext} is the density operator corresponding to both atoms being at a temperature T at time $t = -\tau$ [31]. In Fig. 11.6b the fidelity F is plotted as a function of the temperature T for the displacements and trap frequencies shown in Fig. 11.6a. This figure shows that one can achieve very high fidelities in realistic situations.

11.3.2 Two-qubit gates in magnetic microtraps

We now consider the implementation of a switching potential by means of electromagnetic trapping forces. We first discuss the possibility of obtaining the desired state dependence by assuming some improvements on devices which are now experimentally available [84, 85, 86]. Then we compute the performance of a quantum gate for realistic trapping parameters.

11.3.2.1 Microscopic electromagnetic trapping potential

The interaction between the magnetic dipole moment of an atom in some hyperfine state $|F, m_F\rangle$ and an external static magnetic field \vec{B} entails an energy $U_{\text{magn}} \approx g_F \mu_B m_F |\vec{B}|$ depending on the atomic internal state via the quantum number m_F (here μ_B is the Bohr magneton and g_F is the Landé factor). On the other hand, the Stark shift induced on an atom by an electric field \vec{E}

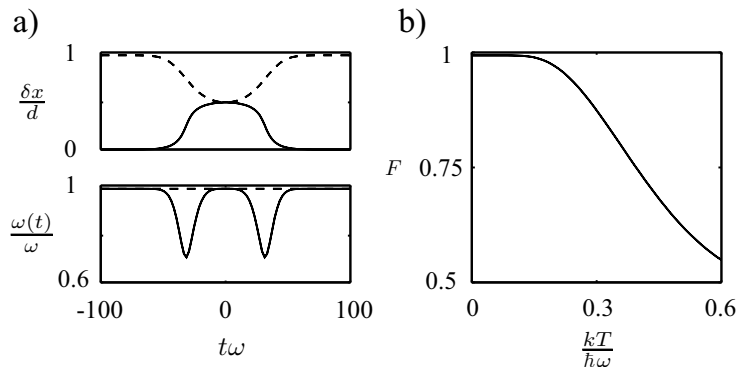


Fig. 11.6: a) Upper plot: Displacements $\delta x^a(t)/d$ (solid line) and $1 + \delta x^b(t)/d$ (dashed line). Lower plot: Trap frequencies $\omega^a(t)/\omega$ (solid line) and $\omega^b(t)/\omega$ (dashed line). b) Fidelity F against temperature $kT/\hbar\omega$ for ^{87}Rb with $a_s = 5.1\text{nm}$. Here $\omega = 2\pi \times 100\text{kHz}$ and $d = 390\text{nm}$.

gives a state-independent energy $U_{\text{el}} \approx \frac{1}{2}\alpha|\vec{E}|^2$, where α is the atomic polarizability. The interplay between these two effects can be exploited in order to obtain a trapping potential whose shape depends on the atomic internal state. As an example, we consider an atomic mirror with an external magnetic field [84, 85, 86], providing confinement along two directions with trapping frequencies which can range from a few tens of kHz up to some MHz. Microscopic electrodes can be plugged on the mirror's surface [87], thus allowing for the design of a potential with the characteristics described in Sect. 11.2.3.

11.3.2.2 Loading and moving atoms within the trap

Several schemes of loading atoms into the trap have been envisaged (see for example [84, 85, 86]). Most of them rely on an intermediate stage where atoms can be trapped and cooled without coming in contact with the magnetic mirror. This pre-loading trap can be either initially displaced from the surface, or close to it but based on a different trapping mechanism (for instance an evanescent wave mirror, where different internal states can be trapped by gravity [88] before the atoms can be put in the right states for magnetic trapping), to be replaced by the electromagnetic microtrap with a gradual switch-on of the electric and bias magnetic fields in the final stage of loading [87]. This could also allow for implementing a controlled filling of the trap sites, in a similar way to that already discussed in Sec. 11.3.1. A further feature to be implemented in view of performing more complex algorithms is the arrangement of several gate potentials in a periodic pattern, and the possibility of transporting atoms within this structure. An example would be given by two adjacent rows of potential minima, shiftable with respect to each other, where atoms could

be loaded. A system like the one suggested in Sect. 11.3.2.1 could allow in principle to obtain such a configuration, since the magnetic field minima can be shifted parallel to the surface by rotating the bias magnetic field. In this way it should be possible to move some atoms, while holding others in place by means of additional local electric fields [84, 85, 86]. Provided that atoms can be addressed individually, which is needed even for performing a one-bit quantum gate, a procedure for implementing a simple quantum algorithm could be the following: perform a gate between two suitably chosen atoms, being close to each other but belonging to different rows, then mutually displace the rows and select another pair of atoms, including one of those coming out from the previous gate. Repeat until the algorithm has been operated, applying the required one-qubit rotations in between the above steps and possibly performing some of them in parallel.

11.3.2.3 Switching the trap potentials state selectively

We choose for the states $|a\rangle$ and $|b\rangle$ the same hyperfine structure states of ^{87}Rb considered in the previous Section, which are low-magnetic field seekers. If both particles are in state $|a\rangle$, there is no interaction-induced phase shift, as already discussed in Sec. 11.2.3.2. The results for both particles in state $|b\rangle$ are shown in Fig. 11.7. The time dependence of ϕ^{bb} is step-like (Fig. 11.7a): the collisional phase is incremented at times $t_k \equiv (2k - 1)T/4$, when the atoms meet at the center of the well, and remains constant at intermediate times, when they separate again. The influence of the interaction on the atomic motion can be seen from Fig. 11.7b, depicting the overlap between the evolved interacting two-atom state $|\psi^{bb}(t)\rangle$ and the corresponding state $|\psi_{(0)}^{bb}(t)\rangle$ computed without taking into account the interaction. The curve has local minima at times t_k , signalling that a collision is taking place, and shows a global decrease corresponding to a slight delay of the interacting motion with respect to the non-interacting one. As it can be seen from Fig. 11.7c, this effect is not dramatic: the oscillation period in the presence of interaction is increased just by $\delta T \approx 2 \times 10^{-3}T$ (with the parameters used here), and the harmonic potential ensures that the system comes periodically back to its initial state. After 7 oscillations we get a phase shift due to the interaction of π , whereas the perturbative formula (11.25) gives $7\phi_T^{bb} \approx 0.98\pi$. Therefore we choose $\tau = 7(T + \delta T) \approx 0.15\text{ms}$: the overlap between the initial and the evolved wave function at that time is $|\langle \psi^{bb}(\tau) | \psi^{bb}(0) \rangle|^2 \approx 0.996$. The behavior turns out to be quite different [89] when the atoms are in different internal states: the phase shift increases more rapidly, but after a few oscillations the system does no longer come back to the initial state. This has a simple explanation. The two atoms collide as soon as the one being in state $|b\rangle$, moving within the potential $m\omega^2 x^2/2$, reaches its turning point, where the other atom is trapped.

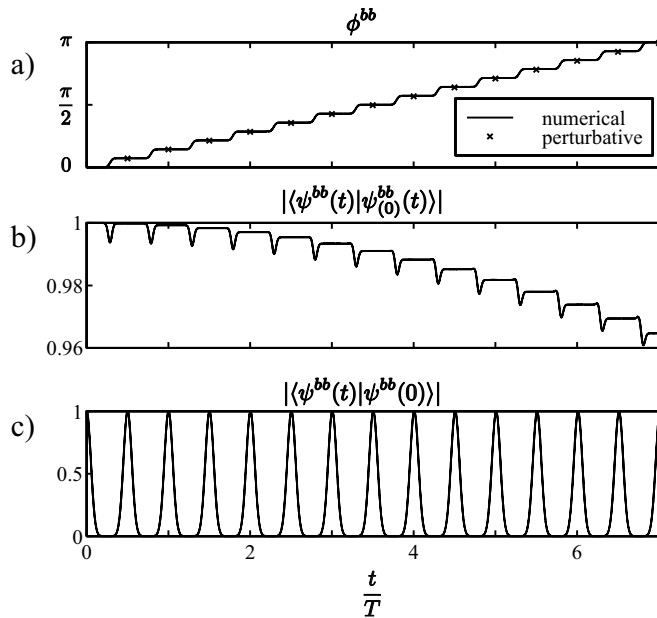


Fig. 11.7: Dynamics during gate operation, with both atoms in state $|b\rangle$: a) interaction-induced phase shift - the circles refer to the perturbative calculation (11.25); b) projection of the evolved state on the corresponding state evolved without interaction; c) projection of the evolved state on the initial one. We choose $\omega \approx 23.4$ kHz and $\omega_y = \omega_z = 150$ kHz, corresponding to ground-state widths $a_x \approx 50$ nm, $a_y = a_z \approx 28$ nm, with the initial wells having frequency $\omega_0 = 2\omega$ and displaced by $x_0 = 3\sqrt{2}a_x$. We take for the scattering length the known value for ^{87}Rb , *i.e.* $a_s^{bb} \approx a_s^{ab} = 5.1$ nm. Time is in units of the oscillation period T .

The interaction time is therefore longer than if both atoms were in state $|b\rangle$. Indeed, in that case they meet at the trap center, with their maximal velocity. This explains why the system picks up a bigger phase shift per oscillation period in the present case. On the other hand, the collision excites the motion of the atom in state $|a\rangle$ within its own well, and therefore the initial state is no longer recovered. This problem can be avoided if the potential minimum for state $|a\rangle$ is displaced along the transverse direction from the one for state $|b\rangle$ by means of an additional electrostatic field [84, 85, 86], so that the atoms interact if and only if they are both in state $|b\rangle$. This problem would not exist in an adiabatic scheme for the gate operation, when the shape of the potential is changed slowly with respect to the atomic motion. This will be the subject of future investigation.

11.3.2.4 Gate fidelity

The calculation of the fidelity in this case has to take into account the symmetrization of the wave function under particle interchange, expressed by an operator S to be explicitly inserted into Eq. (11.34):

$$F = \min_{\varphi} \left\{ \text{tr}_{\text{ext}} \left[\langle \tilde{\varphi} | \mathcal{U} S (|\varphi\rangle\langle\varphi| \otimes \rho_{\text{ext}}) S^\dagger \mathcal{U}^\dagger | \tilde{\varphi} \rangle \right] \right\}, \quad (11.35)$$

With the parameters quoted above, we obtain $F > 0.98$. In order to reach such a fidelity, timing has to be quite precise, with a resolution of the order of $10^{-3}T$ corresponding to tens of ns in this case.

11.4 Parallel quantum computing

In this Section, we will discuss how quantum gates based on controlled collisions can be exploited for quantum computing. It is clear that, with the realization of a universal two-bit gate, any quantum computation can be performed, just as it is the case with other implementations. On the other hand, manipulations such as moving and switching potentials offer a great deal of parallelism [43, 44] not available in other systems.

We will focus our attention on implementations in optical lattices. Some of the ideas could readily be translated into arrays of magnetic microtraps, if the distances between the individual potential wells could be made much shorter than present-day state-of-the-art of nanofabrication. In such a situation, adiabatic variants of the switching operations (see comment at the beginning of Sec. 11.2.3) can be used to create multi-particle entangled clusters of neighboring atoms, similar as with moving potentials. Details of this analysis will be presented somewhere else [89].

One may ask, what can be done in optical lattices that cannot be done in other implementations? The answer to this question depends on a number of experimental conditions such as the possibility of creating regular filling structures and, like in ion-traps, on the possibility of addressing single atoms individually. In the following, we will first (Sec. 11.4.1) give an example of what can be done with controlled lattice movements in conventional set-ups i.e. with random filling of the lattice sites and without any control of the position of individual atoms. We will see that this already allows one to perform interesting spectroscopic studies of the degree of entanglement between the atoms thus created. Next (Sec. 11.4.2), we will describe what can be done if one achieves a regular occupation of the lattice sites and can address the atoms individually. Under such circumstances, an efficient implementation of quantum error correction and of a quantum memory (concatenated Shor code) is possible. Furthermore, fault tolerant versions of certain quantum gates and

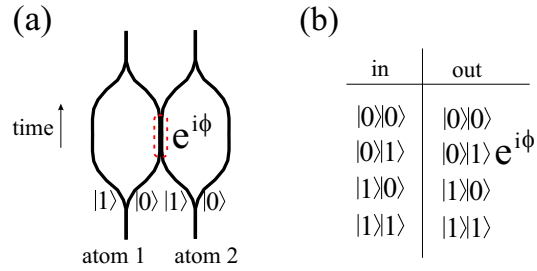


Fig. 11.8: Atom-interferometric process realizing the quantum gate. (a) Two-particle interferometer; (b) Truth table.

of quantum error correction can be implemented straightforwardly, as will be sketched in (Sec. 11.4.3). Finally, in Sec. 11.4.4, we describe how auxiliary atomic levels can be used to realize highly selective entanglement operations, where individually selected atoms are swept across the lattice to create GHZ states [90] of a large number of particles. Together with 11.4.2 and 11.4.3, this scheme has all the ingredients that are necessary for an efficient realization of fault-tolerant quantum computing.

11.4.1 Multi-particle entanglement operations

The two-qubit gates described in Sec. 11.3 correspond abstractly to an atom interferometer as shown in Fig. 11.8. The interferometer has two inputs which are the two atoms trapped at neighboring potential wells. By shifting the potentials back and forth as described in Secs. 11.2.2, only one combination of paths of the two particles overlaps and leads to a phase shift, namely the paths corresponding to state $|a\rangle_1$ for the left particle and $|b\rangle_2$ for the right particle. To emphasize the role of the internal states as *logical* states, we shall henceforth use the notation $|0\rangle \equiv |a\rangle$ and $|1\rangle \equiv |b\rangle$ and neglect the kinetic phases ϕ^a , ϕ^b as they appear in (11.12). Furthermore, we drop the atomic index as long as there is no danger of confusion.

The logical truth table corresponding to the interferometric process is shown in Fig. 11.8. [A similar identification of logical states can be made in magnetic traps as is pointed out in Sec. 11.2.3.4. The labelling of the paths for the left particle in the interferometer has to be interchanged in this case.] For $\phi = \phi^{01} = \pi$ this realizes a phase gate [1]. The phase gate and the set of all one-bit unitary transformations, which can be realized by Raman laser pulses on the internal states $|0\rangle$ and $|1\rangle$, define a *universal set of quantum gates*. [91, 92, 93, 94]

An important difference between optical lattices and other implementations is given by the global effect of the lattice manipulations. To illustrate

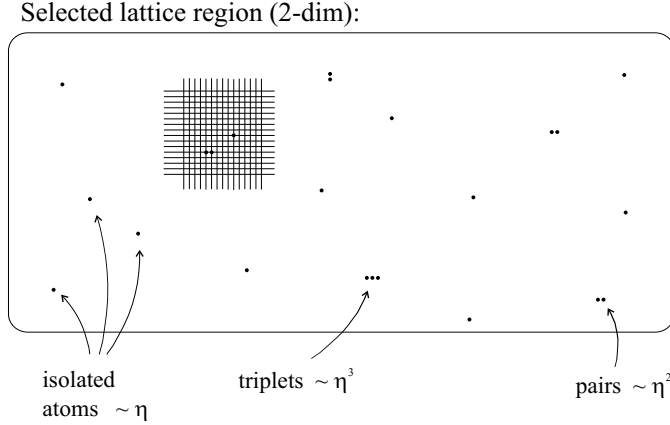


Fig. 11.9: Random occupation of a two dimensional lattice with single atoms.

this point, consider first a two dimensional lattice as in Fig. 11.9 with random occupation of the sites and a filling factor $\eta \ll 1$, where η is defined as the average number of atoms per lattice site. Let us assume that the loading of the lattice can be accomplished in such a way that there are no multiply occupied lattice sites, i.e. that each lattice site is occupied by no more than a single atom. Then, in any region of the lattice, one will find isolated atoms, pairs of neighboring atoms, triplets, and so forth, with a relative frequency proportional to η , η^2 , η^3 , respectively. Consider now the following *Ramsey experiment* [95] where initially all atoms are prepared in the internal state $|0\rangle$ and in the motional ground state of their individual potential wells. In some selected region of the lattice, the following sequence of operations is applied: (1) a $\pi/2$ laser pulse brings all atoms into a superposition of the internal states $|0\rangle$ and $|1\rangle$; (2) the lattice is shifted across one lattice site and then, after a variable length of time, shifted back to its original position, (3) finally a second $\pi/2$ pulse is applied to the region. The effect of this sequence is illustrated in Fig. 11.10. For a group of $N = 1, 2, 3, \dots$ neighboring atoms, the lattice shift corresponds to a *N-particle interferometric process*. Specifically, one obtains the following transformations. For isolated atoms:

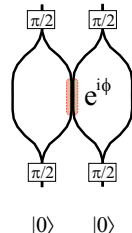
$$|0\rangle \longrightarrow |0\rangle; \quad (11.36)$$

for pairs of neighboring atoms:

$$|00\rangle \longrightarrow \frac{1 + e^{i\phi}}{2}|00\rangle + \frac{1 - e^{i\phi}}{2}|\text{BELL}\rangle; \quad (11.37)$$

and for triplets of neighboring atoms:

$$|000\rangle \longrightarrow \frac{1 + e^{i\phi}}{2}|000\rangle + \frac{1 - e^{i\phi}}{2}|\text{GHZ}\rangle; \quad (11.38)$$

$$|\Psi\rangle = \frac{1+e^{i\phi}}{2}|00\rangle + \frac{1-e^{i\phi}}{2}|\text{BELL}\rangle$$


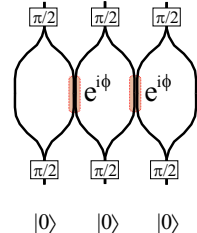
$$|\Psi\rangle = \frac{1+e^{i\phi}}{2}|000\rangle + \frac{1-e^{i\phi}}{2}|\text{GHZ}\rangle$$


Fig. 11.10: Entanglement of pairs (left) and triplets (right) of neighboring atoms by a single lattice shift.

where we have used the notation

$$|\text{BELL}\rangle = \frac{1}{\sqrt{2}} \{ |0\rangle|+\rangle - |1\rangle|-\rangle \},$$

$$|\text{GHZ}\rangle = \frac{1}{\sqrt{2}} \{ |0\rangle|+\rangle|1\rangle - |1\rangle|-\rangle|0\rangle \}, \quad (11.39)$$

and $|\pm\rangle = (|0\rangle \pm |1\rangle)/\sqrt{2}$. The expressions for groups of more particles become more complicated and shall be ignored in the present discussion. It is clear that for $\phi = \pi$ Bell- and GHZ states [96, 90] are created by a *single* lattice shift at various places within the region. This corresponds to an ensemble of 2-bit and 3-bit quantum gates, respectively, acting simultaneously at different lattice sites. To analyze the states (11.37) and (11.38) spectroscopically one could measure the state of the atoms in a final step of the above Ramsey sequence e.g. by a fluorescence measurement. It is clear that by such a measurement the entangled states will be destroyed. On the other hand, by repeating this sequence many times with different samples, one can measure the fluorescence signal as function of the phase ϕ (interaction time). Under ideal circumstances, all isolated atoms will remain in the dark state $|0\rangle$ while all fluorescence signals come from Bell ($\sim \eta^2$) or GHZ ($\sim \eta^3$) states [97]. To check that entangled states, rather than mixtures, are created in the process, the experiment is performed with different interaction times, e.g. times corresponding to $\phi = \pi$ and $\phi = 2\pi$. For entangled states as in (11.37) and (11.38) all fluorescence signals will vanish at $\phi = 2\pi$, while this will not be the case if the states created by the atomic collisions are mixtures of classical many-particle states. More generally, by measuring the *visibility* of the fluorescence signal one may study the *fidelity of the entanglement* created in the process, and its dependence on certain noise sources such as a finite temperature of the atoms. This way, the curve plotted in Fig. 11.6b) could be tested experimentally.

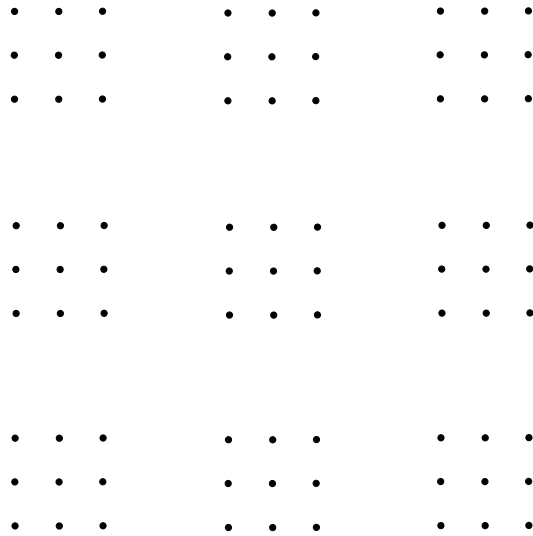


Fig. 11.11: Ordered arrangement of atoms in an optical lattice (see also Fig. 11.3).

11.4.2 Quantum error correction

To employ these entanglement operations for quantum computing, one has to have precise control over the number and the location of atoms that are involved in the collisional process. In addition to the ability of addressing single atoms, one therefore has to achieve a certain *ordered occupation of the lattice sites*. As described in Sec. III.A., Fig. 11.3, this can be by achieved by controlling the intensity of the trapping laser at sufficiently low temperatures. This way optical crystals with periodic patterns of atoms can be created as indicated in Figs. 11.11 and 11.15 [98] Under such circumstances the parallelism of the lattice manipulations can be exploited advantageously. On one side, similar logical operations can be performed simultaneously at different locations on the lattice. On the other side, as we have seen in Fig. 11.10, a single lattice shift can entangle whole groups of atoms. Two types of such entanglement operations are shown in Fig. 11.12. One involves only the logical states $|0\rangle$ and $|1\rangle$, while the second uses a third atomic level as a “transport state” (see Sec. 11.4.4), into which any atom must first be activated, before it can participate in an entanglement operation. In the following, we will first discuss applications of the shift operation as in Fig. 11.12(a). Later, in Sec. 11.4.4 we will consider a more flexible (“sweep”) operation shown in Fig. 11.12(b).

An application of shift operations as described in Fig. 11.12(a) concerns the realization of a *quantum memory*, where a qubit $\alpha|0\rangle + \beta|1\rangle$ (with unknown coefficients α and β) is encoded in the quantum state of a larger block of atoms

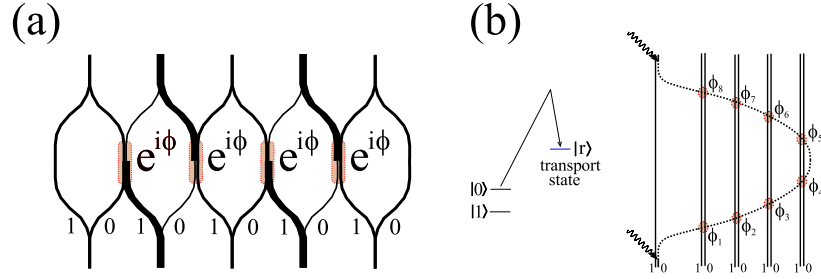


Fig. 11.12: (a) “Shift operation”: The internal atomic states $|0\rangle$ and $|1\rangle$ couple to different lattice potentials that are moved against each other as explained in Sec. 11.3.1.3. This corresponds to a multi-particle interferometer where the same phase shift is acquired whenever two paths temporary overlap. By simple lattice manipulations, therefore, entire groups of atoms become entangled. (b) “Sweep operation”: For more selective entanglement operations, a third atomic level $|r\rangle$ is used [99]. In this scheme, only atoms in the level $|r\rangle$ are moved, whereas the states $|0\rangle$ and $|1\rangle$ are kept in the same potential. At the beginning of an entanglement operation, the atoms are first excited from one of the states $|0\rangle$ or $|1\rangle$ to the state $|r\rangle$ before the lattice is moved. This scheme is much more selective in the sense that those atoms which shall participate in a gate operation are first activated, before they couple to the moving lattice, and the collisional phases ϕ_j can be varied for each interaction individually.

and stabilized against decoherence with the help of quantum error correction [47, 48, 49, 50, 51, 52, 53, 54]. A particular quantum code that is able to protect a qubit against general 1-bit errors (spin flip and phase flip) has been proposed by Shor [47]. It is a 9-bit code where the codewords

$$\begin{aligned} |0_S\rangle &= 2^{-3/2}(|000\rangle + |111\rangle)(|000\rangle + |111\rangle)(|000\rangle + |111\rangle) \\ |1_S\rangle &= 2^{-3/2}(|000\rangle - |111\rangle)(|000\rangle - |111\rangle)(|000\rangle - |111\rangle) \end{aligned} \quad (11.40)$$

consist of products of certain GHZ states. Abstractly speaking, the encoding operation consists of a mapping (embedding) of the qubit’s 2-dimensional Hilbert space \mathcal{H} into a 2^9 -dimensional Hilbert space of the form

$$\mathcal{H} \ni \alpha|0\rangle + \beta|1\rangle \mapsto \alpha|0_S\rangle + \beta|1_S\rangle \in \mathcal{H}_E \subset \mathcal{H}^{\otimes 9}. \quad (11.41)$$

To stabilize the encoded information against decoherence, the code must be measured and corrected on a time scale $\tau \ll 1/9\gamma$ where γ is the rate of decoherence for a single qubit. This is possible since all errors that may occur on any one of the qubits of the codewords (11.40) map the code into a family of 2-dimensional subspaces of $\mathcal{H}^{\otimes 9}$ which are all orthogonal on \mathcal{H}_E [47].

The Shor code (11.40) can be implemented efficiently in a two dimensional lattice configuration [100] as in Fig. 11.11, by using the shift operation of

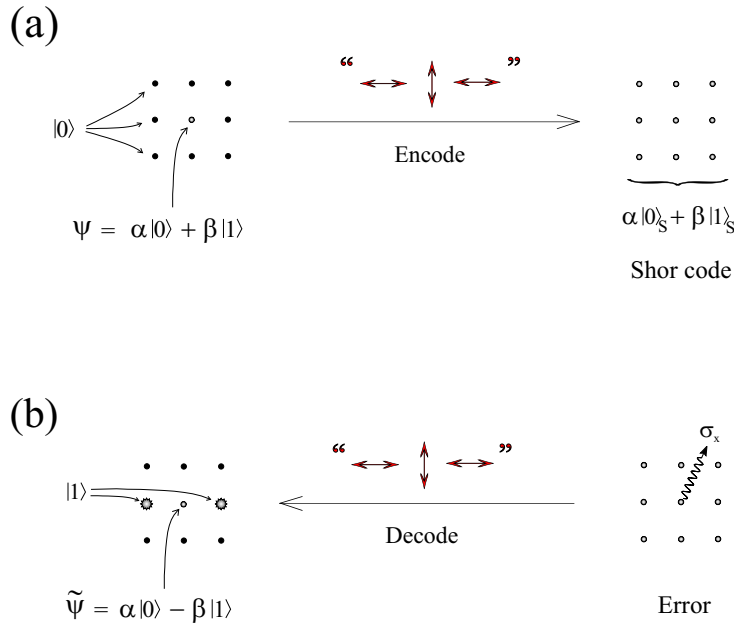


Fig. 11.13: (a) Encoding of a qubit into a block of 3×3 atoms; (b) Decoding and syndrome measurement.

Fig. 11.12(a). To see this, imagine that the qubit/atom whose state is to be encoded is surrounded by neighboring atoms as in Fig. 11.13. The idea is of course to encode the central qubit in the whole block of 3×3 qubits. Initially the central atom is in the unknown state $|\psi\rangle = \alpha|0\rangle + \beta|1\rangle$ while all neighboring atoms are in state $|0\rangle$. As is shown in Appendix B, the initial state is transformed into the Shor code by a simple sequence of horizontal and vertical lattice shifts combined with certain 1-bit rotations, as indicated in Fig. 11.13(a). By this process, the information contained in ψ is so to speak de-localized over the whole block of 9 atoms. To check whether an error has occurred on one of the qubits, the block is first decoded by the inverse transformation [50], which involves the same sequence of lattice shifts as the encoding. Subsequently, one measures which of the neighboring atoms are in the state $|1\rangle$. In the language of quantum error correction, the surrounding atoms of the central qubit in Fig. 11.13(b) are the carriers of the *error syndrome* [50], meaning that their state gives information regarding what type of error occurred and, more importantly, which unitary 1-bit rotation has to be applied to the central qubit to restore it to the original state. In a fluorescence measurement, this information corresponds to a specific pattern of bright and dark atoms surrounding the central qubit. For example, in Fig. 11.13(b) a spin flip has occurred in the central qubit. This means that the state of the

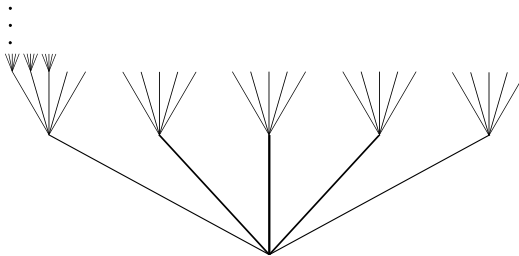


Fig. 11.14: Concatenated quantum coding. At each coding level, a single qubit is encoded in a block of a larger number of qubits, here 5. (See e.g. [62]).

block is transformed into $\alpha\sigma_x^{\text{ctr}}|0_S\rangle + \beta\sigma_x^{\text{ctr}}|1_S\rangle$ where σ_x^{ctr} is the corresponding Pauli spin operator associated with the central atom. By the decoding operation of Fig. 11.13(b), this state is mapped into a product state of 9 qubits in which the neighboring atoms in the central row are both in the (bright) state $|1\rangle$, while the other surrounding atoms are in the (dark) state $|0\rangle$. The central atom is in a state equivalent to $|\psi\rangle$ up to a unitary transformation. Similar fluorescence patterns are obtained if a phase error occurs in the central atom or an arbitrary 1-bit error on any of the atoms in the block. A complete table of the error syndrome is given in the Appendix.

The essential point is that the measurement on the surrounding atoms does not reveal nor destroy the state of the central atoms (the coefficients α and β remain unknown throughout the process). If the sequence of operations “decode-correct-encode” is repeated sufficiently often within the decoherence time $1/9\gamma$ of the block, the state ψ may be protected over arbitrarily long times, in principle. Here one assumes, of course, that the decoding and encoding operations themselves are *free of errors*. In our situation this means that all phases acquired in the atomic collisions can be perfectly controlled. Since these operations will always bear some imperfection/imprecision, the probability that an error is introduced by an imperfect operation increases/accumulates with repeated applications of these operations. The general solution to this quantum-memory problem was given by Knill and Laflamme [57] and by others [58, 59, 60], and requires a *concatenation of encoding operations* as shown schematically in Fig. 11.14. The number of required concatenation steps depends on how long the qubit is to be stored. It can be shown [57] that, given the precision of the operations is above a certain threshold, a qubit can be stored for an arbitrary long time, where the number of qubits required for encoding (i.e. the length of the code) grows polynomially with the length of the storage time. In the optical lattice configuration, a concatenation of the encoding can be implemented straightforwardly. Imagine that, in the central block in Fig. 11.11, the center atom is initially in state $|\psi\rangle = \alpha|0\rangle + \beta|1\rangle$



Fig. 11.15: Concatenated quantum coding in an optical lattice. At each coding level, two-dimensional lattice displacements with an increasing periodicity are applied. The nested character of Fig. 11.14 is here reflected by a self-similar filling pattern of the lattice.

(similar as in Fig. 11.13) whereas all other atoms are in state $|0\rangle$. This means that both the surrounding atoms in the center block and the atoms of all the other blocks are initially in state $|0\rangle$. The first step of the encoding operation is identical as in Fig. 11.13 and results in the configuration where the center block is in a superposition of the Shor code words $|0_S\rangle$ and $|1_S\rangle$, whereas the surrounding blocks remain in state $|0\rangle$. In the second step, the same operation is repeated on a larger scale, i.e. the lattice is shifted across a larger distance such as to make the *blocks* temporarily overlap while the 1-bit operations of the first step are now repeated on corresponding atoms of the outer blocks. As a result, the information $|\psi\rangle$ originally carried by the center atom is now delocalized over $9 \times 9 = 81$ atoms! This scheme may be iterated as indicated in Fig. 11.15. When in the second (and higher-order) encoding step the blocks are brought to overlap, one has to make sure that only phases between corresponding atoms of the different blocks are accumulated. The most elegant way to achieve this would be with the aid of a technique where the 0 and 1 states are displaced vertically before the atoms are moved. This could be implemented in a three-dimensional lattice configuration[101]. The shift operation is then really a “lift & shift” operation. The collisional interaction is then only switched on by varying the vertical displacement, after the blocks have been moved horizontally. If such a lifting technique can not be implemented, e.g. in a truly two-dimensional configuration, then during the horizontal motion

there will be also collisions between non-corresponding atoms, for example the atoms in the right column of one of the blocks with atoms in the left column of a neighboring block. To avoid these unwanted phase shifts, it is possible to vary the velocity of the lattice movement in such a way that during unwanted collisions a phase of $e^{2\pi i}$ is acquired. This method is clearly more susceptible to decoherence. On the other hand, our numerical studies have shown [31], that by an appropriate choice of the displacement function $\theta(t)$ in Fig. 11.4, the phase of a single collision can, in principle, be controlled with a very high precision (with fidelity ≥ 0.9997) and the probability for exciting phonons remains correspondingly small [102].

It does not seem impossible that $\theta(t)$ could be controlled precisely enough to meet the threshold of fault-tolerant computation [62], but we have not yet made detailed numerical investigations for this situation. In summary, the method of *concatenated coding* can be implemented in optical lattices by repeated sequences of lattice displacements on *self-similar filling structures*.

11.4.3 Fault-tolerant computing

In a quantum computer, we do not only wish to store quantum information, but also to process it in a quantum algorithm. To prevent an accumulation of errors during the calculation due to imperfect gate operations, one needs to use fault-tolerant quantum gates that act on the encoded information. Furthermore, errors should be corrected fault tolerantly, that is, without decoding the information (and therefore exposing the qubit to decoherence). The general theory of fault-tolerant computation has been developed by several researchers [62]. In optical lattices, many of such fault-tolerant operations have a geometrically intuitive implementation. For example, if two qubits are encoded in blocks of 9 atoms each, as in Fig. 11.13, a controlled-NOT operation can be implemented by moving one block on top of the other so that each pair of corresponding atoms from the two blocks share a single potential well and acquire a phase shift $e^{i\pi}$. [This is a straightforward generalization of the situation in Fig. 11.8]. When a $\pi/2$ pulse is applied on one of the blocks before and after the blocks are shifted, a fault-tolerant realization of the CNOT gate, with a truth table as in Fig. 11.16 is realized. The minus sign may be eliminated by applying a $3\pi/2$ pulse instead of the second $\pi/2$ pulse. Similarly, one can find a simple fault-tolerant realization of the NOT gate, while for example the Hadamard transform is more involved and requires a measurement with auxiliary qubits. Whether or not one can find similarly *efficient* implementations for a complete set of fault tolerant gates, is still under investigation.

To check whether an error has occurred during a gate operation, one has to measure whether the blocks are still in a superposition of the correct code-

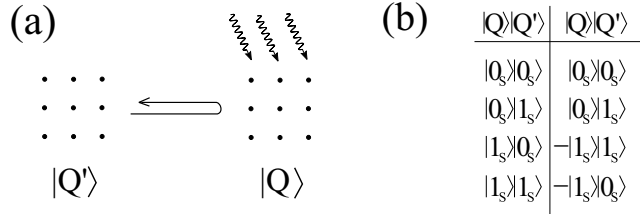


Fig. 11.16: Implementation of a fault-tolerant CNOT gate.

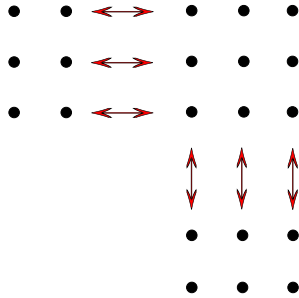


Fig. 11.17: Implementation of fault-tolerant error correction.

words. For the Shor code, this can be done in the following way [47], see Fig. 11.17: To detect a spin-flip, one has to measure the parity of the first two atoms in any row and compare it to the parity of the last two atoms of every row. To do this one would use an “Armada” of 3×2 ancillas in the state $(|00\rangle + |11\rangle)(|00\rangle + |11\rangle)(|00\rangle + |11\rangle)$, which approaches the block from the left in Fig. 11.17 by moving the lattice horizontally. To measure the parities, the Armada is moved on top of the first two columns of the data block so that the atoms interact pairwise with atoms of the data block and acquire a phase shift of $e^{i\pi}$. To satisfy the criteria for fault tolerance, we need to avoid collisions while the ancillas are moved on top of the code, and thus need a “lift & shift” implementation of the operation, as mentioned earlier. Suppose there was a spin-flip in one of the atoms of the first row. Then the state of the ancillary atoms after the interaction reads $(-|00\rangle + |11\rangle)(|00\rangle + |11\rangle)(|00\rangle + |11\rangle)$, and the error will be detected by measuring the parity of the ancillas in each row, after applying a Hadamard transform. In a second run, the Armada is reset in the initial state and then is moved on top of the last two rows of the block, and so on. To detect a phase-flip, a similar procedure is used with an Armada of 2×3 atoms that approaches the block in Fig. 11.17 from *below* by moving the lattice vertically. Since these ancillas should measure any change of sign in any of the GHZ states that make up the codewords (11.40), they have to be

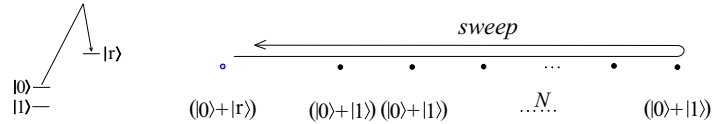


Fig. 11.18: Realization of an $(N + 1)$ -particle GHZ state by a single sweep operation.

prepared in the state $|000000\rangle + |111111\rangle$. A phase flip can then be detected as previously, where now a Hadamard transform has to be applied to the block first, before the “attack” starts from below. In the specific implementation using optical lattices, one could also think about other schemes using only a single row of ancilla atoms on each side of the data block in Fig. 11.17 as realized in Fig. 11.3b).

11.4.4 Selectivity and “sweep operations”

The examples discussed so far make use of the parallelism of the lattice shift to implement certain multi-particle entanglement (or gate) operations efficiently. On the other hand, the shift operation as described in Fig. 11.12(a) is too rigid, when certain operations should apply to a selected group of atoms only. This problem can in principle be solved by using a third atomic level $|r\rangle$ as indicated in Fig. 11.12(b). In this scheme, the level $|r\rangle$ couples dominantly to a transport lattice [99], while the “logical states” $|0\rangle$ and $|1\rangle$ are kept in the same potential. At the beginning of an entanglement operation, the atoms are first excited from one of the states $|0\rangle$ or $|1\rangle$ to the state $|r\rangle$, before the lattice is moved. This scheme is much more selective in the sense that those atoms which shall participate in a gate operation are first activated, before they can participate in the lattice movement. All operations that we have discussed can then be realized in the same manner, with the additional property that only those atoms, to which the operation $|1\rangle \rightarrow |r\rangle$ is applied, will participate. With this additional feature, it is clear, that *universal computations* can be implemented.

Another merit of this scheme is that one can realize more flexible entanglement operations. Consider, for example, a 1-dimensional situation as in Fig. 11.18 with a string of N atoms initially prepared in the product state $(|0\rangle + |1\rangle)^{\otimes N}$ and a selected additional atom (left) in the state $(|0\rangle + |r\rangle)$. By moving the transport lattice, the selected atom is swept across the N lattice sites. During that motion, it interacts with each of the N atoms thereby transforming the state of each atom into $e^{i\phi^0}|0\rangle + e^{i\phi^1}|1\rangle$, with a differential phase $\phi = \phi^1 - \phi^0$. The resulting total state is of the form

$$|0\rangle(|0\rangle + |1\rangle)(|0\rangle + |1\rangle) \cdots (|0\rangle + |1\rangle)$$

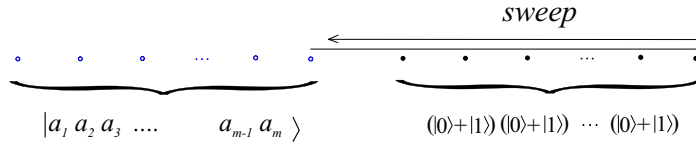


Fig. 11.19: Implementation of the quantum Fourier transform by a sweep operation with variable speed.

$$+|r\rangle e^{iN\phi^0} (|0\rangle + e^{i\phi}|1\rangle)(|0\rangle + e^{i\phi}|1\rangle) \cdots (|0\rangle + e^{i\phi}|1\rangle). \quad (11.42)$$

As long as the collisional phases are different ($\phi \neq 0$) for the two logical states, ϕ can be varied with the speed of this sweep operation. For $\phi = \pi$ one obtains a $N + 1$ -particle GHZ state (see Fig. 11.18) which can easily be brought to the standard form

$$|\psi\rangle = \frac{1}{\sqrt{2}} (|0\rangle|0\rangle|0\rangle \cdots |0\rangle + |1\rangle|1\rangle|1\rangle \cdots |1\rangle). \quad (11.43)$$

Note that for the creation of this state only a single sweep operation is required!

This scheme can be generalized in several directions. By varying the speed by which the lattice is moved during the sweep operation, the phases can be controlled individually for each atom of the string as indicated in Fig. 11.12, allowing for more complex entanglement operations. As a final example consider a configuration as in Fig. 11.19(b), with a “source register” consisting of a string of m atoms in the state $|a\rangle = |a_1 a_2 a_3 \cdots a_m\rangle$, $a_j \in \{0, 1\}$ and a “target register” of m further atoms in the state $(|0\rangle + |1\rangle)^{\otimes m}$, similar as in Fig. 11.18. The state vector $|a\rangle = |a_1 a_2 a_3 \cdots a_m\rangle$ should be interpreted as a binary representation of the number $a = a_1 2^{m-1} + a_2 2^{m-2} + \dots + a_m 2^0$. Consider now the following operation where the source register is first activated to couple to the transport lattice, meaning that each of the atoms 1 to m that is in state $|1\rangle$ is excited to state $|r\rangle$. Next, the lattice is moved to the right so that atoms of the source and the target register interact; this motion continues with variable speed until the source register completely overlaps with the target register. It is helpful to mentally decompose this operation into discrete steps. In the first step, the transport lattice is shifted one lattice site to the right such that the m th atom of the source register interacts with the first atom of the target register. One can tune the interaction time such that a certain phase shift is acquired during this interaction, namely $\phi = 2\pi/2^m$. In the next step, the transport lattice is moved one lattice site further to the right such that now the m th atom of the source register interacts with the *second* atom of the target register, while at the same time the $m - 1$ th atom of the source register interacts with the first atom of the target register. In this step, the interaction time is made double as long as in the first step, so

that $\phi = 2\pi/2^{m-1}$, and so on. After the lattice has been moved across m sites in this vein, the total state of the source and the target register is given by

$$\begin{aligned} |a_1 a_2 a_3 \cdots a_m\rangle \otimes (|0\rangle + e^{2\pi i 0.a_1 a_2 \dots a_m} |1\rangle) \\ (|0\rangle + e^{2\pi i 0.a_2 \dots a_m} |1\rangle) \\ \cdots (|0\rangle + e^{2\pi i 0.a_m} |1\rangle). \end{aligned} \quad (11.44)$$

Finally, the lattice is shifted back to the original position without changing the phases any more (modulo 2π , see earlier remark, or the process can be made symmetric such that only half the phase values are accumulated during the motion to the right while the second halves of the phase values are accumulated when the lattice is brought back to its original position.) The overall effect of this sweep operation can be summarized in the form

$$|a\rangle | \rangle \longrightarrow e^{i\Phi(a)} |a\rangle |\mathcal{F}(a)\rangle \quad (11.45)$$

wherein $|a\rangle$ and $| \rangle$ denote the initial state of the source and the target register, and $|\mathcal{F}(a)\rangle = \frac{1}{\sqrt{2^m}} \sum_{y=0}^{2^m-1} e^{2\pi i a y / 2^m} |y\rangle$ is the quantum Fourier transform of $|a\rangle$ [103]. The additional phase factor $e^{i\Phi(a)}$ accounts for a possible phase shift arising from collisions among different atoms of the source, if no vertical displacement of the transport lattice is possible.

As described, this method gives a very immediate way of implementing the quantum Fourier transform. Note that for a superposition of different input states the source and the target register become entangled. To apply the method in the Shor algorithm [104, 105], for example, additional steps have to be taken. A detailed discussion of this method, together with possible applications, will be presented somewhere else [106]. This final example demonstrates a remarkable flexibility of the entanglement operations that are possible in optical lattices and similar systems, offering new perspectives for efficient implementations of quantum algorithms.

11.5 Final remarks

It is clear that, at the present time, most of the experimental requirements have yet to be realized, before one can implement quantum computing. There are, however, recent achievements in cooling and trapping of atoms in optical lattices and in magnetic microtraps which make it seem possible that some of these elements could be implemented in the laboratory in the near future. There are short-term and long-term perspectives. Essential for all quantum information experiments is a successful *cooling* of the atoms to the ground state of a three dimensional lattice. Numerical calculations [31] using realistic parameters give $kT < 0.2\hbar\omega$ as a critical value. Under these circumstances,

one could perform interesting Ramsey-type spectroscopic studies of the fidelity of multi-particle entanglement as discussed earlier. To do this, neither single-atom addressability is required nor are regular filling structures. When the latter requirements can be realized, on the other hand, coding experiments can be done and a quantum memory be implemented. Finally, if one can find three-level schemes with different scattering phases for the logical states, universal computations can be performed. The parallelism of the lattice could then be exploited for efficient implementations of fault-tolerant quantum computing.

We have discussed multi-particle entanglement schemes mainly in the context of optical lattice implementations. Some of these ideas could readily be adopted in implementations with magnetic microtraps if one uses adiabatic schemes. A basic requirement for this is the possibility of creating quantum dots that are spatially sufficiently close to each other. These ideas will be discussed somewhere else [89].

Acknowledgments

We thank E. Hinds, J. Schmiedmayer, M. Weitz and T. W. Hänsch for many useful discussions. We also thank David DiVincenzo and Andrew Steane for helpful discussions on fault-tolerant quantum computing during the Benasque Workshop 1998. H.-J.B. likes to thank Manny Knill for a helpful discussion on the problem of concatenated coding. One of us (T. C.) thanks M. Traini and S. Stringari for the kind hospitality at the Physics Department of Trento University, and the ECT* for partial support during the completion of this work. This work was supported in part by the Österreichischer Fonds zur Förderung der wissenschaftlichen Forschung, the European Community under the TMR network ERB-FMRX-CT96-0087, the Institute for Quantum Information GmbH, and by the Schwerpunktsprogramm “Quanten-Informationsverarbeitung” der Deutschen Forschungsgemeinschaft.

11.A One particle in a moving harmonic potential

11.A.1 Hamiltonian

The center of the potential with frequencies ω_x , ω_y and ω_z is assumed to be given by $\bar{\mathbf{x}}(t) = (\bar{x}(t), 0, 0)$ and the Hamiltonian reads

$$H = H_x + H_y + H_z, \quad (11.46)$$

where $H_z = \hbar\omega_z(a_z^\dagger a_z + 1/2)$, $H_y = \hbar\omega_y(a_y^\dagger a_y + 1/2)$, and

$$H_x = \hbar\omega_x \left(a_x^\dagger a_x + \frac{1}{2} + (a_x^\dagger + a_x) \frac{\bar{x}(t)}{\sqrt{2}} + \frac{\bar{x}(t)^2}{2} \right). \quad (11.47)$$

The a 's are bosonic destruction operators and $\bar{x}(t)$ is given in harmonic oscillator units. We will concentrate on the x -direction leave out the subscript x and normalize energies to $\hbar\omega$.

11.A.2 Exact solution

The Schrödinger equation for the Hamiltonian Eq. 11.47 can be solved exactly [107, 73]. To do so we define

$$H_0 = a^\dagger a + \frac{1}{2}, \quad (11.48)$$

$$K(t, -\tau) = \frac{1}{\sqrt{2}} \int_{-\tau}^t ds \bar{x}(s) e^{i(s+\tau)} \quad (11.49)$$

and

$$\beta(t, -\tau) = i \int_{-\tau}^t ds \left(K(s, -\tau) \{ \partial_s K^*(s, -\tau) \} + \frac{i\bar{x}(s)^2}{2} \right). \quad (11.50)$$

If initially at time $-\tau$ the system is in the state $|\Psi(-\tau)\rangle = |0\rangle$, where $|n\rangle$ is the n -th harmonic oscillator eigenstate we get

$$|\Psi(t)\rangle = e^{i\Re\{\beta(t, -\tau)\}} \sum_n \frac{(-iK(t, -\tau)e^{-i(t+\tau)})^n}{\sqrt{n!}} |n\rangle. \quad (11.51)$$

The kinetic phase ϕ is thus given by the phase of the overlap of $|\Psi(t)\rangle$ with the instantaneous ground state $D(\bar{\mathbf{x}}(t))|0\rangle$, where $D(\gamma) = \exp(\gamma a^\dagger - \gamma^* a)$ denotes the displacement operator

$$\phi = -\arg \left(\langle 0 | D(\bar{\mathbf{x}}(t))^\dagger | \Psi(t) \rangle \right). \quad (11.52)$$

The interaction phase can be found by Eq. (11.7) with the known $|\Psi(t)\rangle$.

11.A.3 Corrections to the adiabatic approximation

We assume $\bar{x}(t)$ to be an analytic function of t and that $\bar{x}(t) \gg \partial_t \bar{x}(t) \gg \partial_t^2 \bar{x}(t) \gg \dots \gg \partial_t^n \bar{x}(t)$. By expanding in orders of the time derivatives we can write for $K(t', -\tau)$

$$K(t', -\tau) = \frac{1}{\sqrt{2}} \left(i^{N+1} \int_{-\tau}^{t'} ds \{ \partial_s^{N+1} \bar{x}(s) \} e^{i(s+\tau)} - \sum_{n=0}^N i^{n+1} \{ \partial_s^n \bar{x}(s) \} e^{i(s+\tau)} \Big|_{s=-\tau}^{s=t'} \right), \quad (11.53)$$

where N is a positive integer. Note that if we may neglect all terms of order greater than $\partial_t \bar{x}(t)$ and start in a coherent state $|\Psi(-\tau)\rangle = D(\bar{x}(-\tau) + i\partial_t \bar{x}(t)|_{t=-\tau})|0\rangle$ the state will always be a coherent state with $\langle x(t)\rangle = \bar{x}(t)$ and $\langle p(t)\rangle = \partial_t \bar{x}(t)$.

Now we assume for simplicity that $\bar{x}(\tau) = \bar{x}(-\tau) = 0$, $(\partial_t \bar{x}(t))|_{t=-\tau} = (\partial_t \bar{x}(t))|_{t=\tau} = 0$ and $(\partial_t^n \bar{x}(t))|_{t=-\tau} = (-1)^n (\partial_t^n \bar{x}(t))|_{t=\tau}$ for $n > 1$. The system is assumed to be in the state $|\Psi(-\tau)\rangle = |0\rangle$, initially. We keep all the terms to fourth order in the derivatives (in the integrand) and find

$$K(t, -\tau) = \frac{1}{\sqrt{2}} \left(\{i(\partial_t^2 - \partial_t^4)\bar{x}(t)\} (e^{i(t+\tau)} - 1) - \{\partial_t^3 \bar{x}(t)\} (e^{i(t+\tau)} + 1) \right), \quad (11.54)$$

and

$$\beta(t, -\tau) = \frac{1}{2} \int_{-\tau}^t ds \left(\{\partial_s \bar{x}(s)\}^2 + \{\partial_s^2 \bar{x}(s)\}^2 \right) + \frac{1}{2} \{\partial_t^2 \bar{x}(t)\}^2 (1 - e^{-i(t+\tau)}). \quad (11.55)$$

If we choose $(t + \tau) = 2n\pi$ with integer n the largest correction to the approximation to the kinetic phase discussed in Sec. 11.2.2.1 is of third order. Also the amplitude of the first excited state is of third order as can be seen from Eq. (11.54).

11.B Quantum error correction and the implementation of Shor's code

Consider a one-dimensional configuration with a string of n atoms, where $x_0, x_1, x_2, \dots, x_n \in \{0, 1\}$ label the internal state of the atoms at position $0, 1, 2, \dots, n$ of the lattice. An elementary lattice-shift operation as given in Fig. 11.12(a) is then described as

$$LX : \quad |x_0, x_1, x_2, \dots, x_n\rangle \mapsto e^{-i \sum_j (x_{j+1} \bmod 2) x_{j+1} \varphi_{j+1}} |x_0, x_1, x_2, \dots, x_n\rangle \quad (11.56)$$

where the phase φ_{j+1} in the exponent depends on the interaction time and the interaction strength between two atoms at the lattice site $j + 1$, and the addition is performed modulo 2. Note that two neighboring atoms at the sites j and $j + 1$ contribute to the exponent if and only if $x_j = 0$ and $x_{j+1} = 1$. The variables x_j can only take on the values 0 and 1. In all examples we discuss here, $\varphi_j = \varphi = \text{constant}$ and is the same for all lattice sites.

The operation (11.56) defines a generalized phase gate that acts on a group of n neighboring atoms via shifting the lattice across one lattice site. It can easily be seen that, for example when combined with $\pi/2$ -pulses as in Fig. 11.10, LX produces the entangled states (11.37) and (11.38) for $n = 2$ and $n = 3$.

In two dimensional lattices, the logical variables x_{kl} are labeled by two indices, where k is the horizontal index and l the vertical index. The phase gates corresponding to horizontal and vertical lattice shifts are then defined as

$$\begin{aligned} LX|\{x_{kl}\}\rangle &= e^{-i\sum_j(x_{jl}+1 \bmod 2)x_{j+1,l}\varphi_{j+1,l}}|\{x_{kl}\}\rangle \\ LY|\{x_{kl}\}\rangle &= e^{-i\sum_j(x_{kj}+1 \bmod 2)x_{k,j+1}\varphi_{k,j+1}}|\{x_{kl}\}\rangle \end{aligned} \quad (11.57)$$

as an obvious generalization of (11.56).

It is clear that the operations can be further generalized to lattice shifts across an arbitrary number of lattice sites and along arbitrary directions. There are interesting topological questions in this general situation. For the present discussion, however, the gates LX, LY as defined in (11.57) are sufficient and we will set $\varphi_{k,l} = \pi$. Apart from these gates, we will only need single-particle operations, in particular the Pauli-operators $\sigma_{x,j}, \sigma_{y,j}, \sigma_{z,j}$ and the Hadamard transformation ($\pi/2$ pulse) $H_j = (\sigma_{z,j} + \sigma_{x,j})/\sqrt{2}$ applied to an atom with index j .

Consider now a configuration of 3×3 atoms as in Fig. 11.13, where the central atom is in the unknown state $|\psi\rangle = \alpha|0\rangle + \beta|1\rangle$ while all surrounding atoms are initially in the state $|0\rangle$. Let us first look at the special case when $|\psi\rangle = |0\rangle$, that is, the central atom is in the state $|0\rangle$ as well. If we apply a $\pi/2$ pulse to each atom of the block and then the operation LX, we obtain a tensor product of three GHZ states where each row of the block is in the same state $(0+1)0(0-1) - (0-1)1(0+1)$. (For notational brevity, we suppress the bracket notation in the following and identify $0 \equiv |0\rangle$ and $1 \equiv |1\rangle$). This state can be transformed to the form $000 - 111$ by applying H_1 to the first atom and $H_3\sigma_{z,3}$ to the third atom of each row. The operation LX, supplemented by one-qubit rotations, produces thus one of the code words in (11.40).

To realize a quantum memory, an *unknown* state $\psi = \alpha 0 + \beta 1$ of the central atom is to be encoded into an entangled 9-bit state as in (11.41). Let us write the initial (unencoded) state of the block in the form

$$|\text{bare}\rangle = 0_1 0_2 0_3 0_4 (\alpha 0_5 + \beta 1_5) 0_6 0_7 0_8 0_9 \quad (11.58)$$

where the first, second, and third triplet refers to the upper, center, and lower row of the block in Fig. 11.13. To encode ψ into a corresponding superposition of both codewords, lattice movements in both horizontal and in vertical direction are required. In detail, the *encoding operation* is given by

$$ENC = H_{46} \circ LX \circ H_{456} \circ LY \circ \sigma_{x;369} H_{134679} \circ LX \circ H^s \quad (11.59)$$

whose essential part is a sequence of three lattice movements, **horizontal - vertical - horizontal**, with certain 1-bit unitary transformations in between. In the notation used here, H^s denotes a Hadamard transform applied to each of the 8 syndrome atoms, whereas $H_{ijk\dots}$ and $\sigma_{z;ijk\dots}$ are single-qubit rotations applied to the selected atoms i, j, k, \dots , only. Applied to the state (11.58), *ENC* produces

$$\begin{aligned} ENC |\text{bare}\rangle &= \alpha(000 - 111)(001 - 110)(000 + 111) \\ &\quad \beta(000 + 111)(100 + 011)(000 - 111) \\ &\equiv \alpha 0_L + \beta 1_L. \end{aligned} \tag{11.60}$$

The codewords 0_L and 1_L are equivalent to the Shor code (11.40), as we shall see presently.

The *decoding operation* is given by the inverse of (11.59),

$$DEC = H^s \circ LX \circ H_{134679} \sigma_{x;369} \circ LY \circ H_{456} \circ LX \circ H_{46} \tag{11.61}$$

involving the same lattice movements, but the 1-bit operations carried out in reverse order. To see explicitly how one can correct an error occurring on one of the qubits $j = 1, 2, \dots, 9$, we apply the error operators $\sigma_{x,j}$, $\sigma_{y,j}$, or $\sigma_{z,j}$ to the encoded state $\alpha 0_L + \beta 1_L$. Then we apply the decoding operation *DEC* and measure the state of the syndrome atoms. The code 0_L and 1_L is error correcting if every possible error is mapped into a syndrome state different from $0_1 0_2 0_3 \ 0_4 0_6 \ 0_7 0_8 0_9$, and for each syndrome we can tell which unitary transformation has to be applied to the central qubit to restore it to its original state [it is not necessary that all errors are mapped to mutually orthogonal subspaces [47]]. The following table gives for each error the corresponding syndrome and the state of the central qubit:

error	syndrome	central qubit
none	000 00 000	$\alpha 0 + \beta 1$
$\sigma_{x,1}$	110 00 000	$\alpha 0 - \beta 1$
$\sigma_{x,2}$	101 00 000	$\alpha 0 - \beta 1$
$\sigma_{x,3}$	011 00 000	$\alpha 0 - \beta 1$
$\sigma_{x,4}$	010 10 010	$\alpha 0 + \beta 1$
$\sigma_{x,5}$	000 11 000	$\alpha 0 - \beta 1$
$\sigma_{x,6}$	010 01 010	$\alpha 0 + \beta 1$
$\sigma_{x,7}$	000 00 110	$\alpha 0 - \beta 1$
$\sigma_{x,8}$	000 00 101	$\alpha 0 - \beta 1$
$\sigma_{x,9}$	000 00 011	$\alpha 0 - \beta 1$
$\sigma_{y,1}$	100 00 000	$\alpha 0 - \beta 1$
$\sigma_{y,2}$	111 00 000	$\alpha 0 - \beta 1$
$\sigma_{y,3}$	001 00 000	$\alpha 0 - \beta 1$
$\sigma_{y,4}$	000 01 000	$\alpha 1 - \beta 0$
$\sigma_{y,5}$	010 00 010	$\alpha 1 - \beta 0$
$\sigma_{y,6}$	000 10 000	$\alpha 1 - \beta 0$
$\sigma_{y,7}$	000 00 100	$\alpha 0 - \beta 1$
$\sigma_{y,8}$	000 00 111	$\alpha 0 - \beta 1$
$\sigma_{y,9}$	000 00 001	$\alpha 0 - \beta 1$
$\sigma_{z,1}$	010 00 000	$\alpha 0 + \beta 1$
$\sigma_{z,2}$	010 00 000	$\alpha 0 + \beta 1$
$\sigma_{z,3}$	010 00 000	$\alpha 0 + \beta 1$
$\sigma_{z,4}$	010 11 010	$\alpha 1 - \beta 0$
$\sigma_{z,5}$	010 11 010	$\alpha 1 + \beta 0$
$\sigma_{z,6}$	010 11 010	$\alpha 1 - \beta 0$
$\sigma_{z,7}$	000 00 010	$\alpha 0 + \beta 1$
$\sigma_{z,8}$	000 00 010	$\alpha 0 + \beta 1$
$\sigma_{z,9}$	000 00 010	$\alpha 0 + \beta 1$

In Fig. 11.13, the syndrome atoms visually encircle the unknown qubit that is to be protected. If any of the 9 qubit suffers a spin flip, a phase flip, or both, the error can be detected by measuring the state of the syndrome atoms

after the decoding operation has been applied to the group. This could be done by a fluorescence measurement where atoms in state 1 and 0 correspond to “bright” and “dark”, respectively. For example, according to above table, the pattern

$$\begin{array}{ccc} 0 & 0 & 0 \\ 1 & \psi' & 1 \\ 0 & 0 & 0 \end{array}$$

tells us that a spin flip has occurred in the central atom, whereas

$$\begin{array}{ccc} 0 & 0 & 0 \\ 0 & \psi' & 0 \\ 1 & 1 & 0 \end{array}$$

reveals a spin flip in the left atom of the lower row, and

$$\begin{array}{ccc} 0 & 1 & 0 \\ 1 & \psi' & 1 \\ 0 & 1 & 0 \end{array}$$

corresponds to a phase flip in any of the atoms of the central row. In any case, the state ψ' of the central qubit after the detection of an error is related to the initial state ψ via a (known) unitary operation U : $\psi' = U\psi$, which can be obtained from the third column of the syndrome table given above.

The fact that the encoding operation involves only 3 lattice movements provides a specific example of a “parallelization of a quantum circuit” [43, 44]. We have not proven that 3 is really the minimum number of entanglement operations needed; there might be still faster sequences. The original Shor code can be recovered from this code by applying an additional vertical lattice shift, LY, and certain 1-bit rotations.

References

- [1] CIRAC, J. I., and ZOLLER, P., 1995, *Phys. Rev. Lett.* **74**, 4091.
- [2] MONROE, C., MEEKHOF, D. M., KING, B. E., ITANO, W. M., and WINELAND, D. J., 1995 *Phys. Rev. Lett.* **75**, 4714.
- [3] TURCHETTE, Q. A., WOOD, C. S., KING, B. E., MYATT, C. J., LEIBFRIED, D., ITANO, W. M., MONROE, C., and WINELAND, D. J., 1998, *Phys. Rev. Lett.* **81** 3631;
- [4] KING, B.E., MYATT, C.J., TURCHETTE, Q.A., LEIBFRIED, D., ITANO, W.M., MONROE, C., and WINELAND, D.J., 1998, *Phys. Rev. Lett.* **81** 1525;

- [5] MONROE, C., LEIBFRIED, D., KING, B.E., MEEKHOF, D.M., ITANO, W.M., and WINELAND, D.J., 1997, *Phys. Rev. A* **55**, R2489.
- [6] STEANE, A., 1997, *Appl. Phys. B* **64**, 623.
- [7] STEVENS, D., BROCHARD, J., and STEANE, A., 1998, *Phys. Rev. A* **64**, 623.
- [8] JAMES, D.F.V., GULLEY, M.S., HOLZSCHEITER, M.H., HUGHES, R.J., KWIAT, P.G., LAMOREAUX, S.K., PETERSON, C.G., SANDBERG, V.D., SCHAUER, M.M., SIMMONS, C.M., TUPA, D., WANG, P.Z., and WHITE, A.G., quant-ph/9807071.
- [9] TURCHETTE, Q. A., HOOD, C. J., LANGE, W., MABUCHI, H., and KIMBLE, H. J., 1995, *Phys. Rev. Lett.* **75**, 4710.
- [10] MAÎTRE, X., HAGLEY, E., NOGUES, G., WUNDERLICH C., GOY, P., BRUNE, M., RAIMOND, J. M., and HAROCHE, S., 1997, *Phys. Rev. Lett.* **79**, 769.
- [11] HAGLEY, E., MATRE, X., NOGUES, G., WUNDERLICH, C., BRUNE, M., RAIMOND, J. M., and S. HAROCHE, S., 1997, *Phys. Rev. Lett.* **79**, 1.
- [12] PELLIZZARI, T., GARDINER, S.A., CIRAC, J.I., and ZOLLER, P., 1995, *Phys. Rev. Lett.* **75**, 3788.
- [13] CIRAC, J. I., ZOLLER, P., MABUCHI, H., and KIMBLE, H. J., 1997, *Phys. Rev. Lett.* **78**, 3221.
- [14] VAN ENK, S. J., CIRAC, J. I., and ZOLLER, P., 1998, *Science* **279**, 205.
- [15] LAW, C.K. and KIMBLE, H.J., 1997 *J. Mod. Opt.* **44**, 2067.
- [16] GHERI, K.M. SAAVEDRA, C., TÖRMÄ, P., CIRAC, J.I., and ZOLLER, P., 1998, *Phys. Rev. A* **58**, R2627.
- [17] ASPECT, A., GRANGIER, P., and ROGER, G., 1981, *Phys. Rev. Lett.* **47**, 460.
- [18] ASPECT, A., GRANGIER, P., and ROGER, G., 1982, *Phys. Rev. Lett.* **49**, 91.
- [19] ASPECT, A., DALIBARD, A., and ROGER, G., 1982, *Phys. Rev. Lett.* **49**, 1804.
- [20] KWIAT, P.G., MATTLE, K., WEINFURTER, H., ZEILINGER, A., SERGIENKO, A.V., and SHIH, Y.H., 1995, *Phys. Rev. Lett.* **75**, 4337; BRENDDEL, J., GISIN, N., TITTEL, W., and ZBINDEN, H., quant-ph/9809034; KWIAT, P.G., WAKS, E., WHITE, A.G., APPELBAUM, I., and EBERHARD, P.H., quant-ph/9810003; CABRILLO, C. CIRAC, J.I. GARCIA-FERNANDEZ, P., and ZOLLER, P., 1999, *Phys. Rev. A* **59**, 1025.

- [21] BOUWMEESTER, D., PAN, J. I., MATTLE, K., EIBL, M., WEINFURTER, H., and ZEILINGER, A., 1997, *Nature* **390**, 575.
- [22] BOSCHI, D., BRANCA, S., DE MARTINI, F., HARDY, L., and POPESCU, S., 1998, *Phys. Rev. Lett.* **80**, 1121.
- [23] FURUSAWA, A., SORENSEN, J. L., BRAUNSTEIN, S. L., FUCHS, C. A., KIMBLE, H. J., and POLZIK, E. S., 1998, *Science* **282**, 706.
- [24] PAN, J. W., BOUWMEESTER, D., WEINFURTER, H., and ZEILINGER, A., 1998, *Phys. Rev. Lett.* **80**, 3891.
- [25] BOUWMEESTER, D., PAN, J.-W., DANIELL, M., WEINFURTER, H., and ZEILINGER, A., 1999, *Phys. Rev. Lett.* **82**, 1345.
- [26] CORY, D. G., FAHMY, A. F., and HAVEL, T. F., 1997, *Proc. Natl. Acad. Sci. USA* **94**, 1634.
- [27] GERSHENFELD, N. A., and CHUANG, I. L., 1997, *Science* **275**, 350.
- [28] CORY, D. G., MASS, W., PRICE, M., KNILL, E., LAFLAMME, R., ZUREK, W. H., HAVEL, T. F., and SOMAROO, S. S., 1998, *Phys. Rev. Lett.* **81**, 2152.
- [29] JONES, J. A., MOSCA, M., and HANSEN, R. H., 1998, *Nature*, **393**, 344.
- [30] BRAUNSTEIN, S.L., CAVES, C.M., JOZSA, R., LINDEN, N., POPESCU, S., and SCHACK R., quant-ph/9811018.
- [31] JAKSCH, D., BRIEGEL, H.-J., CIRAC, J. I., GARDINER, C. W., and ZOLLER, P., 1999, *Phys. Rev. Lett.* **82**, 1975.
- [32] *Laser manipulation of Atoms and Ions*, 1992, edited by E. ARIMONDO, W. D. PHILLIPS, and F. STRUMIA, (North Holland, Amsterdam); see also *Special issue on Laser cooling and trapping of atoms*, JOSA B **6** No. 11 (1989); *ibid.* **2** No. 11 (1985).
- [33] CHU, S., 1998, *Rev. Mod. Phys.* **70**, 686.
- [34] COHEN-TANNOUJJI, C., 1998, *Rev. Mod. Phys.* **70**, 707.
- [35] PHILLIPS, W. D., 1998, *Rev. Mod. Phys.* **70**, 721.
- [36] ANDERSON, M. H., ENSHER, J. R., MATTHEWS, M. R., WIEMAN, C. E., and CORNELL, E. A., 1995, *Science*, **269**, 198.
- [37] BRADLEY, C. C., SACKETT, C. A., TOLLETT, J. J., and HULET, R. G., 1995, *Phys. Rev. Lett.* **75**, 1687.
- [38] DAVIES, K. B., MEWES, M.-O., ANDREWS, M. R., VAN DRUTEN, N. J., DURFEE, D. S., KURN, D. M. and KETTERLE, W., 1995, *Phys. Rev. Lett.* **75**, 3969.
- [39] HALL, D. S., MATTHEWS, M. R., WIEMAN, C. E., and CORNELL, E. A., 1998, *Phys. Rev. Lett.* **81**, 1543; *ibid.* **81**, 4532.

- [40] HALL, D. S., MATTHEWS, M. R., ENSHER, J. R., WIEMAN, C. E., and CORNELL, E. A., 1998, *Phys. Rev. Lett.* **81**, 1539; *ibid.* **81**, 4531.
- [41] STAMPER-KURN, D. M., ANDREWS, M. R., CHIKKATUR, A. P., INOUE, S., MIESNER, H.-J., STENGER, J., and KETTERLE, W., 1998, *Phys. Rev. Lett.* **80**, 2027.
- [42] BRENNEN, G.K., CAVES, C.M., JESSEN, P.S., and DEUTSCH, I.H., 1999, *Phys. Rev. Lett.* **82**, 1060.
- [43] MOORE, C., and NILSSON, M., 1998, Los Alamos preprint server quant-ph/9804034.
- [44] MOORE, C., and NILSSON, M., 1998, Los Alamos preprint server quant-ph/9808027.
- [45] FREEDMAN, M. H., and MEYER, D. A., Los Alamos preprint server quant-ph/9810055.
- [46] KITAEV, A. YU., and BRAVYI, S. B., Los Alamos preprint server quant-ph/9811052.
- [47] SHOR, P. W., 1995, *Phys. Rev. A* **52**, R2493.
- [48] STEANE, A. M., 1996, *Phys. Rev. Lett.* **77**, 793; *ibid.*, 1996, *Proc. Roy. Soc. Lond. A* **452**, 2551.
- [49] CALDERBANK, A. R., and SHOR, P. W., 1996, *Phys. Rev. A* **54**, 1098.
- [50] LAFLAMME, R., MIQUEL, C., PAZ, J.-P., and ZUREK, W. H., 1996 *Phys. Rev. Lett.* **77**, 198.
- [51] EKERT, A., and MACCHIAVELLO, C., 1996, *Phys. Rev. Lett.* **77**, 2585.
- [52] BENNETT, C. H., DIVINCENZO, D. P., SMOLIN, J. A., and WOOTTERS, W. K., 1996, *Phys. Rev. A* **54**, 3825.
- [53] KNILL, E., and LAFLAMME, R., 1997, *Phys. Rev. A* **55**, 900.
- [54] For a review on the subject of quantum error correction (and on quantum computing in general) see, for example, STEANE, A.M., 1998, *Rept. Prog. Phys.* **61**, 117-173.
- [55] SHOR, P. W., 1996, in *Proc. 37th Symposium on the Foundations of Computer Science*, (IEEE Computer Society Press), p. 56; quant-ph/9605011.
- [56] STEANE, A. M., 1997, *Phys. Rev. Lett.* **78**, 2252.
- [57] KNILL, E., and LAFLAMME, R., 1996, quant-ph/9608012.
- [58] AHARONOV, D., and BEN-OR, M., 1996, quant-ph/9611025.
- [59] KITAEV, A. YU. 1997, *Russ. Math. Surv.* **52**, 1191; *ibid.*, quant-ph/9707021.
- [60] KNILL, E., LAFLAMME, R., and ZUREK, W., 1997, *Science* **279**, 342.

- [61] GOTTESMAN, D., 1998, *Phys. Rev. A* **57**, 127.
- [62] For a review on the subject of fault-tolerant computing and for further references see, for example, PRESKILL, J., 1997, quant-ph/9705031.
- [63] HAMANN, S.E., HAYCOCK, D.L., KLOSE, G., PAX, P.H., DEUTSCH, I.H., and JESSEN, P.S., 1998, *Physical Review Letters* **80** 4149.
- [64] MENNERAT-ROBILLIARD, C., LUCAS, D., GUIBAL, S., TABOSA, J., JURCZAK, C., COURTOIS, J.-Y., and GRYNBERG, G., 1999, *Physical Review Letters* **82** 851.
- [65] DEPUE, M. T. , MCCORMICK, C. , WINOTO, S.L. , OLIVER, S. and WEISS, D.W., 1999, *Physical Review Letters* **82** 2262.
- [66] FRIEBEL, S., D'ANDREA, C., WALZ, J., WEITZ, M., and HÄNSCH, T.W., 1998, *Phys. Rev. A* **57**, R20.
- [67] HINDS, E. A., BOSHIER, M. G., and HUGHES, I. G., 1998, *Phys. Rev. Lett.* **80**, 645.
- [68] WEINSTEIN, J.D., and LIBBRECHT, K.G., 1995, *Phys. Rev. A* **52**, 4004.
- [69] VULETIC, V., HÄNSCH, T. W., and ZIMMERMANN, C., 1996, *Europhys. Lett.* **36**, 349.
- [70] VULETIC, V., FISCHER, T., PRAEGER, M., HÄNSCH, T. W., and ZIMMERMANN, C., 1998, *Phys. Rev. Lett.* **80**, 1634.
- [71] DENSCHLAG, J., UMSHAUS, G., and SCHMIEDMAYER, J., 1998, *Phys. Rev. Lett.* **81**, 737; SCHMIEDMAYER, J., 1995, *Phys. Rev. A* **52**, R13.
- [72] The justification parallels the arguments presented in the context of the pseudo-potential approximation in BEC see, e.g., H. T. C. STOOFF, M. BIJLSMA, and M. HOUBIERS, *J. Res. Natl. Inst. Stand. Technol.* **101**, 443 (1996).
- [73] see, e.g., GALINDO, A., PASCUAL, P., *Quantum Mechanics II* (Springer Berlin 1991).
- [74] KAGAN, YU., SURKOV, E.L., and SHLYAPNIKOV, G.V., 1996, *Phys. Rev. A* **54**, R1753.
- [75] JAKSCH, D., BRUDER, C., CIRAC, J. I., GARDINER, C. W., and ZOLLER, P., 1998 *Phys. Rev. Lett.* **81**, 3108.
- [76] FISHER, M.P.A., WEICHMAN, P.B., GRINSTEIN, G., and FISHER, D.S., 1989, *Phys. Rev. B* **40**, 546.
- [77] BRUDER, C., FAZIO, R., and SCHÖN, G., 1993, *Phys. Rev. B* **47**, 342.
- [78] KRAUTH, W., CAFFAREL, M., and BOUCHARD, J.-P., 1992, *Phys. Rev. B* **45**, 3137.

- [79] SHESHADRI, K., KRISHNAMURTHY, H.R., PANDIT, R., and RAMAKRISHNAN, T. V., 1993, *Europhys. Lett.* **22**, 257.
- [80] FINKELSTEIN, V., BERMAN, P.R., and GUO, J., 1992, *Phys. Rev. A*, **45**, 1829.
- [81] WEINER, J., BAGNATO, V.S., ZILIO, S., and JULIENNE, P.S., 1999, *Rev. Mod. Phys.* **71**, 1.
- [82] TIESINGA, E., VERHAAR, B.J., and STOOF, H.T.C., 1993, *Phys. Rev. A*, **47**, 4114.
- [83] SCHUMACHER, B., 1996, *Phys. Rev. A* **54**, 2614.
- [84] ROACH, T.M., ABELE, H., BOSCHER, M.G., GROSSMAN, H.L., ZETIE, K.P., and HINDS, E.A., 1995, *Phys. Rev. Lett.* **75**, 629.
- [85] HINDS, E.A., BOSCHER, M.G., and HUGHES, I.G., 1998. *Phys. Rev. Lett.* **80**, 645;
- [86] HINDS, E.A., 1999, to appear in *Proc. R. Soc. London*.
- [87] SCHMIEDMAYER, J., 1998, *Eur. Phys. J. D* **4**, 57.
- [88] OVCHINNIKOV, YU.B., MANEK, I., and GRIMM, R., 1997, *Phys. Rev. Lett.* **79**, 2225.
- [89] CALARCO, T. *et al.*, unpublished.
- [90] GREENBERGER, D. M., HORNE, M., and ZEILINGER, A., 1989, in *Bell's Theorem, Quantum Theory, and Conceptions of the Universe*, M. Kafatos, editor, Kluwer, Dordrecht, The Netherlands, p. 69.
- [91] BARENCO, A., BENNETT, C.H., CLEVE, R., DIVINCENZO, D.P., MARGOLUS, N., SHOR, P., SLEATOR, T., SMOLIN, J.A., and WEINFURTER, H., 1995, *Phys. Rev. A* **52**, 3457; and references cited therein.
- [92] DEUTSCH, D., BARENCO, A., and EKERT, A., 1995, quant-ph/9505018.
- [93] BENNETT, C. H., 1995, *Phys. Today* **48**, 24.
- [94] DIVINCENZO, D. P., 1995, *Phys. Rev. A* **51**, 1015.
- [95] N. F. Ramsey, *Rev. Mod. Phys.* **62**, 541 (1990).
- [96] BELL, J.S., 1964, *Physics* **1**, 195.
- [97] For small filling factors, the signals coming from different groups of atoms could even be spatially resolved.
- [98] Other proposals for selectively filling optical lattice sites exist (Martin Weitz, private communication), using infrared superlattices to load the (logical) lattice with a certain, well defined spacing between the atoms.
- [99] In ^{87}Rb and ^{23}Na one could use $|a\rangle \equiv |F = 1, m_F = -1\rangle$, $|b\rangle \equiv |F = 2, m_F = 2\rangle$ and $|c\rangle \equiv |F = 1, m_F = 1\rangle$.

- [100] Freedman and Meyer [45] have independently identified Shor's code as a two-dimensional topological quantum code (see also Kitaev's work [46, 59]). The connection between their results and our lattice implementation remains to be clarified.
- [101] Here we assume that one is able to selectively load a two-dimensional "sheet" in a three-dimensional lattice.
- [102] It remains the practical question, how well the polarization $\theta(t)$ can be controlled in the experiment.
- [103] CLEVE, R., EKERT, A., MACCHIAVELLO, C., and MOSCA, M., 1998, *Proc. Roy. Soc. Lond.* **454**, 339.
- [104] SHOR, P. W., 1995, quant-ph/9508027; *ibid.*, 1997, *SIAM J. Computing* **26**, 1484.
- [105] EKERT, A., and JOSZA, R., 1996, *Rev. Mod. Phys.* **68**, 733.
- [106] BRIEGEL, H.-J. *et al.*, unpublished.
- [107] GARDINER, C.W., *Quantum Noise* (Springer Berlin 1991)

Chapter 12

Moving optical lattices

In this chapter we discuss some of the details needed to obtain the results of the preceding publications (chapters 9 and 11). We concentrate on optical lattices and leave out details on magnetic microtraps. We also discuss some of the experiments suggested in chapter 9.

12.1 State selective optical potentials

In this section we want to investigate the interaction between three energy levels of an atom with a standing light wave. The results presented here are the starting point of the calculations in chapter 9 for an optical lattice that can be moved state selectively.

12.1.1 Optical potential for a three level atom

We consider the case of one internal ground state $|0\rangle$ and two excited states $|1\rangle$ and $|2\rangle$ of an atom interacting with a classical laser beam with frequency ω . Like in Sec. 7.1 we adiabatically eliminate the excited states of the atom and neglect spontaneous emission (cf. Sec. 7.1.2). We find a Schrödinger equation for the evolution of the wave function $|\Psi_0(t)\rangle$ of the particles in internal state $|0\rangle$ with the Hamiltonian given by

$$H = \frac{p^2}{2m} + V_0(x), \quad (12.1)$$

where the optical potential is $V_0(x) = V_0^{(1)}(x) + V_0^{(2)}(x)$ and

$$V_0^{(j)}(x) = -\frac{\Omega_j(x)^2}{4|\delta_j|}. \quad (12.2)$$

x and p are the coordinate and momentum operators respectively. The mass of the atom is m the detuning δ_1 (δ_2) between the atomic transition frequency

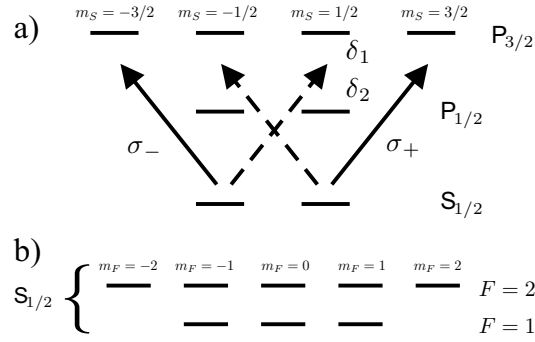


Fig. 12.1: Atomic level structure for e.g. ^{23}Na and ^{87}Rb . a) Fine structure and b) Hyperfine structure.

ω_{10} (ω_{20}) and the laser field is given by $\delta_1 = \omega_{10} - \omega$ ($\delta_2 = \omega_{20} - \omega$). We denote the Rabi frequency which is proportional to the electric field strength and the dynamic polarizability of the atom between states $|0\rangle$ and $|1\rangle$ ($|2\rangle$) by Ω_1 (Ω_2).

12.1.2 State selective optical potential

We shall now consider an atom with the level structure given in Fig. 12.1 interacting with σ_+ and σ_- polarized standing waves and detunings δ_1 and δ_2 from the excited levels as shown in Fig. 12.1. The laser beam σ_+ couples the level $S_{1/2}$ with $m_s = 1/2$ to the level $P_{3/2}$ with $m_s = 3/2$. This situation corresponds to the one described in Sec. 7.1 and thus yields an optical potential of the form Eq. (7.19). Furthermore the laser σ_+ couples the level $S_{1/2}$ with $m_s = -1/2$ with the levels $P_{3/2}$ with $m_s = 1/2$ and $P_{1/2}$ with $m_s = 1/2$. This situation corresponds to the one described in Sec. 12.1.1 and yields an optical potential of the form Eq. (12.2). In Fig. 12.2 we show the resulting level shift for the two ground states due to the interaction with the σ_+ polarized light. As can be seen from this figure it is possible to make the ac-stark shift equal to zero for the level $S_{1/2}$ with $m_s = -1/2$ by choosing the laser frequency correspondingly. The same holds for the interaction of the laser σ_- with the roles of the two ground state energy levels exchanged. It is thus possible to produce an optical lattice where the optical potential of the levels $S_{1/2}$ with $m_s = \pm 1/2$ is purely due to σ_{\pm} polarized light which we will assume in the following. We denote the optical potentials felt by the levels $S_{1/2}$ with $m_s = \pm 1/2$ due to the σ_{\pm} light as $V_{\pm}(x)$.

In Fig. 12.1b the hyperfine structure levels of the ground states $S_{1/2}$ with $m_s = \pm 1/2$ are shown. The level shift of these states is related to $V_{\pm}(x)$ by

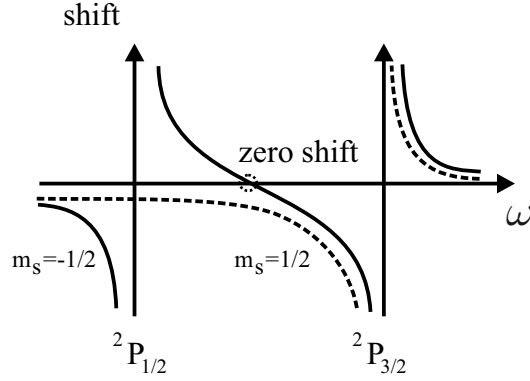


Fig. 12.2: Schematic ac-stark shift of the atomic levels $S_{1/2}$ with $m_s = 1/2$ (dashed curve) and with $m_s = -1/2$ (solid curve) due to the laser beam σ_+ as a function of the laser frequency ω . Note that the ac-stark shift of the level $S_{1/2}$ with $m_s = -1/2$ can be made 0 by choosing the laser frequency correspondingly.

the Clebsch–Gordan coefficients

$$\begin{aligned}
 V_{|F=2, m_F=2\rangle}(x) &= V_+(x), \\
 V_{|F=1, m_F=1\rangle}(x) &= \frac{3}{4}V_+(x) + \frac{1}{4}V_-(x), \quad \text{and} \\
 V_{|F=1, m_F=-1\rangle}(x) &= \frac{1}{4}V_+(x) + \frac{3}{4}V_-(x).
 \end{aligned} \tag{12.3}$$

These are the optical potentials for the three hyperfine levels we used in chapter 9.

12.1.3 Laser configuration

The two standing waves σ_{\pm} can be produced out of two running counter-propagating waves with the same intensity. The corresponding setup is shown in Fig. 12.3. Moreover it is possible to move nodes of the standing waves by changing the angle of the polarization between the two running waves. Let $\{e_x, e_y, e_z\}$ be three unit vectors in space pointing along the $\{x, y, z\}$ direction, respectively. The position dependent part of the electric field of the two running waves $\mathbf{E}_{1,2}$ is given by

$$\begin{aligned}
 \mathbf{E}_1 &\propto e^{ikx} (\cos(\varphi)e_z + \sin(\varphi)e_y), \\
 \mathbf{E}_2 &\propto e^{-ikx} (\cos(\varphi)e_z - \sin(\varphi)e_y).
 \end{aligned} \tag{12.4}$$

The sum of the two electric fields is thus

$$\mathbf{E}_1 + \mathbf{E}_2 \propto \cos(kx - \varphi)\sigma_- - \cos(kx + \varphi)\sigma_+, \tag{12.5}$$



Fig. 12.3: Laser configuration for a state selective optical potential. Two standing circular polarized standing waves are produced out of two counterpropagating running waves with an angle 2φ between their polarization axes.

where $\sigma_{\pm} = e_y \pm ie_z$. Thus the optical potentials are given by

$$V_{\pm}(x) \propto \cos^2(kx \pm \varphi). \quad (12.6)$$

By changing the angle φ it is possible to move the nodes of the two standing waves in opposite directions. Since these two standing waves act as internal state dependent potentials for the hyperfine states as given in Eq. (12.3) it becomes clear that the optical lattices can be moved in opposite directions for different internal states allowing for state selective interactions between the trapped atoms. This enables the implementation of conditional dynamics in optical lattices which is one of the requirements for doing quantum computation.

12.1.4 Resulting optical potential

According to Eq. (12.3) the most general form of the optical potential for a hyperfine level is given by

$$V(x) = V_0 (\alpha \sin^2(kx - \varphi) + \beta \sin^2(kx + \varphi)), \quad (12.7)$$

with $\alpha + \beta = 1$. The position x_0 of the minimum which is at $x = 0$ for $\varphi = 0$ of this potential is given by

$$x_0 = \frac{1}{2k} \arctan((\beta - \alpha) \tan(2\varphi)). \quad (12.8)$$

If we expand around this minimum to second order we find the frequency of the potential as

$$\omega^2 = \omega_0^2 [\alpha \cos(2kx_0 - 2\varphi) + \beta \cos(2kx_0 + 2\varphi)], \quad (12.9)$$

where $\omega_0^2 = 2k^2V_0/m$. Note that in this case also the minimum of the potential $V(x_0)$ changes with the angle φ .

12.2 Evolution of atoms in moving lattices

In this section we want to investigate the time evolution of a particle in a moving optical lattice potential as well as how to describe the interaction between two particles trapped in the optical lattice. The calculations presented here are the starting point of the calculations presented in chapter 9. A shortened version of these calculations can also be found in Sec. 11.A.

12.2.1 One particle in a moving optical lattice

Let us assume the optical potential to be moved along the x -axis approximate the potential for the atom being moved by a harmonic potential with constant frequency and thus concentrate on the one-dimensional Hamiltonian

$$H = \left(a^\dagger a + \frac{1}{2} + (a^\dagger + a) \frac{\bar{x}(t)}{\sqrt{2}} + \frac{\bar{x}(t)^2}{2} \right). \quad (12.10)$$

a and a^\dagger are the destruction and creation operator of the harmonic oscillator. The displacement of the center of the trap is given by $\bar{x}(t)$. Energies are given in units of ω and all the lengths in units of the harmonic oscillator ground state size $a_0 = \sqrt{1/m\omega}$. All the calculations presented here can be generalized to the case of an optical potential with varying oscillator frequency [1].

12.2.1.1 Exact solution

The Hamiltonian Eq. (12.10) can be solved exactly [2]. To do so we define

$$H_0 = a^\dagger a + \frac{1}{2}, \quad (12.11)$$

and

$$K(t, t_0) = \frac{1}{\sqrt{2}} \int_{t_0}^t ds \bar{x}(s) e^{i(s-t_0)}, \quad (12.12)$$

to obtain for the state vector

$$|\Psi_R(t)\rangle = e^{iK(t,t_0)a^\dagger} e^{iH_0(t-t_0)} |\Psi(t_0)\rangle \quad (12.13)$$

the equation of motion

$$\partial_t |\Psi_R(t)\rangle = \left(-ia - K(t, t_0) \{ \partial_t K^*(t, t_0) \} - i \frac{\bar{x}^2(t)}{2} \right) |\Psi_R(t)\rangle. \quad (12.14)$$

This equation is easily solved and we obtain for the state vector

$$|\Psi(t)\rangle = e^{-iH_0(t-t_0)} e^{-i\Im\{\beta(t,t_0)\}} D(-iK(t, t_0)) |\Psi(t_0)\rangle, \quad (12.15)$$

where $\beta(t, t_0)$ is given by

$$\beta(t, t_0) = \int_{t_0}^t ds \left(K(s, t_0) \{ \partial_s K^*(s, t_0) \} + \frac{i\bar{x}(s)^2}{2} \right), \quad (12.16)$$

and $D(\gamma) = \exp(\gamma a^\dagger - \gamma^* a)$ denotes the displacement operator. If initially at time t_0 the system is in the coherent state $|\Psi(t_0)\rangle = |0\rangle$, where $\langle x|n\rangle = \varphi_n(x)$ are the harmonic oscillator eigenstates we find

$$|\Psi(t)\rangle = e^{-i\Im\{\beta(t, t_0)\}} \sum_{n=0}^{\infty} \frac{(-iK(t, t_0)e^{-i(t-t_0)})^n}{\sqrt{n!}} |n\rangle. \quad (12.17)$$

12.2.1.2 Expansion in derivatives of $\bar{x}(t)$

If we assume that $\bar{x}(t)$ is an analytic function with respect to t and that $1 \approx \bar{x}(t) \gg \partial_t \bar{x}(t) \gg \partial_t^2 \bar{x}(t) \dots$ we expand in these derivatives and write for $K(t', t_0)$

$$K(t', t_0) = \frac{1}{\sqrt{2}} \left(i^{N+1} \int_{t_0}^{t'} ds \{ \partial_s^{N+1} \bar{x}(s) \} e^{i(s-t_0)} - \sum_{n=0}^N i^{n+1} \left[\{ \partial_s^n \bar{x}(s) \} e^{i(s-t_0)} \right] \Big|_{s=t_0}^{s=t'} \right), \quad (12.18)$$

where N is a positive integer. Note that if we may neglect terms of order $\partial_t^2 \bar{x}(t)$ and start in a coherent state $|\Psi(t_0)\rangle = |\bar{x}(t_0) + i\partial_t \bar{x}(t)|_{t=t_0}\rangle$ the state will always be a coherent state with $\langle x(t) \rangle = \bar{x}(t)$ and $\langle p(t) \rangle = \partial_t \bar{x}(t)$.

Now we assume for simplicity that $\bar{x}(t) = \bar{x}(t_0) = 0$, $\partial_t \bar{x}(t) = \partial_t \bar{x}(t_0) = 0$ and $\partial_t^n \bar{x}(t) = (-1)^n \partial_t^n \bar{x}(t_0)$ for $n > 1$. The system is assumed to be in the state $|\Psi(t_0)\rangle = |0\rangle$, initially. We will calculate the expansion of the state $|\Psi(t)\rangle$ in terms of the harmonic oscillator eigenfunctions $\varphi_n(x)$ and keep all terms to fourth order in the derivatives (in the integrand) and find

$$K(t, t_0) = \frac{1}{\sqrt{2}} \left(\{ i(\partial_t^2 - \partial_t^4) \bar{x}(t) \} (e^{i(t-t_0)} - 1) - \{ \partial_t^3 \bar{x}(t) \} (e^{i(t-t_0)} + 1) \right), \quad (12.19)$$

and

$$\beta(t, t_0) = -\frac{i}{2} \int_{t_0}^t ds \left(\{ \partial_s \bar{x}(s) \}^2 + \{ \partial_s^2 \bar{x}(s) \}^2 \right) + \frac{1}{2} \{ \partial_t^2 \bar{x}(t) \}^2 (1 - e^{-i(t-t_0)}). \quad (12.20)$$

If we choose $(t - t_0) = 2n\pi$ the corrections compared to the adiabatic approximation are of third order.

12.2.2 Interaction between two particles

We consider two particles interacting via a short range potential. They are assumed to be trapped in two different harmonic wells that move against each other. The distance between the two wells is $\Delta(t)$. The two particles should have the same mass and the two harmonic wells are assumed to have the same frequency ω . Furthermore we assume the two particles to be distinguishable. The Hamiltonian is given by (in harmonic oscillator units)

$$H = \frac{p_1^2}{2} + \frac{p_2^2}{2} + \frac{1}{2} (x_1^2 + (x_2 - \Delta(t))^2) + u_1 \delta(x_1 - x_2) \quad (12.21)$$

At $t = t_0$ we assume the system to be in the state $\Psi(x_1, x_2, t_0) = \varphi_0(x_1)\varphi_0(x_2 - \Delta(t_0))$. Note that in this case $\Delta(t_0)$ will usually be different from 0. The interaction strength is given by $u_1 = 2a_s$, where a_s is the s-wave scattering length in units of a_0 . we define the quantities $R = (x_1 + x_2 - \Delta(t_0))/2$, $r = x_1 - x_2 + \Delta(t_0)$, $P = p_1 + p_2$ and $p = (p_1 - p_2)/2$. and find $H = H_R + H_r$, where $H_R = P^2/4 + (R - \alpha_R(t))^2$ with $\alpha_R(t) = (\Delta(t) - \Delta(t_0))/2$ and

$$H_r = p^2 + \frac{1}{4}(r - \alpha_r(t))^2 + u_1 \delta(r - \Delta(t_0)), \quad (12.22)$$

where $\alpha_r(t) = \Delta(t_0) - \Delta(t)$. We have already solved the equation of motion for the center of mass motion in Sec. 12.2.1 and will now investigate the influence of the interaction on the relative motion.

The harmonic oscillators for particle 1 and 2 are assumed to start to move at time t_0 with zero velocity $\partial_{t_0} \alpha_r = 0$ and acceleration $a_0 = \partial_{t_0}^2 \alpha_r$. Furthermore they are assumed to have their center positions at the same place at $t = t_1$, i.e., $\alpha(t_1) = \Delta(t_0)$ and are moving at a constant velocity $v = \partial_{t_1} \alpha_r$. The energy shift due to the interaction in first order perturbation theory in u_1 is given by

$$\Delta E(t) = \frac{u_1}{\sqrt{2}} \int_{-\infty}^{\infty} dr \langle \Psi(t) | r \rangle \delta(r - \Delta(0)) \langle r | \Psi(t) \rangle, \quad (12.23)$$

where $|\Psi(t)\rangle$ is the state evolving with H_r when $u_1 = 0$ (initial condition being the ground state). Thus we find for the phase shift

$$\phi_{\text{int}} = \int_{-\infty}^{\infty} dt \Delta E(t) = \frac{u_1}{\sqrt{2}|v|} \left(1 - \frac{a_0}{v} e^{-\frac{1}{4v^2}} \sin(t_1 - t_0) \right), \quad (12.24)$$

neglecting all the derivatives of α_r of third and higher order. Since the phase ϕ_{int} should be of order 1, u_1 has to be of the order of v . Note that by choosing $t_1 - t_0 = 2n\pi$ the first order correction in ϕ_{int} vanishes so that the corrections due to moving the lattice are of third order in the derivatives. However, there might be additional corrections to the above result of order u_1^2 arising from doing perturbation theory in u_1 .

12.2.3 Numerical calculations

To find simple analytic results which give some insight into the behavior of the system we have constrained ourselves to the simplest models up to now. In the numerical calculations we performed in chapter 9 more details were taken into account and we want to show here how we solved the resulting equations numerically. We will not use normalized units in this case since now the frequency of the harmonic oscillators is allowed to change with time (cf. Sec. 12.1.4). The Hamiltonian of two interacting particles in a three dimensional lattice moving along the z axis is given by

$$H = \frac{\mathbf{p}_1^2}{2m} + \frac{\mathbf{p}_2^2}{2m} + V_1(\mathbf{x}_1, t) + V_2(\mathbf{x}_2, t) + u\delta(\mathbf{x}_1 - \mathbf{x}_2) + V_0(t), \quad (12.25)$$

where

$$V_1(\mathbf{x}_1, t) = \frac{m\omega_1^2}{2}(x_1^2 + y_1^2) + \frac{m\omega_1(t)^2}{2}(z_1 - \bar{z}_1(t))^2, \quad (12.26)$$

and

$$V_2(\mathbf{x}_2, t) = \frac{m\omega_2^2}{2}(x_2^2 + y_2^2) + \frac{m\omega_2(t)^2}{2}(z_2 - \bar{z}_2(t))^2. \quad (12.27)$$

$V_0(t)$ is determined by the energies of the centers of the harmonic potentials for the two particles which according to Sec. 12.1.4 will change with time. We assume that $\omega_1(0) = \omega_2(0) = \omega$ and define $\mathbf{x} = \{x, y, z\}$ and $\bar{\mathbf{x}}_i(t) = \{0, 0, \bar{z}_i(t)\}$, where $i = 1, 2$. $u = 4\pi a_s \hbar^2 / m$ is the interaction strength determined by the s -wave scattering length a_s . We rewrite the Hamiltonian in time dependent relative and center of mass coordinates defined by $\mathbf{r} = \mathbf{x}_1 - \bar{\mathbf{x}}_1 - \mathbf{x}_2 + \bar{\mathbf{x}}_2$ and $\mathbf{R} = (\mathbf{x}_1 - \bar{\mathbf{x}}_1 + \mathbf{x}_2 - \bar{\mathbf{x}}_2)/2$ and find

$$\begin{aligned} H &= \frac{\mathbf{p}^2}{2\mu} + \frac{\mathbf{P}^2}{2M} + \frac{\mu\omega^2}{2}\mathbf{r}^2 + \frac{M\omega^2}{2}\mathbf{R}^2 + \frac{m\Omega_+^2}{2}\left(2R_z^2 + \frac{r_z^2}{2}\right) \\ &\quad + \frac{m\Omega_-^2}{2}(R_z r_z) + u\delta(|\mathbf{r} + \bar{\mathbf{x}}_1 - \bar{\mathbf{x}}_2|) + V_0(t). \end{aligned} \quad (12.28)$$

Here we have defined $M = 2m$, $\mu = m/2$, $\Omega_+^2 = (\omega_1^2 + \omega_2^2 - 2\omega^2)/2$ and $\Omega_-^2 = \omega_1^2 - \omega_2^2$. For the wave function we use the ansatz

$$\begin{aligned} \Psi(\mathbf{R}, \mathbf{r}, t) &= \sum_{\mathbf{n}, \mathbf{m}} c_{\mathbf{n}, \mathbf{m}} \phi_{n_x}\left(r_x, \frac{\beta}{\sqrt{2}}\right) \phi_{n_y}\left(r_y, \frac{\beta}{\sqrt{2}}\right) \phi_{n_z}\left(r_z, \frac{\beta}{\sqrt{2}}\right) \\ &\quad \times \phi_{m_x}(R_x, \beta\sqrt{2}) \phi_{m_y}(R_y, \beta\sqrt{2}) \phi_{m_z}(R_z, \beta\sqrt{2}) \\ &\quad \times \exp(-i(n_x + n_y + n_z + m_x + m_y + m_z + 3)\omega t) \\ &\quad \times \exp\left(-\frac{i}{\hbar} \int_{t_0}^t V_0(t') dt'\right), \end{aligned} \quad (12.29)$$

where $\beta = \sqrt{m\omega/\hbar}$, and the mode functions we use are

$$\phi_n(x, \alpha) = \sqrt{\frac{\alpha^2}{\pi}} \frac{1}{\sqrt{2^n n!}} e^{-\alpha^2 x^2/2} H_n(\alpha x) \quad (12.30)$$

with $H_n(x)$ the Hermite polynomials. We put this ansatz into the Schrödinger equation for the Hamiltonian H and obtain

$$\begin{aligned} \dot{c}_{\mathbf{n}, \mathbf{m}} = & \frac{v}{2} \left\{ \sqrt{n_z} c_{\mathbf{n}-1, \mathbf{m}} e^{i\omega t} - \sqrt{n_z + 1} c_{\mathbf{n}+1, \mathbf{m}} e^{-i\omega t} \right\} \\ & - \frac{V}{2} \left\{ \sqrt{m_z} c_{\mathbf{n}, \mathbf{m}-1} e^{i\omega t} - \sqrt{m_z + 1} c_{\mathbf{n}, \mathbf{m}+1} e^{-i\omega t} \right\} \\ & - i \frac{\Omega_+^2}{4\omega} \left\{ 2(m_z + n_z + 1) c_{\mathbf{n}, \mathbf{m}} \right. \\ & + \sqrt{m_z(m_z - 1)} c_{\mathbf{n}, \mathbf{m}-2} e^{2i\omega t} + \sqrt{(m_z + 1)(m_z + 2)} c_{\mathbf{n}, \mathbf{m}+2} e^{-2i\omega t} \\ & \left. + \sqrt{n_z(n_z - 1)} c_{\mathbf{n}-2, \mathbf{m}} e^{2i\omega t} + \sqrt{(n_z + 1)(n_z + 2)} c_{\mathbf{n}+2, \mathbf{m}} e^{-2i\omega t} \right\} \\ & - i \frac{\Omega_-^2}{4\omega} \left\{ \sqrt{(n_z + 1)m_z} c_{\mathbf{n}+1, \mathbf{m}-1} + \sqrt{n_z(m_z + 1)} c_{\mathbf{n}-1, \mathbf{m}+1} \right. \\ & \left. + \sqrt{m_z n_z} c_{\mathbf{n}-1, \mathbf{m}-1} e^{2i\omega t} + \sqrt{(n_z + 1)(m_z + 1)} c_{\mathbf{n}+1, \mathbf{m}+1} e^{-2i\omega t} \right\} \\ & - i \frac{u}{\hbar} \sum_{\mathbf{n}'} \phi_{n'_z}^* \left(\Delta(t), \frac{\beta}{\sqrt{2}} \right) \phi_{n_z} \left(\Delta(t), \frac{\beta}{\sqrt{2}} \right) \\ & \quad \times \phi_{n'_x}^* \left(0, \frac{\beta}{\sqrt{2}} \right) \phi_{n_x} \left(0, \frac{\beta}{\sqrt{2}} \right) \phi_{n'_y}^* \left(0, \frac{\beta}{\sqrt{2}} \right) \phi_{n_y} \left(0, \frac{\beta}{\sqrt{2}} \right) \\ & \quad \times \exp(i(n_x + n_y + n_z - n'_x - n'_y - n'_z)\omega t) c_{\mathbf{n}', \mathbf{m}}. \end{aligned} \quad (12.31)$$

Here we have defined $v = \beta(\dot{\bar{z}}_2(t) - \dot{\bar{z}}_1(t))$, $V = \beta(\dot{\bar{z}}_1(t) + \dot{\bar{z}}_2(t))$, and $\Delta(t) = \bar{z}_2(t) - \bar{z}_1(t)$. The notation $\mathbf{n}-1$ has to be interpreted as $\mathbf{n}-1 = \{n_x, n_y, n_z - 1\}$ and $\bar{\mathbf{n}} = \{n_y, n_x, n_z\}$. If we assume that initially $c_{\mathbf{n}, \mathbf{m}} = c_{\bar{\mathbf{n}}, \mathbf{m}} \forall \mathbf{n}$ this holds at all times. If initially $c_{\mathbf{n}, \mathbf{m}} = -c_{\bar{\mathbf{n}}, \mathbf{m}} \forall \mathbf{n}$ this holds at all times and the interaction term vanishes. Furthermore states of different m_1 and m_2 are uncoupled and $\phi_n(0, \alpha) = 0$ if n is odd. Using all this facts we may solve the above Eq. (12.31) numerically for ten basis states in each direction by solving systems of coupled differential equations with only 1500 variables.

12.3 Fidelity of a gate operation

12.3.1 Initial motional state

The initial motional state is assumed to be given by $\rho_0(T) \propto \exp(-\beta H)$ where H is the system Hamiltonian ($2d$ harmonic oscillators) for the external degrees

of freedom. This canonical density operator is given by

$$\rho_0(\beta) = (1 - \gamma)^{2d} \prod_{i=1}^{2d} \left(\sum_{n_i=0}^{\infty} |n_i\rangle_i \gamma^{n_i} \langle n_i| \right), \quad (12.32)$$

where $\gamma = \exp(-\beta\hbar\omega)$ and $\beta = 1/kT$ the inverse temperature and d is the number of dimensions we consider (we only consider the cases $d = 1$ and $d = 3$). $|n_i\rangle_i$ is the eigenstate with n_i quanta in the i -th oscillator of H . In all numerical calculations in chapter 9 we kept all the terms up to order γ^2 to calculate the time evolved density operator. Note that if we calculate the time evolution for two internal states moving along the z axis such that they interact with each other the interaction cancels whenever one of the two particles is in state $|1\rangle$ in the x or y direction in the harmonic oscillator for the relative motion.

12.3.2 Calculating the fidelity

We want to find the fidelity of the gate discussed in chapter 9. Therefore we have to compare the case of an ideal gate (subscript i) with the gate that can be realized by our scheme (subscript e). Initially the ideal gate is in the state

$$|\psi_i(0)\rangle = \begin{pmatrix} a \\ b \\ c \\ d \end{pmatrix}, \quad (12.33)$$

where we left out the external degrees of freedom since they are not important in the ideal case. The lines are for internal states $|00\rangle$, $|01\rangle$, $|10\rangle$ and $|11\rangle$, respectively. $|0\rangle$ and $|1\rangle$ denote the two different internal states that represent the qubit (for details see chapter 9). In the ideal case the gate operation transforms the state into

$$|\psi_i(t)\rangle = \begin{pmatrix} a \\ b \\ -c \\ d \end{pmatrix}. \quad (12.34)$$

In the more realistic situation the initial total density operator $\sigma_e(0)$ is given by

$$\sigma_e(0) = \begin{pmatrix} a \\ b \\ c \\ d \end{pmatrix} \rho_0(\beta) \begin{pmatrix} a \\ b \\ c \\ d \end{pmatrix}^\dagger. \quad (12.35)$$

To find the time evolved density operator $\sigma_e(t)$ we have to calculate the time evolution of the external degrees of freedom which depend on the internal

state and is also determined by the choice of how the optical lattice is moved. The movement is chosen such that the fidelity of the gate is optimized (cf. chapter 9). If we denote the time evolution operators for the external degrees of freedom as $U^{00}(t)$, $U^{01}(t)$, $U^{10}(t)$, and $U^{11}(t)$ for the atoms being in internal states $|00\rangle$, $|01\rangle$, $|10\rangle$ and $|11\rangle$, respectively we can write the density operator at time t as

$$\sigma_e(t) = \begin{pmatrix} aU^{00}(t) \\ bU^{01}(t) \\ cU^{10}(t) \\ dU^{11}(t) \end{pmatrix} \rho_0(T) \begin{pmatrix} aU^{00}(t) \\ bU^{01}(t) \\ cU^{10}(t) \\ dU^{11}(t) \end{pmatrix}^\dagger. \quad (12.36)$$

The minimum fidelity F is given by [3]

$$F = \min_{a,b,c,d} \langle \psi_i(t) | \text{tr}_{\text{ext}} \{ \sigma_e(t) \} | \psi_i(t) \rangle, \quad (12.37)$$

where tr_{ext} denotes the trace over the external degrees of freedom. As shown in chapter 10 this fidelity can be calculated analytically by noting that the expression to be minimized depends only on the square of the modulus of a, b, c, d .

12.4 Ramsey experiment

In chapter 9 a number of possible new experiments are briefly mentioned. The possible new experiments listed there include the measurement of the s -wave scattering length a_s and of the spatial correlation function of the particles trapped in the optical lattice. We will here theoretically describe the basic steps that are needed to perform such experiments. This will help to clarify the brief description of the experiments suggested in the publication (chapter 9).

We assume a two level atom to be trapped in a selectively movable optical lattice (cf. Sec. 12.1). The creation (annihilation) operators for the two levels are given by a_γ^\dagger (a_γ) and b_γ^\dagger (b_γ) where γ labels the different sites of the optical lattice. In order to simplify the notation we will assume the particles in state $|a\rangle$ to be kept at the same position while the atoms in $|b\rangle$ are moved in the optical potential. The first step is to apply a Ramsey pulse described by the unitary evolution

$$U_{R1}^\dagger \begin{pmatrix} a_\gamma \\ b_\gamma \end{pmatrix} U_{R1} = \begin{pmatrix} c_\gamma & e^{i\psi_\gamma} s_\gamma \\ -e^{-i\psi_\gamma} s_\gamma & c_\gamma \end{pmatrix} \begin{pmatrix} a_\gamma \\ b_\gamma \end{pmatrix}. \quad (12.38)$$

Then the lattice is moved and after a time t a second Ramsey pulse is applied described by the unitary evolution

$$U_{R2}^\dagger \begin{pmatrix} a_\gamma \\ b_\nu \end{pmatrix} U_{R2} = \begin{pmatrix} \bar{c}_\gamma & e^{i\bar{\psi}_\gamma} \bar{s}_\gamma \\ -e^{-i\bar{\psi}_\gamma} \bar{s}_\gamma & \bar{c}_\gamma \end{pmatrix} \begin{pmatrix} a_\gamma \\ b_\nu \end{pmatrix}. \quad (12.39)$$

where $\nu = \gamma$ if the lattice is moved back to its starting position. Otherwise ν is the label of the site which was moved to site γ between the two Ramsey pulses. ψ_γ and $\bar{\psi}_\gamma$ are the phases of the Ramsey pulses in site γ and $c_\gamma^2 + s_\gamma^2 = \bar{c}_\gamma^2 + \bar{s}_\gamma^2 = 1$.

The time evolution between the two Ramsey pulses is given by

$$U_t = \exp \left(-i \sum_j \left((\phi - \Delta) n_j^b + U^a n_j^a (n_j^a - 1)/2 + U^b n_j^b (n_j^b - 1)/2 \right) - i \sum_{jl} \Theta_{jl} n_j^a n_l^b \right), \quad (12.40)$$

where $\Delta = \delta t$ with δ the detuning of the Ramsey pulse and ϕ is the kinetic phase defined in Eq. (9.4). U^a , U^b and Θ_{jl} are the phase shifts due to interactions. The number operators are $n_j^a = a_j^\dagger a_j$ and $n_j^b = b_j^\dagger b_j$. The time evolution of the annihilation operators is given by

$$U_t^\dagger a_j U_t = a_j \exp \left(-i U^a (n_j^a - 1) - i \sum_l \Theta_{jl} n_l^b \right), \quad (12.41)$$

and

$$U_t^\dagger b_j U_t = b_j \exp \left(i(\Delta - \phi) - i U^b (n_j^b - 1) - i \sum_l \Theta_{lj} n_l^a \right). \quad (12.42)$$

12.4.1 Occupation numbers

We will now show how by measuring the number of particles in the internal state $|b\rangle$ after doing the sequence of operations described above one is able to discriminate different initial states like Mott insulator and superfluid states. Also it will become evident that it is possible to determine the scattering lengths for the particles in the optical lattice.

Initially all the particles are assumed to be in the internal state $|a\rangle$ and described by the initial state $|\Psi_0\rangle$. We want to find the expectation value

$$\langle n_\gamma^b \rangle_t = \langle \Psi_0 | U_{R1} U_t U_{R2} n_\gamma^b U_{R2} U_t U_{R1} | \Psi_0 \rangle, \quad (12.43)$$

which can be simplified

$$\langle n_\gamma^b \rangle_t = \bar{s}_\nu^2 \langle U_{R1}^\dagger n_\nu^a U_{R1} \rangle_0 + \bar{c}_\nu^2 \langle U_{R1}^\dagger n_\gamma^b U_{R1} \rangle_0 - 2\bar{s}_\nu \bar{c}_\nu \Re \left\{ e^{i\bar{\psi}_\nu} \chi \right\}, \quad (12.44)$$

where $\langle \rangle_{t'}$ denotes the expectation value at time t' and χ is defined by

$$\chi = \langle U_{R1}^\dagger U_t^\dagger b_\gamma U_t a_\nu^\dagger U_t U_{R1} \rangle_0. \quad (12.45)$$

Simplifying the first two terms yields

$$\begin{aligned} \langle n_\gamma^b \rangle_t &= \bar{s}_\nu^2 \left(s_\nu^2 \langle n_\nu^b \rangle_0 + c_\nu^2 \langle n_\nu^a \rangle_0 + 2s_\nu c_\nu \Re \left\{ \langle e^{i\psi_\nu} b_\nu a_\nu^\dagger \rangle_0 \right\} \right) \\ &\quad + \bar{c}_\nu^2 \left(s_\gamma^2 \langle n_\gamma^a \rangle_0 + c_\gamma^2 \langle n_\gamma^b \rangle_0 - 2s_\gamma c_\gamma \Re \left\{ \langle e^{i\psi_\gamma} b_\gamma a_\gamma^\dagger \rangle_0 \right\} \right) \\ &\quad - 2\bar{s}_\nu \bar{c}_\nu \Re \left\{ e^{i\bar{\psi}_\nu} \chi \right\}. \end{aligned} \quad (12.46)$$

The expectation value χ may be written in several different forms. We might find it useful to use

$$\chi = e^{i\alpha} \langle e^{i \sum_j ((\Theta_{\nu j} - \delta_{j,\gamma} U^b) n_j^b - (\Theta_{j\gamma} - \delta_{j,\nu} U^a) n_j^a)} a_\nu^\dagger b_\gamma \rangle_{0+}, \quad (12.47)$$

where $\langle \rangle_{0+}$ denotes the expectation value for the state $U_{R1} |\Psi_0\rangle$, and we have defined $\alpha = \Delta - \phi - U^a + \Theta_{\nu\gamma}$, or the form

$$\begin{aligned} \chi &= \langle \exp \left\{ i \sum_j \left[(\Theta_{\nu j} - \delta_{j,\gamma} U^b) \left(c_j^2 n_j^b + s_j^2 n_j^a + s_j c_j \left\{ e^{i\psi_j} b_j a_j^\dagger + \text{h.c.} \right\} \right) \right. \right. \\ &\quad \left. \left. - (\Theta_{j\gamma} - \delta_{j,\nu} U^a) \left(c_j^2 n_j^a + s_j^2 n_j^b - s_j c_j \left\{ e^{i\psi_j} b_j a_j^\dagger + \text{h.c.} \right\} \right) \right] \right\} \\ &\quad \left(c_\nu a_\nu^\dagger + e^{-i\psi_\nu} s_\nu b_\nu^\dagger \right) \left(c_\gamma b_\gamma - e^{-i\psi_\gamma} s_\gamma a_\gamma \right) \rangle_0 e^{i\alpha}. \end{aligned} \quad (12.48)$$

12.4.2 Special cases

12.4.2.1 Mott phase

We first want to consider the case $|\Psi_0\rangle = \prod_j |n_j^a\rangle_j$ where $|n^a\rangle_j$ is the Fock state with n particles in state $|a\rangle$ at site j and $\nu = \gamma$. We find

$$\langle n_\nu^b \rangle_t = n_\nu (\bar{s}_\nu^2 c_\nu^2 + \bar{c}_\nu^2 s_\nu^2) - 2\bar{s}_\nu \bar{c}_\nu \Re \left\{ e^{i\bar{\psi}_\nu} \chi \right\}, \quad (12.49)$$

with

$$\chi = e^{i(\Delta - \phi - \psi_\nu)} n_\nu s_\nu c_\nu \prod_j \left(c_j^2 e^{-i(\Theta_{j\nu} - U^a \delta_{j,\nu})} + s_j^2 e^{i(\Theta_{\nu j} - U^b \delta_{j,\nu})} \right)^{n_j - \delta_{j,\nu}}. \quad (12.50)$$

12.4.2.2 Superfluid phase

For an initial state $|\Psi_0\rangle = \frac{M^{-N/2}}{\sqrt{N!}} (\sum_{j=0}^{M-1} a_j^\dagger)^N |0\rangle$ where M is the number of sites we obtain

$$\langle n_\gamma^b \rangle_t = \frac{N}{M} (\bar{s}_\nu^2 c_\nu^2 + \bar{c}_\nu^2 s_\nu^2) - 2\bar{s}_\nu \bar{c}_\nu \Re \left\{ e^{i\bar{\psi}_\nu} \chi \right\}, \quad (12.51)$$

where

$$\chi = \frac{N}{M} c_\nu s_\gamma e^{i(\Delta - \phi - \psi_\gamma)} \left(\frac{1}{M} \sum_{j=0}^{M-1} \left(c_j^2 e^{-i(\Theta_{j\gamma} - U^a \delta_{j,\nu})} + s_j^2 e^{i(\Theta_{\nu j} - U^b \delta_{j,\gamma})} \right) \right)^{N-1}. \quad (12.52)$$

12.4.2.3 Gutzwiller ansatz

We use a Gutzwiller wave function $|\Psi_0\rangle = \prod_j \left(\sum_{n=0}^N f_n^{(j)} |n\rangle_j \right)$ as the initial state and find

$$\langle n_\gamma^b \rangle_t = \bar{s}_\nu^2 c_\nu^2 \langle n_\nu^a \rangle_0 + \bar{c}_\nu^2 s_\gamma^2 \langle n_\gamma^a \rangle_0 - 2\bar{s}_\nu \bar{c}_\nu \Re \left\{ e^{i\bar{\psi}_\nu} \chi \right\}, \quad (12.53)$$

where

$$\chi = c_\nu s_\gamma e^{i(\Delta - \phi - \psi_\gamma)} \prod_j \left\{ \sum_{n=0}^{N-1} ((\sqrt{n+1} - 1) \delta_{j,\nu} + 1) ((\sqrt{n} - 1) \delta_{j,\gamma} + 1) f_{n-\delta_{j,\gamma}+\delta_{j,\nu}}^{(j)*} f_n^{(j)} \left(c_j^2 e^{-i(\Theta_{j\gamma} - U^a \delta_{j,\nu})} + s_j^2 e^{i(\Theta_{\nu j} - U^b \delta_{j,\gamma})} \right)^{n-\delta_{j,\gamma}} \right\}. \quad (12.54)$$

References

- [1] Yu. Kagan, E.L. Surkov, and G.V. Shlyapnikov, *Phys. Rev. A* **54**, R1753, (1996).
- [2] A. Galindo, P. Pascual, *Quantum Mechanics II* (Springer Berlin 1990).
- [3] B. Schumacher, *Phys. Rev. A* **54**, 2614 (1996).